From midplane to planets : the chemical fingerprint of a disk

Eistrup, C.

From Midplane to Planets
The Chemical Fingerprint of a Disk

Christian Eistrup

From Midplane to Planets
The Chemical Fingerprint of a Disk

Proefschrift

ter verkrijging van
de graad van Doctor aan de Universiteit Leiden,
op gezag van Rector Magnificus prof. mr. C.J.J.M. Stolker,
volgens besluit van het College voor Promoties
te verdedigen op dinsdag 16 oktober 2018 klokke 10.00 uur

door

Christian Eistrup

geboren te Hørsholm, Denemarken
in 1988

Promotor:	Prof. dr. E.F. van Dishoeck
Co-promotor:	Dr. C. Walsh (University of Leeds)
Overige leden:	Prof. dr. E.A. Bergin (University of Michigan)
	Prof. dr. H.M. Cuppen (Radboud Universiteit Nijmegen)
	Prof. dr. C. Mordasini (Universität Bern)
	Prof. dr. I.A.G. Snellen
	Prof. dr. H.J.A. Röttgering

Cover artwork: adapted from "ALBEDO" by Kasper Eistrup
Cover layout: Iris Nijman
Image in "Acknowledgement"-section:
http://www.clker.com/clipart-pink-elephant-12.html

ISBN: 978-94-028-1202-2

An electronic version of this thesis can be found at www.strw.leidenuniv.nl/∼eistrup

Til mor, far og Astrid, for støtten til at tage springet!

The stars are for everyone to see, yet for no one to touch and control. So let go, sit back, relax, be fascinated, become curious, and wonder. The Universe can open and broaden your mind!

Contents

1 Introduction

Since the dawn of time, two fundamental questions have caused amazement and wondering for humanity: Where do we come from? Are we alone? Although these questions are multifaceted, they are both addressed in the science of astronomy.

"Where do we come from?" seeks a coherent series of events, mechanisms and effects leading from the beginning of our Universe up until we ask the very question. And then asking the question "are we alone?" begs an understanding of our own "place" in the Universe, "why" we are able to philosophise and ask these questions, and ultimately, if someone or something else outside the Earth, or outside the Solar System, might be asking the same questions. In other words: is life unique to the Earth, or is there life outside it?

Addressing this requires input and expertise from several branches of science: physics, astronomy, chemistry, geology and biology, to mention some. The last two branches concern the evolution of a planet and of life on it, when the planet has already formed. The first three branches, on the other hand, can be used to predict to formation and evolution of planets.

1.1 Planets and exoplanets

A planet is, as currently defined by the International Astronomical Union (IAU), a celestial body that (1) is in orbit around the Sun, (2) has sufficient mass for its self-gravity to overcome rigid body forces so that it assumes a hydrostatic equilibrium (nearly round) shape, and (3) has cleared the neighbourhood around its orbit. Out of nine celestial bodies in our Solar System historically recognised as planets before the above IAU definition of 2006, eight of them satisfy these requirements, leaving out Pluto, which is now considered a dwarf planet.

Until quite recently (mid 1990s), the planets in the Solar System were the only ones known to orbit a main-sequence star. Since the first detection of a planet, a so-called exoplanet[1], in the 51 Pegasus system by Mayor & Queloz (1995), an entire new field has erupted which is now flourishing in astronomy, namely exoplanet science. Given the basic challenge that planets and exoplanets are much smaller and much dimmer than their stellar hosts, thus intuitively very difficult to "see" through observations, a range of inventive and creative techniques have had to be developed for the detection of exoplanets. Only one of these, the direct imaging technique, can detect the signal from an exoplanet by simply observing the sky. This is due to advanced techniques, such as coronagraphy, whereby the observed starlight can be dimmed, so that the exoplanet signal does not drown in the stellar signal (see e.g. Marois et al. 2010). All other detection techniques used to this day, the radial velocity (RV) and transit methods, transit-timing variations, microlensing and astrometry, produce indirect detections of exoplanets, by observing the light from the host star and tracking changes in this light that are caused by the presence of a planet.

After more than 20 years of searching for exoplanets, almost 4000 have been confirmed to date. A "confirmed" exoplanet is one that has been detected using multiple detection techniques, thereby ruling out signals that may not come from

[1] Extra-solar planet, orbiting another star than the Sun

planet interactions. The efforts going into searching for exoplanets have included the use of the world's most advanced telescopes, both on ground and in space, including such facilities as ESO's Very Large Telescope in Paranal, Chile, NASA's Hubble Space Telescope, as well as dedicated exoplanet hunting space missions such as NASA's Kepler, with more facilities planned for operation in the near future. However, smaller telescopes are also very effective, with the Lick Observatory, the Haute Provence Observatory, the Danish Telescope in La Silla, Chile, and the MEarth-project all having pioneered exoplanet discoveries.

The confirmed planets can be straightforwardly compared to the eight planets in the Solar System, in terms of sizes (planetary radii), masses and orbital distances from their host stars. This comparison shows that the exoplanets detected so far are mostly very different from the eight Solar System planets, rendering the Solar System architecture and planetary characteristics quite special. Predictions based on the sample of exoplanets so far point to planets being very common around stars in our galaxy, with Cassan et al. (2012) predicting 1.6 planets per star for the Milky Way. Dressing & Charbonneau (2013) suggest that exoplanets 0.5-4 times the radius of the Earth should be common around M dwarf stars.

The exoplanets vary greatly in size and orbital distance. Most exoplanets detected are small like the Earth, and they orbit close to their host stars (at fractions of an AU) [2], but biases in the detection techniques play a crucial role here: the larger (for the transit and transit timing variations methods) and more massive (for the radial velocity, astrometry and microlensing methods) an exoplanet is, and the closer it orbits its host star (for the transit, transit timing variations and radial velocity methods), the easier the planet is to detect. Everything from sub-Earth sized planets (Barclay et al. 2013) to super Jupiter-sized exoplanets have been detected, and even multiple exoplanets orbiting the same star (see e.g. Gillon et al. 2017). All kinds of planets and planetary system architectures therefore seem possible.

Two goals of exoplanet science are 1) understanding the outcome scenarios of planet formation, and what exoplanets with certain characteristics tell us about how the exoplanets formed and evolved, and 2) finding habitable exoplanets, and ultimately the search for signatures of life on such planets, to be able to answer the fundamental question posed in the beginning of this text: Are we alone? An additional goal is also to construct an inventory of planets orbiting all types of stars, after all, the close to 4000 confirmed exoplanets are still few considering the predicted number of planets in the Milky Way galaxy: 1.6 exoplanets per star, with $\sim 10^{11}$ stars in the galaxy.

1.2 Making planets

Connecting detected exoplanets to how they were formed is an exciting and active field of astronomy. It links the hunt for, and study of exoplanets, to the field of star and planet formation. Planets form around stars, largely from the same type of material that the stars form from. The whole process starts when a large volume

[2] See exoplanet.eu

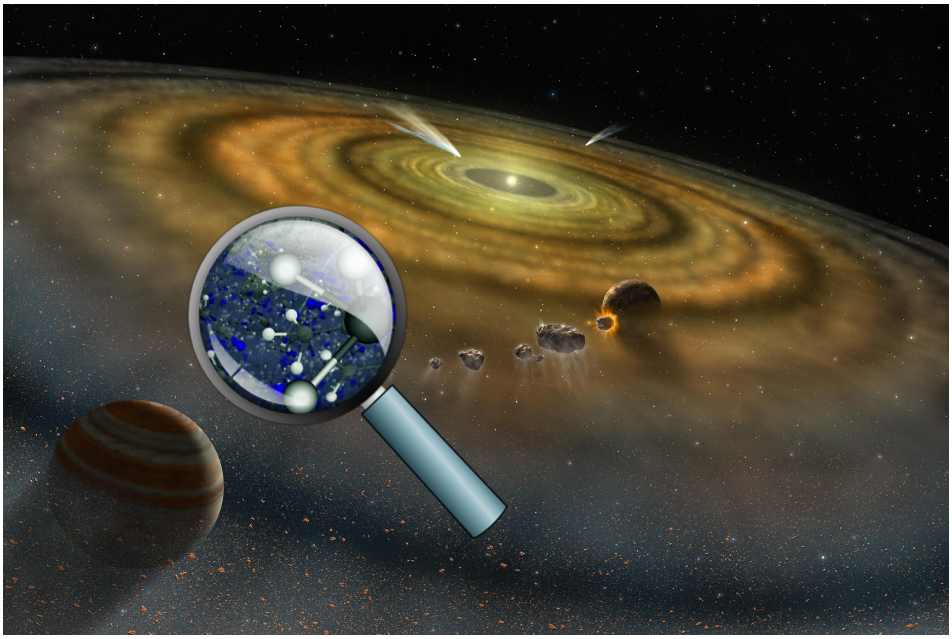

Figure 1.1: Artist's impression of planets forming in a protoplanetary disk of gas and dust. Solid impactors are seen hitting down on a planet. A zoom-in (under the magnifying glass) reveals that the gas and the dust are made up of molecules. *Composite image by Iris Nijman made from artist's impressions by NASA and by B. Saxton / NRAO / AUI / NSF.*

of space filled with gas and dust (a so-called molecular cloud) collapses under its own gravity, with material in the cloud compactifying on a smaller and smaller scale (see review by Li et al. 2014). In the centre of this collapse a protostar is formed and, because of the non-zero initial angular momentum of the material in the molecular cloud, gas and dust start rotating around the protostar in a protoplanetary disk. The material in this disk moves inwards towards the star, but this happens slower than the gravitational free-fall time, because the gas in the disk exerts an outwards pressure, and because the whole disk is rotating, thus adding an outwards pointing centrifugal force.

The dust in the disk will tend to settle gravitationally to the midplane of the disk, and will move closer towards the star than the gas. This is because the dust will dynamically decouple from the gas, when it has grown larger than a few microns. A dust grain will then no longer feel the outwards and upwards gas pressure, but will attempt to move in a Keplerian orbit around the protostar. However, since the dust is immersed in gas, it feels the gas as a head wind, and it thus moves slower in its orbit. This mean that the gas will slow down the dust grain, the dust grain will lose angular momentum, and will drift inwards. The efficiencies of these slowing mechanisms for dust grains depend on the size of the grains, with larger grains, around one centimeter in size, moving faster through the disk than smaller grains (see Lambrechts & Johansen 2012).

These grains consist of initially μm-sized silicates and carbonaceous material, and may have their surfaces covered with ice, depending on the temperature at their distance away from the protostar. The colder it is, the more different volatile molecules will be below their freezing point, and thus be frozen out onto the grain surfaces. In a typical protoplanetary disk, such volatile molecules are H_2O, which freezes out at temperatures below $\sim$180 K (dependent upon density and pressure), and CO_2, CH_4 and CO freezing out at decreasingly lower temperatures. The radial position in the disk midplane where the freeze-out rate of a given molecule onto a grain surface matches the thermal desorption rate of that same molecule off the grain surface is called the *iceline* for that molecular species. Icelines are important in the context of protoplanetary disks, as they largely define where in a disk, depending on the temperature and density structures, a molecular species is in the gas and ice phase.

The grains grow larger over time, mostly due to agglomeration at locations in the disk midplane that can facilitate a pile-up of grains. This can happen due to radial bumps in the gas-pressure profile (Pinilla et al. 2012), or due to streaming instabilities (Youdin & Goodman 2005), amongst other mechanisms. With a large enough concentration of solid bodies of different sizes, the larger bodies (planetesimals) above kilometer sizes can accrete smaller bodies called pebbles (Lambrechts & Johansen 2012) of centimeter to meters in size. This can lead to growing the planetesimals even larger, and when they reach tens-to-hundreds of kilometers in size they can start shaping themselves as spheres (see Fig. 1.1). Finally, when they reach several times the mass of the Earth, the bodies will be massive enough to have surrounding gas in the disk collapse down on their surfaces, in what is known as run-away gas accretion.

Upon accretion of the surrounding gas, a gas giant planet has been formed, of which the Solar System planets Jupiter and Saturn are examples. This is one theory for how planets are formed, the so-called core accretion theory, see Pollack et al. (1996). A planet forming through core accretion can experience a depletion in the material, solid and gas that it can form from. This happens if the planet forms late, after other planets have already used up material, or if it forms in a less massive disk, or in certain parts of the disk, with less material. In such situations some steps towards becoming a gas giant can be halted, and the results will be a less massive planet. Ice giants, like Uranus and Neptune, have icy cores and atmospheres made of hydrogen and helium, that are smaller than the atmospheres of Jupiter and Saturn. Lastly, giant planets can potentially also form by gravitational collapse of material locally in a protoplanetary disk, if the disk is massive enough. This scenario is called gravitational instability (Takahashi & Inutsuka 2014), and it is proposed as the explanation for giant exoplanets orbiting their host stars at large radii, from tens to hundreds of AU.

1.3 Protoplanetary disks, and the era of ALMA

Studying disks and planet formation has undergone a quantum leap in recent years, due to extraordinary new observational facilities, first and foremost ALMA (the

Atacama Large Millimeter/submillimeter Array located in the Atacama Desert in Chile). ALMA, with its extraordinary spatial and spectral resolution power for radio frequencies from 84 to 950 GHz, has opened up opportunities for constraining structures of gas and dust, temperatures, densities, and molecular compositions of protoplanetary disks. All of these are vital for understanding how disks evolve, and, importantly, how planets may form inside them (see Williams & Cieza 2011, for a pre-ALMA summary).

ALMA has unveiled complex physical structures for both the gas and dust in disks, and also detected simple and complex chemical species in the gas. Some prominent findings of ALMA have been the detection of a dust trap (likely induced by a planet) in a transitional disk (in the object IRS 48 by van der Marel et al. 2013), the detections of dusty rings of millimeter sized dust around young stars (see e.g. ALMA Partnership et al. 2015; Andrews et al. 2016, and Fig. 1.2), and dust being concentrated closer to the star than the gas, which extends out to larger radii (see Facchini et al. 2017). The dust concentration close to the star points to dust evolution (although differences in optical depths of gas and dust also play roles): grains in the protoplanetary disk settle toward the disk midplane, and subsequently migrate radially towards the protostar, enhancing the dust concentration there. The rings of dust indicate that substructure exists in the dust concentration close to the protostar. The largely azimuthally symmetric nature of this substructure, as in the cases for the disks TW Hya and HL Tau, points to the millimeter-sized dust depleting in orbits of specific radii around the protostar: this could be a sign of protoplanets in the process of accreting, or already having accreted the surrounding dust in their orbits in order to grow larger, but there are also other explanations. However, the best evidence for ongoing planet formation, is in transitional disks because of the depth of the gas and dust cavities there (van der Marel et al. 2016).

The revelations of dust traps and ringed substructure in the dust emission from disks were therefore the first sparks in the field of observational planet formation. ALMA was also recently used to infer planets in formation around the protoplanetary disk HD 163296, this time not using dust emission, but instead the emission lines from carbon monoxide (CO), and specifically the subtle variations in the orbital speed of the CO gas, variations of order five to tens of percent, which only ALMA has the sensitivity to detect. These small orbital speed variations were linked to radial changes to the gas pressure induced by the presence of planets forming in the disk. Together, two teams of reseachers (Pinte et al. 2018; Teague et al. 2018) predicted three giant planets in formation around HD 163296.

Other examples of predictions of protoplanetary presence around protostars include the detection of spiral structures in the dust emission from a disk (e.g. Pérez et al. 2016; Hall et al. 2018), although thus far such spiral structures are rare. Hydrodynamical simulations have shown that a sufficiently massive planetary object orbiting at a large radius can stir up the dust structure inside the planet, and cause spiral structures in dust (Dong et al. 2015). The indications are thus plentiful, and the evidence growing, that ALMA is indeed able to detect signs of planets in formation, opening up an observational laboratory to test existing physical model predictions of how planet formation takes place.

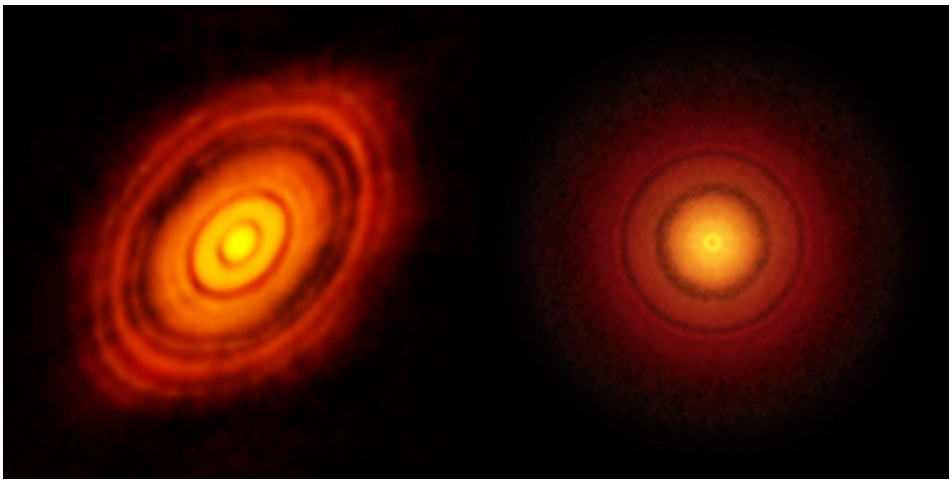

Figure 1.2: Images of millimeter dust emission from the disks around HL Tauri (left) and TW Hydrae (right). Rings are seen around both protostars. *Credit left: ALMA Partnership et al. (2015), credit right: Andrews et al. (2016).*

Another aspect of protoplanetary disks and planet formation that ALMA has opened up is the mapping of the chemical (gas-phase) inventory of disks. With unrivalled spectral resolution, ALMA can detect spectral signatures of both simple molecules, like CO, HCN and HCO^+, and more complex ones, like H_2CO and CH_3OH, to mention a few. Other facilities, like the space missions *Spitzer* and *Herschel* have detected additional molecules emitting in the infra-red, and far-infra-red, respectively. Pontoppidan et al. (2014) gives an overview of detections by *Spitzer* such as CO_2, H_2O, C_2H_2 and HCN. Hogerheijde et al. (2011) detected cold H_2O and Salinas et al. (2016) detected NH_3, both using *Herschel*.

Observations of the disk around TW Hydrae (the left image in Fig. 1.2) have for one revealed much less CO gas than expected (see e.g. Nomura et al. 2016; Kama et al. 2016a; Schwarz et al. 2016). Efforts with ALMA have also been put into tracing the CO iceline through observations of molecular species that can only exist in the gas-phase when CO is frozen out. N_2H^+ and DCO^+ are such molecules, and they have been successfully detected by Qi et al. (2013); Öberg et al. (2015). The detection of CN in disks has similarly been used to trace the exposure and penetration of UV radiation on disks, and hence their dust structure (Cazzoletti et al. 2018).

In addition to ALMA observations, optical and near-infrared facilities have also contributed with new insights on planet formation. Recently, Keppler et al. (2018) revealed images of a planet in formation around the young star PDS 70, which was detected using observations from the VLT/SPHERE, the VLT/NaCo and the Gemini/NICI telescopes and instruments. This discovery was the first-ever direct image of a forming planet, and it highlights the value of multi-wavelength observations (e.g. millimeter/submillimeter and optical/near-infrared) of protoplanetary

disks, for a more detailed understanding of planet formation.

Because planets are forming in these disks, they will form from material containing these molecules, and by knowing how much of each molecule there is in the disks, and where it is located, predictions can be made as to the molecular composition of the planets. This can be predicting the relative amounts of CO_2 and H_2O, but more importantly the relative amounts of elemental carbon, oxygen, and nitrogen that goes into forming the planets.

1.4 Astrochemistry: laboratory, simulations and observations

Understanding the chemical composition in planet-forming regions is essential for predicting the compositions of the planets that form therein. In turn, given the growing chemical characterisations of exoplanet atmospheres, astrochemistry is essential for tracing the formation histories of these planets.

So what is the chemical composition of planet-forming material, i.e. the gas and ice-covered dust residing in the disk midplane? The answer to this is a link between observational exoplanet science, which has already detected CO, H_2O and CH_4 (Swain et al. 2008; Barman et al. 2015) in the atmospheres of exoplanets, and the science of protoplanetary disks and planet formation. The chemical composition of the latter must be what sets the chemical content of the former. There are at least two challenges to answering the questions.

First challenge. It is difficult to determine the chemical composition in the protoplanetary disk midplanes, even with ALMA. This is due to the upper layers of the disks obstructing the emission coming from the midplane, meaning it is mostly emission from the upper layers of the disk that can be observed. Since these upper layers have different physical conditions than the midplane, in that they are more diffuse, warmer, and experience more UV radiation from the protostar, the chemistry in these layers is different from the chemistry in the midplane, and the chemical compositions of the upper layers can thus not be used as probe for the midplane composition (see e.g. Walsh et al. 2015). However, successful efforts have been made by Zhang et al. (2017) to probe the CO in the midplane through detections of CO isotopologues, but it remains difficult to probe other gas species in the region (although for less volatile molecules this is due to them being frozen out in the outer regions, rather than intermediate layer obscuration).

Second challenge. Should it be assumed that the chemical composition in the midplane is directly inherited from the parent molecular cloud, such that the molecules in the cloud survived the trip to the midplane (Madhusudhan et al. 2014; Mordasini et al. 2016), and subsequently the incorporation into a planet? Or will chemical reactions happen along the way, thereby changing the chemical composition of the material? The molecules in the inner, hotter part of the disk could also be assumed completely reset (dissociated into atoms, see Visser et al. 2009; Pontoppidan et al. 2014) upon arrival in the disk midplane, followed by either LTE condensation when the disk cools, or chemical kinetics dictating the reactions between the atoms (Willacy et al. 1998; Aikawa & Herbst 1999; Vasyunin

et al. 2008).

With the currently available data from astrochemical laboratories there is now a good basis both for binding energies for molecules to surfaces, and reaction rate coefficients for chemical kinetics in both gas phase and in the ice (see review by Cuppen et al. 2017). These coefficients can be used to construct chemical models that can simulate the kinetics of chemical reactions in space, based on balancing reaction rates that are forming versus destroying a given molecule. The rates of different reactions depend on physical conditions such as temperature and density, as well as the assumed timescale (more chemical changes can take place over longer time), and the abundances of ions and radicals, which are in turn products of ionisation by e.g. galactic cosmic rays. Given high enough temperatures and densities, local thermodynamic equilibrium (LTE) can be attained, at which point the equilibrium abundances of molecules can be computed via Gibbs' Free Energy minimisation.

LTE conditions may be present close to the star, or in a Hot Jupiter atmosphere, but in the colder disk midplane such conditions are not achieved. Therefore chemical kinetics is a more appropriate approach in these environments. Chemical kinetics are computationally slower and more complicated to handle than Gibbs' Free Energy minimisation, because of the larger amount of chemical species and reactions to account for, with a need to solve up to 1000 differential equations, and choosing appropriate numerical solvers and parameters to achieve a stable solution. Added complications are the uncertainties associated with the reaction rate coefficients, the need to treat gas-phase chemistry, gas-grain interactions and grain-surface chemistry simultaneously, and the question on how to parameterise grain-surface ice chemistry.

Several disk chemistry codes are available, codes that couple chemistry with disk physics (temperature, density, radiation field etc.). These are codes like the ProDiMo code (Woitke et al. 2009) and the DALI code (Bruderer et al. 2014). Other codes treat the chemistry independently of the physics, such as the BADASS code (Walsh et al. 2015). The different codes employ various degrees of complexity with regards to the different types of chemistry that they are focusing on: gas-phase, gas-grain interaction, or grain-surface chemistry, as well as assumptions for the physical conditions and feedback effects between physical and chemical evolution. Due to computational limitations, the codes are usually either treating the physical-chemical feedback effects self-consistently (the DALI code), but with limitations regarding chemical complexity (especially grain-surface chemistry), or treating especially said grain-surface chemistry extensively, but with no feedback effects from chemical to physical evolution (the BADASS code). The codes take their reaction rate coefficients from publicly available databases such as KIDA/OSU[3] or UDfA[4].

The BADASS code has a more extensive treatment of ice chemistry than the other codes. This code includes not only atom-addition (hydrogenation), but also radical-radical or radical-molecule reactions involving ice species that thermally diffuse from one surface site to another (e.g. $\mathrm{iCO} + \mathrm{iOH} \longrightarrow \mathrm{iCO_2} + \mathrm{iH}$, where

[3]http://kida.obs.u-bordeaux1.fr/networks.html
[4]http://udfa.ajmarkwick.net

"i" denotes ice species). Because the gas and dust in the dense disk midplane can be assumed to be thermally balanced, the gas-phase chemistry can be treated simultaneously with these chemical effects on the grains. This also means that the code can treat adsorbed molecules (molecules that bind to the grain surface from the gas-phase) as a part of the grain-surface chemistry, even if the temperature is higher than the freeze-out temperature prescribed by the binding energy of the molecule, because diffusion across the ice surface is faster than desorption due to the lower barrier for the former. This effect is a consequence of the treatment of freeze-out in the chemical kinetics framework: a chemical species does not simply exist as gas inside its iceline, and as ice outside it. The freeze-out and desorption terms for a given molecule in the rate coefficients framework are always both at play, and the iceline is simply the radial location where temperature and density lead to the two terms matching each other. But a molecule can still freeze out inside the iceline, and still thermally desorb from the grain surface outside of it, thus allowing for interesting chemical effects in the vicinity of icelines.

Chemical kinetics, including complex grain-surface chemistry, allows for a comprehensive treatment of chemistry for volatile molecules (molecules with a low binding energy) in the midplanes of disk. Chemical kinetics codes are thus important for predicting how the chemical composition in the midplane evolves over time, and what the composition of the material will be when it is being incorporated into planets and other celestial bodies.

1.5 Combining astrochemistry and planet formation

Planet formation models have thus far mostly assumed that the chemical composition of the planet-forming material was inherited from the parent molecular cloud, and remained chemically inert until incorporation into planets (see e.g. Ali-Dib 2017; Alibert et al. 2013; Mordasini et al. 2016). Because a certain set of molecular abundances has then been assumed for the planet-forming disk midplane, this simplification has meant that at any radial point in the disk (with a given temperature) it was known which molecular species were in gas-phase and which were ices on grains. This would only depend on the binding energies of the molecules.

Depending on where a planet is then assumed to be formed, and which stage of formation it is in (only growing from solid material, or also accreting gas), its final composition could be estimated, from the molecules at that location in the disk. Especially the relative amounts of elemental carbon and oxygen at the location (see Fig. 1.3) would then set the chemical basis for bulk and atmospheric chemistry in the planet, where chemistry is likely closer to equilibrium conditions (see e.g. Mollière et al. 2015) than was the case in the protoplanetary disk midplane. Planet formation modelling efforts that have included treatment of chemical evolution in the disk midplane before forming planets include Cridland et al. (2016, 2017). However, they focused on the final chemical composition of the formed planetary atmospheres, rather than the chemical changes to the gas and ice in the disk midplane occurring before initiation of planet formation.

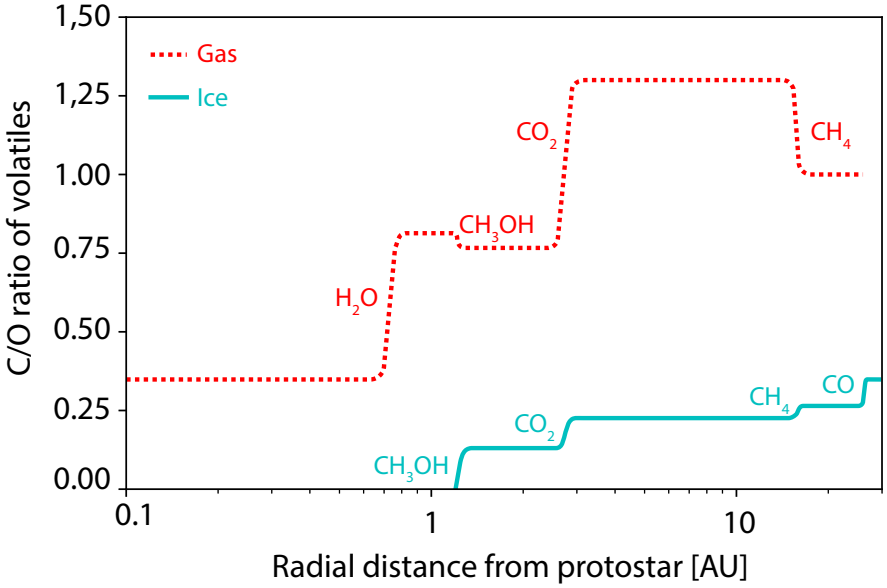

Figure 1.3: Carbon-to-oxygen (C/O) ratios of gas and ice in the disk midplane as a function of distance from the protostar. Each vertical transition marks the iceline region of the molecule noted next to the transition. Overall C/O ratio is 0.34, therefore the gas has this value close to the star where all volatile molecules are in the gas, and the ice has the value in the colder, outer disk where all volatile molecules are ices on grains. No chemical reactions are included besides freeze-out of molecules onto grain surfaces, and desorption of molecules off the surfaces of grains. *Image credit: Iris Nijman and Christian Eistrup*

Another key question in modelling especially giant planet formation is if their atmospheres are built mostly from gas accretion, or from impacting icy solids. Cridland et al. (2016, 2017) assumed only gas accretion at play for building a planet atmosphere, whereas Mordasini et al. (2016) found that by accreting gas and icy pebbles onto the giant planets, their atmospheric compositions ended up dominated by that of the pebbles, rather than that of the accreted gas. However, it is still debated to which extent, and for which impactor sizes and velocities, the solid bodies will be gravitationally scattered by the planets, rather than accreted (see e.g. Birnstiel et al. 2016; Johansen et al. 2014a; Bitsch et al. 2015). Because the answer to this question remains unclear, the evolution of the chemical composition of both the gas and ice in the midplane of a disk are of interest in the context of formation of giant planet atmospheres.

Öberg et al. (2011b) realized that the C/O ratios of gas and ice changes with disk radius due to the sequential, temperature-dependent freeze-out of the main volatiles, such as H_2O, CO_2 and CO. In Fig. 1.3 an estimate of carbon and oxygen content in the gas and ice as a function of radius can be seen, assuming the overall carbon-to-oxygen ratio (C/O ratio) to be 1/3, with abundances taken from Table 2 of Marboeuf et al. (2014). Changes to the gas and ice content of carbon and

oxygen, respectively are seen at five distinct locations, namely (from inside to out) at the icelines of H_2O, CH_3OH, CO_2, CH_4 and CO (as marked in the figure). The icelines are not sharp. This is because the temperature and density-dependent balance between freeze-out and desorption makes for a radial range of change from gas to ice (outward), rather than sharp steps. This is thus slightly different from Fig. 2 in Öberg et al. (2011b), which assumed sharp transitions from gas to ice. However, the big question remains: is it a good assumption that the planet-forming gas and ice in the disk midplane do not change chemically over time? And in case it does change, under which circumstances (temperature, density, ionisation level, and time frame) do changes occur?

In case the material does change (chemical evolution) it could have far-reaching consequences for the understanding of planet formation. First and foremost, changing chemistry for pre-Solar conditions could be compared to the current chemistry of the Solar System (e.g. planets and comets), to constrain which conditions the Solar System may have been subject to during its formation and evolution. Second, a treatment of disk midplane chemical kinetics incorporated into planet formation models may provide a more complete picture of the chemical makeup of exoplanets and their atmospheres.

1.6 Comets as fossils of planet-forming material

Planets are not the sole outcome of disk evolution: in the icy outer parts of disks, there are also left-over planetesimals made from the solid material that was not incorporated into larger bodies (see reviews by Mumma & Charnley 2011; A'Hearn 2011). These planetesimals are called comets, and consist mostly of volatile ices. Comets have been monitored and observed for decades, with comet 1P/Halley being one of the most famous comets. It is a short-period comet visible with the naked eye on the night sky every ∼75 years, and its appearance has been reported through millennia. It has a perihelion of 0.6 AU, thus inside the orbit of the Earth, making it an easy comet to study while on its close encounters with the Sun. The last encounter was in 1986, at which point the *Giotto* spacecraft came within close vicinity to it, enabling the detection of several molecular species in comet 1P's coma (Eberhardt 1999).

Besides *Giotto*, ESA's *Rosetta* mission recently accomplished landing a module (*Philae*) on comet 67P/Churyumov-Gerasimenko, as well as providing images of a comet with unprecedented detail (see Fig. 1.4). One of many interesting results from the *Rosetta* mission was the detection of abundant molecular oxygen at O_2 (moxy) at a level $\sim 4\%$ with respect to H_2O ice in the coma of 67P (Bieler et al. 2015). This was a surprising discovery, since O_2 ice is not thought to be abundant in molecular clouds. This result led to a re-analysis of data from the *Giotto* mission revealing similar levels of O_2 ice in comet 1P. O_2 ice may thus be a common ice species on comets in the Solar System.

Comets are considered relatively pristine composition-wise. Because they have likely formed from icy grains colliding and sticking, the ice composition on comets could possibly trace the icy volatile chemical history of our Solar System. Thou-

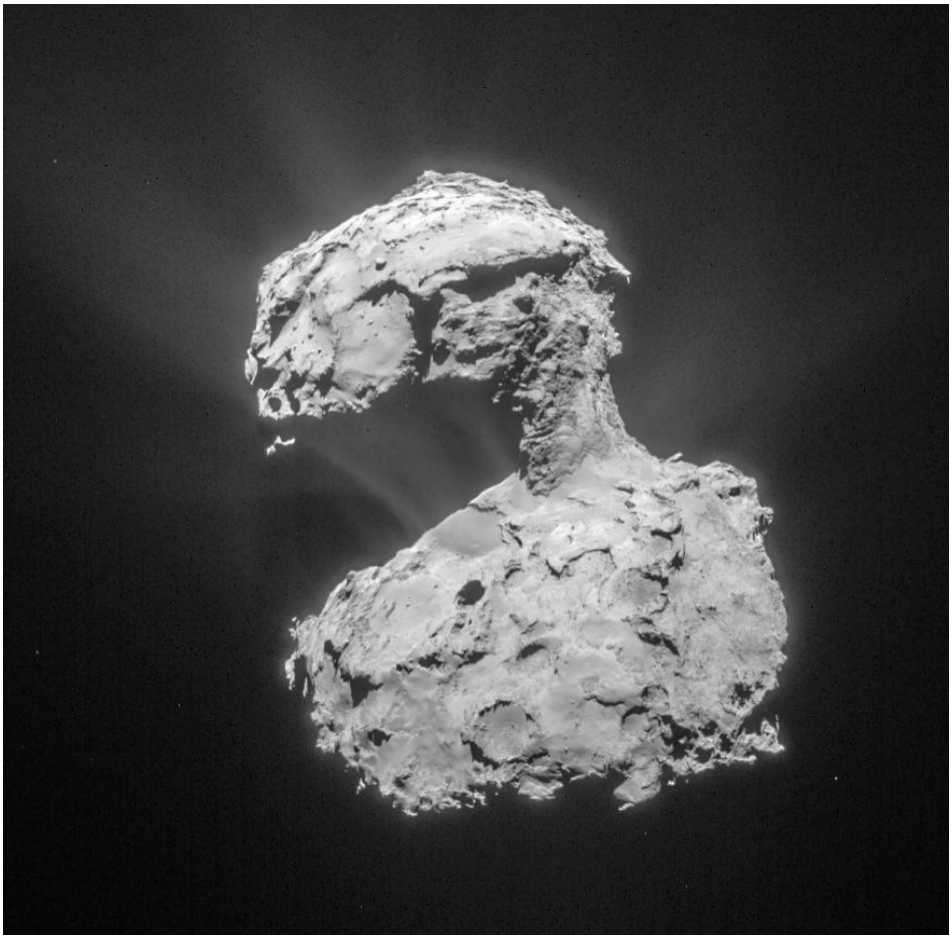

Figure 1.4: Image of comet 67P taken by the ESA *Rosetta* mission *Image credit: ESA/Rosetta/NAVCAM*

sands of comets are known nowadays, and even the detections of exocomets orbiting other stars than the Sun have been claimed (Matrà et al. 2017a,b). In the Solar System many molecular species have been detected in comets, as seen in the cometary volatile inventory compiled by Le Roy et al. (2015). More is thus known about cometary composition than about exoplanet atmospheric compositions, and because comets likely play a role in planet formation (as planetesimals forming planetary cores, and as impactors "polluting" exoplanet atmospheres), it is important to understand the chemical evolution and composition of the comets as a fossil of protoplanetary disk chemistry.

1.7 This thesis

Rapid advances have been made in recent years in fields relating to planets and planet formation. The theoretical understanding of protoplanetary disk physics and evolution has come far, likewise for planet formation. From an observational point-of-view, the dust and gas inventory of an increasing amount of diverse disks are being mapped out by ALMA (with new detections also made possible with *Spitzer* and *Herschel* space missions), and chemical compositions of disks, primarily in the upper layers, are being determined. Alongside, with the use of state-of-the-art facilities like ESO's VLT, the *Hubble* Space Telescope, and NASA's *Kepler* mission, a zoo of exoplanets of all sizes are being discovered, and pushing the current technology to the limit has revealed signs of several molecules in the atmospheres of some exoplanets (Snellen et al. 2010; Birkby et al. 2013; Kreidberg et al. 2014; Sing et al. 2016) .

A remaining challenge is understanding the chemical histories of the end-products: the planets, planetesimals and comets. What sets the molecular composition of planet atmospheres? How does the planet formation process affect the chemical make-up of the planets? While astronomers and planet formation experts have assumed the disk midplane composition to be chemically inert, thereby simplifying the incorporation of "chemistry" into their physical planet formation models, results from astrochemistry show a rich chemistry in disks, with chemical reactions under different physical conditions likely causing chemical changes to the material over time. The disk midplane, being the region of the disk relevant to planet formation, remains difficult to probe observationally, and is also too cold to be assumed to be in chemical equilibrium.

This thesis contributes a necessary step forward by simulating the composition and chemical evolution of the volatile midplane material using one of the powerful tools for understanding of interstellar chemistry that astrochemistry has to offer: chemical kinetics models. This thesis aims to test what effects chemical kinetics may have on the composition of the midplane material under the different conditions that a protoplanetary disk midplane may be subjected to. This, in turn, may lead to new insights into the chemical composition and formation histories of planets, exoplanets and comets.

Chapter 2: This chapter, employing the BADASS code, explores the effects of a static physical protoplanetary disk midplane with varied chemical conditions

and ionisation levels on the chemical evolution over an assumed timescale of 1 Myr. The initial chemical composition, either fully molecular or fully atomic, is tested for effects on the chemical composition by 1 Myr. Likewise is the ionisation level, which assumes two non-zero levels, to test the dependence of ionisation on the chemistry. Lastly, the difference between gas-phase chemistry-only (including freeze-out and desorption) and grain-surface chemistry is explored. Despite this multidimensional approach, there are general trends in the results which constrain the effects of the different assumptions.

Amongst other results, it is found that no significant chemical evolution occurs only when chemical starting conditions are saturated molecules, and the ionisation level is low. The results also reveal that, in addition to gas-phase chemistry, grain-surface chemistry has a unique impact on the chemical evolution, pointing to a need to treat ice chemistry comprehensively in chemical kinetics codes.

Chapter 3: This chapter expands on Chapter 2. A physically evolving midplane structure is assumed (rather than a static one), which is cooling and losing material over a timescale of 7 Myr, thus considering a longer disk lifetime than in Chapter 2. Different chemical starting conditions and ionisation levels are considered here as well. Special attention is given to the evolution of the elemental carbon-to-oxygen ratios in the gas and in the ice, and how these ratios change along with changing chemical composition. This chapter opens up a new paradigm of disk midplane chemistry, in that it makes time-dependent predictions on the long-term chemical composition of the material in the midplane, and these results serve as more realistic chemical inputs to planet formation models than previous "chemically inert" assumptions.

The results show that the chemical composition of protoplanetary disk midplanes is continuously evolving over a timescale of 7 Myr, resulting in the radial C/O ratio profile for gas decreasing with time, and the C/O ratio profile for ice increasing with time (away from the initial conditions seen in Fig. 1.3). It is also found that an evolving physical disk structure only affects chemical evolution by shifting icelines inwards as a consequence of decreasing temperatures. Chemical evolution between icelines is largely the same for physically static and evolving disks. In the outer icy disk, a chemical steady state is reached by 7 Myr, suggesting that a certain (temperature dependent) set of icy disk midplane abundances are reached independent of initial assumptions about chemical composition, given a proper timescale to evolve. Also, the simultaneous treatment of gas-phase, gas-grains and grain-surface chemistry leads to a depletion of CO from the gas-phase inside its thermal iceline, due to the chemical conversion of CO into less volatile forms, such as CO_2 ice, on the grain surfaces. This effect creates a "fake" CO iceline, in agreement with reported observations of the CO iceline in TW Hydrae at a higher temperature than prescribed by the CO binding energy (Zhang et al. 2017).

Chapter 4: This chapter digs into a finding in Chapter 2: O_2 ice is being chemically produced to within 1-10% of H_2O ice for a specific subset of physical and chemical conditions. Because this abundance matches with the surprising observations of O_2 ice on Comet 67P by the ESA *Rosetta* mission, the production of icy O_2 in the colder, comet-forming region of the pre-Solar nebula is investigated

in Chapter 4. The BADASS model is expanded to include the available laboratory and modelling results for O_3 ice chemistry, and two parameters controlling the efficiency of grain-surface reactions are varied to constrain under which conditions O_2 ice may have been synthesised in-situ on a grain or cometary surface in the pre-Solar nebula.

The results do show a sweet spot in the parameter space where O_2 ice, as well as the related H_2O_2 and O_3 ice all match the observed abundances in comet 67P. However, this sweet spot assumes somewhat extreme values for some reactions involving O_3, and for some grain-surface parameters, that are currently not fully supported by laboratory results. Thus, while more laboratory results on grain-surface reactions would be welcomed to improve the treatment of O_3 in chemical kinetics codes, a primordial origin (i.e. formed in the parental cloud from which our Solar System originated) remains the best explanation for the abundance of O_2 ice in comets 67P and 1P.

Chapter 5: This chapter continues in the path of understanding cometary origins by constraining their formation via chemistry. Comets exhibit a wide diversity of compositions that may be explained by disk chemistry in radius and time. In turn, the diversity in comets may help to understand the diversity in exoplanet atmospheric compositions, if these atmospheres are indeed fed by icy, solid impactors. The evolving chemical abundances over 7 Myr from Chapter 3 are compared to measured abundances of volatiles and simple organics from 15 well studied comets, in order to highlight where in this pre-Solar nebula, and when during disk evolution, the comets are most likely to have formed, given the compositional differences in the disk from Chapter 3. A χ^2 method comparing observed and modelled abundances is used to compute maximum likelihood surfaces, and estimate where and when each comet is most likely to have formed, given by the best overall match between observed and modelled molecular abundances.

The results are used to propose a taxonomy for comet families based on chemical similarity to the chemical composition of the disk midplane in which they once formed.

1.8 Main conclusions

- (Chapter 2 and 3) Disk midplane chemistry matters! Chemistry will always alter the molecular abundances and the elemental composition of gas and ice in a protoplanetary disk midplane, unless the disk inherits stable ice species from the parent cloud, and the ionisation is low.

- (Chapter 2 and 3) Ionisation, in particular from cosmic rays, is essential for chemical evolution. Ionisation initiates chemical evolution in the disk midplane, and the higher the ionisation level, the shorter the timescale for chemical evolution.

- (Chapter 2) At an early stage of chemical evolution ($\sim$0.1 Myr at high ionisation), beginning from atomic chemistry, O_2 ice is produced at an abundance

with respect to water similar to the abundances measured in the comae of comets 1P and 67P.

- (Chapter 3) Chemical evolution taking place in a disk midplane will generally act to lower the elemental carbon-to-oxygen ratio of the gas, and increase the ratio for the ice. Chemical evolution also leads to the generation of a "fake" CO iceline that lies at a higher-than-expected temperature.

- (Chapter 4) Modelling of chemical evolution of ices in the pre-Solar nebula with the inclusion of O_3 chemistry, does not show the same abundance of O_2 ice as was found in Chapter 2 (without O_3). Therefore, a primordial origin remains the most likely explanation for the detections of O_2 ice in comets 1P and 67P.

- (Chapter 5) Chemical evolution models of disk midplanes can be used to constrain the formation histories of comets in the Solar System, when compared to abundances of molecular species in the comets.

- (This thesis) Modelling chemical kinetics in protoplanetary disk midplanes is an important tool for predicting the compositions of planets, as well as for tracing the formation histories of observed planets, exoplanets, planetesimals and comets.

1.9 Future outlook

In just a few years, the James Webb Space Telescope will be launched, which will provide exciting new insights into the contents of exoplanet atmospheres and ice species on grains in protoplanetary disks as well as the molecular reservoir in the disk atmosphere within the planet-forming region. In addition, the ESO Extremely Large Telescope will be able to dig even deeper into the compositions of atmospheres of not only Hot Jupiters, but also smaller and colder exoplanets, and disks. It is thus in the near future that further observational constraints will be put on planet formation theories and exoplanet atmospheres, and it is thus timely to incorporate more comprehensive treatments of chemistry into the already highly developed planet formation models on the market today.

The next step is to incorporate an understanding of disk midplane chemical evolution into planet formation models. It is key that planet formation modellers and astrochemists get together to properly combine the physical and chemical tools that are available today. It is also key that multiple combinations of physical and chemical codes and inputs are tested, to check for general trends, but also because there likely is no size fits all. The zoo of observed exoplanets speaks its own language. The Solar System is likely not the standard outcome of planetary system architecture and design. And in order to understand planetary systems in general, a range of physical and chemical scenarios are needed to simulate it and draw insights.

The planet formation and disks community and the exoplanet community also have important upcoming discussions: what do we know about exoplanets and

their compositions, are they actually forming in rings around protostars depleted from millimeter-sized dust, and from which mechanisms, gas accretion or impacting solids, did they gain their atmospheres with a given C/O ratio?

Let chemistry meet planet formation, let chemistry meet exoplanets, and let that constitute a next important step in understanding the diversity of planets and exoplanets, and let it add a piece in the puzzling path for human kind to better understand its origins, and drive the ambition to discover life in space.

Finding extraterrestrial life is the ultimate motivation for me to learn, progress, reach dead-ends, discover, fail (it happens, and it is ok!), and ultimately achieve new insights. I am convinced that the detection of biosignatures on a rocky planet in the temperate zone around its host star will constitute a paradigm shift in human kind's understanding of itself, and its place and importance in the Universe. I think that the discovery will eventually humble human kind, and make us realise that we are not that special, but that we are fortunate enough to inhabit a small place in the vast cosmos, a pale blue dot[5], that we should care well for.

One thing that all humans on the Earth have in common is that we share occasional dark nights with beautiful bright dots spread across the tapestry above us. The universal tale that we are all together on our little Earth, here, somewhere in the cosmos, is a tale of peace, a tale of unison, a tale that should make us realise commonalities, rather than differences. It is my hope (and something I will actively contribute to) that astronomy can continue spreading a universal sense of fascination, of awe, of excitement and of peace for everyone on our planet, and that that can help human kind for generations to come in the future.

[5]Quote: Carl Sagan

2 Setting the volatile composition of (exo)planet-building material

Does chemical evolution in disk midplanes matter?

C. Eistrup, C. Walsh & E.F. van Dishoeck
Published in Astronomy and Astrophysics, 2016

Abstract - The atmospheres of extrasolar planets are thought to be built largely through accretion of pebbles and planetesimals. Such pebbles are also the building blocks of comets. The chemical composition of their volatiles are usually taken to be inherited from the ices in the collapsing cloud. However, chemistry in the protoplanetary disk midplane can modify the composition of ices and gases.

Aim: To investigate if and how chemical evolution affects the abundances and distributions of key volatile species in the midplane of a protoplanetary disk in the 0.2–30 AU range.

Methods: A disk model used in planet population synthesis models is adopted, providing temperature, density and ionisation rate at different radial distances in the disk midplane. A full chemical network including gas-phase, gas-grain interactions and grain-surface chemistry is used to evolve chemistry in time, for 1 Myr. Both molecular ("inheritance" from the parent cloud) and atomic (chemical "reset") initial conditions are investigated.

Results: Great diversity is observed in the relative abundance ratios of the main considered species: H_2O, CO, CO_2, CH_4, O_2, NH_3 and N_2. The choice of ionisation level, the choice of initial abundances, as well as the extent of chemical reaction types included are all factors that affect the chemical evolution. The only exception is the "inheritance scenario" with a low ionisation level, which results in negligible changes compared with the initial abundances, regardless of whether grain-surface chemistry is included. The grain temperature plays an important role, especially in the critical 20-28 K region where atomic H no longer sticks long enough to the surface to react, but atomic O does. Above 28 K, efficient grain-surface production of CO_2 ice is seen, as well as O_2 gas and ice under certain conditions, at the expense of H_2O and CO. H_2O ice is produced on grain surfaces only below 28 K. For high ionisation levels at intermediate disk radii, CH_4 gas is destroyed and converted into CO and CO_2 (in contrast with previous models), and similarly NH_3 gas is converted into N_2. At large radii around 30 AU, CH_4 ice is enhanced leading to a low gaseous CO abundance. As a result, the overall C/O ratios for gas and ice change significantly with radius and with model assumptions. For high ionisation levels, chemical processing becomes significant after a few times 10^5 yrs.

Conclusions: Chemistry in the disk midplane needs to be considered in the determination of the volatile composition of planetesimals. In the inner <30 AU disk, interstellar ice abundances are preserved only if the ionisation level is low, or if these species are included in larger bodies within 10^5 yrs.

2.1 Introduction

The discovery of more than 2000 extrasolar planets by the radial velocity and transiting techniques (e.g., Udry & Santos 2007; Borucki et al. 2011; Batalha et al. 2013; Fischer et al. 2014) has signaled the next phase in exoplanet research: the characterization of their atmospheres. Simple molecules such as CO, H_2O and perhaps CO_2 and CH_4 are being detected in a growing number of exoplanet atmospheres (e.g., Seager & Deming 2010; Snellen et al. 2010; Birkby et al. 2013; Fraine et al. 2014; Crossfield 2015; Sing et al. 2016). These atmospheres are thought to be built up largely by the accretion of pebbles and planetesimals in the natal protoplanetary disk (see Johansen et al. 2014b and Benz et al. 2014 for reviews), hence the atmospheres should reflect the chemical composition of the disk. There are two different views on how to treat the chemistry in the midplanes of disks, depending on the scientific focus and heritage.

Planet formation and population synthesis models (e.g., Ida & Lin 2004, 2008; Alibert et al. 2013) consider multiple physical effects taking place in a protoplanetary disk, such as gravitational interactions between bodies, orbital excitation and eccentricity damping, gas drag, accretion of material onto planets, and planet migration in the gaseous disk. Hence, there is a high degree of physical complexity and detail to planet formation processes in these simulations. However, these models do not contain any detailed chemistry. Either they simply use the observed chemical abundances in interstellar ices and assume that these abundances are preserved during disk evolution, or they assume that thermodynamic equilibrium is attained so that chemical abundances are controlled by temperature and pressure only (e.g., Mousis et al. 2010; Johnson et al. 2012; Moses et al. 2013; Marboeuf et al. 2014; Thiabaud et al. 2015b). The main observational test is through statistical comparisons with the observed populations of exoplanets and their predicted compositions.

The alternative view starts from detailed physico-chemical models of protoplanetary disks which are closely linked to, and tested by, a wide variety of astronomical observations (see reviews by Williams & Cieza 2011 and Armitage 2011). Starting from an assumed (static) surface density distribution, scale height and disk flaring, such models first determine the temperature structure of dust and gas heated by the central star through calculation of the full radiative transfer of the dust and the thermal balance of the gas (e.g., Dullemond et al. 2007; Nomura & Millar 2005; Woitke et al. 2009; Bruderer 2013). This physical model is then coupled with an extensive gas-grain chemistry network to solve the kinetic chemistry equations at each point in the disk and compute the chemical composition of the gas and ice as a function of time (e.g., Bergin et al. 2007; Furuya & Aikawa 2014; Cleeves et al. 2014d; Reboussin et al. 2015; Walsh et al. 2012, 2015). Since planets are formed in the midplanes of disks, it is particularly important to consider the composition and evolution in the midplanes. To what extent is the initial chemical composition of material that is accreted onto a protoplanetary disk preserved, and what happens to the material after it reaches the midplane of the disk, i.e., to what extent is it reset (Visser et al. 2009; Pontoppidan et al. 2014)? Does planetesimal formation happen so fast that ices are incorporated into large bodies early on in

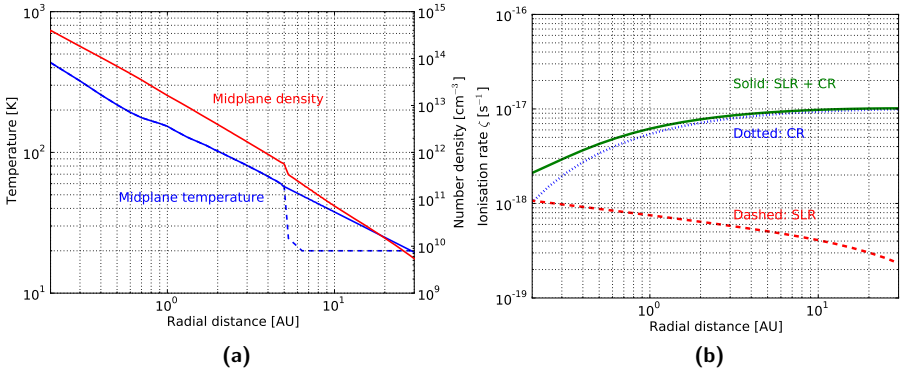

Figure 2.1: (a) The temperature $T(R)$ in K (blue) and number density $n(R)$ in cm^{-3} (red) profiles for the disk midplane. The solid blue line indicates the adjusted temperature profile (as described in the text). The original temperature profile from Alibert et al. (2013) beyond 5.2 AU is indicated by the dashed blue line. (b) The ionisation rate $\zeta(R)$ in s^{-1} adopted for the disk midplane. The red dashed line depicts the contribution to the ionisation rate from short-lived radionuclides (SLRs) only. The blue dotted line is the contribution from external cosmic rays (CRs) only. The solid green line represents the total ionisation rate (SLRs and CRs) as a function of radial distance.

the evolution, preventing further chemical processing (Zhang et al. 2015)?

Additional clues to the chemical evolution in disks come from the observations of comets in our own solar system (Mumma & Charnley 2011). Cometary records suggest that the chemical composition of the pre-solar nebula has been at least partially preserved in the comet-forming zone throughout its lifetime, pointing to little or no chemical processing. However, the original composition of the material that was present in the protoplanetary disk around the Sun when it formed remains unknown, and studies of other disks are needed to provide a framework for our own solar system. Particularly interesting are the recent results from the ESA *Rosetta* mission finding significant amounts of O_2 in comet 67P/C-G (see Bieler et al. 2015), with similarly high O_2 abundances inferred for comet Halley from a re-analysis of the *Giotto* data (Rubin et al. 2015). Abundances as high as a few % of solid O_2 with respect to solid H_2O are not yet fully understood. Lastly, the deuteration of water and organics also provides insight into the history of the pristine material from the ISM (see Ceccarelli et al. 2014).

In their planet population synthesis models, Marboeuf et al. (2014) assumed the initial chemical abundances to be inherited directly from the interstellar ices observed in dense interstellar clouds. A set of eight volatile molecules (H_2O, CO, CO_2, CH_4, H_2S, CH_3OH, N_2, and NH_3, species also considered in this work) were homogeneously distributed in their model disk midplane with relative ratios consistent with interstellar ice observations (Gibb et al. 2004; Öberg et al. 2011a; Boogert et al. 2015). Depending on the physical conditions in different parts of the midplane, as well as the sublimation temperatures of the species, these molecules could then either be assigned to the gas or ice, with the threshold set by the icelines

of the species. Icelines (or snowlines) mark the radius in the disk midplane beyond which species exist solely in ice form and are thus depleted from the gas. This occurs at the radius where the accretion rate onto grain surfaces (or freezeout) exceeds the desorption rate from grain surfaces due to the negative temperature gradient in the midplane. The relative rates of these processes are very strong functions of temperature leading to a narrow transition region from gas to ice (moving outwards in radius). The position of the midplane iceline for a particular species will depend on its volatility (i.e., its binding energy). Marboeuf et al. (2014) do not consider any chemical reactions in their models, besides freezeout and desorption.

The positions of the icelines are important because they determine which species are gas and ice at any location in the disk, and thus which material is available to build larger bodies (solids only). If, for example, a giant planet is forming in the disk, the composition of its core will reflect the ice compositions at the different positions in the disk through which the forming planet has moved. The composition of the planet's atmosphere, on the other hand, will reflect the gas composition at the position where the planet becomes massive enough to accrete an atmosphere onto its surface from the surrounding gas in the disk. Moreover, accretion of icy bodies may still pollute the atmosphere. These pebbles and planetesimals migrate through the disk due to radial drift and may therefore have originated at larger radii. Depending on the pebble and planetesimal sizes, the migration of these objects also affects the location of the icelines (see, e.g., Piso et al. 2015).

Particularly important is the C/O ratio of the solid and gaseous material in the disk (Öberg et al. 2011b). The ratio depends not only on the different volatilities of the chemical species but also on their production or destruction as a consequence of chemical processing. Since H_2O and CO_2 (which are both O rich) freeze out at higher temperatures than species that are more C rich, such as CH_4 and CO, the C/O ratio depends on both the physical structure and chemistry in the disk. Ultimately, the chemical composition of a planet's core and its atmosphere may thus differ depending on the history of the disk, the formation location of the planet, and any subsequent migration.

To address these questions, we use a physical disk model, in particular its midplane temperature and density, which is the same as that considered in the Marboeuf et al. (2014) population synthesis models. We compute the abundances of chemical species with time using a comprehensive chemical network and different sets of assumptions (see below) to investigate the degree to which chemical evolution/processing affects the resulting abundances of key volatiles in the disk midplane. The sensitivity of our results to the choice of (i) initial chemical abundances (parent cloud "inheritance" or chemical "reset"), (ii) the physical conditions (in particular ionisation level), and (iii) the types of chemical reactions included in the model, are also investigated, with details provided in Sect. 5.2. This generates eight different simulations, the results of which are presented in Sect. 5.3. Sect. 5.4 discusses the validity of the "inheritance" and "reset" scenarios, the implications for planet formation, and the extent to which the results hold for other disk models. Sect. 2.5 summarises the conclusions from this work.

Table 2.1: Initial abundances (with respect to H_{nuc}) for atomic and molecular initial abundances setups. The binding energies E_b for all species are also listed.

Species	Atomic	Molecular	E_b[K]
H	9.1×10^{-5}	5.0×10^{-5}	600
He	9.8×10^{-2}	9.8×10^{-2}	100
H_2	5.0×10^{-1}	5.0×10^{-1}	430
N	6.2×10^{-5}		800
O	5.2×10^{-4}		800
C	1.8×10^{-4}		800
S	6.0×10^{-6}		1100
H_2O		3.0×10^{-4}	5770
CO		6.0×10^{-5}	855
CO_2		6.0×10^{-5}	2990
CH_4		1.8×10^{-5}	1090
N_2		2.1×10^{-5}	790
NH_3		2.1×10^{-5}	3130
CH_3OH		4.5×10^{-5}	4930
H_2S		6.0×10^{-6}	2743
O_2		0	1000
HCN		0	3610
NO		0	1600

2.2 Methods

2.2.1 Physical disk model

The protoplanetary disk is taken from the models of Alibert et al. (2013), Marboeuf et al. (2014), and Thiabaud et al. (2015b) which provide the midplane temperature $T(R)$, pressure $p(R)$, and surface density profiles $\Sigma(R)$ with radius, R. The disk has a parameterised surface density profile[1],

$$\Sigma(R) = \Sigma_0 \cdot \left(\frac{R}{5.2\text{AU}}\right)^{-\gamma} \cdot \exp\left(\frac{-R}{a_C}\right)^{2-\gamma}, \tag{2.1}$$

where, $a_C = 20$ AU, $\gamma = 0.8$ (see the prescription in Alibert et al. 2013, Table 1), and a_C and γ are constrained by observations (Andrews et al. 2010). The surface density is $\Sigma(5.2\text{ AU}) = 16$ g cm^{-2} at $R = 5.2$ AU and the disk is truncated at $R_{\text{out}} = 30$ AU. The total mass of the disk is

$$M_{\text{disk}} = \int_{R_0}^{R_{max}} 2\pi R\Sigma(R)\, dR \; = 1.3 \times 10^{-3} M_\odot \approx 0.13\text{MMSN},$$

with $R_0 = 0.05$ AU, R_{max} defined as the radius at which the cumulative disk mass calculated from inside out reaches the total disk mass within 1%, $\Sigma(R)$ taken from Eq. 2.1, and MMSN $= 1 \times 10^{-2} M_\odot$ from Weidenschilling (1977).

The focus here is on the midplane of the disk, where the gas and dust temperatures are assumed to be coupled. Physical disk models have been developed to explain a wide variety of observations where the emission usually arises from higher up in the disk atmosphere, and where gas/grain decoupling for temperature is significant. However, since the disk vertical structure is not relevant for planet formation in the midplane, a midplane-only model is used here.

The radial grid used here consists of 119 points from $R = 0.2$ AU to $R = 30$ AU, with radial step sizes of $\Delta R = 0.1$ AU and 1 AU, inside and outside of 10 AU, respectively.

The disk model includes irradiation from a central star with a spectral type similar to the Sun. The temperature profile from Alibert et al. (2013) is slightly adjusted to remove two features: (i) a physically unrealistic drop at 5.2 AU, and (ii) an imposed lower temperature limit of 20 K in the outer disk. The profile used here follows their profile in the range 0.2 AU $\leq R <$ 5.3 AU, and uses a power-law function $T \propto R^{-0.6}$ to extrapolate 5.3 AU $\leq R \leq$ 30 AU, in agreement with full 2D radiative transfer models of protoplanetary disks (see, e.g., Bruderer et al. 2014). This adjustment is shown in Fig. 2.1a. In this work, the solid blue temperature profile in Fig. 2.1a is used throughout the disk, whereas the original Alibert et al. (2013) profile in the outer disk is given by the blue dashed profile. No adjustments are made to the pressure profile from Alibert et al. (2013).

The temperature in the model decreases from $T = 434$ K at $R = 0.2$ AU to $T = 19.5$ K at $R = 30$ AU in the outer disk. The number density over this radial

[1] From Marboeuf et al. 2014, Eq. (1)

Table 2.2: Chemical reaction types included in the two versions of the chemical network.

Reaction type	Reduced chemical network	Full chemical network
Two-body gas-phase reactions	x	x
Direct cosmic ray ionisation	x	x
Cosmic ray-induced photoreaction	x	x
Grain-cation recombination	x	x
Freezeout	x	x
Thermal desorption	x	x
Photodesorption		x
Grain-surface cosmic ray-induced photoreaction		x
Grain-surface two-body reaction		x

range spans about 5 orders of magnitude, reaching almost $n = 10^{15}$ cm^{-3} close to the star, and dropping to about $n = 10^{10}$ cm^{-3} at 30 AU.

Two different levels for the ionisation rate throughout the disk are considered, a low level and a high level. In particular, recent models have shown that cosmic rays can be excluded from disks by the combined effects of stellar winds and magnetic field structures (Cleeves et al. 2013a, 2014a). The purpose of these two levels of ionisation is to investigate the effect on chemical reactions that are driven by ionisation. Fig. 2.1b shows the ionisation level profiles used in the simulations.

The case with *low ionisation level* considers ionisation originating from the decay products of short-lived radionuclides (henceforth referred to as SLRs) only. Low ionisation is labeled as "SLR". The implementation of this ionisation source into the simulations is done using a simplified version of the prescription given in Eq. 30 in Cleeves et al. (2013b),

$$\zeta_{\rm SLR}(R) = (2.5 \cdot 10^{-19}\,{\rm s}^{-1}) \left(\frac{1}{2}\right) \left(\frac{\Sigma(R)}{\rm g\ cm^{-2}}\right)^{0.27}, \tag{2.2}$$

where $\zeta_{\rm SLR}$ is the SLR ionisation rate per H_2 molecule in s^{-1} and $\Sigma(R)$ is the surface density of a disk at a given radius R (see Eq. 2.1). The simplification ignores the original time dependence of the ionisation rate, as given in Cleeves et al. (2013b); however, including the time dependence will change the ionisation rate by no more than a factor of 2. With this low ionisation level, a higher degree of ionisation is obtained in the inner, denser disk midplane compared with the outer disk (see the red dashed curve in Fig. 2.1b). This is because the SLR ionisation rate scales with the midplane number density of SLRs, which is assumed to be homogeneous and thus scales with $\Sigma(R)$, see Eq. 2.1.

On the other hand, the case of *high ionisation level* (green solid profile in Fig. 2.1b) considers contributions from the decay products of SLRs and from cosmic rays (henceforth referred to as CRs), originating externally to the disk (high ionisation is labeled as SLR + CR). Such a high ionisation level has been used in many disk models in the midplane, (see, e.g., Semenov et al. 2004). These CRs are able to penetrate the disk to induce UV photons in the disk midplane via

$$H_2 \xrightarrow{CR} {H_2}^+ \xrightarrow{e^{-*}} {H_2}^* \longrightarrow H_2, \tag{2.3}$$

with the resulting photons generated by radiative decay of H_2^* (see Prasad & Tarafdar 1983). The CR-ionisation rate contribution, $\zeta_{\rm CR}$, is treated by assuming the following parameterised prescription:

$$\zeta_{\rm CR}(R) \approx \zeta_0 \cdot \exp\left(\frac{-\Sigma(R)}{96\ {\rm g\ cm^{-2}}}\right), \tag{2.4}$$

where $\zeta_{\rm CR}$ is the CR-ionisation rate per H_2 molecule as function of radius R, $\zeta_0 = 10^{-17}{\rm s}^{-1}$ is the assumed upper limit to the ionisation rate, and the exponential term represents an attenuation effect for high surface densities (see, e.g., Umebayashi & Nakano 2009). Hence, a higher CR-ionisation rate is reached in the outer disk midplane than in the inner disk (opposite to the case with SLRs

only), as represented by the blue dotted profile in Fig. 2.1b. Mutual neutralisation following collisions of ions with grains can lower the ionisation level, as shown by Willacy et al. (1998). This effect is taken into account in this work. Deuterium chemistry, however, is not considered here, but will be addressed in a separate paper with overlapping authors (Furuya et al. 2016).

2.2.2 Chemical model

A detailed network is used to compute the chemical evolution of all species, in which many different reactions and pathways are included. The gas-phase chemistry is from the latest release of the UMIST Database for Astrochemistry (see McElroy et al. 2013) termed RATE12. Gas-grain interactions and grain-surface chemistry are included (as described in Walsh et al. 2015, and references therein). The chemistry is solved time-dependently at each radial grid point in the disk. The chemical evolution is assumed to be isolated at these grid points with no exchange of material between the grid points during the evolution. The differences in chemistry at the different points are therefore dictated only by the differences in physical conditions $T(R)$, $n(R)$, and $\zeta(R)$. Different chemical species have different volatilities, and thus different temperatures below which the phase change from gas to ice occurs. For each species a binding energy, E_b (K), is adopted. These values are given in Table 2.1.

Two different versions of the chemical network were utilised to obtain better insight into the importance of different processes: a reduced chemical network, and a full chemical network. The types of chemical reactions considered in the network versions are outlined in Table 2.2. The reduced chemical network comprises gas-phase chemical reactions, freezeout of gas-phase species onto grain surfaces to form ices, and desorption of ice species off grain surfaces back into the gas phase. The full chemical network also contains grain-surface chemistry in addition to the reactions included in the reduced chemical network. For the reduced chemistry this means that a chemical species becomes non-reactive as soon as it freezes out onto the surface of a grain, and that freeze-out and desorption of a species depend on the accretion and thermal desorption rates only. Photodesorption is excluded from the reduced chemical network to enable direct comparison to model results of Marboeuf et al. (2014), whose only desorption mechanism is thermal desorption. For the full chemistry, on the other hand, photodesorption is included, and chemical processing can continue after freezeout. The motivation behind using a reduced and full chemical network, respectively, is to quantify the effects of gas-phase chemistry, and grain-surface chemistry, respectively.

The simulations are run with two different sets of initial abundances: atomic species or molecular species (see Table 2.1 for an overview of the initial species in each type of input). All abundances in this paper are with respect to the total number of H nuclei. The molecular abundances in Table 2.1 are values representative of interstellar ices (see Öberg et al. 2011a, Boogert et al. 2015, and Tables 1 and 2 in Marboeuf et al. 2014). For both sets of initial abundances (atomic and molecular) the elemental ratios are consistent.

The choice of these initial abundances is motivated by the following two sce-

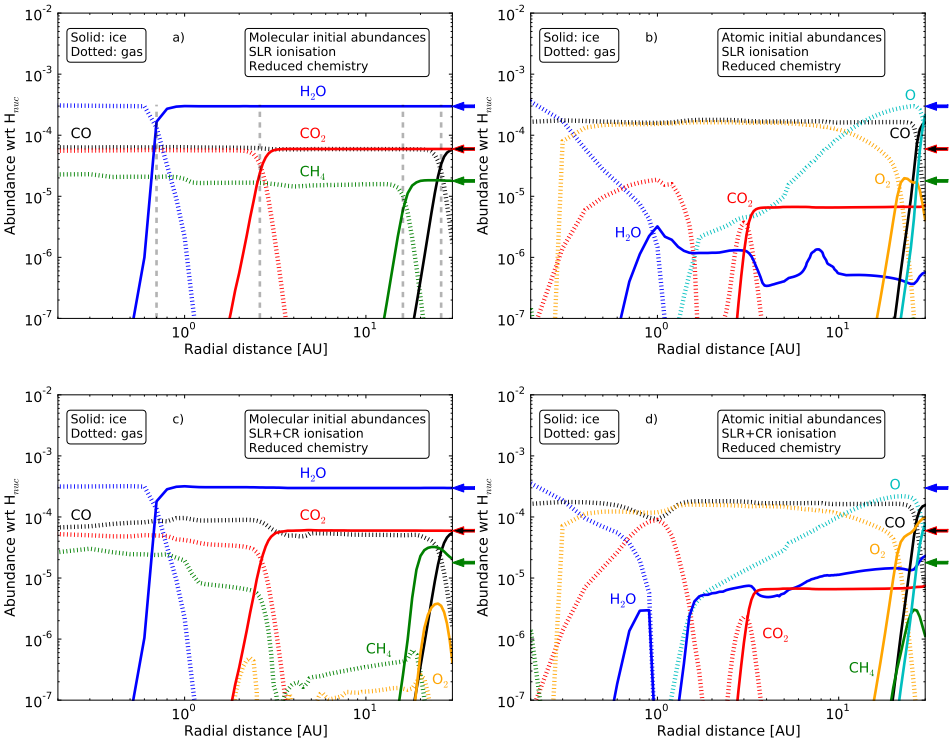

Figure 2.2: Final abundances with respect to total H nuclei density as function of radial distance R from the star for key volatile species, when using the reduced chemical network (see Table 2.2). In all panels, the solid lines show the ice abundances and the dotted curves show the gas abundances. The top two panels show the results for the low ionisation case (SLRs only) and the bottom two panels show those for the high ionisation case (SLRs and CRs). The left-hand panels show the results when assuming the "inheritance" scenario and the right-hand panels show those when assuming the "reset" scenario (see Table 1). (see Table 2.1). The arrows on the right-hand side of each plot indicate the initial abundances of H_2O, CO_2, CO, and CH_4 gases in the "inheritance" scenario. CO and CO_2 share the same arrow (red with black filling), because they have the same initial abundances. The grey, dashed, vertical lines in panel a) indicate the iceline positions of H_2O, CO_2, CH_4 and CO, respectively, from the inner to the outer disk. The positions of these icelines are the same in the other panels.

narios about the history of the midplane material. The first scenario is that the material going into protostellar systems is inherited from the cloud out of which the protoplanetary disk collapsed and formed. This scenario is denoted "inheritance", and it implies that the material has the same composition as found in dark clouds, especially their ices (see Marboeuf et al. 2014; Mumma & Charnley 2011). The second scenario is the case where the material coming from the dark cloud experiences heating events from the protostar (i.e., accretion bursts or regular stellar irradiation). These heating events are assumed to alter the chemistry in disks significantly (see, e.g., Visser et al. 2015). In the extreme case, the chemistry is "reset", meaning that the molecules are assumed to be dissociated into atoms out to $R = 30$ AU, which can then reform molecules and solids in a condensation sequence, as traditionally assumed for the inner solar nebula (e.g. Grossman 1972). Hence, the scenario considering atomic initial abundances is denoted "reset". Early chemical models of protoplanetary disks often assumed a set atomic initial abundances (e.g., Willacy et al. 1998; Aikawa et al. 1999; Semenov et al. 2004; Vasyunin et al. 2008; Walsh et al. 2010); however, these early models also did not typically include a comprehensive grain-surface network and focussed solely on the gas-phase chemistry. Early models that did include grain-surface chemistry (e.g. Willacy 2007; Walsh et al. 2010) were limited to simple atom-addition stemming from Tielens & Hagen (1982) and Hasegawa & Herbst (1993). Here, a more comprehensive grain-surface network is used which includes radical-radical recombination, atom addition, and also ice processing (Garrod et al. 2008). This work differs from earlier protoplanetary disk models in that we directly compare and quantify the effects of the "inheritance" versus "reset" scenarios for a single disk model using a comprehensive gas-grain chemical network.

Important for investigating chemical evolution is also the size of the grains in the disk midplane, which affects the rates of grain-surface chemical reactions, as well as gas-grain interactions such as freezeout. Here, spherical grains are considered. Fixed sizes of $r_{\rm grain} = 0.1\mu{\rm m} = 10^{-5}$ cm and fixed grain number density 10^{-12} with respect to H nuclei are assumed. Dust settling from the upper layers of a disk onto the disk midplane is assumed to happen on a timescale shorter than 1 Myr (Dullemond & Dominik 2004; Aikawa et al. 1999), and this settling will increase the dust density relative to that for the gas. On the other hand, dust coagulation may decrease the dust surface area compared with that of standard ISM dust (Dullemond & Dominik 2005). The consequences of assuming fixed values are briefly discussed in Sect. 5.4.

All simulations are run for $t = 1$ Myr. The lifetime of a disk before gas dispersal is found to be in the range < 1 to 10 Myr based on observations (see Williams & Cieza 2011; Fedele et al. 2011). The time evolution of the results is briefly discussed in Sects. 5.3 and 5.4.

2.3 Results

This section presents the results from the chemical evolution simulations for key volatiles which contribute significantly to the C/O ratio in the gas and ice: CO,

CO_2, H_2O, CH_4, O_2, O, HCN and NO (O_2, O, HCN and NO are presented only where relevant). Chemical evolution results for the key nitrogen bearing species N_2 and NH_3 are also presented. Fig. 2.2 presents the results for the reduced chemistry, and Fig. 2.3 those for the full chemistry. All figures show midplane abundances of chemical species with respect to H_{nuc} as a function of radial distance (in AU) from the central star. The arrows to the right of each panel indicate the initial abundance levels assumed for the "inheritance" scenario, see Table 2.1. Colour coding of arrows matches that of the plots. CO and CO_2 have the same assumed initial abundances.

In Fig. 2.2a, the icelines for each key volatile considered here have positions at 0.7, 2.6, 16 and 26 AU, with temperatures of 177, 88, 28 and 21 K for H_2O, CO_2, CH_4, and CO, respectively (see icelines marked as dashed vertical lines in Fig. 2.2a). The CO iceline is furthest out, because CO is more volatile than the other species, due to its low binding energy, see Table 2.1. The positions of the icelines of these four volatiles are indicated with arrows in the top parts of each plot presented here.

2.3.1 Reduced chemical network

Figs. 2.2a and 2.2c show the final abundances for the key volatiles when assuming molecular initial abundances, for the low ionisation and high ionisation case, respectively. This is the "inheritance" scenario. Fig. 2.2a, assuming a low ionisation level, shows negligible changes in the ice abundances of each species (i.e., the initial molecular cloud abundances are preserved), and only minor changes to the gas-phase abundances within each iceline (<10% for CO and <30% for CH_4).

For the higher ionisation rate (see Fig. 2.2c), the picture looks slightly different. Larger changes in gas-phase abundances are seen here for all the species inside their respective icelines: up to 43% for CO_2, up to 62% for CO, and several orders of magnitude for CH_4. However, the H_2O, CO_2, and CO ice abundances outside their respective icelines are preserved with their initial assumed abundances. This is due to the almost instantaneous freezeout onto grains of these species under the cold and dense physical conditions found in the outer disk, in conjunction with the assumed chemical non-reactivity of these species upon freezeout in the reduced form of the chemical network.

The largest difference in the gas-phase abundances in Fig. 2.2c when compared with those in Fig. 2.2a is the destruction of CH_4 gas between $1 < R < 15$ AU, as well as the production of CH_4 ice, reaching a peak abundance higher than the initial abundance level between 20 and 25 AU, and also the production of O_2 ice from 20 to 30 AU. The differences in the outer disk can be ascribed to the increasing ionisation level here, as seen in Fig. 2.1b. The higher ionisation rate creates a destruction pathway for abundant gas-phase species, such as CO, which releases a small proportion of free C and O into the gas-phase for incorporation into other C- and O-bearing molecules, such as CH_4 (via the initiating ionisation-dependent reaction between CO and He^+, see Aikawa & Herbst 1999) and O_2, via gas-phase reactions (also discussed in Walsh et al. 2015). Beyond their respective icelines, CH_4 and O_2 freeze out onto grain surfaces almost instantaneously whereby

they become depleted from the gas and are thus protected from further chemical modification. The gas-phase abundances of both species are not preserved within their respective icelines (16 AU for CH_4 and 21 AU for O_2) because these species are also destroyed in the gas-phase by CR-induced photons (see reaction sequence 2.3).

Figs. 2.2b and 2.2d show the results for the low and high ionisation cases (top and bottom panels, respectively) using atomic initial abundances. In this "reset" scenario, it is assumed that the gas has undergone an extreme heating event which has fully erased the prestellar composition (see Sect. 3.2.3). For both ionisation levels, H_2O and CO are the dominant gas-phase species in the very innermost region of the disk midplane, $R < 0.3$ AU. For $R \geq 0.3$ AU, gas-phase CO and O_2 are efficiently produced and reach similar abundance levels ($\sim 1.6 \times 10^{-4}$ for O_2 and $\sim 1.8 \times 10^{-4}$ for CO) out to their respective icelines at 21 AU for O_2 and 26 AU for CO. Gas-phase O_2 is much more abundant (by at least 2 orders of magnitude) in this "reset" scenario than in the "inheritance" scenario. In the "reset" scenario O_2 is formed is the gas-phase via $O + OH \longrightarrow O_2 + H$ (see Walsh et al. 2015), and remains in the gas-phase because it is very volatile (binding energy of $E_b = 1000$ K), and only freezes out at 24 K, see Table 2.1. Outside the CO iceline, the CO ice abundance reaches the same level as that for the gas inside the iceline. This CO abundance is about half the H_2O initial abundance in the "inheritance" scenario. The remainder of the available oxygen (63%) in the outer disk remains in atomic form. These are oxygen atoms that have not had sufficient time to form molecules before freezeout. 30 AU is just around the atom oxygen iceline (which is at 29 AU), so both O gas and ice account for the total O abundance of 3.3×10^{-4}, making atomic oxygen the most abundant O carrier here, almost twice as abundant as CO ice. This result is particular to the reduced chemistry case because all species are rendered chemically inert upon freezeout; in reality, atomic oxygen on and within ice mantles is highly reactive (see, e.g., Linnartz et al. 2015).

Between $R = 0.2$ and 1.6 AU, gas-phase CO_2 is produced for both ionisation levels. The abundance reaches 9.0×10^{-5} for the high ionisation case at $R = 1$ AU (Fig. 2.2d), which is about 5 times higher than the abundance peak for low ionisation at $R = 1$ AU (see Fig. 2.2b). For both low and high ionisation rates, CO_2 ice reaches an abundance of only about 10% of the value assumed in the "inheritance" scenario outside the CO_2 iceline. In addition, H_2O ice is not efficiently produced in the outer disk in this "reset" scenario. The "reset" scenario H_2O abundance levels resemble abundance levels of H_2O naturally produced in the gas phase of $10^{-7} - 10^{-6}$ (see Hollenbach et al. 2009). The abundance of H_2O ice is about an order of magnitude larger in the high ionisation case, showing that ion-molecule reactions in the gas-phase are contributing to the formation of water in the absence of grain-surface chemistry. However, the peak H_2O ice abundance of 2.3×10^{-5} (reached at 30 AU in Fig. 2.2d) remains more than an order of magnitude lower than the initial H_2O abundance assumed in the "inheritance" scenario. The high ionisation level in Fig. 2.2d also aids the formation of CH_4 ice beyond its iceline, reaching a peak abundances of 3.0×10^{-6}. However, as also found for H_2O and CO_2 ice, the maximum abundance reached for CH_4 is only 17% of the assumed initial abundance for the "inheritance" scenario.

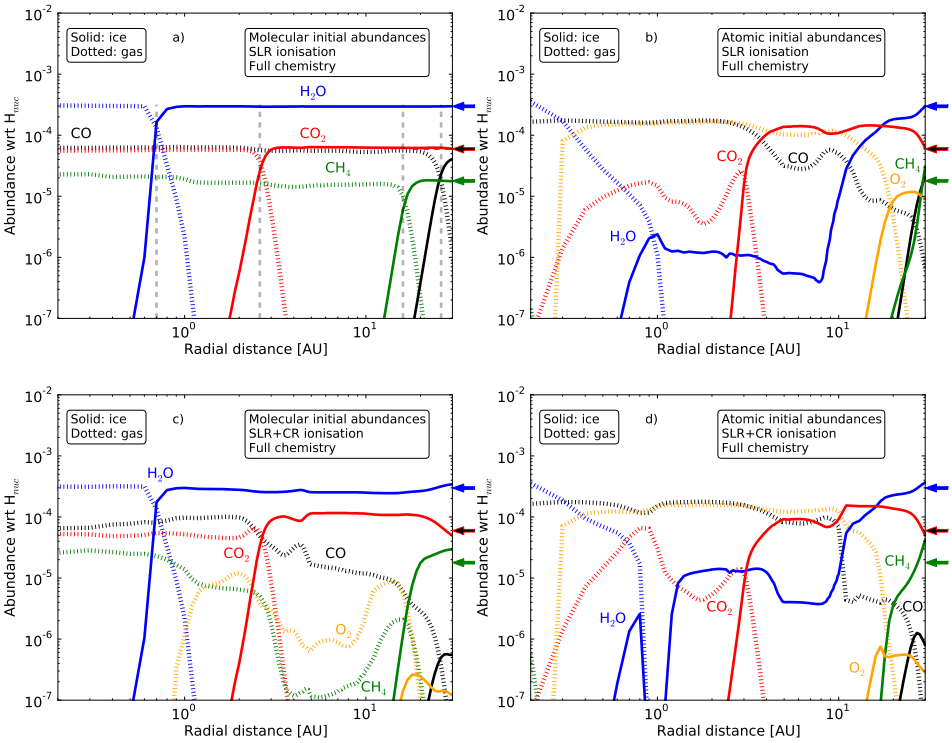

Figure 2.3: Final abundances with respect to total H nuclei density as function of radial distance from the star R for key volatile species, when using the full chemical network (see Table 2.2). In all panels, the solid lines show the ice abundances and the dotted curves show the gas abundances. The top two panels show the results for the low ionisation case (SLRs only) and the bottom two panels show those for the high ionisation case (SLRs and CRs). The left-hand panels show the results when assuming the "inheritance" scenario and the right-hand panels show those when assuming the "reset" scenario (see Table 1). (see Table 2.1). The arrows on the right-hand side of each plot indicate the initial abundances of H_2O, CO_2, CO, and CH_4 gases in the "inheritance" scenario. CO and CO_2 share the same arrow (red with black filling), because they have the same initial abundances. The grey, dashed, vertical lines in panel a) indicate the iceline positions of H_2O, CO_2, CH_4 and CO, respectively, from the inner to the outer disk. The positions of these icelines are the same in the other panels.

2.3.2 Full chemical network

Fig. 2.3a shows the chemical evolution results when assuming the "inheritance" scenario and a low ionisation rate (SLRs only) for the full chemical network. The abundance behaviour in this figure is practically indistinguishable from that for the case using the reduced chemical network (see Fig. 2.2a), that is, the initial assumed abundances are preserved in both the gas and the ice. For the higher ionisation rate case (SLRs and CRs, Fig. 2.3c) the picture is different. Chemical processing by cosmic-ray-induced reactions in both gas and ice occurs, and is most noticeable within the icelines of each species. A large reduction in the gas-phase CO abundance beyond 2 AU is seen, in contrast with the reduced chemistry results. This decrease in CO gas (and ice beyond the iceline) coincides with an overall enhancement in CO_2 ice in the outer disk. CO molecules accreting onto the grain surfaces can react with OH radicals produced in the ice via photodissociation of H_2O ice by CR-induced photons in the full chemistry. This produces CO_2 ice in-situ on the grain surfaces via the reaction

$$\mathrm{CO_{surf}} + \mathrm{OH_{surf}} \longrightarrow \mathrm{CO_{2,surf}} + \mathrm{H_{surf}}, \tag{2.5}$$

which is responsible for the rise in the CO_2 ice abundance between 3 and 15 AU (doubling the initially assumed CO_2 abundance). Within this radial region the dust temperature is between 27 K and 78 K, and because H atoms are very volatile ($E_\mathrm{b} = 600$ K) they can rapidly thermally desorb from the grain surface, impeding further grain-surface reactions involving atomic H. In the outermost disk between 20 and 30 AU, the temperature drops to $T \approx 19.5$ K, enabling the more efficient retention of H atoms arriving from the gas or produced in-situ within the grain mantles, and thereby increasing the relative rate of H_2O ice production via the reaction,

$$\mathrm{OH_{surf}} + \mathrm{H_{surf}} \underset{\gamma_\mathrm{CR}}{\rightleftharpoons} \mathrm{H_2O_{surf}}. \tag{2.6}$$

This reaction is more efficient than Reaction (2.5) under these colder conditions. Although balanced by destruction due to photodissociation, the abundance of H_2O ice is increased at the expense of CO_2 ice beyond 20 AU.

CH_4 gas is destroyed between 1 and 16 AU in the full chemistry, similar to the case for the reduced chemistry (see Fig. 2.2c). The reactions responsible for this destruction of CH_4 at 10 AU, are

$$\mathrm{CH_4} \xrightarrow{\gamma_\mathrm{CR}} \mathrm{CH_2} \xrightarrow{\mathrm{H}} \mathrm{CH_3} \xrightarrow{\mathrm{O}} \mathrm{H_2CO}, \tag{2.7}$$

$$\mathrm{CH_2} \xrightarrow{\mathrm{NO}} \mathrm{HCNO} \xrightarrow{\mathrm{O}} \mathrm{CO} \xrightarrow{\mathrm{OH}} \mathrm{CO_2}, \tag{2.8}$$

where γ_CR indicates photodissociation by cosmic-ray induced photons. The carbon is thus converted from CH_4 into CO_2 and H_2CO, but the conversions require CRs (i.e. high ionisation). However, H_2CO does not reach an abundance of more than 10^{-12}, so CO_2 is the main reservoir for the carbon converted from the CH_4 gas, see Fig. 2.4. Some carbon from CH_4 is also converted into unsaturated hydrocarbons in the gas phase (as also seen in Aikawa et al. 1999), eventually forming gas-phase C_2H_4. This is the reservoir for the converted carbon in the reduced

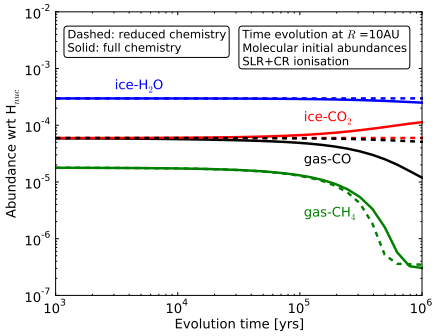

Figure 2.4: Abundance evolution with time for CO gas, CO_2 ice, H_2O ice and CH_4 gas. Dashed curves are for the reduced chemistry, solid curves are for the full chemistry. Additional time-dependent plots are supplied in Appendix 2.A

chemistry, because CO_2 ice requires gran-surface chemistry to form, and hence CO_2 ice does not increase in abundance in the reduced chemistry case. For the full chemistry, however, this C_2H_4 subsequently freezes out onto grain surfaces, undergoes hydrogenation, and forms C_2H_6 which reaches a final abundance of 8.6×10^{-6}, approximately an order of magnitude lower than that of CO_2 (1.2×10^{-4}).

The reaction $CO + He^+$ reported by Aikawa et al. (1999), turning carbon from CO into CH_4 and other hydrocarbons, is found here to be a relatively minor channel as compared to the reactions between CH_4 and He^+, and ${H_3}^+$, respectively, turning CH_4 into CO. The result of this is an efficient conversion of carbon from CH_4 into CO. Outside the CO_2 iceline, this conversion is enhanced. This enhancement is due to the accretion of CO onto grain surfaces, and subsequent rapid reaction of CO with OH to form CO_2, a reaction not included in the models of Aikawa et al. (1999).

The destruction of CO gas due to the conversion into CO_2 has been suggested by e.g. Nomura et al. (2016) to explain the depletion of CO gas inside the CO iceline of the protoplanetary disk TW Hya. Kama et al. (2016a) reported overall carbon depletion in the disk atmospheres of some protoplanetary disks using results from a single-dish survey of CO ($J = 6 - 5$) and [CI]($^3P_1 - ^3 P_0$) line emission with APEX. Schwarz et al. (2016) reported CO depletion in TW Hya from CO isotopologue emission observations with ALMA. Detailed modelling confirmed that carbon is likely depleted in the disk around TW Hya by a factor of ≈ 100 (Kama et al. 2016b, see also Du et al. 2015). This is in good agreement with the CO gas abundance just inside the CO iceline in Fig. 2.3c, and the results presented here therefore provide a possible explanation for the presence of this inner-disk CO depletion, found inside of, but somewhat mimicking, the actual CO iceline in TW Hya.

At a temperature of 37.7 K (at $R = 10$ AU), CO_2 freezes out immediately after production. The abundance increase in CO_2 ice follows the destruction of CH_4 gas, as seen in Fig. 2.4 which presents the time evolution. It is interesting

that this effect is seen under these specific physical conditions, with temperatures ranging from 40 to 150 K. This indicates that the CH_4 destruction happens at radii between the H_2O and CH_4 icelines, where H_2O is not chemically active in gas-phase reactions. More generally, for the high ionisation level, the chemical processing becomes significant after a few times 10^5 yrs. That is shown in Appendix 2.A, where jumps in abundance levels are presented for our four key volatiles between 100 kyr and 500 kyr.

When considering initial atomic abundances (Figs. 2.3b and 2.3d) a similar radial behaviour (although not identical) is seen when comparing the results for reduced and full chemistry. Inside the icelines, mainly gas-phase H_2O, O_2 and CO are produced, reaching peak abundances of 3.6×10^{-4}, 1.6×10^{-4}, and 1.8×10^{-4}, respectively. Not as much gas-phase CO_2 is produced within the iceline. Comparing the results for low and high ionisation, the peak abundances of gaseous CO_2 are 2.5×10^{-5} and 6.6×10^{-5}, respectively, and a negligible amount of gas-phase CH_4 is formed. For the high ionisation rate, Fig. 2.3d, a larger amount of H_2O ice (an order of magnitude at 2 AU) is produced between 1 and 10 AU, than with a low ionisation rate (Fig. 2.3b), as is also seen in the model using the reduced chemical network. For H_2O ice, a dip in the abundance is seen around 7 AU in Fig. 2.3d. This is an effect of the competing productions of H_2O ice and SO_2 ice. At 4 AU, SO_2 ice is produced more slowly than H_2O ice, and reaches a final abundance of 2.7×10^{-6}. At 7 AU, however, the lower temperature favours a more efficient and fast production of SO_2 ice, which is able to lock up atomic O, thereby impeding the simultaneous production of H_2O ice.

Can these models produce abundant O_2 in gas or ice? Significant gaseous O_2 is formed in the inner disk starting from atomic abundances, as discussed above. Using the low ionisation rate (see Fig. 2.3b), O_2 ice reaches an appreciable abundance of 1–10% that of H_2O ice between 15 and 30 AU, similar to that seen in the results using the reduced chemical network. However, little O_2 ice is found when using the higher ionisation rate, indicating that O_2 ice is susceptible to chemical processing by CR-induced photons. In Fig. 2.3c using molecular initial abundances, O_2 gas is also produced from 1 AU out to 15 AU but in smaller amounts than starting from atomic initial abundances. It reaches a peak abundance of a few percent of that of H_2O ice at 2 AU.

2.3.3 Main nitrogen reservoirs

Figs. 2.5 shows the final abundances for N_2, NH_3, HCN and NO (HCN and NO only where relevant) for the full chemistry. Results for both low and high ionisation levels, and both gas and ice species, are plotted in each figure. Fig. 2.5a are the results when assuming molecular initial abundances (i.e. the "inheritance" scenario), whereas Fig. 2.5b are those assuming atomic initial abundances (i.e. the "reset" scenario). For the "inheritance"-scenario with low ionisation, the initial abundances are largely preserved, as for the C- and O-bearing species, and the icelines are of NH_3 and N_2 are nicely outlined at 2.5 and 30 AU, at temperatures of 90 and 20 K, respectively. These icelines are marked with dashed vertical lines in Figs. 2.5a. However, for high ionisation there is a destruction of NH_3

and production of N_2 at ≈ 1.5 AU. The reaction pathways responsible for these features are as follows:

$$NH_3 \xrightarrow{XH^+} NH_4{}^+ \xrightarrow{e^-} NH_2 \xrightarrow{NO} N_2 \tag{2.9}$$

$$NH_3 \xrightarrow{OH} NH_2 \xrightarrow{NO} N_2 \tag{2.10}$$

$$NH_3 \xrightarrow{\gamma_{CR}} NH_2 \xrightarrow{NO} N_2 \tag{2.11}$$

NH_3 is converted into N_2 both through ion-molecule reactions (reaction sequence 2.9), as well as through CR-induced photoreactions (reaction sequences 2.10 and 2.11). The timescale of this conversion is a few times 10^5 yrs, as was found for the cases of H_2O, CO, CO_2 and CH_4 and discussed earlier in Section 2.3.2.

When considering atomic initial abundances in Fig. 2.5b, atomic N is seen to form N_2 gas quickly (as also shown and discussed in Schwarz & Bergin 2014), which is the dominant bearer inside 10 AU. This holds regardless of the assumed ionisation level. In the outer disk, HCN ice is the main reservoir, being 5-10 times more abundant than NH_3 ice outside 10 AU. For low ionisation around 1 AU, NO and HCN are the second and third most abundant N-bearing species, although more than an order of magnitude less abundant than N_2. In the outer disk, NH_3, N_2, and NO all reach ice abundances factors of a few to ten times less than the HCN ice abundance. HCN is produced on very short timescales (< 1 yr) in the gas-phase via the following reaction sequence,

$$C \xrightarrow{H_2} CH_2 \xrightarrow{H_2} CH_3 \xrightarrow{O} HCO \xrightarrow{N} HCN, \tag{2.12}$$

with subsequent freeze-out of HCN onto grains. NO is produced mainly via the well-known gas-phase reaction between N and OH, whereas NH_3 ice is formed in situ on the grain surfaces via hydrogenation of atomic N (see also Walsh et al. 2015). Even with grain-surface chemistry included, when beginning with atomic initial abundances, NH_3 ice formation is less efficient than that for those species more reliant on gas-phase formation followed by freezeout.

2.4 Discussion

2.4.1 Compositional diversity at different radii: inheritance vs reset

The third column of Table 2.3 shows the final abundances for the full chemical model with low ionisation level and molecular initial abundances at three different radii throughout the disk midplane (see Fig. 2.3a). This is the model for which the results show best preservation of the initial abundances (listed in Table 2.1 for the "inheritance" case). The remaining columns show the fractional abundances of each species at each radial distance for all other models using full chemistry relative to this reference model. The fractional abundances have been calculated

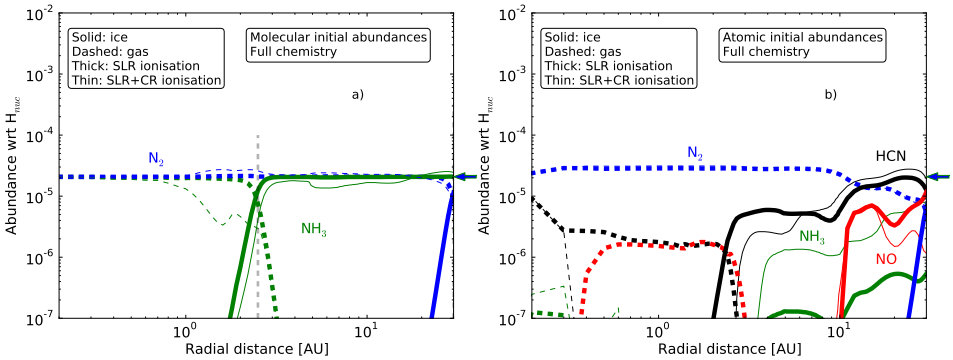

Figure 2.5: Final abundances for the major nitrogen species obtained with the full chemical network. Solid curves show ice abundances, dashed curves show gas abundances. Thin curves are for low ionisation level, and thick curves are for high ionisation level. The physical conditions and initial abundances in Fig. 2.5a are identical to those considered in Fig. 2.3a and c. Likewise, for Fig. 2.5b the assumptions are identical to those in Fig. 2.3b and d. The arrow on the right-hand side of each plot indicate the initial abundances of N_2 and NH_3. They have the same initial abundances and hence share arrow. The grey, dashed, vertical line in panel a) indicates the iceline position of NH_3. The position of the iceline is the same in panel b). The iceline of N_2 is at 30 AU, and therefore not seen.

using the formula given in the footnote of Table 2.3. Fractional abundance values smaller than 1 means abundances lowered relative to the reference model whereas values larger than 1 means increased abundances. Values of 0 indicate abundances more than two orders of magnitude lower than for the reference model, so as to avoid large numbers in the table. A value of 1 means no change from the reference model. Three different radii are considered which span the radius of the disk and probe three distinct regions: (i) H_2O-ice rich only (1 AU), (ii) H_2O-ice rich and CO_2-ice rich (10 AU), and (iii) volatile-gas poor (30 AU, i.e., gas fully depleted of volatiles via freezeout).

At $R = 1$ AU, CO gas is enhanced in all three models by factors of 1.5 to 2.5, with a greater enhancement seen in the atomic case. This is generally at the expense of all other considered species: H_2O ice and gas, CH_4 gas, and CO_2 gas. Both CH_4 gas and H_2O ice show extreme depletion for the atomic cases, for the reasons discussed in Sect. 5.3.

Moving to 10 AU, i.e., beyond the CO_2 iceline, a different behaviour is seen. CO_2 ice is enhanced by factors of 1.5 to 1.8 in the other three models, this time generally at the expense of CO and CH_4 gas and H_2O ice. The extreme depletion of water ice in the atomic cases also extends into this region. However, an enhancement of a factor 1.3 is seen in CO gas for the atomic case and high ionisation, showing that the higher ionisation rate can also facilitate gas-phase formation as well increased ice processing.

Moving outwards to 30 AU, where most volatiles have accreted onto grain surfaces, different behaviour is seen yet again. This time CH_4 ice is enhanced by a factor of 1.7 to 2.4 at the expense of CO gas and ice (with the latter depleted by almost an order of magnitude) for the high ionisation cases. H_2O and CO_2 ice are

Table 2.3: Fractional differences in key volatiles between different simulations using full chemistry at $R = 1$, 10, and 30 AU with respect to the reference model (the abundances for which are given in the column labelled "Mol. low ion.")

Radial distance	Species	Abundance	Fractional deviation[1]		
		(Reference model)			
		Mol. low ion.	Mol. high ion.	Atom. low ion.	Atom. high ion.
$R = 1$ AU	*Gas*				
	H_2O	2.2×10^{-6}	1.03	0.5	0
	CO	6.4×10^{-5}	1.52	2.5	2.4
	CO_2	5.8×10^{-5}	0.9	0.26	0.53
	CH_4	1.9×10^{-5}	0.74	0	0
	Ice				
	H_2O	3.0×10^{-4}	1	0	0
$R = 10$ AU	*Gas*				
	CO	5.3×10^{-5}	0.23	0.95	1.31
	CH_4	1.6×10^{-5}	0.02	0	0
	Ice				
	H_2O	3.0×10^{-4}	0.83	0.04	0.04
	CO_2	6.3×10^{-5}	1.79	1.73	1.46
$R = 30$ AU	*Gas*				
	CO	1.2×10^{-6}	0.01	0.53	0.02
	Ice				
	H_2O	3.0×10^{-4}	1.14	1	1.22
	CO	4.1×10^{-5}	0.01	0.5	0.02
	CO_2	6.0×10^{-5}	0.83	1.04	0.84
	CH_4	1.8×10^{-5}	1.67	1.71	2.36

[1] Formula for calculating fractional deviations: deviation=abundance(comparison model)/abundance(reference model). The reference model, "Mol. low ion.", is that for which the initial abundances are mainly preserved throughout the midplane. In all subsequent column labels, "Mol" and "Atom" refer to molecular and atomic initial abundances, and "low" and "high" refer to a low assumed ionisation rate (SLRs only) and a high ionisation rate (SLRs and CRs), respectively
.

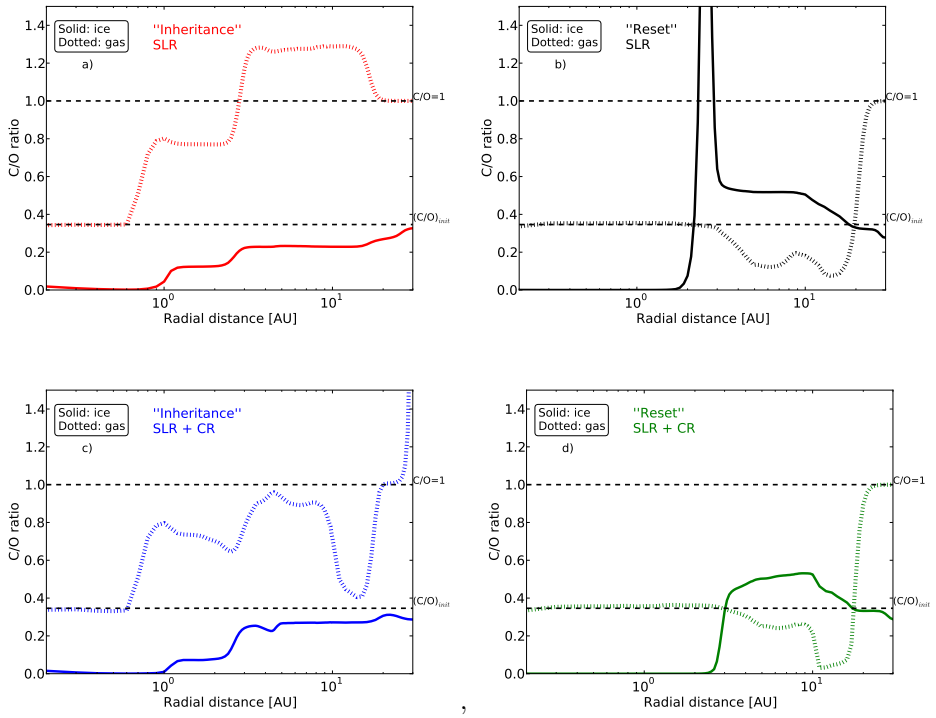

Figure 2.6: C/O ratios in the gas (dashed lines) and ice (solid lines) for the 4 full chemistry model setups as described in the text.

enhanced and depleted by up to 22% and 17% respectively, with high ionisation only. Little change is seen for low ionisation, despite beginning the calculation with atomic abundances. For this scenario, it appears that in the outer disk (30 AU), the resulting abundances of CO_2 and H_2O ice reproduce the inherited values to within a few percent.

Finally, it is important to recognize that at all radii and in all scenarios, including the full "reset" case, the chemistry is not in thermodynamic equilibrium, i.e., the abundances are not simply set by the overall elemental abundances and pressure (see also the discussion in Henning & Semenov 2013).

2.4.2 C/O ratio

The results in Table 2.3 show that for different sets of assumptions or models setups, a large diversity is seen in the resulting computed abundances of dominant C- and O-bearing volatiles. The deviations are also radially dependent, and align with the positions of icelines. The percentage deviations are sufficiently large to affect the C/O ratio in the gas and ice which will go into forming the building

blocks of planets.

Fig. 2.6 shows the C/O ratios for gas (dashed) and ice (solid) species in the four different model setups using the full chemistry. In the calculation of the ratio, all dominant C- and O-bearing species were taken into account. In addition to the main considered volatiles (CO, H_2O, CO_2 and CH_4), these also include CH_3OH, O_2, HCN, NO, and atomic O where appropriate. The horizontal lines indicate the canonical C/O ratio (at 0.43) and C/O = 1.

For the "inheritance" scenario and low ionisation (Fig. 2.6a), the C/O ratio for the gas resembles a step function. Moving outwards in radius, the steps coincide with the icelines of H_2O, CO_2, and CH_4, respectively. This profile is very similar to that in Fig. 4 in Öberg et al. (2011b) in which the C/O ratios in the gas and ice were assumed to be dictated solely by the positions of icelines. Only for the case of "inheritance" and low ionisation level is there a region in the disk, between 3 and 16 AU, in which the gas is carbon rich, i.e., C/O > 1. The ice ratio for the same model shows that overall the ice remains carbon poor (or oxygen rich), but does become relatively more carbon rich moving outwards in the disk as the icelines for CO_2 and CH_4 are surpassed.

Considering the "inheritance" scenario with the high ionisation level (Fig. 2.6c), the chemical processing induced by CRs has a noticeable affect on the C/O ratio in the gas and ice. The C/O gas-phase ratio remains less than 1 everywhere due to the destruction of CH_4 gas and the production of O_2 gas. The gas-phase C/O ratio appears to increase significantly beyond 26 AU; however, this is beyond the CO iceline where most molecules (except H_2) are depleted from the gas. The C/O ice ratio looks similar to that for the case of low ionisation. The ratio is a bit higher for the low ionisation case within 3 AU (73% at 1.6 AU), and slightly lower beyond 3 AU (15% at 10 AU) reflecting the repartitioning of atomic carbon and oxygen from H_2O ice into CO_2, CO, and O_2 (see Fig. 2.3).

Turning attention to the "reset" scenarios in Figs. 2.6b and 2.6d, the picture changes significantly. Between 3 and 16 AU the C/O ratio in the ice is higher than that in the gas (although both ice and gas remain carbon poor). This is opposite to both "inheritance" cases; the dominant carriers of gas-phase C and O in these models in this region are CO and O_2, and the dominant ice component is CO_2 ice as opposed to H_2O ice. Thus the C/O ice ratios tends towards ≈ 0.5 whereas in the gas it tends towards ≈ 0.3.

The peak at ≈ 2.5 AU for the profile in Fig. 2.6d is due to HCN ice being produced and freezing out at a slightly higher temperature than CO_2. This causes an increase in the C/O ice ratio in this local region (see Fig. 2.5b). It is only seen in the low ionisation case because N-bearing species formed via gas-phase chemistry in the inner disk (< 3 AU) are able to survive to 10^6 yrs. The presence or otherwise of this large peak is dependent upon the relative binding energies of HCN and CO_2 assumed in the model; recent measurements of thermal desorption of pure HCN ice do derive a higher binding energy than both CO_2 and NH_3 (e.g., Noble et al. 2013), but in a mixed ice they may be more similar.

The C/O ratio plots in Fig. 2.6 highlight that the different model setups considered here (especially the "inheritance" versus "reset" scenarios) result in very different C/O ratio profiles for the material in the planet-forming regions of the

disk midplane.

2.4.3 Implications for planet formation and comets

2.4.3.1 Giant planet atmospheres

Giant planets can accrete their atmospheres either directly from the surrounding gas or through accretion of icy planetesimals, or both. In addition, radial migration of a forming planet can influence the makeup of the resulting atmosphere as the planet moves through a gradient in gas and icy planetesimal composition. Fig. 2.6a suggests that if only accretion from the gas is considered, a gas-giant planet forming between 3 and 16 AU may be able to form a carbon-rich atmosphere in the case of "inheritance" with low ionisation rates. For high ionisation rates, the atmosphere would still be relatively carbon rich with respect to the canonical ratio (horizontal dashed lines at C/O ratio 0.34 in Figs. 2.6), yet with a ratio which remains < 1. In both cases, the atmosphere can be polluted by accreting icy planetesimals which are oxygen rich, lowering C/O in the planet's atmosphere.

For the "reset" scenario, a gas-giant planet forming between 3 and 16 AU would accrete C-poor gas; however, if the volatile component accreted by the planet were dominated by icy planetesimals, the resulting atmosphere may become carbon rich relative to the canonical value.

The low abundance of ice (relative to the gas) inside the CO_2 iceline for the "reset" scenario is also interesting from the perspective of the overall core-envelope partitioning. If the core of the planet was to form from the solid material available at 1 AU in Fig. 2.3d, then the bulk of the planet would not be built up of volatile ices, but rather of more refractory components (rocks). The composition of the forming atmosphere will then be set solely by the composition of gas accreted onto the forming planet.

The CO_2-rich ice mantles formed beyond 16 AU in the "reset" scenario also have an interesting implication for the first stage of planet formation, the formation of pebble-sized objects. The sticking efficiency of 100μm-sized CO_2 ice particles was recently determined to be an order of magnitude lower than that for similarly sized H_2O ice particles (Musiolik et al. 2016). Hence, under these particular conditions, the first steps of planet formation may be impeded.

2.4.3.2 Cometary composition

With molecular initial abundances (i.e., "inheritance"), the composition is generally preserved (with a few already mentioned exceptions, see Sect. 5.3). Hence, planetesimals forming under these specific conditions will be composed of "inherited" material. The overlap in the composition of comets, considered pristine remnants of the solar nebula, and interstellar ices certainly supports the hypothesis that a significant fraction of disk midplane material may be inherited from the molecular cloud (see, e.g., Mumma & Charnley 2011; Öberg et al. 2011a). For the "reset" case, cometary and interstellar abundances would be significantly different, at least for comets formed inside 30 AU.

It is interesting to consider whether a protoplanetary disk midplane, which inherits only water ice, is able to synthesis O_2 at a level similar to that seen in comets because this could be an observational constraint on the "inheritance" scenario. Our models can produce significant amounts of O_2 gas in the inner disk, as was also seen and discussed in full 2D protoplanetary disk models of Walsh et al. (2015). Bieler et al. (2015) find an O_2-to-H_2O ice ratio of $\approx 4\%$ in comet 67P/C-G, with O_2 closely associated with the H_2O ice. They concluded O_2 was likely primordial in origin, i.e., originating from the parent molecular cloud and/or protostellar envelope. This result is surprising due to the high reactivity of O_2 ice. The confirmation of O_2 in comet 1P/Halley at a level similar to that in 67P/C-G suggests that O_2 is a dominant cometary component (Rubin et al. 2015). In Figs. 2.3a and 2.3c, molecular oxygen is produced only for the high ionisation case and reaches a peak abundance of $< 0.1\%$ that of water ice. This reflects the efficient conversion of O_2 into water ice, once formed. The "reset" case with low ionisation produces more O_2 gas and ice with respect to H_2O ice, but it remains difficult to envisage a scenario in which H_2O and O_2 ice would be well mixed. Nevertheless, these results are sufficiently interesting to warrant a detailed study exploring a broader range of parameter space, which will be conducted in future work.

HCN has been detected in numerous comets with an abundance ratio of the order of a few $\times 0.1\%$ relative to water (see, e.g., Mumma & Charnley 2011; Wirström et al. 2016). The results presented here show that HCN ice is unlikely to be produced in-situ via the processing of ices containing only N_2 and NH_3, which is opposite to the case for O_2.

2.4.4 Caveats of model assumptions

Several assumptions have been made in our models, in addition to the set of initial abundances, the ionisation rate, and the chemical network used. We have considered only a single temperature and density profile, as well as single dust-grain size and density. Although the disk surface density used is typical of those derived for nearby protoplanetary disks (see, e.g., Williams & Cieza 2011), in reality, disk midplane temperature profiles depend on a multitude of parameters including, disk mass, stellar spectral type, dust distribution and opacity, and disk flaring index (which influences the amount of UV absorbed and/or scattered by the disk surface layer). The iceline locations determined here are consistent with those determined in protoplanetary disk models which are considered to be representative of the pre-solar nebula (see, e.g., Öberg et al. 2011b, and references therein). For disks around warmer stars, the icelines would move outwards in radius, with the opposite result for disks around colder stars. All else being equal, this will only affect the radial extent over which we see each chemical effect. A significantly warmer inner disk will also allow gas-phase reactions with reactions to occur more readily which may perturb the chemistry differently to that seen here. Also, our adopted disk structure is static in time. This was chosen to keep focus on chemical evolution for fixed physical conditions. Future work will utilise an physical disk model that is evolving in time.

There is observational evidence for both dust-grain settling and growth in protoplanetary disks (e.g., Dullemond & Dominik 2004, 2005; Williams & Cieza 2011). Settling towards the midplane will increase the dust-to-gas mass ratio, whereas dust growth to $\approx$ mm sizes, will act in the opposite sense to decrease the total available surface area for freezeout and grain-surface reactions. The combination of both effects can either decrease or increase the total surface area of dust grains per unit volume. A smaller surface area (i.e., generally larger grains) will decrease the rate of freezeout (although freezeout is found to be almost instantaneous at the high densities of disk midplanes), and decrease the rate of grain-surface processing of ice mantles. Hence, this will lessen the effects of grain-surface chemistry, particularly for the case of high ionisation. Larger dust grains are also able to drift inwards as they become decoupled from the gas and affect the locations of icelines, by as much as 60% (as argued by Piso et al. 2015). The effects of different grain sizes will be investigated and addressed in future work.

Only two ionisation levels have been assumed here, to probe what are considered to be two extreme cases; however, there is also speculation in the literature that the pre-solar nebula may have been exposed to an increased cosmic-ray rate due to nearby supernovae early in the Sun's lifetime (see, e.g., the review by Adams 2010). We have demonstrated here that a relatively high level of ionisation causes more chemical processing than a lower level. We would expect this trend to continue for ionisation levels $\gg 10^{-17}$ s^{-1}. A lower level of ionisation would likely not have any effect, as the low level considered here is already seen not to significantly alter the chemistry. An increase or decrease in total disk mass (or surface density) will have the same effect as decreasing and increasing the ionisation rate due to CRs (especially in the outer disk), and increasing and decreasing the ionisation rate due to SLRs (especially in the inner disk).

The choice of initial abundances in the "inheritance"-scenario assumes an instant transition from molecular cloud phase to the disk midplane for the gas, with no chemical processing taking place "on the way". Likewise, the "reset"-scenario assumes all gas content to be dissociated into atoms at the time it reaches the midplane. These two sets of abundances are extremes. Recent models indicate that chemical processing of the material does take place on its way to the midplane (Drozdovskaya et al. 2016), so a realistic initial composition of the material is more likely to be a mix of atoms and molecules. Considering the extreme cases, however, provides insight into the degree of chemical processing taking place.

Finally, we extracted our chemical abundances at a single time step only, at 10^6 yrs, which is considered to be representative of the lifetime of the pre-solar nebula and nearby young protoplanetary disks (e.g., Williams & Cieza 2011; Henning & Semenov 2013). A shorter time would lead to less extreme effects due to ion-molecule reactions and CR-induced photoreactions, because these reactions typically have long timescales ($\gtrsim 10^5$ yrs) (see Fig. 2.4); however, this strongly depends on the assumed cosmic-ray ionisation rate. A longer time would lead to the opposite case. The ALMA detection of gaps and rings in the disk around the young ($< 10^6$ yr) protostar, HL Tau, suggests that grain growth and planet(esimal) formation in protoplanetary disks may occur much earlier than heretofore considered (ALMA Partnership et al. 2015); hence, shorter chemical timescales are worthy

of further investigation in future work. Specifically, in our models, assuming the "inheritance"-scenario and high level of ionisation, significant changes to the abundances of key volatiles take place after a few times 10^5 yrs (for more details, see Appendix 2.A).

2.5 Conclusions

The models presented in this work have examined the importance of kinetic chemistry on the molecular composition (gas and ice) in protoplanetary disk midplanes. The main conclusions are listed below.

- The disk midplane composition reflects that of interstellar ices only for the case of low ionisation (SLRs only) in the "inheritance" scenario. The partitioning between gas and ice is determined solely by iceline positions, as is assumed in the planet population synthesis models. The inclusion of grain-surface chemistry has a negligible effect.

- Assuming a higher rate of ionisation (SLRs plus CRs) and inheritance leads to an increase in the abundance of CH_4 ice beyond its iceline, and a significant depletion of gas-phase CH_4 in the critical region between 1 and 15 AU. Cosmic-ray-induced chemistry enables the release of free carbon from CO in the outer disk (> 15 AU) which is incorporated into gas-phase methane which freezes out. This naturally leads to low gas-phase CO abundances as is observed in some disks. On the other hand, cosmic-ray-induced chemistry efficiently destroys methane gas in the CH_4-poor region. The conclusion holds whether grain-surface chemistry is included or not.

- When grain-surface chemistry is considered, the CO_2 ice to H_2O ice ratio is increased, with CO and CH_4 gas destroyed at the expense of an increase in CO_2 ice. The critical reactions are the photodissociation of H_2O ice to form OH radicals within the ice mantle, which subsequently react with CO to form CO_2 ice. This reaction is able to proceed faster than H + OH recombination within ≈ 20 AU because the very volatile H atoms are quickly lost to the gas phase for grains warmer than 20 K. Beyond this radius, the reformation of water ice wins. The partitioning between N_2 and NH_3 is similarly affected.

- For the extreme "reset" scenario in which all elements are initially in atomic form, the picture changes significantly. Without grain-surface chemistry, gas-phase CO, O_2, and atomic oxygen are the main carbon and oxygen-bearing species beyond 1 AU. The chemistry does not have sufficient time to incorporate all available initial elemental oxygen into molecules by 10^6 yrs. Gas-phase water and CO_2 do form and subsequently freeze out, albeit achieving much lower abundances than in the "inheritance" scenario. A higher ionisation level helps to increase the production of H_2O and CH_4.

- With grain-surface chemistry, the abundances of H_2O and CO_2 ice increase significantly, demonstrating the absolute necessity of grain-surface chemistry

for the synthesis of these two dominant ice components. The final abundance ratios reached in the very outer disk (30 AU) for H_2O and CO_2 are similar to those for the inheritance scenario, regardless of the ionisation level; however, the higher ionisation level does impede the abundance of O_2 ice at the levels seen in comets and enables a conversion from CO to CH_4.

- In the reset scenario, species other than the main considered volatiles are also produced in non-negligible quantities: O_2, HCN, and NO. The higher ionisation level generally helps the production of HCN and NO (at the expense of N_2 and NH_3) and impedes the survival of O_2 ice.

- The inclusion of chemistry has a significant impact on the C/O ratio of both gas and ice in the planet-forming region which is expected to influence the resulting composition of forming planet(esimal)s. The ices remain, on the whole, dominated by oxygen (i.e., C/O < 1). For both inheritance cases, the gas is carbon rich relative to the canonical value; however only for the low ionisation case is there a reservoir of gas-phase material with C/O > 1. For both "reset" scenarios, the ice becomes more carbon rich than the gas, which is opposite to the "inheritance" case.

The results presented here show that under certain conditions, highlighted above, chemistry can have a profound effect on the composition of the planet-forming material in disk midplanes. Chemistry influences the partitioning of elemental carbon, oxygen, and nitrogen, into molecules of differing volatilities, such that the positions of ice lines alone, are not necessarily adequate for determining the ratio of C/O in neither the gas, nor the ice. Only under the extreme case of full inheritance and low ionisation, are the elemental ratios determined solely by the positions of icelines. This conclusion is also similar to that for the assumption that ices are already locked up in larger bodies by $\approx 10^5$ yr.

The work presented here follows the time evolution of chemistry in a static protoplanetary disk which is the simplest physical case. In reality, disk conditions evolve with time, at the same time as planetesimals are forming and migrating within the midplane. Future plans include determining the influence of chemistry in an evolving protoplanetary disk (where the density, temperature, and ionisation rate also vary with time), and to couple the outputs of these models with planet formation tracks to determine, in a quantitative manner, the influence on the resulting composition of gas-giant planetary atmospheres.

Acknowledgements: The authors thank Amaury Thiabaud and Ulysses Marboeuf for making their disk density and temperature profile available and for many inspiring discussions. The authors also thank Karin Öberg for a fruitful discussion about CO gas depletion inside the CO iceline. Astrochemistry in Leiden is supported by the European Union A-ERC grant 291141 CHEMPLAN, by the Netherlands Research School for Astronomy (NOVA), and by a Royal Netherlands Academy of Arts and Sciences (KNAW) professor prize. CW also acknowledges the Netherlands Organisation for Scientific Research (NWO, grant 639.041.335).

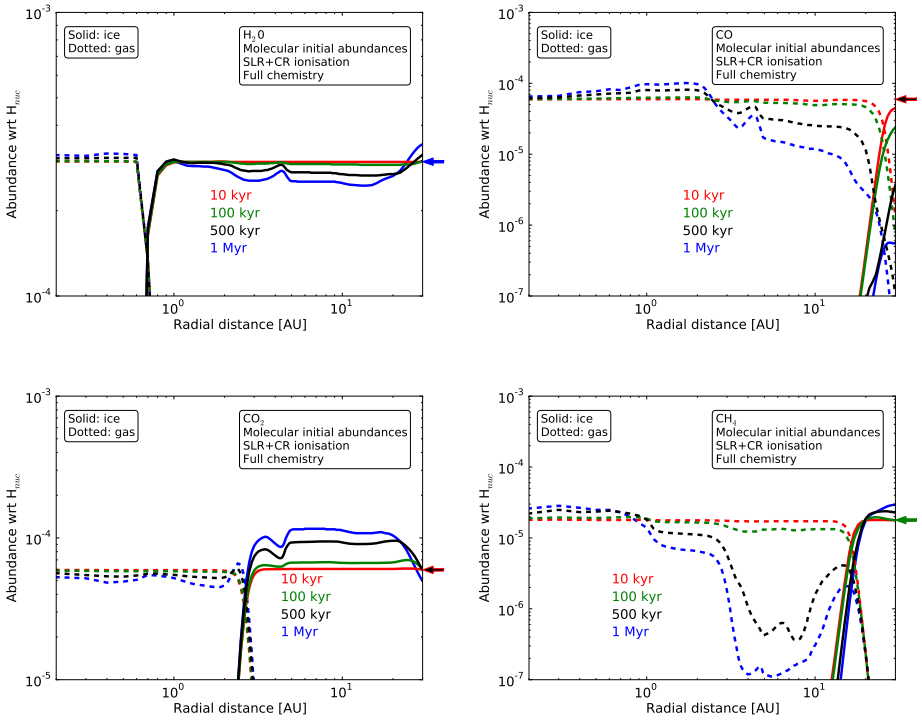

Figure 2.7: Abundances as function of radial distance R of the four key volatiles, taken at four different evolutionary stages. Note the different y-axes ranges. Arrows to the right of each panel indicate the initial abundance level in the case of the "inheritance"-scenario.

2.A Timescales

Fig. 2.7 shows the abundances of the four key volatile, taken at four different evolutionary times. Note the different y-axes ranges. It is seen that significant changes occur between 100 and 500 kyr, that is after a few times 10^5 yrs. This goes for all the four species, gas as well as ice, out to about 25 AU.

It is interesting to see that H_2O and CO_2 are respectively produced and destroyed in the gas phase in the inner disk, and vice versa in the outer disk. For CO and CH_4 there are turn-over radii in the inner disk, inside of which they are both being produced, and outside of which they are both being destroyed. These turn-over radii correspond to the iceline positions of H_2O and CO_2 for the case of CH_4 and CO respectively. This nicely illustrates the dependance on gas phase H_2O and CO_2 for the production/destruction of CO and CH_4 in the gas phase.

3 Molecular abundances and C/O ratios in chemically evolving planet-forming disk midplanes

C. Eistrup, C. Walsh & E.F. van Dishoeck
Published in Astronomy and Astrophysics, 2018

Abstract - Exoplanet atmospheres are thought be built up from accretion of gas as well as pebbles and planetesimals in the midplanes of planet-forming disks. The chemical composition of this material is usually assumed to be unchanged during the disk lifetime. However, chemistry can alter the relative abundances of molecules in this planet-building material.

Aim: We aim to assess the impact of disk chemistry during the era of planet formation. This is done by investigating the chemical changes to volatile gases and ices in a protoplanetary disk midplane out to 30 AU for up to 7 Myr, considering a variety of different conditions, including a physical midplane structure that is evolving in time, and also considering two disks with different masses.

Methods: An extensive kinetic chemistry gas-grain reaction network was utilised to evolve the abundances of chemical species over time. Two disk midplane ionisation levels (low and high) were explored, as well as two different makeups of the initial abundances ("inheritance" or "reset").

Results: Given a high level of ionisation, chemical evolution in protoplanetary disk midplanes becomes significant after a few times 10^5 yrs, and is still ongoing by 7 Myr between the H_2O and the O_2 icelines. Inside the H_2O iceline, and in the outer, colder regions of the disk midplane outside the O_2 iceline, the relative abundances of the species reach (close to) steady state by 7 Myr. Importantly, the changes in the abundances of the major elemental carbon and oxygen-bearing molecules imply that the traditional "stepfunction" for the C/O ratios in gas and ice in the disk midplane (as defined by sharp changes at icelines of H_2O, CO_2 and CO) evolves over time, and cannot be assumed fixed, with the C/O ratio in the gas even becoming smaller than the C/O ratio in the ice. In addition, at lower temperatures (< 29 K), gaseous CO colliding with the grains gets converted into CO_2 and other more complex ices, lowering the CO gas abundance between the O_2 and CO thermal icelines. This effect can mimic a CO iceline at a higher temperature than suggested by its binding energy.

Conclusions: Chemistry in the disk midplane is ionisation-driven, and evolves over time. This affects which molecules go into forming planets and their atmospheres. In order to reliably predict the atmospheric compositions of forming planets, as well as to relate observed atmospheric C/O ratios of exoplanets to where and how the atmospheres have formed in a disk midplane, chemical evolution needs to be considered and implemented into planet formation models.

3.1 Introduction

Over the past 20 years exoplanetary science has evolved from purely detection (e.g. Udry & Santos 2007; Borucki et al. 2011; Batalha et al. 2013; Fischer et al. 2014) to exoplanet characterisation. One example of characterisation is the deciphering of the molecular content of exoplanet atmospheres which has revealed simple molecules such as CO and H_2O, and possibly CO_2 and CH_4 (e.g. Seager & Deming 2010; Snellen et al. 2010; Birkby et al. 2013; Fraine et al. 2014; Crossfield 2015; Sing et al. 2016).

The C/O ratio of an exoplanet atmosphere (usually derived from relative abundances of the simple molecules listed above) has been proposed to be a possible tool to link an exoplanet to its formation site in the natal protoplanetary disk. This is because disk midplanes have a radial gradient of C/O ratios in gas and ice (see e.g. Öberg et al. 2011b). This approach, to couple observed C/O ratios in exoplanets with their possible formation sites, typically assumes that the radial dependence of the midplane C/O ratio is defined solely by the iceline (snowline) positions of the main volatile species in a disk of fixed chemical composition (see e.g. Marboeuf et al. 2014). The position of the iceline for a particular species depends on the temperature structure of the disk midplane, and the binding energy (or desorption energy) of the molecule to ice mantles on dust grains. Icelines thus affect the relative ratios of heavy elements in the gas and ice. For example, beyond the H_2O iceline, the gas is depleted in oxygen whilst the ice is enriched in oxygen. Similar changes occur across the CO_2, CH_4, and CO icelines thereby also altering the local C/O ratio in both the ice and gas. An example of a variable C/O ratio for a disk with a fixed chemical composition (as per the conventional assumption) is shown in Fig. 1 of Öberg et al. (2011b). Due to the step-like features of that figure, caused by icelines, the figure will be referred to as the traditional stepfunction.

Protoplanetary disks are not static objects: over the disk lifetime, from formation to dispersal, typically $\sim 0.1 - 10$ Myr, the disk generally cools, spreads, loses material (via accretion onto the star or dissipation) and thus becomes less dense over time (see the review by Williams & Cieza 2011). Hence, the icelines of volatile species also change in time, generally migrating inwards towards the star (Davis 2005; Min et al. 2011; Harsono et al. 2015). To date, most models exploring the location and evolution of icelines with the explicit goal to link to the composition of planet-building material have assumed static midplane conditions (Öberg et al. 2011b; Madhusudhan et al. 2014; Thiabaud et al. 2015b). Static models are more straightforward to couple with chemical kinetics. Recently Piso et al. (2015, 2016) explored the evolution of elemental ratios across icelines in both a static and viscously evolving disk model including the radial drift of ice-coated grains of different sizes. The temperature structure is kept fixed in time in these models. A similar approach has been adopted by Ali-Dib et al. (2014) and Ali-Dib (2017). Both of these models include dust and pebble dynamics at the expense of kinetic chemistry. Those models which do allow evolving disk midplane conditions also neglect kinetic chemistry for simplicity (see, e.g. Marboeuf et al. 2014; Mordasini et al. 2016).

The impact of kinetic chemistry in planet formation models is yet to be fully

explored due to the increased computational demands in coupling a chemical model with, for example, a planet population synthesis model. This is despite chemical kinetics being a necessity in models explaining protoplanetary disk observations for some 20 years since the first detection of molecules, other than CO, in disk atmospheres (see review by Henning & Semenov 2013). This is now changing, as is the traditional picture of a static disk. Recent examples of kinetic gas-grain chemistry in disks can be found in Helling et al. (2014), Walsh et al. (2015) and Cridland et al. (2016), with different levels of treatment of the chemistry and grain growth. Also, there is growing observational evidence for low gaseous CO abundances which can be attributed to either rapid planetesimal growth or chemical evolution (see e.g. Favre et al. 2013; Bruderer et al. 2012; Reboussin et al. 2015; Kama et al. 2016c; Miotello et al. 2017).

The disk midplanes suffer from a lack of observational constraints on their chemical compositions. This due to the observational difficulty of probing the midplane through the optically thick higher-lying layers of the disk and to the freeze-out of species in the outer disk midplane. Most molecular emission, whether at millimeter or infrared wavelengths, therefore arises from the warm layer at intermediate disk heights (see Bergin et al. 2007, for a review). Even the N_2H^+ emission observed with ALMA, which probes the part of the outer disk where CO is frozen out, arises mostly from layers just above the midplane (Qi et al. 2013; van 't Hoff et al. 2017). Molecules expected to be abundant in midplane ices such as H_2O (Hogerheijde et al. 2011; Du et al. 2017), NH_3 (Salinas et al. 2016), H_2CO (Loomis et al. 2015) and CH_3OH (Walsh et al. 2016) have been detected in the gas-phase but the observations either lack spatial resolution or reflect subsequent gas-phase chemistry, making it difficult to infer the outer disk midplane ice abundances. Ultimately, comet abundances may provide the best constraints on this region, at least for our solar nebula disk.

In contrast, the midplane of the warm inner disk where CO is not frozen out has recently been imaged for the first time through CO isotopologue observations of $^{13}C^{18}O$ by Zhang et al. (2017) for one disk. Such observations are promising, and are perhaps also feasible for other common species, but they require large telescope time investments. Also, the dust continuum emission becomes optically thick in the inner disk, hiding our view of much of the planet-forming midplane. Thus, perhaps ultimately the only information on the midplane chemical composition is to be inferred from the atmospheric compositions of the planets that form out of the midplane, and which remain after the disk is dispersed.

As emphasized in Mordasini et al. (2016), the road from a gaseous disk midplane to an observable exoplanet atmospheric composition is long, requiring many steps, physical (e.g. migration) as well as chemical. A key issue is whether the planets' heavy element enrichment is controlled by the accreted gas or by the accreted (icy) planetesimals. Mousis et al. (2009), Thiabaud et al. (2015a), and Mordasini et al. (2016) found that the dominant delivery mechanism for heavy elements to a forming gas-giant planet atmosphere is accretion of icy planetesimals rather than direct accretion from the gas, at least for planets with masses less than a few times that of Jupiter. The ultimate C/O ratio in the observable part of the planet's atmosphere also depends on how well the sublimated planetesimals

are mixed in the envelope and on the core-envelope partitioning. In any case, it is clear from models such as those of Mordasini et al. (2016), which explicitly include planetary formation and planetesimal accretion processes, that the composition of both the gas and the ice of the evolving parent disk is needed to determine the planetary atmosphere composition.

Eistrup et al. (2016) (herefrom Paper 1) investigated how kinetic chemical evolution affects the composition of volatiles (ice and gas) in a static protoplanetary disk midplane. If interstellar ices are inherited from the collapsing cloud (without alteration) by the protoplanetary disk, then the ice composition is preserved only for the case where there is no source of external ionisation (i.e. no cosmic rays). An important conclusion from Paper 1 is that if chemistry is efficient on a timescale of ~ 1 Myr, then the C/O ratio of the gas and ice remains less than one always within the CO iceline. Only for the case of low ionisation and full inheritance does the C/O ratio approach 1, and this only occurs for the gas: the ice remains oxygen-rich always.

The effects of chemical kinetics on the composition of gas and ice volatiles in evolving protoplanetary disk midplanes remains to be quantified. We here expand upon the work presented in Paper 1 to investigate how changing temperature and density in the disk midplane with time modifies the above conclusions. We also considered how disk mass may affect the composition of planet-building material. We furthermore studied the timescale for chemical changes by extending the lifetime of our disk models to ~ 7 Myr at which point we assumed that planet formation has halted and disk dispersal is advanced.

We investigate a wide parameter space, with somewhat simplified physical structures, and two sets of extreme initial abundances. The two scenarios of initial chemical abundances are: cloud inheritance (hereafter "Inheritance" scenario) and chemical reset (hereafter "Reset" scenario). In the inheritance scenario the initial abundances are molecular, and taken to be those found in ices in the parent molecular cloud. In the reset scenario, the initial abundances are atomic, because all molecules are assumed dissociated by high temperatures close to the young star. Both scenarios include H, H_2 and He initially, with abundance ratios: $N(\mathrm{H})/N(\mathrm{H_2})=10^{-4}$, and $N(\mathrm{He})/N(\mathrm{H_2})=0.17$. Generally, the inner disk midplane should be susceptible to luminosity outbursts that can reset the chemistry, while the outer disk midplane should be expected to inherit the parent cloud abundances, so both scenarios may apply but in different parts of the disk (Pontoppidan et al. 2014). The intention is to investigate chemical trends expected for these two sets of initial conditions and using a more realistic disk, which is becoming cooler and more diffuse over time.

3.2 Methods

The evolving physical disk model from Alibert et al. (2013) was used. This disk model was adopted in planet population synthesis studies. It features time evolution of disk midplane temperature and pressure as a function of radius ($0.2-30$ au) over a timescale of 7 Myr. The approach for calculating the ionisation rate and

chemical evolution follows that presented in Paper 1: we summarise the main aspects here.

3.2.1 Evolving disk model

An evolving disk here refers to a disk that is cooling in time whilst also losing mass. In this work power laws were fitted to the temperature structure evolving in time as originally computed by Alibert et al. (2013).

The disk structure adopted from Alibert et al. (2013) and used in Paper 1 will be referred to as the 0.1 MMSN disk, having an initial mass of $1.3 \times 10^{-3} M_{\odot}$ or 0.13 times the minimum mass solar nebula, or MMSN (Weidenschilling 1977). The reason for fitting power laws was that the initial time-dependent temperature structure from Alibert et al. (2013) featured a step, that is, an unphysical radial drop, at around 5 AU, as well as an artificial lower temperature cut-off at 20 K. Both of these features were smoothed out with a power law profile in Paper 1. The same unphysical drop in temperature was observed for later time steps. In order to smooth out all timesteps, whilst ensuring a temperature profile that is monotonically decreasing in time for all radii, power laws were fitted to all temperature profiles from Alibert et al. (2013). For timesteps up to 400 kyr of evolution, the power laws were fitted using model data from 1 to 2.1 AU, and for all later timesteps from 0.2 to 0.6 AU. The resulting power law fits were then extrapolated to the entire radial range of the disk. This procedure gave the temperature profiles that can be seen for selected timesteps (as labelled) in Fig. 3.1a.

Using these temperature profiles, the midplane density profiles for all timesteps were computed using the midplane pressure profiles from Alibert et al. (2013), assuming H_2 to be the main gas constituent. The resulting midplane number density radial profiles at selected timesteps are shown in Fig. 3.1b.

The surface density profiles at the first timestep were computed using the prescription and values for Table 1, Disk "8" in Alibert et al. (2013). Taking into account disk evolution, the surface density at later timesteps at a radial distance R was computed by scaling the initial surface density $\Sigma_{t=0}(R)$ to the evolution in midplane number density $n(R)$ as seen in Fig. 3.1b. Hence, the surface density at point R at time t is given by

$$\Sigma(R,t) = \Sigma(R, t=0) \times \frac{n(R,t)}{n(R,t=0)}. \tag{3.1}$$

To drive chemical evolution, ionisation of the disk midplane is needed, a conclusion reached by our and other models (see e.g. Helling et al. 2014; Aikawa et al. 1996; Willacy et al. 1998; Walsh et al. 2012; Cleeves et al. 2013b). Paper 1 found that chemical evolution was observed to be significant within 1 Myr evolution time only when short-lived radionuclides (SLRs) and cosmic rays (CRs) were included. In this paper, the contribution to ionization by SLRs and CRs were treated in a similar way to that in Paper 1: the ionisation rate from decay of SLRs is computed using the prescription from Eq. 30 in Cleeves et al. (2014c), including the time-dependent term, which was omitted in Paper 1.

$$\zeta_{\rm SLR}(R,t) = (2.5 \cdot 10^{-19}{\rm s}^{-1}) \left(\frac{1}{2}\right)^{1.04t} \left(\frac{\Sigma(R,t)}{\rm g\ cm^{-2}}\right)^{0.27}. \quad (3.2)$$

The contribution from CRs were calculated assuming attenuation depending on how much material the CRs have to pass through on their way to the midplane. The attenuation factor was calculated using the (now) evolving surface density of the disk in the vertical direction giving the following ionisation rate

$$\zeta_{\rm CR}(R,t) = \zeta_0 \times \exp\left(\frac{\Sigma(R,t)}{96{\rm g\ cm^{-2}}}\right), \quad (3.3)$$

where $\Sigma(R,t)$ is the evolving surface density profile, taken from Eq. 3.1, and ζ_0=10^{-17} s^{-1} (as in Paper 1).

The SLR ionisation rate profiles ("low" ionisation) and the SLR + CR ionisation contribution profiles ("high" ionisation) are plotted at selected timesteps in Fig. 3.1c and d. We note that the SLR ionisation level decreases rapidly with time and becomes very low, of order 10^{-22} s^{-1} by $\sim$ 7 Myr. In contrast, the CR ionisation level increases with time, especially in the inner disk, due to the decreasing surface density.

The timestep grid of Alibert et al. (2013) was adopted, with physical conditions changing for every timestep of their models. However, timesteps were added at early evolutionary stages ($1 - 10^4$ yrs) in order to account for short-term chemical effects. The first timestep in the time grid in this work is 1 yr, and the physical conditions at 1 yr from Alibert et al. (2013) were adopted for this timestep. Four logarithmic decades were applied ranging from 1 to 10^4 yrs, with physical conditions during this time fixed at the conditions at 1 yr. After 10^4 yrs, the time grid and the associated, continuously changing physical conditions of Alibert et al. (2013) were adopted. The time goes up to 7 Myr, in order to also investigate long-term chemical evolution. Until 7 Myr, this disk model goes through 401 timesteps.

3.2.2 Higher disk mass: 0.55 MMSN disk

For investigating the effect of a higher disk mass, a more massive evolving disk physical structure from Alibert et al. (2013) was adopted (Table 1, "Disk 12" of Alibert et al. 2013). The initial mass of this disk is 0.55 MMSN = 0.0055 $M_\odot$, determined in the same manner as was the case for the less massive disk in Paper 1. Since this disk has the same steep temperature drop as was the case with the 0.1 MMSN disk, and also features the 20 K lower temperature limit, power laws were also fitted to the temperature profiles at each timestep. In order to have the temperature profiles decreasing in time monotonically at each radial point, for this disk, the power law fitting was done for the first timestep (1 yr) and the last timestep (7 Myr) for the evolving disk temperature profiles between 1.1 and 1.5 AU. For all intermediate timesteps, power law indices intermediate to the two fitted indices were adopted, so that the power law index is continuously and linearly decreasing in time, with the step-wise decrease in index value being constant for each timestep. The original disk temperature structure from Alibert et al. (2013)

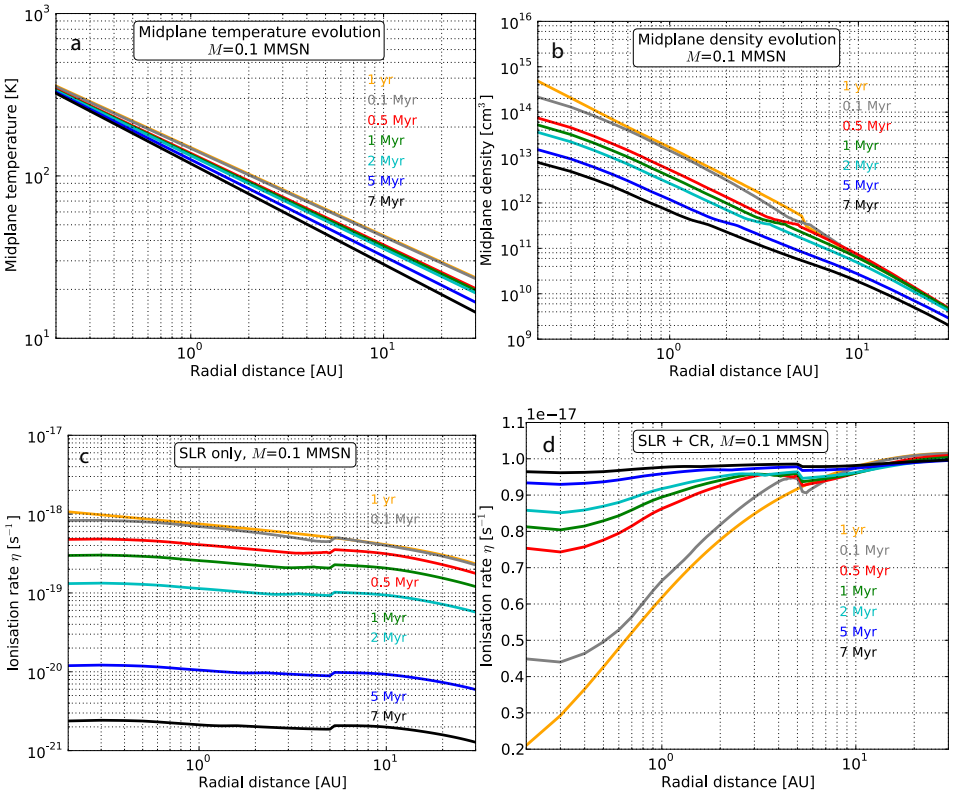

Figure 3.1: Midplane temperature and density (top) and ionisation rates (bottom) as functions of disk radius for different evolutionary times for the 0.1 MMSN evolving disk model. For this model, the starting conditions at 1 yr are given by the orange profiles shown here, which feature slightly different physical conditions than that for the static disk structure adopted by Paper 1 (see text for details).

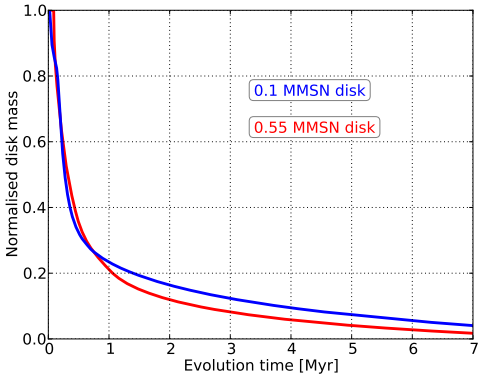

Figure 3.2: Evolving disk masses for the two disks, normalised to the initial disk masses of 0.1 and 0.55 MMSN. For both disks, more than half of the initial mass is lost before 0.5 Myr, and by 1-1.5 Myr evolution, only 20% of the initial masses remain.

was then adopted inside 1.1 AU, whereas the fitted (for first and last timesteps) and imposed power law structures were applied outside 1.1 AU. For the outer parts of the disk, at late timesteps, the temperature gets very low (below 8 K), which is unphysical. A lower limit of 8 K to the temperature was therefore imposed.

The midplane number density and ionization level structures for this 0.55 MMSN disk were computed in the same way as described for the 0.1 MMSN disk in Sect. 3.2.1. The resulting midplane temperature, density and ionisation profiles for the midplane of the 0.55 MMSN disk are presented in Fig. 4.1 (see Appendix). The evolving 0.55 MMSN disk goes through 438 time steps during the 7 Myr modelled evolution. The first timestep is at 1 yr, and from 1 yr through 10^4 yrs the time resolution is the same as for the same early timesteps for the 0.1 MMSN disk model, as described in Section 3.2.1. After 10^4 yrs, the timesteps from Alibert et al. (2013) were adopted.

The disk structures differ for the two different disk masses. Since the ionisation level is dominated by the contribution from CRs at all times throughout the disk (see Fig. 3.1 and 4.1, panels c and d), the decreasing surface density means the degree of ionisation in the inner disk is increasing in time. Because of the higher densities, the degree of ionisation in the inner disk is increasing faster in time for the 0.55 MMSN disk than for the 0.1 MMSN disk.

The temperature structure for the 0.55 MMSN disk is hotter in the inner disk, and has a steeper radial gradient, than that for the 0.1 MMSN disk. The low temperature in the outer disk for the 0.55 MMSN disk is due to lesser heating from irradiation from the central star. This is because more material shields the radiation for the 0.55 MMSN disk than for the 0.1 MMSN disk.

Fig. 3.2 shows the evolution of the disk masses for the two disks, normalised to their initial masses. Both disks experience significant mass loss during the evolution, with the 0.1 MMSN disk losing 95% of its initial mass, and the 0.55 MMSN disk losing 98% of its initial mass, after 7 Myr.

3.2.3 Chemical model

The chemical model included gas-phase chemistry, gas-grain interactions and grain-surface chemistry. The gas-phase chemistry was from the latest release of the UMIST Database for Astrochemistry (McElroy et al. 2013) termed RATE12. The rates for gas-grain interactions and grain-surface chemistry were calculated as described in Walsh et al. (2015, and references therein). A gas-to-dust mass ratio of 100 was adopted. The chemical model used here was identical to the "Full chemistry" setup in Paper 1. Photodissociation and photodesorption due to cosmic-ray induced UV photons were included.

The adopted grain size is 0.1 μm. As discussed in Paper 1, this assumption is certainly not correct, but the effects of grain growth to larger sizes and decreasing midplane gas-to-dust ratios due to settling tend to compensate each other. The important dust parameter for the chemistry is the amount of surface area available for freezeout and subsequent grain-surface chemistry. This is often parameterised as a combination of grain size and number density (set by the assumed gas-to-dust mass ratio). The assumption on the constant grain size will be further discussed in Section 3.3.6.3. More generally, all trends found in this paper are robust but the exact timescale for chemical changes and the magnitude of the chemical changes will depend on the assumed grain size and the gas-to-dust mass ratio.

For details about the two sets of initial abundances (the inheritance and reset scenarios), see Table 1 in Paper 1. The overall C/O ratio utilised is 0.34. In Paper 1 it was found that if the disk was exposed to ionising cosmic rays, efficient production of CO_2 ice and O_2 gas and ice takes place at intermediate disk radii, whereas CH_4 gas was converted to CO and CO_2. Also, if full chemical reset into atoms occurs en route into the disk midplane (e.g. via a shock or a luminosity outburst), then the abundances of dominant volatiles can differ from interstellar values by more than an order of magnitude (see also Drozdovskaya et al. 2016). Most striking was the depletion of H_2O ice advancing enhanced gas-phase CO and O_2. This difference was larger for the case where cosmic rays were excluded from the reset scenario. Helling et al. (2014) also found cosmic rays to be of importance to chemistry that alters the C/O ratio in the midplane. Their results, however, were different from those in Paper 1, due to differences in the grain-surface chemistry utilised.

Throughout this work, whenever distinguishing between gas-phase and icy species is necessary, an "i" in front of a molecule involved in a reaction will denote that the molecule is icy, and a "g" in front will denote a gas-phase molecule. For reference, an iceline is the midplane radius inside of which a given chemical species is in the gas phase, and outside of which the species is in the ice.

3.3 Results

Figure 3.3 shows abundances as a function of radius for selected volatile species in gas and ice after 7 Myr evolution, for four different model setups. As indicated in the boxes in each panel, the model setups explore a range of static and evolving disks, for the inheritance versus reset scenarios, and at both low and high ionisation

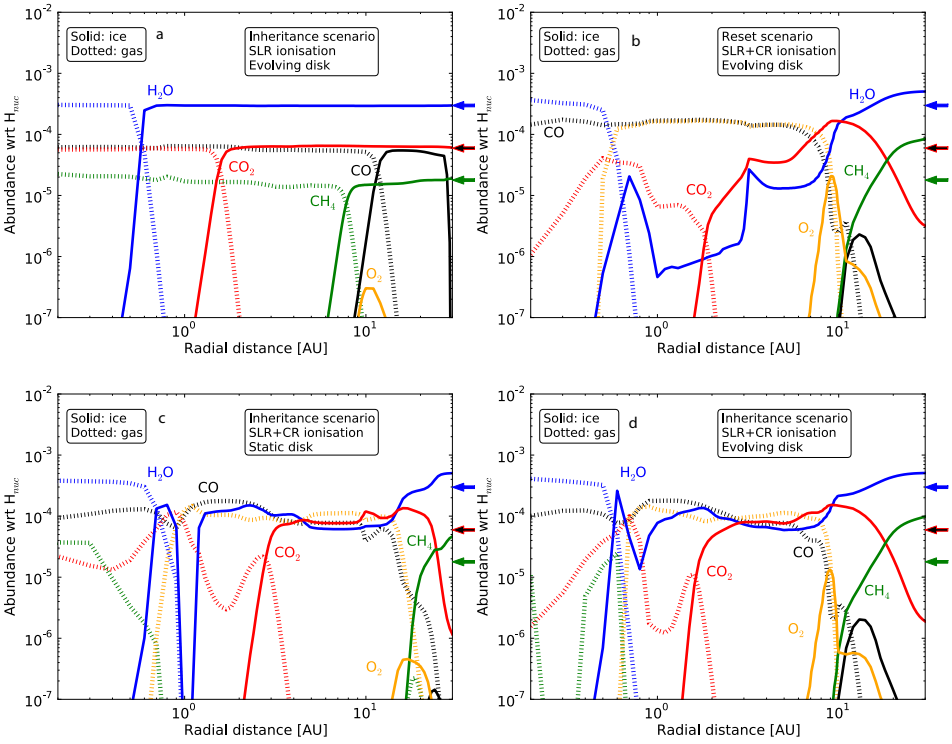

Figure 3.3: Abundances after 7 Myr evolution for four different model setups. Panel a: inheritance scenario with low ionisation and evolving disk structure. Panel b: reset scenario, high ionisation and evolving disk structure. Panel c: Inheritance scenario with high ionisation and static (unchanging) disk structure. Panel d: Inheritance scenario with high ionisation and evolving disk structure. The blue, red-and-black and green arrows to the right of each panel indicate the initial abundances assumed for H_2O, CO/CO_2 and CH_4, respectively, in the inheritance scenario.

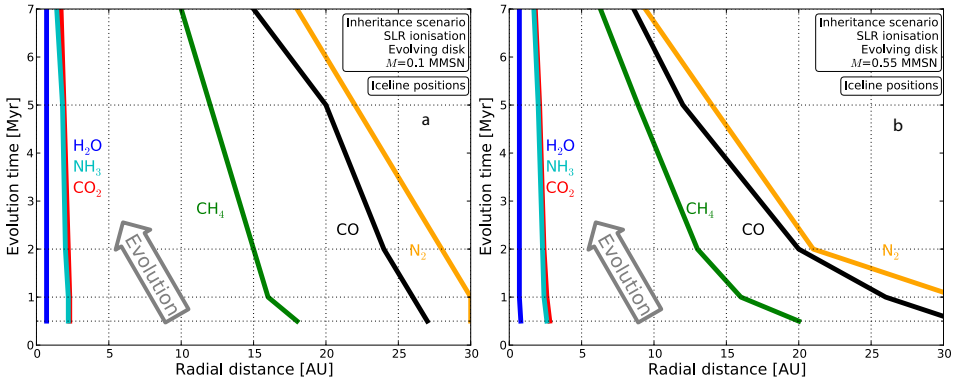

Figure 3.4: Evolving iceline positions for main volatiles, for 0.1 MMSN (left) and 0.55 MMSN (right) evolving disks

levels.

3.3.1 Static versus evolving disk: shifting icelines

In Paper 1 it was found that given low ionisation and inherited initial chemical abundances, chemical evolution was insignificant on the timescale of 1 Myr. Figure 3.3a shows the same case, but now for a physically evolving disk structure (the 0.1 MMSN disk), as described in Section 5.2, and for up to 7 Myr. It is evident from Fig. 3.3a that the chemistry in the midplane remains defined by the iceline positions, and that chemical processing has caused no significant chemical changes. This conclusion holds for the 0.55 MMSN evolving disk structure as well. Hence, the conclusion from Paper 1, that in the case of inherited abundances and low ionisation level, chemical evolution is insignificant, can be extended to a timescale of 7 Myr for these cases.

The main effect of utilising an evolving disk structure instead of a static one is that the icelines shift inwards with time. This in evident when comparing Fig. 3.3c and 3.3d, which both feature the inheritance scenario at high ionisation, but for a static and an evolving disk structure, respectively. For Fig. 3.3d the icelines are shifted inwards in time, whereas for 3.3c the icelines are static corresponding to the static temperature structure. The additional effects of adopting an evolving disk structure instead of a static structure are the retention of H_2O ice around 0.7 AU in panel d and one to two orders of magnitude lower CH_4 gas abundance in the inner disk. The iceline positions for the disks are determined from Fig. 3.3 as the maximum distance R from the star at which a volatile is more abundant in gas than in ice. Fig. 3.4 features the locations of the thermal icelines of selected volatile species as functions of time. The solid profiles indicate the movement of the icelines over time. We note that the axes scales in Fig. 3.4 are linear.

For H_2O, NH_3, and CO_2 in the 0.1 MMSN disk, the icelines shift by 30-35%

between 0.5 and 7 Myr of evolution (e.g. from 0.7 to 0.5 AU for H_2O). For CH_4, CO, and N_2 the icelines are shifted inwards by ∼60%. The larger shifts for the latter, more volatile species are due to the larger decreases in temperature in the outer disk, due to the decreasing slopes of the temperature profiles with time (see Fig. 3.1a). For the 0.55 MMSN disk, the icelines shift farther than for the 0.1 MMSN disk. This is due to the steeper temperature profile for the 0.55 MMSN disk, as can be seen when comparing top left panels in Figs. 3.1 and 4.1. The temperature drops by ∼50% from 0 to 2 Myr at 10 AU in the 0.55 MMSN disk, versus a temperature drop by ∼20% in the 0.1 MMSN disk over the same timeframe and radius.

3.3.2 Timescales of chemical changes

Figs. 3.5 and 3.6 show abundances for five key volatiles as function of midplane radius at six timesteps: 0.1, 0.5, 1, 2, 5 and 7 Myr, for the inheritance scenario model at high ionisation. The left panels are for the 0.1 MMSN disk, and the right panels are for the 0.55 MMSN disk. A time of 0.1 Myr was chosen as the first timestep because it was found in Paper 1 that for the inheritance scenario no chemical changes had taken place yet at this evolution time. An age of 0.5 Myr is representative of the timescale corresponding to the end of the embedded phase of star formation, when the protoplanetary disk is revealed. This was also found in Paper 1 to be the chemical evolution timescale for the high ionisation case. In that work, 1 Myr was considered the full evolution time: here, we consider additional and later timesteps at 2, 5, and 7 Myr. The first is chosen as it is the median age of T Tauri stars and represents the lifetime of the gas-rich protoplanetary disk. A time of 5 Myr represents an aged disk like TW Hya. By 7 Myr the gaseous disk is thought to have fully dissipated resulting in a gas-poor debris disk (see e.g. Fedele et al. 2010, and Fig. 3.2).

As seen in Figs. 3.5 and 3.6, chemistry is continuously ongoing throughout the evolutionary time of 7 Myr. The chemical abundance changes over 7 Myr vary from factors of a few (e.g. a 3 times decrease in H_2O ice abundance at 10 AU in Fig 3.5a to orders of magnitude (e.g. a CH_4 gas depletion at 5 AU in 3.6a, resulting in a significantly different chemical "picture" from the beginning to the end of the evolution. For all species considered in these plots, the shifting icelines can be seen as an inward shift with time of the radius where the gas and ice profiles cross each other.

Overall, with the exceptions of H_2O, CO and CO_2 inside 0.4 AU to be discussed in Section 3.3.3, the trends are similar for the 0.1 MMSN and 0.55 MMSN disks. Thus, in the following discussion only the chemical evolution of the 0.1 MMSN disk case is considered.

To visualise the main chemical changes more clearly, Fig. 3.7 highlights the evolution of key species with time at each of four chosen radial positions: 1, 5, 10 and 30 AU. At 1 AU large changes happen between 1 and 7 Myr. The abundances of CO and O_2 gas seem to converge at the end of the evolution, indicating that a steady state situation may be reached where these two species are the main carbon and oxygen reservoirs. H_2O ice is still dropping in abundance, thus, if evolution

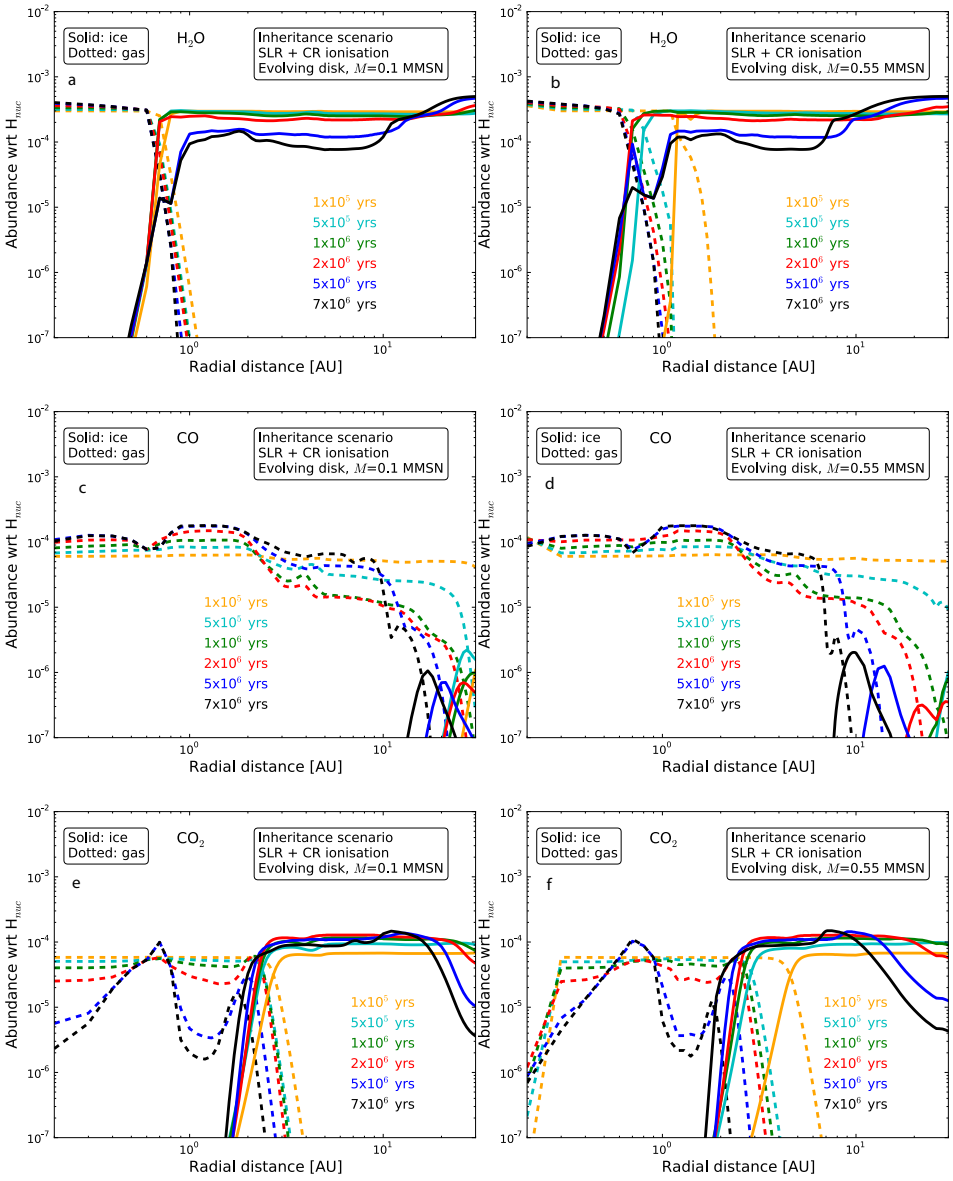

Figure 3.5: Abundances of H_2O, CO and CO_2 gas (dashed) and ice (solid) as a function of midplane radius at five timesteps: 0.5, 1, 2, 5, and 7 Myr. The left-hand and right-hand panels show the 0.1 MMSN and 0.55 MMSN disk results, respectively.

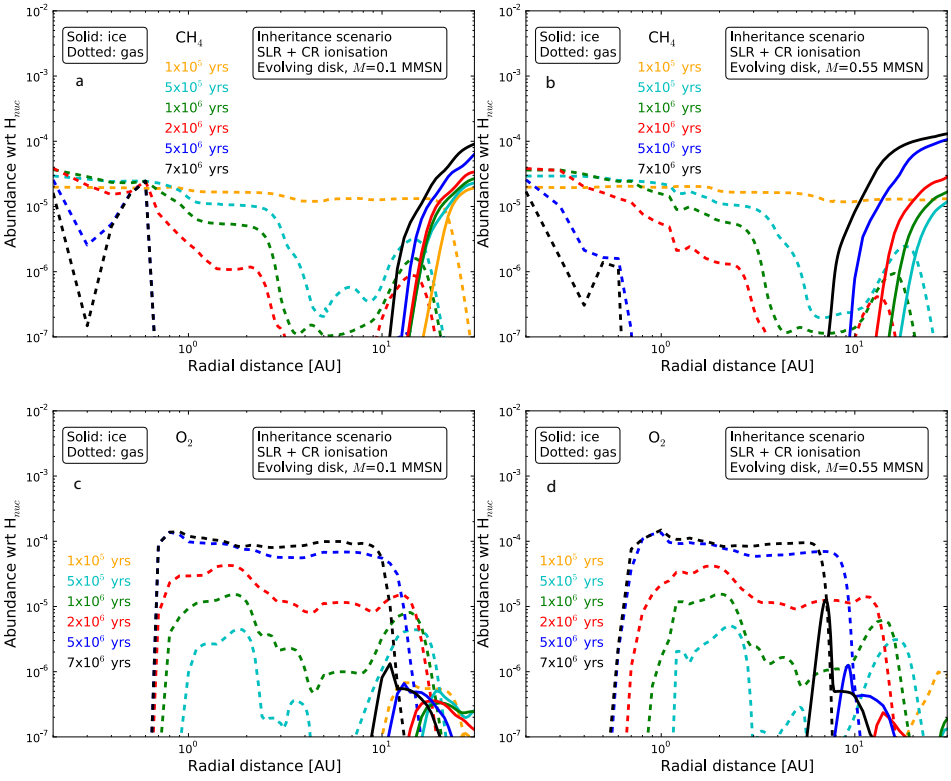

Figure 3.6: Same as Fig 3.5, but for CH_4 and O_2.

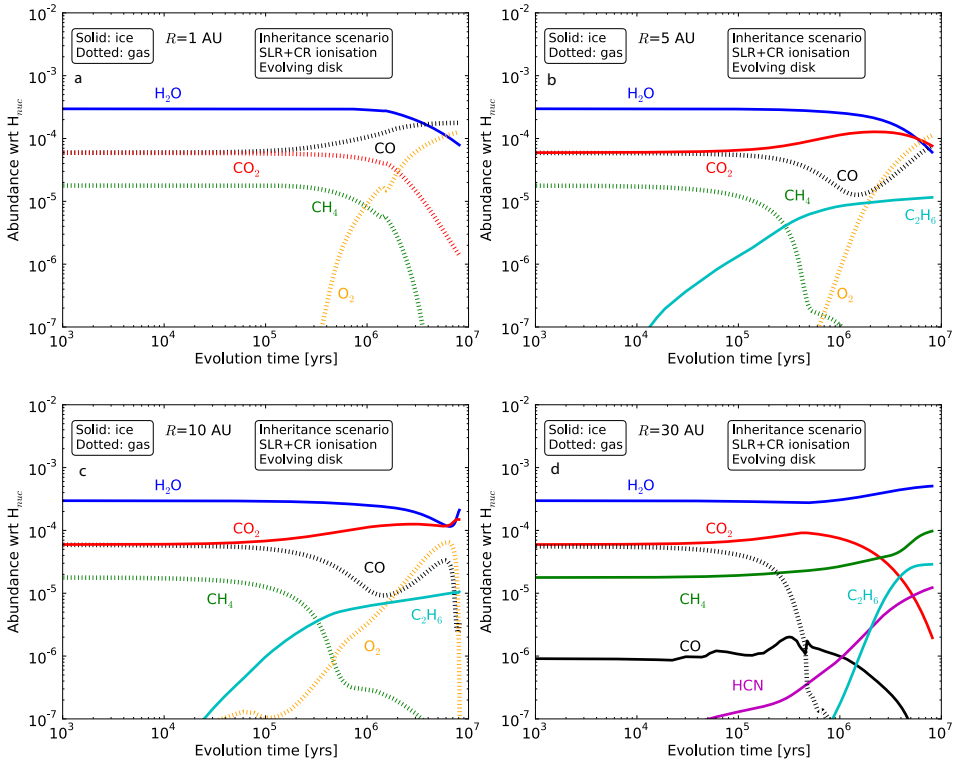

Figure 3.7: Time evolution of selected volatiles, in gas as ice at 1, 5, 10 and 30 AU, for the 0.1 MMSN disk with high ionisation and inheritance.

were to continue for a longer time, a further decrease in H_2O ice abundance would likely be seen.

At 5 AU, no steady state seems to have been reached after 7 Myr. CO and O_2 gas and H_2O and CO_2 ice have near equal abundances to within a factor of two, and a steady increase in C_2H_6 ice abundance is seen throughout the evolution reaching a final abundance of $\sim 10^{-5}$, making it the third most abundant carrier of elemental carbon, accounting for $\sim$ 15% of the carbon. CH_4 gas is depleted due to reactions with He^+, which is a consequence of the high ionisation level, as also mentioned in Paper 1. A "reverse" evolution of CO gas and CO_2 ice is also evident, taking place at about the same time (between ∼1.6-5 Myr), indicating interdependency between production and destruction of CO and CO_2. The decreasing abundance of CO gas and increasing abundance of CO_2 ice from ∼0.1 Myr to ∼2 Myr can be explained by CO gas colliding with the grains, and subsequently reacting fast with OH (faster than CO can desorp) to produce CO_2 on grain surfaces, as also described in Paper 1. The reverse evolution for CO and CO_2, after 2 to 3 Myr, is due to the increasing midplane ionisation level over time (see Fig. 3.1d). For both a static and an evolving disk, the continuous CR ionisation of the midplane causes an increasing CR-induced photon fluence there (we note that the fluence increases faster for the evolving disk due to the evolving ionisation level). This increasing fluence amplifies the photodissociation of CO_2 ice into CO and O on the grains, which starts to dominate over the CO_2 production reaction $iCO + iOH \longrightarrow iCO_2 + iH$. The result is a decrease in CO_2 ice and an increase in CO gas after 2-3 Myr. Thus, for an evolving disk, and the physical conditions considered here, the CO_2 ice abundance reaches a maximum. The more diffuse the midplane becomes over time, the higher the ionisation contribution from CRs stays accordingly, and the shorter time it takes for the CO and CO_2 evolutions to invert, in what will now be referred to as an "abundance inversion".

Going out to 10 AU, the evolution is very similar to that at 5 AU. The main difference is the rapid decrease in O_2 and CO gas abundances at the end of the evolution, which is due to the shifting of the O_2 iceline from outside to inside of 10 AU (see Fig. 3.4), and the destruction of CO gas. The latter is caused by the rapid conversion of CO into CO_2 ice mentioned above. These changes to O_2 and CO gas at 10 AU remove them from the gas phase. An effect of this freeze-out is also the extra availability of O_2 and CO on the grain surfaces which both react to form H_2O and CO_2 ices, which are seen to increase in abundances simultaneously with the freeze-out of CO and O_2.

Out at 30 AU it is cold enough for all volatiles, except CO, to be frozen out initially. As seen in Fig. 3.7, within the abundance limits, CO gas and ice are co-existing because R=30 AU is just inside the initial thermal CO iceline, with the ice abundance accounting for a few percent of the total CO abundance. The CO gas abundance decreases after ∼0.4 Myr, at which point the midplane has cooled enough for the CO iceline to move inwards of 30 AU, after which the CO ice becomes more abundant than the gas. However, the CO ice abundance after about 1 Myr is only a few percent that of the initial CO gas abundance, indicating that CO is processed on grain surfaces upon freeze-out. CO_2 ice is also destroyed after 1 Myr of evolution, but CH_4 ice is steadily produced to become the dominant

carbon-bearing species after 7 Myr.

This production of CH_4 ice at 30 AU is linked to the destruction of CH_3OH ice through photodissociation by CR-induced photons which takes place simultaneously after 1 Myr. CH_3OH ice is destroyed on the grains inside and outside of the location of CO iceline. It is not reproduced from hydrogenation of CO because CO is being converted into CO_2. Outside the CO iceline CO and CH_3OH are both being photodissociated on the grains caused by CR-induced photons, through the reactions

$$\mathrm{iCH_3OH} \xrightarrow{\gamma_{CR}} \mathrm{iCH_3 + iOH} \quad \text{and} \quad \mathrm{iCO} \xrightarrow{\gamma_{\mathrm{CR}}} \mathrm{iO + iC} \tag{3.4}$$

This means low abundances of oxygen-containing complex organic molecules. In the cold outer midplane with temperatures down to around 15 K, the mobility of molecules on the grains is low, so hydrogenation reactions become dominant. $\mathrm{iCH_3 + iH \longrightarrow iCH_4}$ is causing the increase in CH_4 ice abundance, with CH_4 being the dominant carbon carrier after 7 Myr of evolution at 30 AU. Likewise, the hydrogenation of C_2H_4 ice and C_2H_5 ice is responsible for the production of C_2H_6 ice. H_2O ice is formed from hydrogenation of OH leftover from the photodissociation of CH_3OH, including the reaction:

$$\mathrm{iCH_3OH} \xrightarrow{\gamma_{CR}} \mathrm{iCH_2 + iH_2O}. \tag{3.5}$$

The abundance of C_2H_6 ice increases with increasing radial distance. In addition to C_2H_6 ice, HCN ice is also abundantly produced at 30 AU, and these two species jointly account for 40% of the elemental carbon, with CH_4 accounting for an additional 50%, and the remaining 10% is in other molecules, such as CH_3OH (further discussed in Section 3.4.2) by 7 Myr. H_2O ice accounts for more than 99% of the elemental oxygen.

Overall, it is evident from these figures and discussion that chemical evolution continues up to (at least) 7 Myr. That was also a conclusion of Kamp et al. (2013). Under the conditions and assumptions presented here, the majority of changes to the chemical abundances take place between 0.5 and 7 Myr, and as in evident from Fig. 3.5 and Fig. 3.6, the changes are significant (from factors of a few to orders of magnitude changes for all species).

3.3.3 Varying disk masses

Figs. 3.5 and 3.6 present radial abundance distributions at different evolutionary timesteps for CO, CO_2, CH_4, H_2O and O_2. Left panels are for the low mass evolving disk structure. Right panels are for the high mass evolving disk structure.

Overall, when comparing the two disk masses for all five species it is seen that there are no significant differences in the abundance evolutions. However, the temperature structures are different, thus the icelines are located and shifted by different radial distances (see Section 3.3.1). Only in the case for CO_2 gas, is the evolution in the innermost disk (inside 0.4 AU) very different (by up to 3 orders of magnitude). This is due to the high temperatures and densities here, causing the abundance to be dictated by chemical equilibrium. This is more pronounced for the 0.55 MMSN disk, which is warmer in the inner tenth of an AU, than the 0.1 MMSN disk.

3.3.4 Importance of initial abundances: inheritance vs reset

The choice of initial abundances was shown in Paper 1 to have a large effect on the final abundances after 1 Myr of evolution. In Fig. 3.3, panels b and d show abundances after 7 Myr evolution for an evolving disk with a high level of ionisation, with panel b) assuming a reset scenario for the initial chemical abundance, and panel d) assuming the initial abundances to be inherited. Since both cases have assumed the same evolving physical structure, the icelines are identically located in both panels.

Inside the H_2O iceline at ∼0.5 AU, where all species are in the gas phase, similar abundance levels are seen for H_2O, CO and CO_2, in both scenarios. CH_4 gas, on the contrary, is absent from the inner disk in the reset scenario. In relation to this absence, a destruction of CH_4 gas is evident in the inheritance scenario as seen at 1 AU in Fig. 3.7a, which indicates that CH_4 is being continuously destroyed in the gas phase, a destruction happening more slowly inside the H_2O iceline in Fig. 3.3, than it does outside that iceline.

Redirecting focus from the inner to the outer disk, the abundances of the ices outside the O_2 iceline at around 10 AU are very similar (at 30 AU CO_2 is a factor of two different, CH_4 is ∼10% different, and H_2O is only 1% different) when comparing the reset and the inheritance scenarios in Fig. 3.3 b and d for chemical evolution by 7 Myr. Indeed, outside 10 AU the choice of initial abundances seems irrelevant for the resulting abundances, given a long enough evolution time. In other words: in this region, which is very relevant for comet formation, chemical steady state is close, and the fingerprint of the interstellar chemical abundances is erased if the gas disk lasts for 7 Myr.

The inner (mostly) gaseous midplane, and the outer (mostly) icy midplane produce similar abundance ratios independent of the choice of initial abundances. The intermediate region in Fig. 3.3 b and d, roughly between the H_2O and O_2 icelines at 0.5 AU and 10 AU, is quite different. The dominant gas phase species are CO and O_2, both at approximately the same abundance level within a factor of 2, in both the reset and the inheritance scenarios. H_2O and CO_2 ices, however, are one-to-two orders of magnitude lower for the reset scenario than for the inheritance scenario. Looking into the time evolution of CO, O_2, H_2O and CO_2 in the inheritance scenario with high ionisation at 5 AU shown in Fig. 3.7b, it is evident that none of these species have yet reached steady state (although it is close) by 7 Myr. Additional evolution time would therefore likely bring the abundances of H_2O and CO_2 ices in the inheritance scenario further down, and CO and O_2 gases further up, similar to the plot for the reset scenario in Fig. 3.3b.

3.3.5 O_2 as a significant disk midplane molecule

Molecular oxygen is often not considered to be a dominant molecule in planet formation models. The detection of a high abundance of O_2 ice to H_2O ice of $3.8^{+}_{-}0.85$% on Comet 67P reported by Bieler et al. (2015) has triggered models to explain the origin of this molecular oxygen (see Mousis et al. 2016; Taquet et al. 2016).

In disk chemistry models by Walsh et al. (2015) O_2 is abundantly produced in the intermediate layers of a disk. Here, the O_2 evolution in the midplane is traced up to 7 Myr. Fig. 3.6 shows abundance profiles for O_2 at different timesteps for the inheritance scenario. It is evident that between the H_2O and O_2 icelines, the abundance of O_2 gas continuously increases with time. O_2 is produced on the grain surfaces through the following reaction pathway:

$$iH_2S \xrightarrow{H} iHS \xrightarrow{O} iSO \xrightarrow{O} iSO_2 \xrightarrow{H} iO_2, \tag{3.6}$$

O_2 ice subsequently desorbs (if inside the O_2 iceline), and steadily builds up a high abundance of $\sim 10^{-4}$ wrt H_2O over 7 Myr evolution. The initial abundance of H_2S is 6×10^{-6} (20 times lower than the O_2 gas abundance by 7 Myr), and the HS molecule left over from the last step in the reaction chain above is recycled for conversion of more oxygen atoms into O_2 via the second step above. Henceforth, the initial abundance of sulphur is seemingly irrelevant for the final abundance of O_2, since the sulphur merely acts as a catalyst for the conversion of oxygen atoms into molecular oxygen.

3.3.6 Caveats of model assumptions

3.3.6.1 Choice of grain-surface reaction parameters

An important part of the chemical evolution presented here is caused by grain-surface chemistry. The importance of grain-surface chemistry was also highlighted in Paper 1, as well as in Walsh et al. (2014). However, the grain-surface reactions are sensitive to the choice of grain surface parameters. In this work, the barrier height for quantum tunnelling $b_{\rm qt}$ between grain surface sites has been set to $b_{\rm qt} = 1$ Ång, and the ratio of diffusion energy $E_{\rm diff}$ between grain surface sites and molecular binding energy $E_{\rm des}$ has been set to $E_{\rm diff}/E_{\rm des} = 0.5$. This is a conservative take where most grain-surface chemistry happens at moderate temperatures ($\gtrsim$ 25K). If $b_{\rm qt}$ was to be increased, the hydrogenation reactions would be slowed down, and vice versa for decreasing $b_{\rm qt}$. If $E_{\rm diff}/E_{\rm des}$ was to be decreased, then grain-surface radical-radical recombination could happen at lower temperatures. Such changes would affect chemical evolution, but an exploration of this parameter space is left for future work.

3.3.6.2 Dependence on ionisation

As highlighted in several previous studies, including Paper 1, Aikawa et al. (1996), Helling et al. (2014), Cleeves et al. (2014b) and Walsh et al. (2015), the chemical evolution taking place in protoplanetary disk midplanes is highly dependent on the degree of ionisation. The timescale of chemical evolution has been found in this work to scale inversely with the ionisation level. It is found that an ionisation level 10 times higher than that presented here will shorten the chemical evolution time scale 10 times, and vice versa.

In the situation where the midplane is significantly shielded from CR ionisation, for example by a high column density attenuating the CR particles, or by magnetic

field effects (see Cleeves et al. 2013a), then no significant chemical evolution takes place over the disk lifetime of 7 Myr. In the case of complete exclusion of CRs, this is seen in Fig. 3.3a, where the ionisation level is solely based on SLR decay products in the midplane. This ionisation level starts out between 10^{-19} and 10^{-18} s^{-1}, and drops orders of magnitude over the evolution time, as seen in Fig. 3.1c. Thus, for midplane ionisation levels of a few times 10^{-19} s^{-1} or lower, 7 Myr of evolution is insufficient time for the ionisation to cause significant chemical evolution. Along the same lines, if chemical steady state is to be achieved within 1 Myr of evolution, in the outer disk, then the ionisation level has be $\sim 10^{-16} s^{-1}$ (about ten times higher than assumed for high ionisation in the outer disk here) or higher. The effects of X-ray ionisation on disk chemistry in planet-forming midplanes will be explored in future work.

3.3.6.3 Choice of grain sizes and distribution

Like in Paper 1, the physical grain parameters have been kept constant throughout the evolution time. However, in real disks several processes take place for grains during the lifetime of a disk, all of which could change the grain parameters adopted here. These processes include grain settling to the midplane, agglomeration and fragmentation, as well as grain radial drift. The physics of grain evolution has been studied extensively (see e.g. Birnstiel et al. 2016; Kataoka et al. 2014; Okuzumi et al. 2012, and references therein).

One way of theoretically investigating the effects of changing dust parameters, is to simply adopt a different dust size as input for the models. Increasing the dust size will reduce the total surface area-to-mass ratio, prolonging the freeze-out and desorption timescales, and vice versa for decreasing dust size. However, the grain-surface chemical evolution of the ices will likely simply be slowed down for a reduced surface area-to-mass ratio, and sped up for an increased surface area-to-mass ratio. Thus, the same chemical effects might be seen, just on different timescales (see Section 3.2.3). Recent work by Facchini et al. (2017) found that the dust growth timescale in the disk midplane is significantly longer (3 orders of magnitude) than the timescale of freeze out and desorption, for example for CO.

The dust growth timescale is, however, still shorter than the timescale for chemical evolution. Although this means that the grain size utilised for grain-surface reactions here in fact is not static (as assumed) over the chemical evolution time, the grain growth might not affect the chemistry that differently from what has been presented in this work: grain growth likely does not accumulate small compact spherical grains into larger and compact grains with a predictable change in grain surface areas. Rather the growth may lead to fluffy aggregates or grains with uneven surfaces (Blum & Wurm 2008). Hence, the change to the grain surface area-to-mass ratio may not be significant. If grains are subsequently compactified resulting in a reduced grain surface area-to-mass ratio, it may simply lead to the aforementioned longer timescale for grain-surface reactions.

3.4 Discussion

3.4.1 Iceline shifts: comparison to other studies

The positions and movements of volatile icelines have been subject to much investigation recently, see Piso et al. (2015), Ali-Dib (2017), Öberg & Bergin (2016), and references therein. Piso et al. (2015) modelled shifting iceline positions over 3 Myr assuming both radial drift of particles, and a viscous disk with gas accretion. In these models, they found shifted icelines of volatiles compared to a static disk situation. These shifts, however, are not caused by evolving temperature structures as is the case in the present work, but by radial drift of different sized particles. Thus, radial drift can also shift the icelines independently by setting different radii for desorption of icy grain mantles depending on the sizes of the grains. Despite these differences, both evolving temperatures and radial drift of particles act to shift the icelines inwards. Piso et al. (2015) found that the H_2O iceline was shifted inwards by up to 40%, whereas the icelines of CO_2 and CO were shifted inwards by up to 60% and 50%, respectively. These shifts are comparable in size to those found in this work, but not caused by the same mechanism. Thus, the combination of different physical disk evolution effects could possibly result in even larger iceline shifts.

3.4.2 What happens to gaseous CO?

The dominant ices in the outer disk midplane at the end of evolution are all stable molecules, for both choices of initial abundances. For the reset scenario this results from hydrogenation of carbon and oxygen atoms on the grain surfaces, whereas for the inheritance scenario, the oxygen and carbon atoms are mainly supplied from the CR-induced photodissociation of CO and CO_2.

CO gas has been studied extensively through observations of protoplanetary disks. As noted in the introduction several observational studies have found surprisingly weak CO emission from disks, more than can be accounted for by simple freeze-out and photodissociation. In particular for TW Hya, Schwarz et al. (2016) reported depletion by two orders of magnitude through CO isotopologue observations, and Zhang et al. (2017) recently determined the CO midplane iceline with an associated freeze-out temperature of 27^{+3}_{-2} K, higher than expected from the binding energy of pure CO ice ($\sim$ 21K). Zhang et al. (2017) attributed this higher freeze-out temperature to CO being frozen out onto a mix of H_2O and CO_2 ices. In relation to these reported depletions, the findings for CO in this work are interesting. The outer icy disk here is not the only region lacking CO. A decrease in CO gas abundance is also seen to take place for the inheritance scenario for the region between the CO_2 and the CO icelines in Fig. 3.5c around $\sim$3 AU, until 2 Myr of evolution. The effect of CO freezing out and subsequently reacting into CO_2 and chemically converting into other species such as HCN and C_2H_6 means that CO gas is effectively reduced in abundance by up to 2 orders of magnitude, within the CO iceline. This reduction in CO gas, however, is only happening so long as the CR-induced photon fluence is low enough to not dissociate CO_2 into CO on

the grains, as discussed in Section 3.3.2. The models show that chemical CO gas depletion in a disk midplane could therefore be a temporary effect. As discussed earlier, the timescale of CO depletion, which lasts until the abundance inversion takes place, will depend on the ionisation conditions, and thus the density, in the midplane, with a lower ionisation level prolonging the CO depletion timescale.

An additional large drop in CO gas abundance is seen starting by 5 Myr at ∼10 AU for the 0.1 MMSN disk, see Fig. 3.5c (the inheritance scenario). Thus, if one was to determine the CO iceline from depletion of gas-phase CO isotopologues in an old disk like TW Hya, the desorption temperature for CO in this model could appear to be at ∼29 K (similar to the freeze-out temperature for CO found by Zhang et al. 2017) at ∼10 AU, rather than at ∼21 K at 16 AU, for the 0.1 MMSN disk. This appearance of the CO iceline to be at a higher temperature and smaller radius than prescribed by the CO binding energy is due to the chemical depletion of CO gas, happening outside the O_2 iceline, resulting in a "fake" CO iceline. A fake CO iceline was also seen in Paper 1, although that was different from the one here: in Paper 1 the fake iceline was seen outside the CO_2 iceline by 1 Myr, thus at a smaller radius and at an earlier evolutionary stage. The fake iceline seen here coincides with the thermal iceline of O_2, and the reduction in CO gas abundance outside 10 AU is due to the freeze-out of O_2. O_2 ice is hydrogenated into HO_2 ice on the grains, and subsequently dissociated into OH ice. This OH, in turn, reacts with colliding CO to produce CO_2 ice, thereby reducing the CO gas abundance. This effect will be further investigated in future work.

In Fig. 3.8 the abundance evolution of the main carbon-bearing volatiles, CO, CO_2, CH_4, HCN, C_2H_6, CH_3OH are plotted at 10, 20 and 30 AU, alongside "Other", which accounts for the carbon that is not contained in the plotted species. For all three radii, the main contributors to Other are HCO and HNC, as well as complex molecules and hydrocarbons such as C_3H_4, CH_2CO, H_2CCO, CH_3OCH_3 and CH_3COCH_3, which all show abundances $> 10^{-7}$ with respect to H nuclei. It is evident at 10 AU in panel a that CO_2 locks up the majority of the carbon, through the grain-surface reaction with CO and OH, and CO gas is seen to decrease in abundance. Here, C_2H_6 ice is accounting for about 10% of the elemental carbon, with less than 10% of the carbon locked up in Other.

At 20 AU in panel b the picture looks different after 7 Myr. The Other species take up about 30% of the elemental carbon, which is more than any single species alone. At 20 AU, the temperature decreases from about 30 to 18 K during the evolution time. That means that at the end of evolution, all molecules are frozen out onto the grains, and due to the temperature regime, most species are mobile on the grain surfaces, and able to react to form larger complex molecules, like those included in the Other category.

In panel c at 30 AU, the temperature goes down to 15 K after 7 Myr, meaning all species, including H atoms, can stick to the grains. H atoms, along with lowered mobility of molecules on the grain surfaces, means that hydrogenation reactions become dominant. Thus carbon is locked up in CH_4, HCN and C_2H_6 and CH_3OH, with only around 10% elemental carbon in Other species.

Recent work by Yu et al. (2016, 2017) also find this chemical conversion of CO into more complex ices using an evolving disk model in the midplane. Their disks

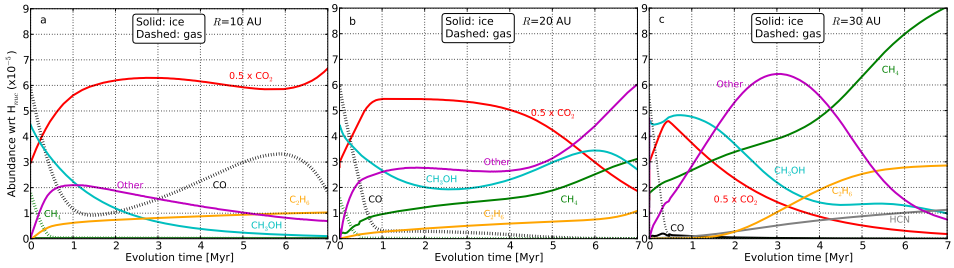

Figure 3.8: Time evolution of the main volatile species at 10, 20 and 30 AU, plotted on linear scales to ease comparison to Fig. 7 of Yu et al. (2016) and Fig. 2 of Yu et al. (2017). The H_2O ice abundance in these plots is at least 80. A rapid decrease of gaseous CO is seen within 1 Myr. The CO_2 ice is plotted at half its abundance to emphasize the steep drop for CO gas before 1 Myr at all three radii.

have temperatures of ∼35-40 K at 20-30 AU. They also found CO destruction in the disk midplane, by modelling chemical evolution using the older RATE06 network. However, their models produce the C_2H_5 radical in the ice, which in this work is hydrogenated into C_2H_6 ice. Also, they find only about 5% increase in their CO_2 ice abundance, indicating that the CO gas destruction is not feeding the production of CO_2 ice on the grains. Reboussin et al. (2015) did see conversion of CO gas to amongst other CO_2 and C_2H_6 ices on the grains using the NAUTILUS model, in agreement with this work. Besides these studies, models focussing on analysis of chemical evolution in disk midplanes are limited. Cridland et al. (2017) used a chemical network to evolve chemistry in the midplane before forming planets out of the material, but did not focus on the chemical response to the (varying) physical conditions and reaction types dominating in the midplane. Helling et al. (2014) found a different effect of chemistry on the C/O ratios that what is seen in this work, because their treatment of grain-surface chemistry was simpler.

3.4.3 Evolving elemental ratios

An important aspect of chemical evolution in a disk midplane is the relation to the composition of exoplanets, particularly their atmospheres. In Paper 1 it was shown that unless the inheritance scenario with low ionisation was considered, the C/O ratio of the chosen model setup changed over the course of 1 Myr of evolution. It was demonstrated that the C/O ratio radial stepfunction in Fig. 1 of Öberg et al. (2011b) was modified. In this work, the evolution of the C/O ratios are traced up to 7 Myr instead of 1 Myr, and the effects of both chemical evolution and the evolving temperature structure are shown.

The longer timescale causes larger changes to the dominant volatile abundances and significant changes to the traditional C/O ratio stepfunction, even more than what was seen Paper 1. The larger abundance changes are apparent in Fig. 3.7, where changes of up to two orders of magnitude are seen from 1-7 Myr, thus significantly larger than the changes happening until 1 Myr (the case from Fig. 4

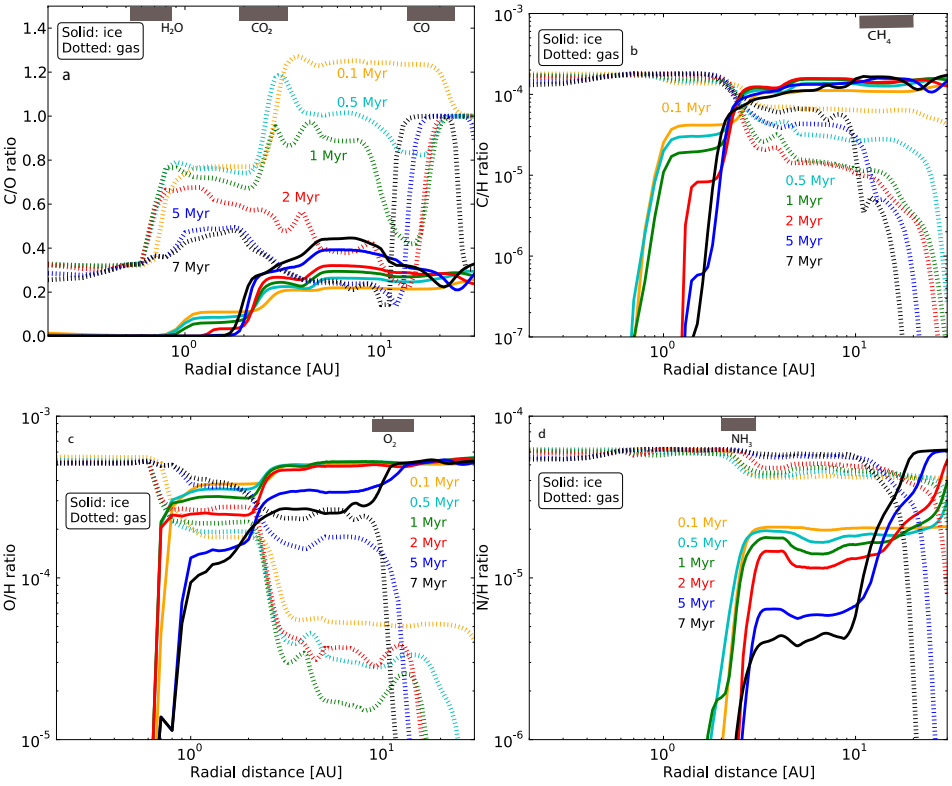

Figure 3.9: Elemental ratios of carbon, oxygen and nitrogen in gas and ice as a function of radius, at six timesteps: 0.1, 0.5, 1, 2, 5 and 7 Myr. Panel a: C/O ratios. Panel b: C/H ratios. Panel c: O/H ratios. Panel d: N/H ratios. Gas profiles are dashed, ice profiles are solid. The y-axes have different scales, in particular in panel 1 the y-axis is linear. The grey boxes indicate the radial regions that the iceline of a volatile move over during the evolution.

in Paper 1). Considering the more realistic scenario of an evolving, cooling disk (see Fig. 3.3 panels b and d) rather than a static one (Fig. 3.3 panel c), similar trends in chemical abundance changes to the static case are seen. The main effect is that volatile icelines are shifted inwards with time, because the disks cool. The physical conditions at each timestep of the simulations determine the chemical composition at that timestep. This holds for all scenarios and tells us that the chemical timescale is faster than the physical timescale in these models, and that a static disk model may be sufficient for modelling chemistry. However, a planet forming in the crossing-zone of an iceline may experience a drastic change to the composition of accreting material over time.

In Fig. 3.9a, b, c and d, the evolving C/O, C/H, and O/H and N/H ratios, respectively, in gas and ice are presented for the evolving 0.1 MMSN disk. The yellow profiles are at 0.1 Myr only, where as yet no significant chemical evolution has taken place, and the ratios are therefore the canonical values corresponding to the input abundances. Thus, for C/O for example, this yellow profile resembles the stepfunction from Öberg et al. (2011b).

For the C/O ratio evolution in panel a, it is clear at later times that the evolving chemistry has caused the C/O ratios in gas and ice to change. At 5 AU, the C/O ratio in the gas drops from 1.2 to 0.3 over the course of 7 Myr. For the ice at the same distance, the C/O ratio increases from 0.2 to almost 0.5, thus making the ice between 3 and 10 AU more carbon rich than the gas. By 7 Myr the C/O ratios in both gas and ice are below 0.5, and thereby the C/O gas and ice ratio profiles are significantly different than the Öberg et al. (2011b) stepfunction, and the profiles correlate with the C/O ratio profiles for the reset scenario from Paper 1. That indicates that steady state is close after 7 Myr of evolution with inherited abundances. It is expected that so long as the initial C/O<1, the same trends would be seen in C/O ratio evolutions, if a different set of elemental ratios were chosen.

The C/H evolution in panel b shows a significant turnover at the CO_2 iceline at 2 AU, with more carbon being contained in gas than in ice inside the iceline, and vice versa outside of it. This iceline is thus critical for the metallicity of the material, and has important implications for the carbon content of the forming planets. Besides this distinct iceline, other features of the C/H ratios are the decreasing level in ice between the CH_3OH (at 1.3 AU by 7 Myr) and the CO_2 icelines. This is due to the destruction of CH_3OH on the grain surfaces, as well as the CO and CO_2 dependent interconversion of C/H ratio in gas and ice between the CO_2 and the O_2 icelines (see Section 3.3.2).

Panel c features the O/H ratio evolution. Here the H_2O, CO_2 and O_2 icelines at ∼0.8, 2 and 10 AU, outline the radii of main changes. Between the H_2O and CO_2 icelines, the ice starts as two times more oxygen rich than the gas, but after 7 Myr, the gas can become 3 times more oxygen rich than the ice. Between the CO_2 and O_2 icelines, the ice starts an order of magnitude more oxygen rich than the gas, but after 7 Myr, the gas and ice are equally oxygen rich. This is due to the increasing abundance of gaseous O_2.

Although this work so far has focussed on carbon and oxygen-bearing species, for completeness the evolving nitrogen content in the material is shown in panel d.

The decreasing nitrogen ice content between 2 and 8 AU is due to the destruction of NH_3 ice (iceline at $\sim$ 2.5AU) in this region, which causes an increased nitrogen level in the gas, with N_2 (iceline at $\sim$20 AU) becoming the main nitrogen gas carrier (see Paper 1 for further discussion). Schwarz & Bergin (2014) also modelled the evolution of nitrogen-bearing species in a disk, and found different partitionings of the nitrogen into HCN, NH_3 and N_2, depending on their model assumptions.

3.4.4 Impact for planet formation and planet atmospheric composition

Recent years has seen enormous effort put into the field of planet formation and planet population synthesis models. Physical effects like grain growth, migration and radial drift, and a planet's acquisition of an atmosphere from a disk have been included in increasingly sophisticated models (see e.g. Lambrechts & Johansen 2012; Alibert et al. 2013; Ali-Dib et al. 2014; Madhusudhan et al. 2014; Benz et al. 2014; Bitsch & Johansen 2016, and references therein). Planet population synthesis models however have neglected chemical evolution, although Cridland et al. (2016, 2017) did consider kinetic chemistry to model the material that go into forming planetary atmospheres.

Mordasini et al. (2016) conducted planet formation synthesis models introducing a "chain" of models to self-consistently predict the atmospheric transmission spectra of a hot Jupiter exoplanet from modelling the formation of the planet as it forms in the disk. One prediction from their work was that for hot Jupiters less massive than a few $M_{\rm Jup}$, heavy element enrichment in the envelope from impacting planetesimal polluters dominate the final atmospheric composition over the enrichment obtained from gas accretion. This is interesting in the context of the findings in this work, that the C/O, C/H, O/H and N/H ratios in both gas and ice evolve over time. For hot Jupiters, it is thus not necessarily the heavy element content of the gas in the disk that will determine the planet's resulting atmospheric elemental ratios.

The findings of this work, that chemistry matters in disk midplanes under certain assumptions, may complicate the challenge of relating observed exoplanet atmospheric elemental ratios to the formation history of the planet. Not only is it shown in this paper that chemical evolution can change the radial elemental ratios in gas and ice over time, but as Mordasini et al. (2016) stated, the disk material - gas or ice - that the atmosphere of the planet is formed from, may have a mixed origin.

The result of these two effects can, however, be explored through modelling. By having a planet atmosphere form from different relative contributions of gaseous and icy material in the disk, and by assuming (as a start) one of the time evolved elemental ratio abundances presented here, the final elemental ratio in the atmosphere, and the resulting transmission spectrum, can be generated. It can then be assessed whether or not the effects are observable, with current or future observational facilities. This would also be a first step to better implement disk chemistry into the "chain" of models, as requested by Mordasini et al. (2016). First attempts at this were indeed carried out by Cridland et al. (2016, 2017). However, they only

considered planets formed inside 4 AU. An expansion of their work would thus be welcomed.

Lastly, the outer disk volatile ice abundances presented here obviously inspire a comparison to observed abundances in comets in the Solar System, in order to constrain the models with Solar System conditions. Such a comparison is currently in progress and will be published in an upcoming paper.

3.5 Summary

In this paper, the implications of chemistry in evolving disk midplanes on the composition of planet-forming material have been investigated.

Chemical evolution is an ionisation-driven long-term effect, which for the disk structures considered here becomes significant after a few times 10^5 yrs of evolution, and goes on until at least 7 Myr, in the region between the H_2O and O_2 icelines ($\sim$0.5-10 AU, for the 0.1 MMSN disk). Considering the more realistic scenario of an evolving, cooling disk rather than a static one, similar trends in chemical abundance changes to the static case are seen. The main effect is that volatile icelines are shifted inwards with time, because the disks cool. Hence, using a static disk structure representative of the conditions in the disk during the accretion epoch of a forming planet may be sufficient for modelling chemistry. Changes of similar magnitudes are seen for all scenarios for the 0.1 MMSN disk and the 0.55 MMSN disk. That means that assuming different disk masses does not significantly affect the chemical evolution. However, higher mass disks than those studied here should be explored.

After 7 Myr of evolution, inside the H_2O iceline and outside the O_2 iceline, the fingerprint of interstellar abundances has been erased, for the high ionisation level, and chemical steady state has been achieved. That is to say, for ice in the outer disk, it becomes irrelevant whether the inheritance or the reset scenario is assumed. In the inner tenths of an AU, chemical equilibrium conditions are likely achieved. An abundance inversion is seen for CO and CO_2 between the CO_2 and CO icelines, where the abundance evolutions invert at a time which depends on the ionisation level. For the high ionisation level, CO gas reaches its minimum abundance by $\sim$1.6 Myr, and CO_2 reaches its maximum abundance at $\sim$2.5 Myr.

By 7 Myr CO gas is seen to deplete inside the CO thermal iceline, from outside the O_2 iceline, which could mimic the iceline being further in and at warmer temperatures than the CO binding energy prescribes. Ice species such as HCN and C_2H_6 become important carbon-bearing species in the outer disk by a few Myr. Between the H_2O and O_2 icelines, O_2 gas is the dominant oxygen bearing species. Just outside the O_2 iceline, it is warm enough for molecules to move on the grain surfaces, but not cold enough for H atoms stick on the grains. This results in the production of larger, more complex molecules on the grain surfaces.

Chemical evolution changes the elemental ratios in the gas and ice significantly over time. This results in a region where the ice has a higher C/O ratio than the gas. In order to relate observed atmospheric C/O ratios in exoplanets to formation locations and conditions in the disk midplane, chemical evolution is

important to consider, independent on whether an atmosphere is built primarily from gas accretion or from planetesimal impacts. Generally, chemical evolution acts to significantly lower the C/O ratio of gas, such that neither the ratio in gas or in ice is at or above unity, but rather the C/O ratios in both gas and ice evolve to be below 0.5 (given an overall C/O ratio of 0.34).

If planet formation lasts for longer than a few times 10^5 yrs in the disk midplane and cosmic ray ionisation is present, then the chemical abundances and elemental ratios in gas and ice will change alongside with planet formation. Henceforth, chemical evolution needs to be addressed when predicting the chemical makeup of planets and their atmospheres, as well as when inferring formation locations of exoplanets based on their observed atmospheric elemental ratios.

Acknowledgements: The authors thank Amaury Thiabaud and Ulysses Marboeuf for making their disk density and temperature profile available and for many useful discussions. The authors also thank Nikku Madhusudhan for a helpful discussion regarding the C/O ratio evolution and its effect on the metallicity, and the referee for useful comments that improved the presentation of the paper. Astrochemistry in Leiden is supported by the European Union A-ERC grant 291141 CHEMPLAN, by the Netherlands Research School for Astronomy (NOVA), and by a Royal Netherlands Academy of Arts and Sciences (KNAW) professor prise. CW also acknowledges the Netherlands Organisation for Scientific Research (NWO, grant 639.041.335) and the University of Leeds for financial support.

3.A Physical structure for 0.55 MMSN disk

Figure 4.1 show the evolving physical structure for the 0.55 MMSN disk, featuring temperature, density and ionisation level evolution.

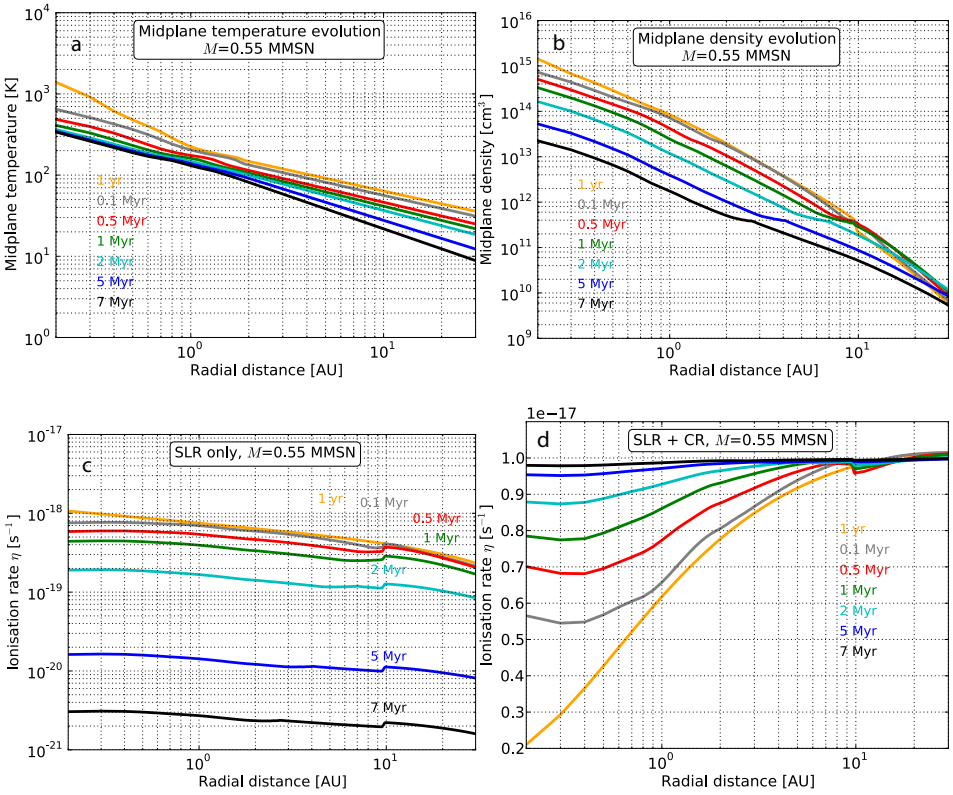

Figure 3.10: Same as for Fig. 3.1, but for the 0.55 MMSN disk.

4 Formation of cometary O_2 ice and related ice species on grain surfaces in the midplane of the pre-Solar nebula

C. Eistrup & C. Walsh
Accepted for publication in Astronomy and Astrophysics

Abstract - The detection of abundant O_2 at 1-10% relative to H_2O ice in the comae of comets 1P/Halley and 67P/Churyumov-Gerasimenko, motivated attempts to explain the origin of the high O_2 ice abundance. Recent chemical modelling of the outer, colder regions of a protoplanetary disk midplane has shown production of O_2 ice at the same abundance as that measured in the comet.

Methods: A thorough investigation is carried out to constrain the conditions under which O_2 ice could have been produced through kinetic chemistry in the pre-Solar nebula midplane. An updated chemical kinetics code is utilised to evolve chemistry under pre-Solar nebula midplane conditions. Four different chemical starting conditions, and the effects of various chemical parameters are tested.

Results: Using the fiducial network, and for either reset conditions (atomic initial abundances) or atomic oxygen only conditions, the abundance level of O_2 ice measured in the comets can be reproduced at an intermediate time, after 0.1-2 Myr of evolution, depending on ionisation level. When including O_3 chemistry, the abundance of O_2 ice is much lower than the cometary abundance (by several orders of magnitude). H_2O_2 and O_3 ices are abundantly produced (at around the level of O_2 ice) in disagreement with their respective abundances or upper limits from observations of comet 67P. Upon closer investigation of the parameter space, and varying parameters for grain-surface chemistry, it is found that for temperatures 15-25 K, densities of $10^9 - 10^{10}$ cm^{-3}, and a barrier for quantum tunnelling set to 2 Å, the measured level of O_2 ice can be reproduced with the new chemical network, including an updated binding energy for atomic oxygen (1660K). However, the abundances of H_2O_2 and O_3 ices still disagree with the observations. A larger activation energy for the $O + O_2 \longrightarrow O_3$ reaction (E_{act}>1000 K) helps to reproduce the non-detection of O_3 ice in the comet, as well as reproducing the observed abundances of H_2O_2 and O_2 ices. The only other case where the O_2 ice matches the observed abundance, and O_3 and H_2O_2 ice are lower, is the case when starting with an appreciable amount of oxygen locked in O_2.

Conclusions: The parameter space investigation revealed a sweet spot for production of O_2 ice at an abundance matching those in 67P and 1P, and O_3 and H_2O_2 ices abundances matching those in 67P. This means that there is a radial region in the pre-Solar nebula from 120-150 AU, within which O_2 could have been produced in-situ via ice chemistry on grain surfaces. However, it is apparent that there is a high degree of sensitivity of the chemistry to the assumed chemical parameters (e.g. binding energy, activation barrier width, and quantum tunnelling barrier). Hence, because the more likely scenario starting with a percentage of elemental oxygen locked in O_2 also reproduces the O_2 ice abundance in 67P at early stages, this supports previous suggestions that the cometary O_2 ice could have a primordial origin.

4.1 Introduction

The detection of abundant molecular oxygen at 1-10% (average 3.8±0.85%) relative to H_2O ice in the coma of comet 67P/Churyumov-Gerasimenko (herinafter 67P: Bieler et al. 2015) came as a surprise, as it was the first detection of O_2 in a comet. This was not expected because O_2 ice has been found to be efficiently converted to H_2O ice in laboratory studies under interstellar conditions (e.g. Ioppolo et al. 2008). Subsequent to this detection, a re-analysis of Comet 1P/Halley data from the *Giotto* mission (Rubin et al. 2015) indicated a similar O_2/H_2O ice ratio (3.8±1.7%), suggesting that indeed O_2 ice may be a common ice species in Solar System comets. These detections thus prompted speculation as to the chemical origin of the O_2 ice. Taquet et al. (2016) modelled the chemical evolution of material from the pre-stellar core stage to the midplane of the formed protoplanetary disk, and found that O_2 ice can be produced at the early stages and survive the transport to the disk midplane. Mousis et al. (2016) found that, if O_2 ice is formed from radiolysis of H_2O ice through the reaction $2\,\mathrm{i}H_2O \xrightarrow{\gamma} 2\,\mathrm{i}H_2 + \mathrm{i}O_2$ (where "i" denotes a molecule in the ice form), then this likely did not happen during the pre-Solar nebula (PSN) disk phase, but rather in the parent cloud, thus supporting the findings of Taquet et al. (2016). Dulieu et al. (2017) performed laboratory experiments to investigate if dismutation of H_2O_2 ice ($2\,\mathrm{i}H_2O_2 \longrightarrow 2\,\mathrm{i}H_2O + \mathrm{i}O_2$) on the cometary surface could be the origin of the O_2 detection. However, this explanation requires a high initial abundance of H_2O_2 ice relative to H_2O ice (twice the detected abundance of O_2, or ∼7%), and a high efficiency for the conversion of H_2O_2 to O_2 in order to match the low detected level of H_2O_2 relative to O_2 of $\sim 6 \times 10^{-4}$. O_3 ice, a molecule chemically related to O_2, H_2O_2 and H_2O, was not detected in the coma of comet 67P, and has an upper limit of 10^{-6} with respect to H_2O ice. It is worth to note here that molecular oxygen is also produced when CO_2 ice is exposed to far-UV radiation (see e.g. Martín-Doménech et al. 2015). However, although this may be viable chemical route to O_2 ice, it does not explain the strong association between the production rates for H_2O and O_2 seen for comet 67P (Bieler et al. 2015). On the other hand, experiments investigating chemistry in CO_2 ice irradiated with 5 keV ions (H^+ and He^+) and electrons (Ennis et al. 2011; Jones et al. 2014) favour the production of ozone (O_3) over molecular oxygen (O_2). These experiments mimic the conditions that ices are exposed to in the outer Solar System, and upon cosmic ray impact.

In Eistrup et al. (2016) (hereafter Paper 1), it was found through chemical kinetic modelling of protoplanetary disk midplanes that O_2 ice could be produced to match the measured cometary abundance by 1 Myr, if the chemical starting conditions were purely atomised and the ionisation level was low ($\sim 10^{-19}$ s^{-1}). Purely atomised starting conditions reflect the assumption that an energetic stellar outburst or accretion heating close to the star could have fully dissociated all volatiles in the midplane, and low ionisation means that the only ionisation source in the midplane is the decay of short-lived radionuclides. This latter scenario assumes that a magnetic field could have shielded the midplane from cosmic rays (as proposed by Cleeves et al. 2013a). This finding sparked interest into whether or not the chemical origin of the O_2 ice could be chemical processing of the icy

material in the pre-Solar nebular (PSN) disk midplane. Most recently Mousis et al. (2018) explored the possibility that turbulent transport of icy grains between the disk midplane and the upper layers of the disk exposed the grains to a stronger cosmic-ray flux thus chemically processing H_2O ice to produce O_2 ice via radiolysis. They find that on a 10 Myr timescale O_2 ice in the midplane remains underproduced by up to two orders of magnitude relative to the abundances observed in the comets. Eistrup et al. (2018) also found that this abundance for O_2 ice be reached on similarly long timescales.

Based on the promising results in Paper 1, this work investigates under which conditions in the PSN midplane O_2 ice could have been chemically produced in-situ to reach the observed abundance level in the comets. This work differs from that in Mousis et al. (2018) in that a full chemical kinetics network is used that follows the chemical connection between H_2O, O_2 and related ice species. A disk model more suitable for the PSN is used, and a more thorough investigation of the O_2 kinetic ice chemistry is conducted. Initial chemical abundances, physical conditions, parameters for grain-surface chemistry, as well as the inclusion of O_3 in the chemical network are all tested to see the effect on the O_2 ice production and abundance.

4.2 Methods

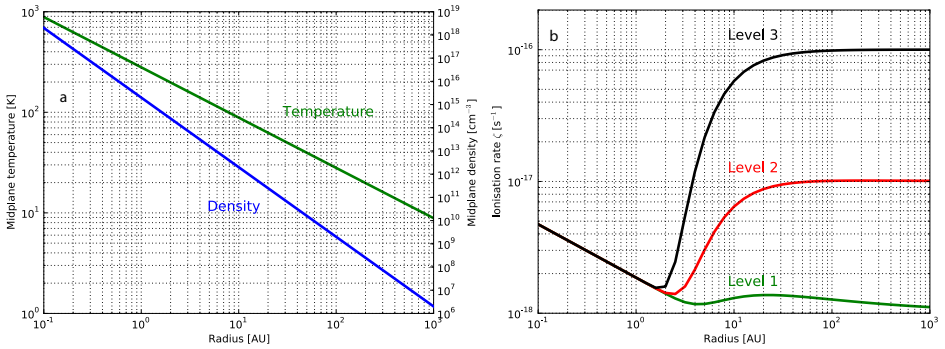

Figure 4.1: a): midplane temperature and density profiles for the pre-Solar nebula. b): ionisation levels utilised in the models. Level 1: SLRs only. Level 2: SLRs + fiducial CRs. Level 3: SLRs + enhanced CRs.

In order to investigate the chemical evolution in the PSN midplane, the physical disk model for the PSN from Hayashi (1981) is utilised. This disk model estimates the structure and mass of the PSN, assuming the total current mass of the planets in the Solar System to be distributed as dust and gas in a protoplanetary disk in equilibrium. The mass of this nebula is $M_{\rm MMSN}$=0.08 $M_\odot$, based on integrating

the PSN surface density structure from Aikawa et al. (1997)[1] from 0.1-1000 AU. This provides temperature and density profiles for the disk midplane, as well as the surface density profile. The latter is used to calculate the attenuation of cosmic rays (herefrom CRs) impinging on the disk, thereby estimating the contribution of CRs to the disk midplane ionisation, as was discussed in detail in Paper 1. The disk structure is static in time, which was shown in Eistrup et al. (2018) to not cause a significantly different chemical evolution from an evolving disk structure, apart from the inward shifting of molecular icelines in response to decreasing temperature with time.

In Figure 4.1a this PSN midplane temperature and density structure is plotted from 0.1-1000 AU. The temperature decreases by two orders of magnitude from ∼900 K to 9 K from the inner to the outer disk, and the density drops from 10^{18} cm^{-3} to 10^{6} cm^{-3}. The dynamic ranges, especially in density, are thus larger than what was used in Paper 1. However, this disk is also extending out to 1000 AU instead of 30 AU in Paper 1. This is because this PSN disk midplane is significantly warmer and more massive than the disk structure in Paper 1 (0.08 $M_{\odot}$ versus 0.01 $M_{\odot}$), thus the relevant temperature regime for O_2 ice chemistry (10-30 K) is found outside 100 AU here.

4.2.1 Ionisation levels

In Paper 1 it was confirmed that ionisation is an important driver of chemistry in disk midplanes (see e.g. Aikawa et al. 1997; Walsh et al. 2015). It was also found that abundant O_2 ice was produced at low ionisation (only radionuclide decay, and no contribution from cosmic rays). Therefore, three different levels of ionisation are explored here: a low level (Level 1, SLRs only), a high level (Level 2, the fiducial level which includes galactic cosmic rays), and an extra high level (Level 3, which includes enhanced cosmic rays), see Figure 4.1b. The two former levels assume the same contributions to the midplane ionisation as was the case for the low and high level in Paper 1: ionisation Level 1 includes only the contribution from short-lived radionuclides (SLRs) in the midplane. Ionisation Level 2 includes in addition CRs impinging on the disk, using the canonical cosmic ray ionisation rate for the local ISM ($\zeta_{H_2} = 10^{-17}$ s^{-1}). Ionisation Level 3 assumes a CR ionisation contribution ten times higher than for ionisation Level 2, based on estimates from e.g. van Dishoeck & Black (1986), Dalgarno (2006) and Indriolo et al. (2015) that the galactic cosmic ray rate ζ_{GCR} could be in the range $\zeta_{H} = 10^{-17} - 10^{-16}$ s^{-1} in diffuse clouds. We explore this enhanced CR scenario because O_2 ice has been found to be efficiently synthesised in experiments studying H_2O ice radiolysis in relation to Solar System icy bodies (see, e.g., lab work by Teolis et al. 2017, and others). For Levels 1 and 2, the ionisation ranges between $10^{-18} - 10^{-17}$ s^{-1} throughout the disk whereas for Level 3, $\sim 10^{-16}$ s^{-1} is reached at radii larger than 10 AU. In the inner disk inside ∼2 AU, all three ionisation levels are the same, because the surface densities here (>600 g cm^{-2}) attenuate the impinging CRs, so that only the SLRs contribute. In the outer, more diffuse disk, the contribution

[1] $\Sigma(R) = 54(R/10\text{AU})^{-3/2}\text{g cm}^{-2}$

from CRs impinging on the disk becomes more dominant, thus leading to three markedly different ionisation levels.

4.2.2 Chemical network

The chemical model used here includes gas-phase chemistry, gas-grain interactions and grain-surface chemistry. The gas-phase chemistry is from the latest release of the UMIST Database for Astrochemistry (McElroy et al. 2013) termed RATE12. The rates for gas-grain interactions and grain-surface chemistry are calculated as described in Walsh et al. (2015, and references therein). A gas/dust mass ratio of 100 is adopted. This setup is similar to the "Full chemistry" setup from Paper 1. The adopted grain size is 0.1 μm.

Four scenarios of initial chemical abundances are explored: the first two are cloud inheritance (hereafter "Inheritance" scenario) and chemical reset (hereafter "Reset" scenario). In the inheritance scenario the initial abundances are molecular (but no O_2 initially), and assumed inherited from the parent molecular cloud. In the reset scenario, the initial abundances are atomic, because all molecules are assumed dissociated prior to arrival in the disk midplane, due to exposure to a sufficiently strong accretion shock en route into the disk, or accretion heating very close to the star leading to high temperatures. The "reset" scenario is of particular interest for this paper because it was for this scenario in Paper 1 that the O_2 ice to H_2O ice ratio was similar to that found in comets 67P and 1P (Bieler et al. 2015; Rubin et al. 2015). Table 4.3 lists the initial atomic and molecular abundances used in these two scenarios. Tables 4.1 and 4.2 list the relevant binding energies for species, and activation barriers for reactions applicable to the O_2 chemistry, respectively. Radiolysis of H_2O ice through the reaction $2\,\mathrm{i}H_2O \xrightarrow{\gamma} 2\,\mathrm{i}H_2 + \mathrm{i}O_2$ and dismutation of H_2O_2 ice through the reaction $2\,\mathrm{i}H_2O_2 \longrightarrow 2\,\mathrm{i}H_2O + \mathrm{i}O_2$ are not explicitly included in the network. For the inheritance scenario, in this chemical network, atomic oxygen can be produced in-situ in the ice mantles via the cosmic-ray induced photodissociation of H_2O ice and other abundant oxygen-bearing molecules therein (e.g., CO_2 ice).

The third and fourth scenarios for the initial chemical abundances are more simple: first, the "Water"-scenario, which assumes initial abundances of gas-phase H, He, H_2 and H_2O. This scenario is intended to investigate if O_2 ice can be produced through processing of H_2O ice. Second, the "Atomic oxygen"-scenario, which assumes gas-phase H, He, H_2 and O as initial abundances. Here it is investigated whether or not O_2 ice production from atoms depends on the presence of elements other than oxygen. Eistrup et al. (2018) showed that H_2S ice on the grain surfaces acts as a catalyst for the conversion of adsorbed oxygen atoms into O_2 ice. Whether or not the sulphur-bearing species are essential for the production of O_2 ice can be tested in these two scenarios, because they exclude sulphur, and only include a source of oxygen in the form of oxygen atoms or H_2O.

Lastly, it is explored if the observed cometary O_2 ice abundance can be maintained if the PSN started out with a percentage (5%) of elemental oxygen locked up in primordial O_2, as was suggested by Taquet et al. (2016).

4.3 Results

In this section the chemical evolution of various species in the PSN are presented in a number of figures. Due to the focus on O_2 ice in this paper, the attention will be on species that are chemically related to O_2 ice (a schematic overview of these species can be found in Cuppen et al. 2010).

4.3.1 PSN abundance evolution

4.3.1.1 Inheritance scenario

Figure 4.2 features abundances as a function of midplane radius for different evolutionary times up to 10 Myr for the inheritance scenario. Left to right are increasing ionisation levels, and top to bottom are H_2O, O_2 and H_2O_2 ices, respectively. H_2O ice is plotted with respect to H_{nuc} abundance, whereas O_2 and H_2O_2 ice are plotted with respect to H_2O ice. The is done to match the convention used in the reporting of cometary abundances. The model details are listed in each panel, along with color coding indicating evolution times. In the middle and lower panels the respective observed limits for O_2 and H_2O_2 ices are marked with orange and red shaded regions, respectively. The orange shading for O_2 ice marks the limits to the mean O_2 ice abundance observed in comet 67P ($3.8\pm0.85 \times 10^{-2}$ with respect to H_2O ice), and the red shading marks the limits for H_2O_2 ice ($6 \pm 0.7 \times 10^{-4}$ wrt O_2 ice, thus $2.34 \pm 0.8 \times 10^{-5}$ wrt H_2O ice (Bieler et al. 2015)). Note that in 67P variations in O_2 over H_2O ice were seen spanning 1-10%.

An evolution time of 10 Myr is chosen because this is assumed to be the maximum lifetime of a gaseous protoplanetary disk, and based on the results from Eistrup et al. (2018), the outer icy disk midplane should have reached steady state by this time. Since the focus in this work is the outer, icy PSN disk midplane, the radial range starts at 50 AU, which lies inside the O_2 iceline ($\sim$ 120 AU at $\sim$29 K).

For ionisation Level 1 in Fig. 4.2a, H_2O ice stays abundant throughout the evolution. For higher ionisations, the H_2O ice abundance decreases with time inside, and increases with time outside $\sim$ 120 AU. This radius marks the O_2 iceline. Panels d to f show the evolution of O_2 ice for the different ionisation levels. The profiles for O_2 ice for ionisation Levels 1 and 2 peak at similar abundance levels of 2-3$\times10^{-3}$ with respect to H_2O ice, which is an order of magnitude lower than the observed abundance. It is seen that for higher ionisation, this abundance is reached faster, with ionisation Level 1 producing of order 10^{-3} with respect to H_2O ice only by 10 Myr.

It is shown that for H_2O_2 ice abundance profiles featured in panels g to i they evolve in a similar way to O_2 (note the same y-axis range as for O_2 ice), and reach peak abundances at $\sim$120 AU by 10 Myr, that are a factor of 2-3 lower than those for O_2 ice. This abundance level is 30-100 times higher than that observed for H_2O_2 ice in comet 67P. For all ionisation levels there are narrow radial regions where the H_2O_2 ice abundance matches the observed levels over a time range defined by the ionisation level (e.g. between 70-80 AU ionisation Level 3 at all times). However,

at these points the O_2 ice abundance does not match that observed.

For the inheritance scenario it is thus seen that O_2 ice is underproduced by at least an order of magnitude, and H_2O_2 is overproduced by up to two orders of magnitude.

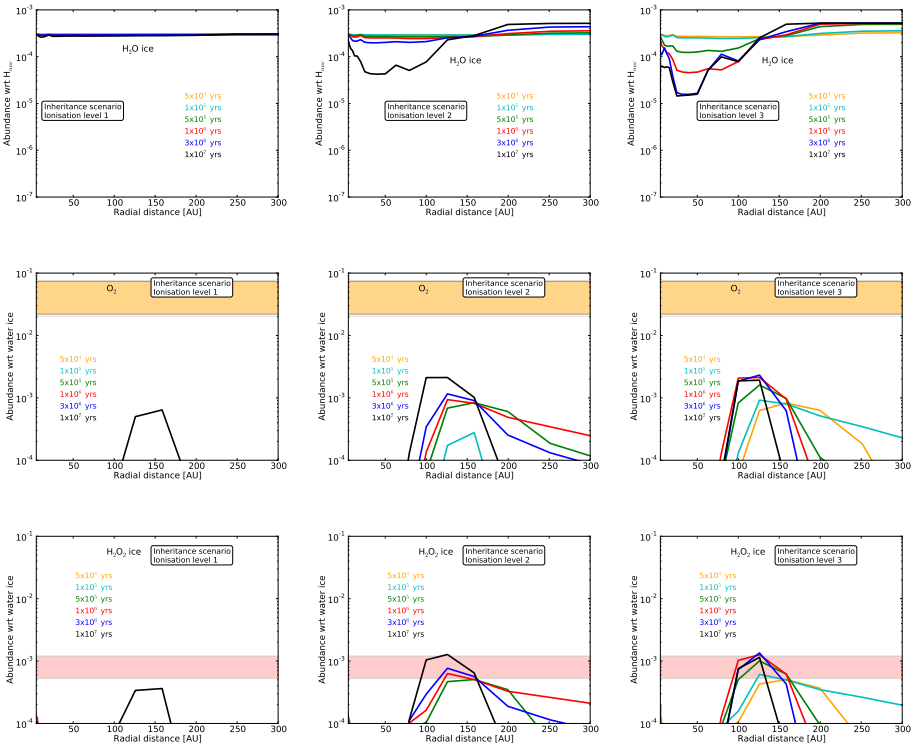

Figure 4.2: Radial abundance profiles for the inheritance scenario at multiple evolutionary time steps. Top to bottom are H_2O, O_2 and H_2O_2. Left to right are increasing ionisation levels. For O_2 and H_2O_2 the limits detected in comet 67P are indicated as yellow and red shaded areas, respectively. The chemical network utilised does not include O_3 chemistry.

4.3.1.2 Reset scenario

The abundance evolution profiles for the reset scenario are shown in Fig. 4.3. For O_2 ice in panels d to f it is seen that a high abundance ($10^{-2}-10^{-1}$ with respect to H_2O ice) is reached for both ionisation Levels 1 and 2, with each reproducing the observed abundance for a large radial range covering 150-300 AU. For ionisation Level 1 the O_2 ice abundance matching the observation is maintained up to 2 Myr. Until 1 Myr between 150-220 AU, the modelled abundance lies above the observations ($>5\times10^{-2}$ with respect to H_2O ice). For Level 2 the abundance level

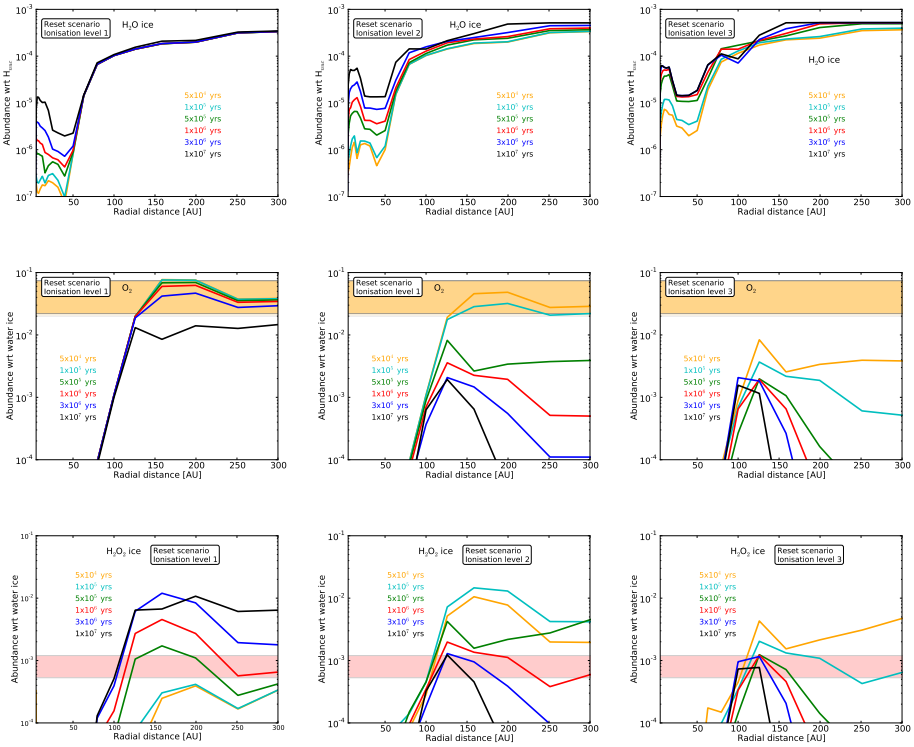

Figure 4.3: Radial abundance profiles for the reset scenario at multiple evolutionary time steps. Top to bottom are H_2O, O_2 and H_2O_2 ices. Left to right are increasing ionisation levels. For O_2 and H_2O_2 the limits detected in comet 67P are indicated as yellow and red shaded areas, respectively. The chemical network utilised does not include O_3 chemistry.

matching the observed values happens between $5 \times 10^4 - 10^5$ yrs in the range 150-200 AU, but subsequently drops to reach 2-3$\times 10^{-3}$ with respect to H_2O ice by 10 Myr. This was also the abundance level reached for O_2 ice by 10 Myr for the inheritance scenario. For ionisation Level 3, the abundance is below the observed level already by 5×10^4 yrs of evolution, and by 10 Myr it also has reached the level of 2-3$\times 10^{-3}$ with respect to H_2O ice. For ionisation Level 1, the abundance remains higher than 2-3$\times 10^{-3}$ with respect to H_2O ice throughout the evolution, indicating that, for both inheritance and reset, at this ionisation level, 10 Myr of chemical evolution is not enough to bring the O_2 ice abundance to what appears to be its steady state level according to the results from the inheritance scenario in Fig. 4.2 (for a description of disk midplane chemical steady state, see Eistrup et al. 2018).

H_2O_2 ice is seen in Fig. 4.3, panels g to i, to evolve significantly over time. For all ionisation levels, H_2O_2 ice is produced over time with the timescale dependent

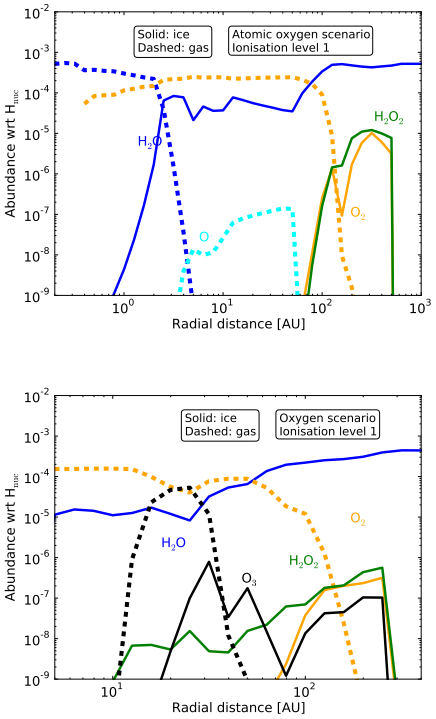

Figure 4.4: Abundances by 10 Myr evolution in the oxygen-only scenario, for ionisation Level 1. a) without O_3 chemistry included. b) with O_3 chemistry included.

on ionisation level. The fastest production is seen for Level 3, where the peak abundance of $>10^{-2}$ with respect to H_2O ice is reached already by 10^5 yrs. On the other hand it takes 0.5 Myr and 3 Myr to reach a similar abundance for Levels 2 and 1, respectively. The H_2O_2 ice is subsequently destroyed after reaching its peak. For ionisation Levels 2 and 3 a steady state abundance of order 10^{-3} with respect to H_2O ice is reached at radii ∼100-120 AU. Beyond this radius it has disappeared by 10 Myr.

4.3.1.3 Water and atomic oxygen starting conditions

Models were also run starting with simpler sets of initial abundances, either with all oxygen already present in H_2O ("Water scenario") or all free ("Atomic oxygen scenario"), in addition to H and He. This was to test the formation of O_2 ice solely from processing of H_2O ice, and the formation via assembly from free oxygen atoms, in the absence of other chemistry. It was found that the water scenario did not, at any point in time or radius, reproduce O_2 ice to the abundance seen in the comets. The maximum abundance was $<10^{-7}$ with respect to H_2O ice, regardless of ionisation level. This is shown in Fig. 4.12, where the gas and ice abundances of O, O_2, H_2O and H_2O_2 are plotted as a function of radius by 10 Myr of evolution.

The atomic oxygen scenario, on the other hand, can reproduce the observed abundance of O_2 ice by 10 Myr, as is seen in panel a of Fig. 4.4. This panel of Fig. 4.4 shows the abundances of H_2O, O, O_3 and H_2O_2 with respect to H_{nuc} as a function of radius, by 10 Myr of evolution. The radial range (80-300 AU) for this reproduction is similar to the range in the reset scenario, but in the atomic oxygen scenario H_2O_2 ice is found to be more efficiently formed than O_2 ice. This scenario will be revisited later.

4.3.2 Including ozone ice chemistry

The chemical network utilised so far has not included O_3. This is because it has not been considered to be an important player in ISM chemistry, as it is formed primarily in the gas-phase via a three-body mechanism. However, data exist on O_3 ice chemistry, as outlined in e.g. Cuppen et al. (2010) and Lamberts et al. (2013). The production pathway to O_3 ice is

$$iO_2 \xrightarrow{iO} iO_3,$$

with a fiducial barrier of 500 K, and the destruction pathway is

$$iO_3 \xrightarrow{iH} iO_2 + iOH,$$

which has no barrier. Hence, it is expected that the pathway to O_3 ice via O_2 ice may impact on the O_2 ice abundance, and will be dependent on the both the availability of free oxygen atoms on the ice, and the efficiency of hydrogenation.

Figure 4.5 presents the evolving abundances of H_2O ice, O_2 ice H_2O_2 ice and O_3 ice as a function of radius for the inheritance scenario, thus now including O_3 ice chemistry. These panels are directly comparable with those in Fig. 4.2. The abundance evolution of O_3 ice is shown in the bottom row. The abundance evolution seen for O_2 ice in panels d to f and for H_2O_2 ice in panels g to i are similar to the trends in Fig. 4.2 for the chemistry without O_3. However, the abundances reached by 10 Myr with O_3 chemistry are lower than those without: both O_2 ice and H_2O_2 ice abundances peak at $\sim 5 \times 10^{-4}$ with respect to H_2O ice, thus a factor of two lower for H_2O_2 ice and a factor of five lower for O_2 ice when compared with the scenario without O_3 chemistry. The peak O_2 ice abundance is almost two orders of magnitude lower than the observed value, and the peak of the H_2O_2 ice is about 20 times higher than the observed value.

For O_3 ice in panels j to l a steady build-up over time is seen. Note that the range on the y-axis range is different for O_3 ice than for H_2O_2 and O_2 ices. The O_3 ice reaches maximum abundance fastest at ionisation Level 3 ($\sim 10^{-4}$ with respect to H_2O ice), thus a factor of five lower than that reached for H_2O_2 ice and O_2 ice, yet two orders of magnitude higher than the observed upper limit at 10^{-6} with respect to H_2O ice for O_3 ice in comet 67P. Only at larger radii (between 150 and 270 AU, depending on evolution time) do the O_3 and H_2O_2 ice abundances fall within the observed limits, although O_2 ice does not. All three ice species thus show similarities in their evolution, and order-of-magnitude similarities in

their peak abundances. The observed large differences between their respective abundances (O_3:H_2O_2:$O_2 \lesssim$1:23.5:39200) are not reproduced by these models.

For the reset scenario, including O_3 chemistry, Fig. 4.6 shows a higher abundance level of O_2, H_2O_2 and O_3 ices than for the inheritance scenario. At ionisation Level 1, O_2 and H_2O_2 ices peak at $\sim 10^{-2}$ with respect to H_2O ice at $\sim$ 150 AU between 0.5-1 Myr evolution, but subsequently drop by about an order of magnitude by 10 Myr. For ionisation Levels 2 and 3, abundance levels for both species of $\sim 10^{-2}$ with respect to H_2O ice are only achieved by 5×10^4 yrs, and the peak abundances by 10 Myr are at $1 - 2 \times 10^{-4}$ with respect to H_2O ice, thus neither matching the observed values of H_2O_2 ice nor of O_2 ice. At no point in time or radius does the reset scenario including O_3 chemistry reproduce the observed mean abundance of O_2 ice. However, for ionisation Levels 1 and 2 the abundance between 150-200 AU reaches above 1% of H_2O ice, which is within the observed range in comet 67P (1-10%).

The O_3 abundance for the reset scenario at ionisation Level 1 starts out high at $1 - 3 \times 10^{-2}$ with respect to H_2O ice between 100-200 AU up to $5{\times}10^5$ yrs. s seen in Fig. 4.6. Note that the higher ratios reached within 70 AU is due to generally low absolute ice abundances (see panels a to c in Fig. 4.6). For ionisation Levels 2 and 3, these high abundances reduce over time leading to a peak of at a few times 10^{-5} with respect to H_2O ice by 10 Myr between 100-120 AU. The maximum abundance achieved by 10 Myr is an order of magnitude higher than the observed upper limit. Only in the wings of the abundance profiles do the models reproduce this upper limit for the entire radial range, depending on evolution time and ionisation level.

The scenarios starting with only H_2O or elemental oxygen were also investigated after the inclusion of O_3 chemistry. However, neither of them reproduced a significant amount of O_2 ice. The abundances by 10 Myr are shown for the oxygen-only scenario in Fig. 4.4b. Upon inclusion of O_3 chemistry, the peak abundance of O_2 ice from panel a (without O_3) drops by at least four orders of magnitude to $<10^{-9}$ with respect to H_2O ice in panel b. Starting with atomic oxygen only therefore does not reproduce the observed abundance. For the water scenario, there is also no O_2 ice. An overview of gas and ice abundances of H_2O, O_2, O_3 and H_2O_2 as a function of radius by 10 Myr of evolution for the inheritance, reset, water and oxygen scenarios is shown in Fig. 4.13.

In none of the tested cases including O_3 chemistry is the O_2 ice abundance reproduced to match the levels observed in the comets.

4.3.3 Exploring the sensitivity of the abundances to assumed grain-surface parameters

The underproduction of O_2 ice and overproduction of H_2O_2 and O_3 ices may be a result of the adsorption and reaction parameters assumed for the network of reactions involving oxygen and hydrogen. If, for example, the reaction $iO_2 \xrightarrow{iO} iO_3$ is too efficient on the grain-surfaces, this could lead to over- and under-production of O_3 and O_2 ices, respectively. This reaction is dependent on the adsorption of atomic oxygen, for which the utilised binding energy here is $E_{\rm bin}$=800 K. This

Table 4.1: Binding energies $E_{\rm bin}$[K] for relevant species

Species	UDfA (used here)	UDfA reference	Penteado et al. (2017)
O	800	Tielens & Allamandola (1987)	1660±60
OH	2850	Garrod & Herbst (2006)	3210±1550
O_2H	3650	Garrod & Herbst (2006)	800
H_2O_2	5700	Garrod & Herbst (2006)	6000±100
O_2	1000	Garrod & Herbst (2006)	898±30
O_3	1800	Garrod & Herbst (2006)	2100±100
H_2O	5700	Brown & Bolina (2007)	4800±100
H	600	Cazaux & Tielens (2002)	650±100
H_2	430	Garrod & Herbst (2006)	500±100

is based on estimates from Tielens & Allamandola (1987). However, recent experimental work by He et al. (2015) experimentally determined a binding energy of $E_{\rm bin}$=1660 K, thus more than doubling the former value. This higher binding energy should act to keep oxygen atoms from desorbing at higher temperatures, thereby facilitating every step in the reaction pathway leading from iO $\xrightarrow{\rm iO}$ iO_2 $\xrightarrow{\rm iO}$ iO_3. On the other hand, at low temperature the mobility of atomic oxygen will be reduced. This latter case could possibly lead to a decreased production of O_3 ice.

In this subsection, the sensitivity of the chemistry to several parameters is explored for single-point models (i.e. single n, T) which cover the temperature and density ranges in the PSN midplane where O_2 ice production is expected, based on the model results described thus far. The first parameter explored is the barrier width for quantum tunnelling $b_{\rm qt}$which is set to either 1 or 2 Å representing the limits to the range of values usually assumed for $b_{\rm qt}$ when modelling grain-surface chemistry, see Cuppen et al. (2017), and references therein. The second parameter is the ratio of the diffusion energy to the molecular binding energy $E_{\rm diff}/E_{\rm bin}$, which is taken to be either 0.3 or 0.5 (see Ruffle & Herbst 2000; Garrod & Herbst 2006, and references therein). This amounts to four combinations of the two reaction parameters. The values of each parameter associated with a given model setup is given in each panel. The values for the grain-surface chemistry used in Eistrup et al. (2016, 2018), are $b_{\rm qt}$= 1Å and $E_{\rm diff}/E_{\rm bin}$ = 0.5. Only the reset scenario is studied here because this is the case for which maximal O_2 ice formation is seen.

4.3.3.1 Abundance mosaics

Figures 4.14, 4.7, 4.15 and 4.16 show the abundances of H_2O ice with respect to $H_{\rm nuc}$, and O_2 ice, O_3 ice and H_2O_2 ice with respect to H_2O ice, again, maintaining the convention used by the comet community. From top to bottom span evolution times from 5×10^4 yr up to 10^7 yr. In each panel in the figures a mosaic of color-

Table 4.2: Activation energies $E_{\rm act}$[K] for relevant grain-surface reactions.

Reaction		$E_{\rm act}$[K]
$OH + H$	$\longrightarrow H_2O$	0
$OH + H_2$	$\longrightarrow H_2O + H$	2100
$O_3 + H$	$\longrightarrow O_2 + OH$	0
$O + O$	$\longrightarrow O_2$	0
$O + O_2$	$\longrightarrow O_3$	500
$OH + O$	$\longrightarrow O_2H$	0
$O_2H + H_2$	$\longrightarrow H_2O_2 + H$	5000
$H + H_2O_2$	$\longrightarrow H_2O + OH$	2000

indicated abundances shows the results across different combinations of midplane temperature (ranging from 10-30 K on the y-axis), and densities (ranging from $10^8 - 10^{10}$ cm^{-3} on the x-axis). The ionisation is kept constant at $\zeta = 10^{-17}$ s^{-1}, approximately the same as ionisation Level 2 from Fig. 4.1 in the outer disk midplane. This ionisation level was seen in Fig. 4.3 (model without O_3) to match the observed O_2 ice abundance early in the evolution (up to 0.1 Myr).

From left to right in each of the Figs. 4.14 to 4.15 two grain-surface reactions parameters are changed. The first one is the barrier width for quantum tunnelling $b_{\rm qt}$ which is either 1 Å (columns one and two, in each figure) or 2 Å (columns three and four, in each figure). The second parameter is the ratio of diffusion energy to molecular binding energy $E_{\rm diff}/E_{\rm bin}$, which can be either 0.3 (columns one and three, in each figure) or 0.5 (columns two and four, in each figure). This amount to four combinations of the two reaction parameters, thus the four columns of mosaics in each figure. The values of each parameter associated with a given model setup is given in each panel.

The range of evolution time steps is chosen to cover both the evolutionary stage at which O_2 ice was abundant in Fig. 4.3 (5×10^4 yr, for ionisation Level $2 \sim 10^{-17}$ s^{-1}), as well as the later stages of disk evolution. The colors in the mosaic are chosen to enable distinguishing between abundance levels that change per order-of-magnitude, with dark red (top color in color bar) representing the highest abundance, and dark blue (bottom color in color bar) representing the lowest. The range of abundance levels in each figure is chosen to cover the full range of abundances produced for each species in the models. By showing the abundance evolutions in this way model results matching the observed abundances of e.g. O_2 ice (1-10% of H_2O ice) will show as orange (second highest color in colorbar) in Fig. 4.7.

For H_2O ice in Fig. 4.14 it is seen that for columns one and two ($b_{\rm qt}$=1 Å) the abundance level largely remains within the initial order of magnitude of 10^{-4} with respect to H_2O ice. For columns three and four ($b_{\rm qt}$=2 Å), some change is seen: especially for the third column ($E_{\rm diff}/E_{\rm bin}$=0.3), the abundance is an order

of magnitude lower for temperatures 25-30 K than for 10-20 K, and the abundance increases with time at 20 K. Turning to Fig. 4.7 for O_2 ice, limited production is seen for columns one and two, with an early peak abundance between $10^{-4} - 10^{-3}$ with respect to H_2O ice at 25 K for $n = 10^8 - 10^9$ cm^{-3} by 5×10^4 yr. More interesting are columns three and four: until 0.5 Myr, abundances of $10^{-2} - 1$ with respect to H_2O ice are reached for temperatures 15-25 K for all densities. Thus the O_2 ice abundance lies above or reproduces the observed values. For these cases, by >1 Myr, the produced O_2 ice is destroyed and reaches $10^{-5} - 10^{-3}$ with respect to H_2O ice by 10 Myr.

Having narrowed in on this parameter range (early evolutionary times, and $b_{\rm qt}$=2 Å), it can now be checked if H_2O_2 and O_3 ices can match the observed levels for the same model parameters. Fig. 4.15 shows the same suite of plots for O_3 ice. Results in columns three and four up to 0.5 Myr evolution show that O_3 ice is abundantly produced, at a similar or higher level than O_2 ice, thus not matching the observed upper limit (darkest shade of blue, $<10^{-6}$ with respect to H_2O ice). The subsequent destruction by >1 Myr does not bring the abundance level much further down, and the O_3 ice abundance is generally similar to that for O_2 ice. O_3 ice only matches the observed upper limit for $T = 10$ K.

In Fig. 4.16, H_2O_2 ice is abundantly produced for $b_{\rm qt}$=2 Å and $E_{\rm diff}/E_{\rm bin}$=0.3. For 25 K it is consistently at a level of $10^{-1} - 1$ with respect to H_2O ice during the entire evolution. For 20 K it is also abundant, although 1-2 orders of magnitude lower than that found at 25 K, and it is less abundant than O_2 ice until ~ 0.5 Myr by 1-2 orders of magnitude. At later times, for 20-25 K, H_2O_2 ice becomes 1-3 orders of magnitude more abundant than O_2 ice. For $E_{\rm diff}/E_{\rm bin}$=0.5 it is produced at levels $10^{-6} - 10^{-3}$ with respect to H_2O ice, depending on density.

4.3.3.2 Abundance evolutions for selected parameter sets

In Section 4.3.3.1 the color mosaics revealed a promising set of physical and chemical parameters that supported the production of O_2 ice in situ under conditions suitable for the PSN: $b_{\rm qt} = 2$ Å (rather than the fiducial value of 1 Å), T=15-25 K, $n = 10^9 - 10^{10}$ cm^{-3} and evolution times up to 0.5 Myr. The ratio of diffusion-to-binding energy for ice species appeared to play a minor role, with both values of 0.3 and 0.5 facilitating O_2 ice production.

In Figure 4.8 evolving abundances are plotted for O_2, O_3, H_2O_2 and O_2H ices with respect to H_2O ice, for the three different temperatures and two densities outlined above, and with $E_{\rm diff}/E_{\rm bin}$=0.3. Details about each plot can be found in the labels. Each panel includes shaded regions indicating the observed abundances for O_2 ice (yellow), H_2O_2 ice (red) and upper limit for O_3 ice (grey).

For all six panels, it is seen that O_2 ice is within the measured abundance values, at least for a period during evolution. In all cases an initial production is seen, with the abundances of O_2 ice across model setups peaking at 30-40% with respect to H_2O ice between $\sim 5 \times 10^4 - 5 \times 10^5$ yrs, with the highest abundances reached at 20 K. For temperatures at 15-20 K, the O_2 ice abundances are generally higher than for T=25K. By $\sim 3 \times 10^5$ to 10^6 yrs, depending on model setup, the O_2 ice abundance drops at least two orders of magnitude below maximum. Hence,

the observed abundance of O_2 ice can be reproduced in all six setups, but only at early times.

Regarding ice species besides O_2, Fig. 4.8 shows that O_3 is the most abundant of the plotted species, at least until 10^5 yrs. At early evolutionary stages, O_3 ice is even more abundant than H_2O ice. This is because the calculations are started with free oxygen atoms (reset scenario). This high level is not seen in the measurements of comet 67P, in which an upper limit of 10^{-6} with respect to H_2O ice was reported.

Likewise for H_2O_2 ice, it is mostly produced at a high abundance ($>10^{-3}$ with respect to H_2O ice) in these models. At 25 K after ~ 0.5 Myr of evolution, H_2O_2 ice is the most abundant of the plotted species. At no point in time in any of the plots does the abundance of H_2O_2 ice match the levels observed (red shaded region): for 15 K it is at least an order of magnitude too low, and between 20-25 K it is overproduced by between a factor of three and two orders of magnitude.

For a ratio of diffusion-to-binding energy of 0.5, similar plots are shown in Fig. 4.9. Between 20-25 K there are evolutionary times when O_2 ice is reproduced to match the observations. However the highest abundance reached is at 20 K. For T=15 K, no reproduction of the observed abundances of neither O_2 ice nor H_2O_2 ice is seen, and O_3 ice is (next to H_2O ice) the dominant carrier of elemental oxygen. At T=25K for $n = 10^9$ cm^{-3}, the abundance of H_2O_2 ice matches that measured in the comet both by $\sim$0.03 Myr and by $\sim$ 3 Myr, and by 0.03 Myr the O_2 ice abundance is only $\sim$ 2 times lower than the observed abundance. Along the same lines, for T=25 K and $n = 10^9$ cm^{-3} by $\sim$ 0.4 Myr O_2 ice matches the observed abundance, and H_2O_2 ice is only $\sim$ 2 times higher than the observed level. This indicates that something close to a match with the observed abundances between both O_2 and H_2O_2 ice abundances with respect to H_2O ice is reached at 25 K. However, all the models are still vastly overproducing the O_3 ice abundance compared with the measurements.

This parameter space investigation has shown that there are sweet spots, both for the physical and chemical setup, where O_2 ice can be produced to match the measurements on comet 67P, even after expanding the grain-surface chemical network to include O_3 ice chemistry. However, the low measured abundance of O_3 ice remains unexplained by the models.

A possible way to adjust the models to lower the O_3 ice production could be to increase the reaction barrier for the $iO_2 \xrightarrow{iO} iO_3$ reaction, where the default barrier is at E_{act}=500 K. Because the abundance levels of O_2 ice and H_2O_2 ice in Fig. 4.9 panel c (T=25K, E_{diff}/E_{bin}=0.5, $n = 10^{-9}$ cm^{-3}, $b_{qt} = 2$Å and $\zeta = 10^{-17}$ s^{-1}) featured evolutionary stages when they were simultaneously in proximity to the observed levels, this model setup is now tested with three different values for the activation energy for the $iO_2 \xrightarrow{iO} iO_3$ reaction. In addition to the fiducial 500 K, also 1000 K and 2000 K activation energies are tested. It is noted that these are likely too high relative to what is known from laboratory work where O_3 is seen to form readily at low temperatures (Lamberts et al. 2013). However, given that O_3 ice is not seen to be efficiently produced in space including comets, the hypothetical situation with a higher barrier is explored, as a means to mitigate as

of yet unknown chemical pathways away from O_3 ice. To compare the effects of these changes, the same tests of activation energies are performed for the setup in panel b in the same figure ($T = 20$ K, keeping all other parameters the same).

In Fig. 4.10 panels a and b, abundances for O_2, O_3 and H_2O_2 ices are plotted as a function of time, with solid, dashed and dotted profiles representing activation energies for the O_3 ice production reaction of 500 K, 1000 K and 2000 K, respectively. In panel a only the abundance of O_2 ice is found to match the observed level. However, in panel b, at 25 K, it is seen that for at $E_{\rm act}$= 2000 K, O_2 ice and H_2O_2 ice are both reproduced to within the observed values between 0.8-1 Myr evolution. For the same evolutionary timescale, O_3 ice is much lower in abundance ($\sim 10^{-16}$ with respect to H_2O ice), thus also agreeing with the upper limit for the cometary abundance. This is therefore a sweet spot in the physical and chemical parameter space, in which the observed abundances of all three species are reproduced. It is noteworthy that the ionisation level for this sweet spot includes the contributions from both SLRs and CRs, whereas it was found in Paper 1 that O_2 ice be reproduced only without CRs. However, the framework here is different from that in Paper 1, as O_3 chemistry and the updated binding energy for atomic oxygen have been included. Note that the anomalously high activation required for O + O_2 is likely masking as of yet unknown routes in the O_3 chemistry.

4.3.4 Including a primordial source of O_2 ice

Here, the results from the scenario starting with 5% of atomic oxygen locked in O_2 is tested, exploring the theory for the primordial origin of O_2 ice, as suggested by Taquet et al. (2016) and Mousis et al. (2016). This is a modification of the inheritance scenario so that remaining oxygen is already locked in molecules (mostly H_2O, CO and CO_2, see the inheritance scenario abundances in Table 4.3). In Fig. 4.11 evolving abundance profiles for this scenario are shown, for temperatures between 15-25 K from left to right, and densities between $10^9 - 10^{10}$ cm^{-3} from top to bottom. The ionisation rate is at $\zeta = 10^{-17}$ s^{-1}, the ratio of diffusion-to-binding energy is 0.5, and the barrier width for quantum tunnelling is 2Å. The activation energy for the O + O_2 reaction is the fiducial value of 500 K.

It is seen in Fig. 4.11, panels a, b, d and e, that an early abundance level of O_2 ice at or above the observed mean is maintained until a few times 10^4 yrs for temperatures between 15-20 K. At 25 K, the abundance of O_2 ice is lower early on, and in particular for n=10^9 cm^{-3} the abundance is $< 10^{-2}$ with respect to H_2O ice, which is outside the observed range. Simultaneously with O_2 ice matching the observed abundance in some cases, the abundance of O_3 ice is 1-2 orders of magnitude lower than O_2 ice by 3×10^3 yrs for all cases except in panel c. Between a few times 10^4 yrs and 10 Myr the O_2 ice abundance decreases by >2 orders of magnitude compared with the initial abundance, and from $\sim 10^5$, yrs O_3 ice is the dominant oxygen carrier of the plotted species. Hence, this scenario can reproduce the observed abundance of O_2 at early stages, and with lower abundances of H_2O_2 and O_3 ices, although abundances for the latter two species are still higher than measured.

4.4 Discussion

The abundance of O_2 ice in comet 67P has motivated much work as to its origin. Rubin et al. (2015), Mousis et al. (2016, 2018), Taquet et al. (2016) and Dulieu et al. (2017) have all attempted to explain the O_2 level from a point of view of possible chemical origins. Mousis et al. (2016) and Rubin et al. (2015) approached the problem by investigating chemical processing of either H_2O ice or H_2O_2 ice into O_2 ice. Mousis et al. (2018) attempted an explanation with a scenario in which ice-covered grains were transported from the midplane to the upper layers of the disk. Here, the grains undergo photochemical processing producing O_2 ice, which is then cycled back to the disk midplane. It is noted that Mousis et al. (2018) only consider the O_2 ice abundances, not H_2O_2 or O_3 ices. On the other hand, Taquet et al. (2016) approached it from a broader point-of-view considering primordial production pathways in the parent cloud, and utilising extensive chemical networks and subsequently tracking the primordially-produced O_2 ice to the disk midplane. While those works all concluded that a primordial origin and subsequent retention of O_2 ice was the most likely, Paper 1 concluded that starting from a fully atomised disk midplane, there is an evolutionary phase during which a range of radii in the outer icy midplane (outside the O_2 iceline) will reasonably reproduce the measured O_2 / H_2O ice level.

The investigation here has taken the step further from Paper 1: exploring the physical and chemical parameter space that may facilitate the production of O_2 ice in-situ in the PSN, and simultaneously tracing the abundances of the chemically related species H_2O_2, O_3 and O_2H, as well as using a more massive disk model more appropriate for the PSN.

4.4.1 Chemical starting conditions

The chemical starting conditions' effects on the O_2 ice production were explored. It is clear that only an atomised start can facilitate the production, although models starting with a percentage of elemental oxygen in O_2 did retain this O_2 ice for a short period of evolution. The presence of atoms other than oxygen (such as sulphur), however, does not have a large impact on the production of O_2 ice. That means that oxygen-only and hydrogenated oxygen species lock up the majority of the available elemental oxygen.

4.4.2 Dependence on ionisation levels

The ionisation levels have been shown to facilitate different chemical evolution of abundances. The chemical timescales are shorter for higher ionisation levels. Ionisation Level 1 only reproduced the observed O_2 abundance for models without O_3, and ionisation Levels 2 and 3 cause similar evolutionary trends, meaning that Level 3 does not facilitate any more O_2 ice production than Level 2. It is noteworthy that the sweet spot for reproduction of O_2, H_2O_2 and O_3 ices to within the observed abundances was found for a ionisation level of $\zeta = 10^{-17}$ s^{-1}, which is the local ISM value for dense clouds. This ionisation resembles ionisation Level

2 at 100-130 AU in the PSN disk midplane (see Fig. 4.1 panel b), which is also the radial range covering the temperature and density of the sweet spot, which is just outside the O_2 iceline.

4.4.3 Changing $E_{\rm bin}$ for atomic oxygen, and inclusion of O_3

O_3 was introduced and included in the chemical network with production through $iO_2 \xrightarrow{iO} iO_3$ (activation energy of 500 K), and destruction through barrierless hydrogenation. After this change, the binding energy $E_{\rm bin}$ for oxygen atoms was increased from 800 K to 1660 K, as measured by He et al. (2015). This change was expected to make oxygen atoms less volatile, thus having them reside on the grain surfaces at higher temperatures than before. This was expected to aid the production of O_2 and O_3 ices through the pathway $iO \xrightarrow{iO} iO_2 \xrightarrow{iO} iO_3$.

The expansion to include O_3 chemistry induces very different behaviours of O_2, O_3, and the chemically related H_2O_2. Still assuming the PSN midplane, and ionisation Level 1, O_2 ice is not reproduced to match the observed cometary abundances.

The updated binding energy for atomic oxygen also had an effect, as the parameter space investigation revealed O_2 ice production matching the observed value, even when including O_3 chemistry. This change made the oxygen atoms less volatile, thus adsorbing to the grain at higher temperatures.

4.4.4 Narrowing down on O_2 ice production

With the lower produced level of O_2 ice after inclusion of O_3 chemistry the question remained if O_2 ice, in any case, can be produced to within the measured levels. Besides updating $E_{\rm bin}$ for atomic oxygen, two parameters for grain-surface chemistry, which had been kept constant thus far were now varied: the barrier width for quantum tunnelling, and the ratio of diffusion-to-binding energy of icy molecules. Adjusting these parameters, in particular the barrier width for quantum tunnelling, appears to have important impacts on the production level of O_2 ice. Increasing the barrier for quantum tunnelling from 1 to 2 Å, for temperatures ranging between 15-25 K, and densities 10^9-10^{10} cm^{-3}, results in O_2 ice produced to within the mean measured level in comet 67P. Increasing the barrier width from 1 to 2 Å lowers the mobility of H and H_2 on the grain-surfaces. This means that O+O reactions proceed more efficiently than hydrogenation of O, O_2 and O_3 ice, which in turn leads to higher abundances of O_2 and O_3 ices for a $b_{\rm qt}$ of 2 Å. Generally, with this wider tunnelling barrier, the measured mean abundance of O_2 ice can be reproduced relatively early in the evolution, from 0.05-0.5 Myr. At 25 K the corresponding level of H_2O_2 ice was close to its observed value. O_3 ice, however, remains more abundant than O_2 ice. Early in the evolution, O_3 ice is even more abundant than H_2O ice, but this is explained by O_3 ice being a precursor to H_2O ice in the reaction pathway

$iO \xrightarrow{iO} iO_2 \xrightarrow{iO} iO_3 \xrightarrow{iH} iOH \xrightarrow{iH} iH_2O$,

due to the availability of free oxygen. Indeed, in Fig. 4.8, showing the time evolution of species, O_3 is the dominant oxygen carrier at early times, and H_2O at later

times. The exception to this are the cases of a low ratio of diffusion-to-binding energy of 0.3, and temperatures of 25 K (panels c and f in Fig. 4.8), where H_2O_2 dominates at later times. Here, a lower diffusion energy and higher temperature means a higher mobility of icy molecules on the grain surface. This leads to OH (the product of O_3 + H) reacting with O_2 ice (precursor to O_3 ice and product of the hydrogenation of O_3 ice), thereby lowering the abundance of O_3 ice, and increasing the abundance of first O_2H ice, and subsequently H_2O_2 ice via the reaction pathway $iO_2 \xrightarrow{iH} iO_2H \xrightarrow{iH} iH_2O_2$.

4.4.5 Activation energy for O_3 ice production pathway

A crucial element in modelling chemical evolution is the assumed activation energies for reactions. Especially for grain-surface chemistry, these energies remain somewhat uncertain, due to the difficulty of estimating them through production rates in the lab. In this work, the fiducial activation energy for the reaction $iO + iO_2 \longrightarrow iO_3$ was E_{act}=500 K (Lamberts et al. 2013), resulting in model O_3 ice at a higher abundance than its parent species, O_2 ice. This means that the modelled abundance of O_3 ice is several orders-of-magnitude higher than the upper limit determined in comet 67P (see Figs. 4.8 and 4.9).

Testing out higher activation energies for the production of O_3 ice (thereby impeding the O + O_2 reaction) revealed that for E_{act}=2000 K, the production of O_3 ice was sufficiently impeded to bring the abundance below the limit observed in the comet. This test simultaneously showed a match between both the abundances of O_2 ice and H_2O_2 ice and the cometary abundances at 25 K between 0.8-1 Myr evolution for an ionisation level of $\zeta = 10^{-17}$ s^{-1}, starting from the reset scenario. Thus, a sweet spot in the parameter space, where all three species match observed abundances, was found. However, it should be emphasised that such a high barrier is not supported in previous analyses of laboratory experiments. An upper limit for the activation energy of O + O_2 of E_{act} = 150 K on amorphous silicate surfaces was derived from experimental results by Minissale et al. (2014). Lamberts et al. (2013) required an activation energy of E_{act} = 500 K in order to reproduce experimental results from Ioppolo et al. (2010) of O_3 production on thick ices, and in agreement with this result, Taquet et al. (2016) were able to reproduce the low abundances O_3 and O_2H on ice mantles in dark clouds using an activation energy of E_{act} = 300 K.

In this work O_3 has remained overproduced for these levels of activation energies, even when increasing it to E_{act} = 1000 K. Only using an artificially high energy of E_{act} = 2000 K for the O + O_2 reaction lowered the abundance of O_3 ice to the observed level. This could suggest that as-of-yet unknown reactions may be missing from the network: reactions involving either O_2 or O that do not lead to O_3 (so O and O_2 get locked up in other molecules than O_3) and/or new routes for destruction of O_3 ice.

4.4.6 Location of O_2 ice production sweet spot in PSN disk midplane

Taking the sweet spot for matching abundances of O_2 ice, H_2O_2 ice and O_3 ice, it is interesting to look at where in the PSN disk midplane the physical conditions for this match may be satisfied.

A close look at Fig. 4.1a shows that indeed in the radial range ∼100-130 AU is found a temperature of ∼25 K and is found a density of $10^9 - 10^{10}$ cm^{-3}. Thus, for the sweet-spot O_2 ice production scenario, this would be the predicted radial range for formation of both comets 1P and 67P, and a formation time scale by 0.8-1 Myr, given the model assumptions. This radial range is 2-3 times larger than the orbit of the present day Kuiper belt (30-50 AU).

4.4.7 Primordial origin of O_2 ice

A scenario that did predict early presence of O_2 ice to within the observed level, and H_2O_2 ice and O_3 ice orders of magnitude lower than that of O_2 ice, is the scenario starting with an initial abundance of O_2 of ∼5% with respect to the total elemental oxygen abundance, which was inspired by the results of Taquet et al. (2016) assuming that the O_2 is inherited from the parent cloud. Given early formation of the comets (by thousands to tens of thousands of years after formation of the PSN midplane), this scenario remains likely for the formation of the ices, and the fiducial values of $b_{\rm qt}$ = 1 Å and $E_{\rm act}$= 500 K for the O + O_2 reaction in the ice. This scenario agrees with the findings of Taquet et al. (2016).

4.5 Conclusion

Since the somewhat unexpected detection of abundant O_2 ice in the coma of comet 67P, several studies have attempted to explain the origin of the O_2. Building on the results from Paper 1, this work has investigated the possibility of in-situ formation of O_2 ice on grains in the midplane of the PSN disk midplane.

While a high abundance of O_2 ice, matching that observed in comet 67P, was reproduced outside the O_2 ice in the PSN disk midplane at intermediate evolutionary stages when assuming the initial chemistry to be reset, the same production was not seen after including O_3 ice chemistry into the chemical network. For the fiducial choice of parameters for grain-surface chemistry, and an activation energy of 500 K for the $O + O_2 \longrightarrow O_3$ reaction on the grains, O_3 ice was in most cases found to be the dominant oxygen-carrier next to H_2O ice, and O_2 ice was orders of magnitude too low in abundance compared to the abundance observed in comet 67P.

In order to test the sensitivity of the production of O_2, O_3, and H_2O_2 ices to the assumed parameters for grain-surface chemistry, in particular the barrier width for quantum tunnelling $b_{\rm qt}$ and the ratio of diffusion-to-binding energy of ice molecules $E_{\rm diff}/E_{\rm bin}$, a parameter space investigation was conducted. Several temperatures and densities were also tested, and the reset scenario assumed for initial abundances. This led to a sweet-spot set of parameters being revealed: $b_{\rm qt}$=

2Å, $E_{\rm diff}/E_{\rm bin} = 0.3 - 0.5$ T=15-25 K and $n = 10^9 - 10^{10}$ cm^{-3} which facilitated O_2 reproduction matching the observed level. However, the abundances of O_3 and H_2O_2 ices were still in disagreement with the observed values by orders of magnitude.

As a last adjustment of the chemistry intended to lower the O_3 ice abundance, the activation energy for production of O_3 ice from the association of O and O_2 ices was increased in order to mitigate possible unknown chemical pathways away from O_3. For an activation energy of $E_{\rm act}$ = 2000 K, $E_{\rm diff}/E_{\rm bin}$ = 0.5, and the remaining physical and chemical conditions as given above, the abundances of O_2 ice, H_2O_2 ice, and the upper limit for O_3 ice in the comet were all reproduced. This matches a formation location in the PSN disk midplane between 120-150 AU, just outside the O_2 iceline. However, this high activation energy for O_3 ice production is not supported by laboratory estimates, and thus more laboratory work is needed to determine potential missing chemical pathways for O_3 ice chemistry.

A model starting out with a percentage of elemental oxygen locked in O_2 and thus assuming a primordial origin of O_2, also reproduced the observed abundance of O_2 ice at early stages of evolution, without increasing $E_{\rm act}$ for the O + O_2 reaction. Here, the O_3 and H_2O_2 ice abundances were below the O_2 ice abundance, but not matching the observed abundance levels. However, since the observed abundances of all three ices species are only reproduced in this work in the case for a set of rather extreme choices for the chemical parameters, the most plausible explanation for the origin of the cometary O_2 ice remains the primordial one, as originally proposed by Taquet et al. (2016).

Acknowledgements: The authors thank Ewine van Dishoeck and Arthur Bosman for many useful discussions and comments that helped the investigation and improved the quality of the manuscript. The authors also thank an anonymous referee for their review of this work. Astrochemistry in Leiden is supported by the European Union A-ERC grant 291141 CHEMPLAN and the Netherlands Research School for Astronomy (NOVA). CW also acknowledges the Netherlands Organisation for Scientific Research (NWO, grant 639.041.335) and the University of Leeds for financial support.

4.A Appendix: additional figures

Fig. 4.12 shows the gas and ice abundances of O, O_2, H_2O and H_2O_2 as a function of radius by 10 Myr of evolution, for the chemical network without O_3 chemistry. Fig. 4.13 shows the gas and ice abundances of O_2, H_2O and H_2O_2 and O_3 as a function of radius by 10 Myr of evolution, for the chemical network including O_3.

Table 4.3: Initial abundances (with respect to H_{nuc}) for atomic (reset scenario) and molecular (inheritance scenario) setups.

Species	Atomic	Molecular
H	9.1×10^{-5}	5.0×10^{-5}
He	9.8×10^{-2}	9.8×10^{-2}
H_2	5.0×10^{-1}	5.0×10^{-1}
N	6.2×10^{-5}	
O	5.2×10^{-4}	
C	1.8×10^{-4}	
S	6.0×10^{-6}	
H_2O		3.0×10^{-4}
CO		6.0×10^{-5}
CO_2		6.0×10^{-5}
CH_4		1.8×10^{-5}
N_2		2.1×10^{-5}
NH_3		2.1×10^{-5}
CH_3OH		4.5×10^{-5}
H_2S		6.0×10^{-6}
O_2		0

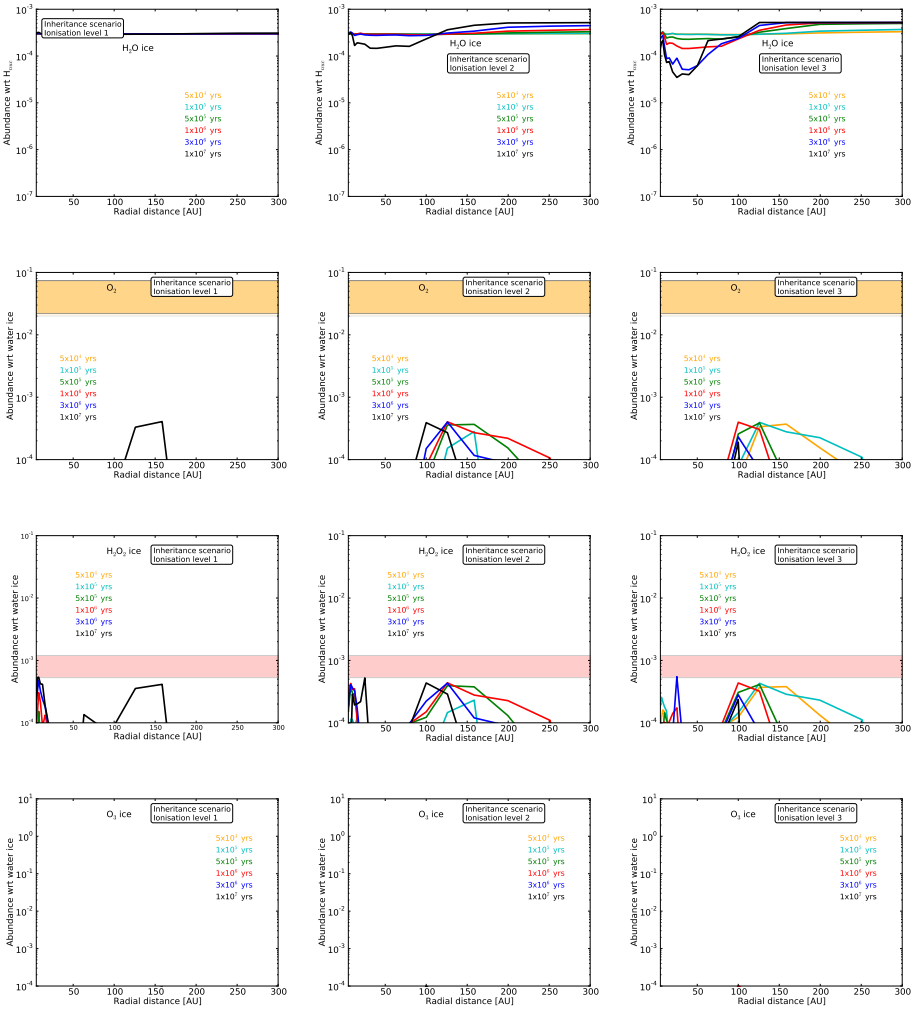

Figure 4.5: Radial abundance profiles for the inheritance scenario at multiple evolutionary time steps. Top to bottom are H_2O, O_2 and H_2O_2 and O_3 ices. Left to right are increasing ionisation levels. For O_2, H_2O_2, and O_3 the limits, and upper limit, detected in comet 67P, are indicated as yellow, red and grey shaded areas, respectively. The chemical network utilised includes O_3 chemistry.

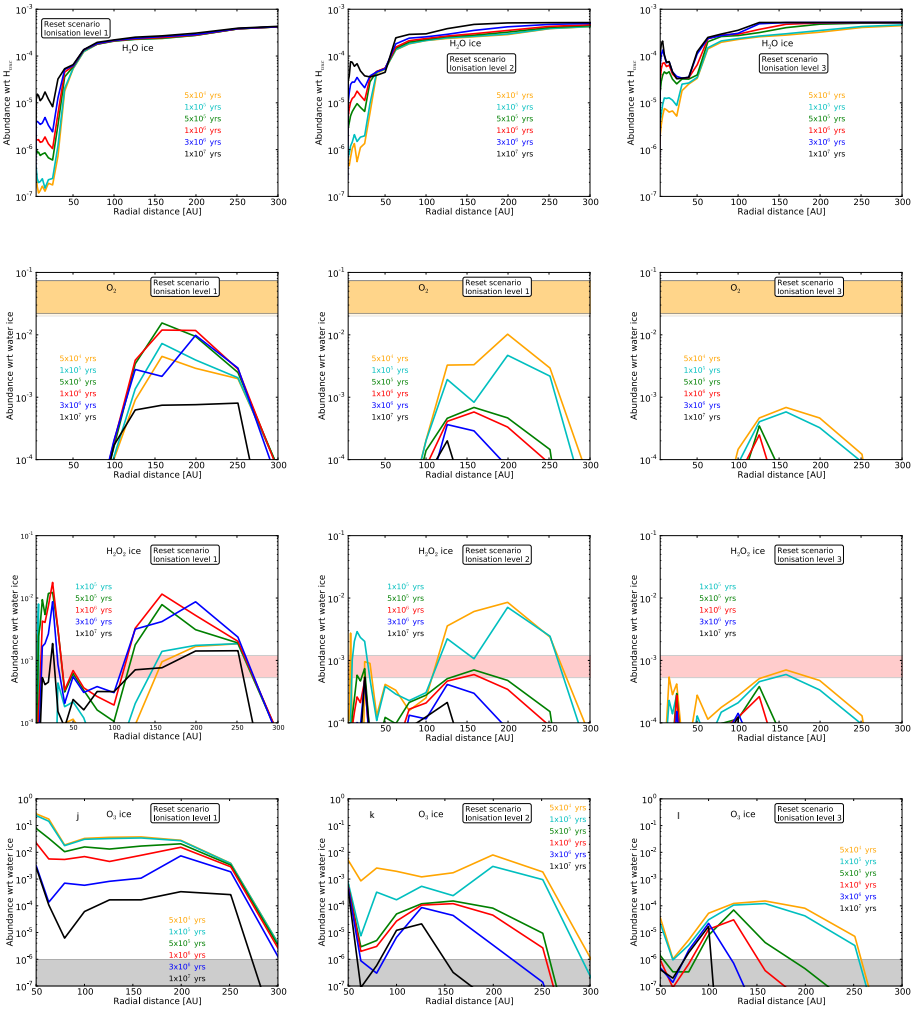

Figure 4.6: Radial abundance profiles for the reset scenario at multiple evolutionary time steps. Top to bottom are H_2O, O_2 and H_2O_2 and O_3 ices. Left to right are increasing ionisation levels. For O_2, H_2O_2, and O_3 the limits, and upper limit, detected in comet 67P, are indicated as yellow, red and grey shaded areas, respectively. The chemical network utilised includes O_3 chemistry.

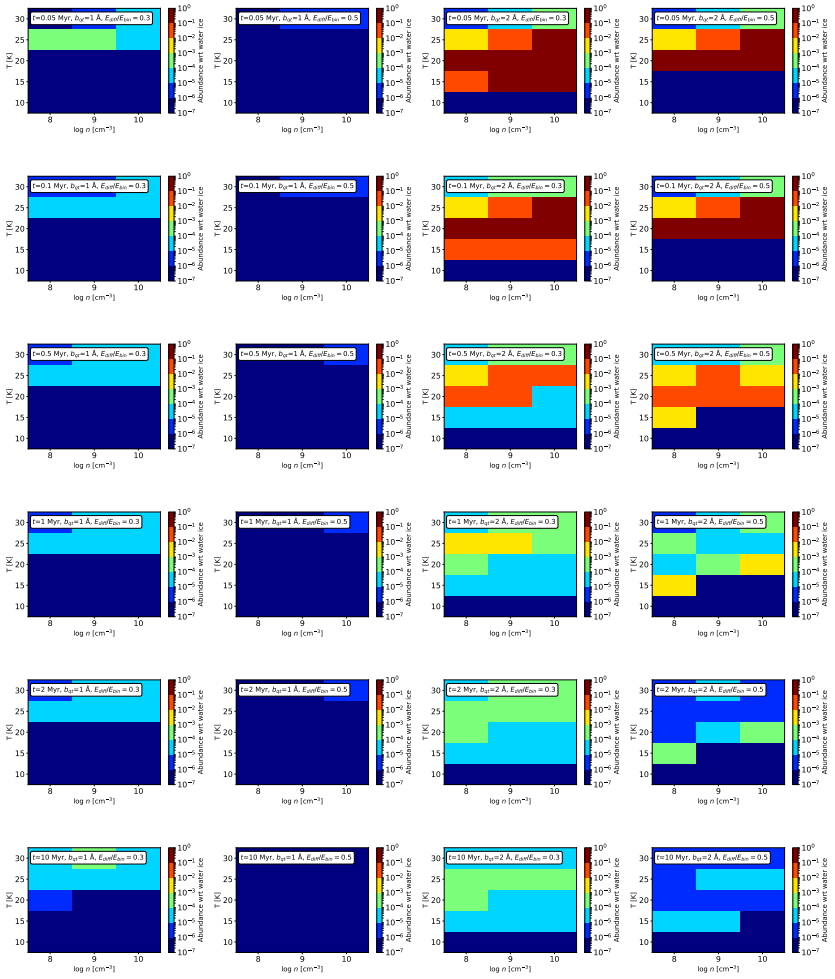

Figure 4.7: Abundances (given as colors) for O_2 ice as function of midplane density (x-axes), and temperature (y-axes) at different evolutionary steps for the reset scenario. From left to right are abundances from model runs with different parameters for grain-surface reactions: columns one and two feature b_{qt}= 1 Å, columns three and four feature b_{qt}= 1 Å, columns one and three are with $E_{\rm diff}/E_{\rm bin}$= 0.3, and columns two and four are with $E_{\rm diff}/E_{\rm bin}$= 0.5. Top to bottom are different evolutionary times, from 0.05 Myr (top) to 10 Myr (bottom). To the right of each plot is a colorbar, indicating the abundance level with respect to H_2O ice for each color. The chemical network utilised includes O_3 chemistry. Orange matches cometary O_2 abundances.

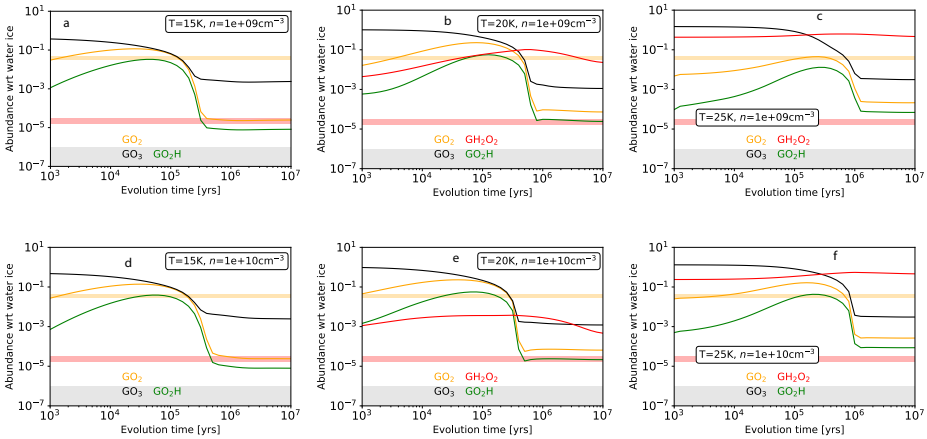

Figure 4.8: Evolving abundances as function of time for the reset scenario for six different combinations of temperature (15, 20, or 25 K), density (10^9 or 10^{10} cm^{-3}) and molecular diffusion-to-binding energy ratio of 0.3. The barrier width for quantum tunnelling is $b_{qt} = 2$ Å. The orange shaded regions indicates the limits to the measured abundance of O_2 ice in the coma of comet 67P. The red shaded regions indicates the limits to the measured abundance of H_2O_2, and the top of the grey shaded region marks the upper limit to the measured abundance of O_3 ice in comet 67P. The chemical network utilised includes O_3 chemistry.

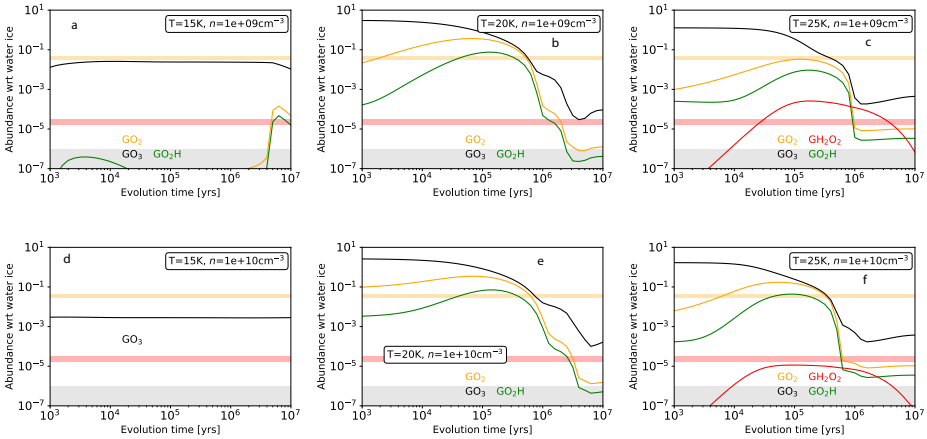

Figure 4.9: Evolving abundances as function of time for the reset scenario for six different combinations of temperature (15, 20 or 25 K), density (10^9 or 10^{10} cm^{-3}) and molecular diffusion-to-binding energy ratio of 0.5. The barrier width for quantum tunnelling is $b_{qt} = 2$ Å. The orange shaded regions indicates the limits to the measured abundance of O_2 ice in the coma of comet 67P. The red shaded regions indicates the limits to the measured abundance of H_2O_2, and the top of the grey shaded region marks the upper limit to the measured abundance of O_3 ice in comet 67P. The chemical network utilised includes O_3 chemistry.

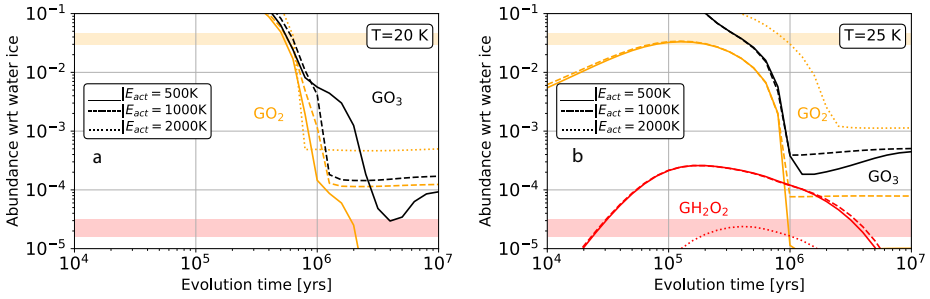

Figure 4.10: Evolving abundances for O_2 ice, H_2O_2 ice and O_3 ice for three different activation energies for the reaction iO + iO_2. a) is for T=20 K. b) is for T= 25 K. The barrier width for quantum tunnelling is $b_{qt} = 2$ Å, and the molecular diffusion-to-binding energy is 0.5.

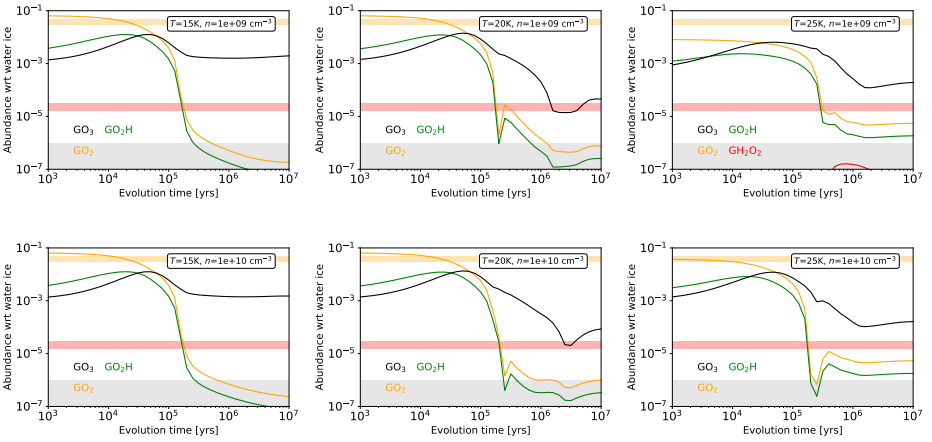

Figure 4.11: Evolving abundances as function of time for the inheritance scenario, plus 5% extra elemental oxygen as O_2, for six different combinations of temperature (15, 20 or 25 K), density (10^9 or 10^{10} cm^{-3}) and molecular diffusion-to-binding energy ratio of 0.5. The barrier width for quantum tunnelling is $b_{qt} = 2$ Å. The orange shaded regions indicates the limits to the measured abundance of O_2 ice in the coma of comet 67P. The red shaded regions indicates the limits to the measured abundance of H_2O_2, and the top of the grey shaded region marks the upper limit to the measured abundance of O_3 ice in comet 67P.

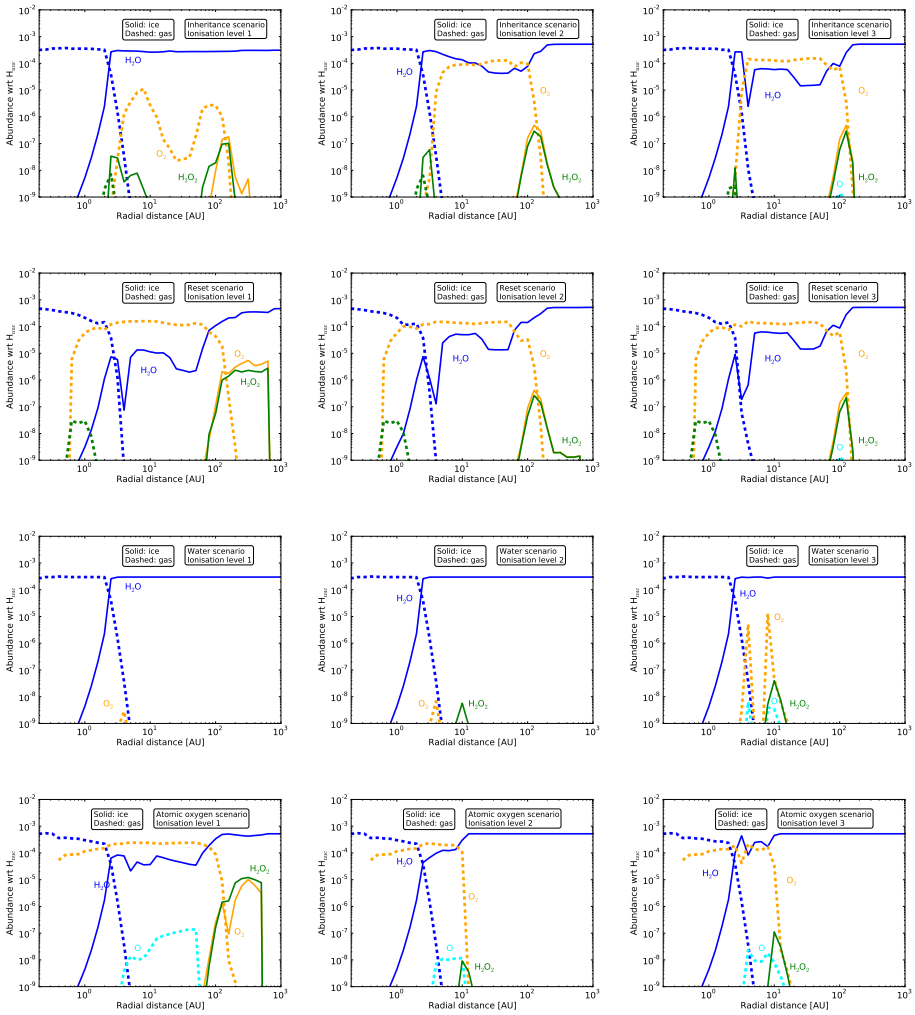

Figure 4.12: Abundances by 10 Myr evolution for. Top to bottom are the inheritance scenario, the reset scenario, the water scenario, and the oxygen scenario, see the panels. Left to right are changing ionisation levels. The chemical network utilised does not include O_3 chemistry.

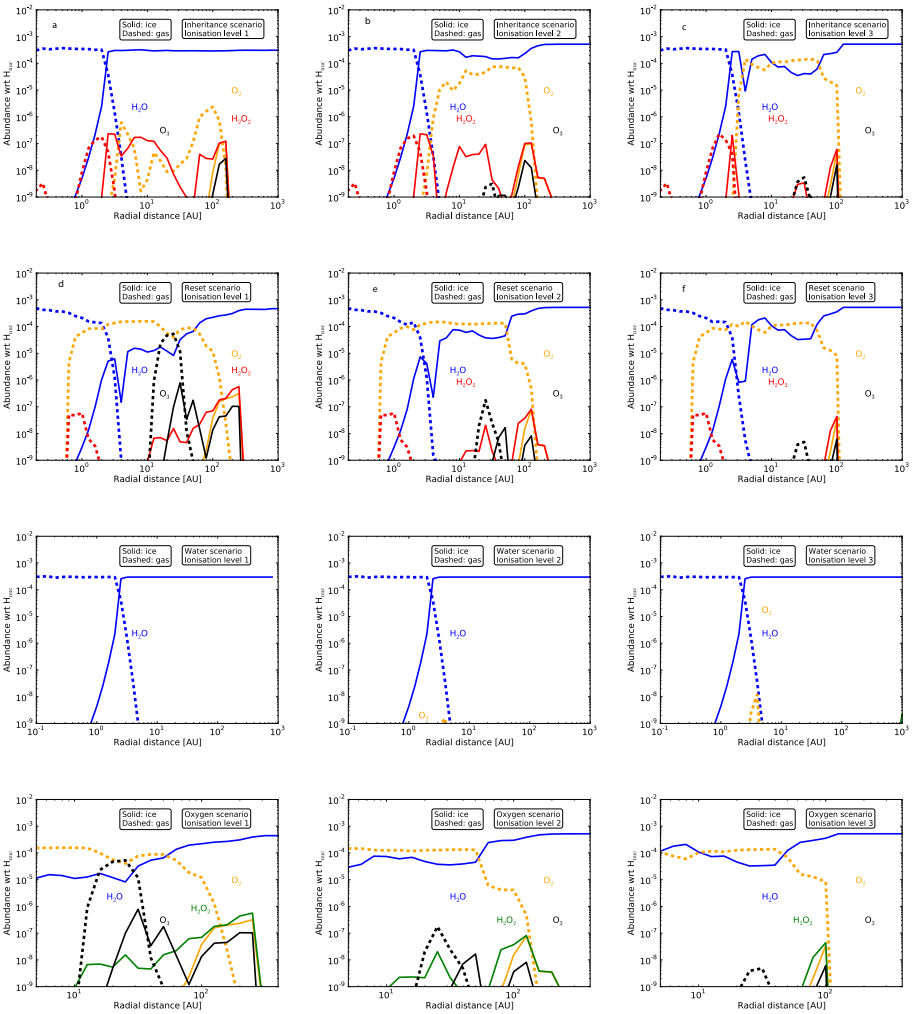

Figure 4.13: Abundances by 10 Myr evolution for. Top to bottom are the inheritance scenario, the reset scenario, the water scenario, and the oxygen scenario, see the panels. Left to right are changing ionisation levels. The chemical network utilised includes O_3 chemistry.

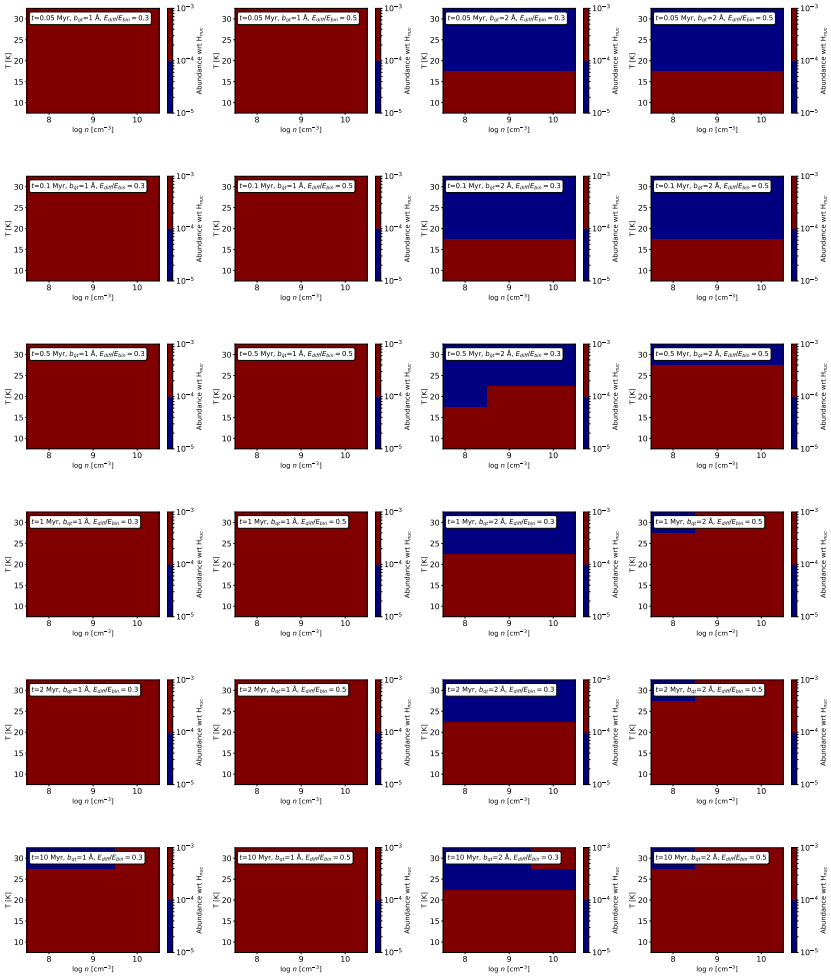

Figure 4.14: Abundances (given as colors) for H_2O ice as function of midplane density (x-axes), and temperature (y-axes) at different evolutionary steps for the reset scenario. From left to right are abundances from model runs with different parameters for grain-surface reactions: columns one and two feature b_{qt}= 1 Å, columns three and four feature b_{qt}= 1 Å, columns one and three are with $E_{\rm diff}/E_{\rm bin}$= 0.3, and columns two and four are with $E_{\rm diff}/E_{\rm bin}$= 0.5. Top to bottom are different evolutionary times, from 0.05 Myr (top) to 10 Myr (bottom). To the right of each plot is a colorbar, indicating the abundance level with respect to $H_{\rm nuc}$ for each color. The chemical network utilised includes O_3 chemistry.

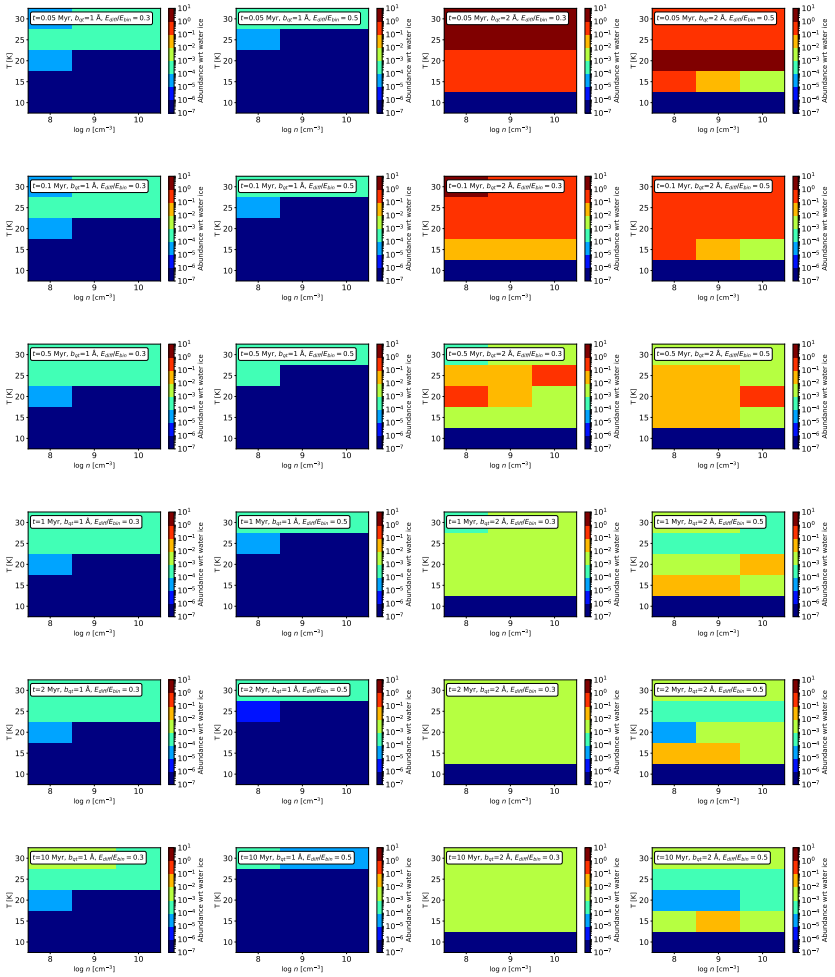

Figure 4.15: Abundances (given as colors) for O_3 ice as function of midplane density (x-axes), and temperature (y-axes) at different evolutionary steps for the reset scenario. From left to right are abundances from model runs with different parameters for grain-surface reactions: columns one and two feature b_{qt}= 1 Å, columns three and four feature b_{qt}= 1 Å, columns one and three are with $E_{\rm diff}/E_{\rm bin}$= 0.3, and columns two and four are with $E_{\rm diff}/E_{\rm bin}$= 0.5. Top to bottom are different evolutionary times, from 0.05 Myr (top) to 10 Myr (bottom). To the right of each plot is a colorbar, indicating the abundance level with respect to H_2O ice for each color. The chemical network utilised includes O_3 chemistry. Darkest hue of blue matches the upper limit for cometary O_3 abundances.

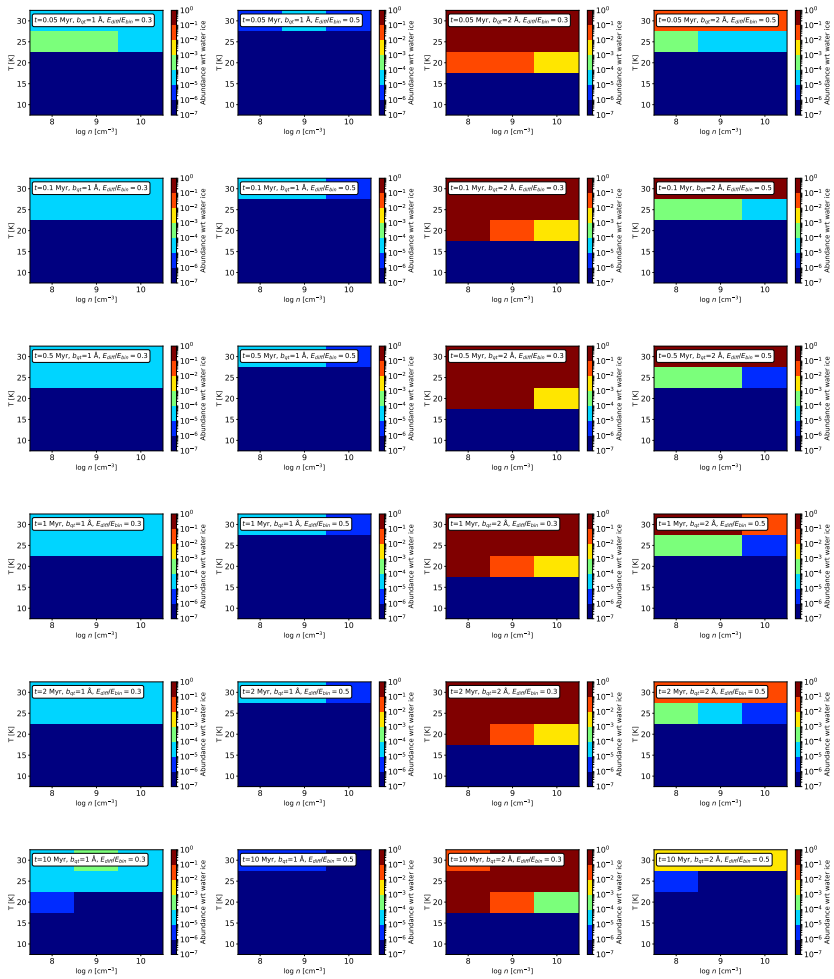

Figure 4.16: Abundances (given as colors) for H_2O_2 ice as function of midplane density (x-axes), and temperature (y-axes) at different evolutionary steps for the reset scenario. From left to right are abundances from model runs with different parameters for grain-surface reactions: columns one and two feature b_{qt}= 1 Å, columns three and four feature b_{qt}= 1 Å, columns one and three are with $E_{\rm diff}/E_{\rm bin}$= 0.3, and columns two and four are with $E_{\rm diff}/E_{\rm bin}$= 0.5. Top to bottom are different evolutionary times, from 0.05 Myr (top) to 10 Myr (bottom). To the right of each plot is a colorbar, indicating the abundance level with respect to H_2O ice for each color. The chemical network utilised includes O_3 chemistry. Lightest hue of blue matches the cometary H_2O_2 abundances.

5 Matching protoplanetary disk midplane chemical evolution to cometary compositions

A chemical evolution taxonomy for comets

C. Eistrup, C. Walsh, D. Carr, M. Drozdovskaya & E.F. van Dishoeck
In preparation for Astronomy and Astrophysics

Abstract - Comets are planetesimals left over from the formation of planets in the Solar System. They reside far away from the Sun, and are built up of pristine ices that may trace the chemical history of the Solar System. With a growing number of observed molecular abundances in many comets, and an improved understanding of chemical evolution in protoplanetary disk midplanes, comparisons can be made between models and observations, that could potentially constrain the formation histories of comets.

Aim: To carry out the first statistical comparison between cometary volatile ice abundances and modelled evolving abundances in a protoplanetary disk midplane. A χ^2-method is used to determine maximum likelihood surfaces for 15 different comets to have formed at a given time (up to 8 Myr) and place (out to 30 AU) in the pre-Solar nebula midplane.

Methods: This is done using observed volatile abundances for 15 comets, and the evolution of volatile abundances from chemical modelling in disk midplanes. Two assumptions for the chemical modelling starting conditions (cloud inheritance or chemical reset), as well as two different sets of cometary species (parent species, with or without sulphur species) are investigated.

Results: When considering all parent species (ten molecules) in the reset scenario the χ^2 likelihood surfaces show a characteristic trail in the parameter space with high likelihood of formation between 30 AU at early times and 15 AU at later times, for five comets. This trail roughly traces the CO iceline. For the inheritance scenario, somewhat good agreement is found for five comets, suggesting they formed inside 15 AU. When only considering carbon and oxygen bearing species good agreement is found for ten comets for the reset scenario, also suggesting they formed at or inside the CO iceline, but possibly at different times during the 8 Myr timescale. Comparing the carbon and oxygen bearing species to the inheritance scenario also shows the same trends as for the inheritance scenario with the full sample of species considered.

Conclusions: A statistical comparison between observed and modelled chemical abundances in comets and comet-forming regions is potentially a powerful tool for constraining cometary formation histories. Reducing the number of considered species to only carbon and oxygen bearing species (seven species in total) constrains the formation of 14 out of 15 comets to the vicinity of the CO iceline (moving from ∼30 to ∼15 AU over time), with chemistry having been (partially) reset early in the pre-Solar nebula. These comets did not previously fall into the same taxonomical categories together, therefore this chemical constraint may be proposed as an alternative taxonomy for comets. Based on the most likely time for each of these comets to have formed during the disk chemical evolution, a formation time classification for these 14 comets is proposed.

5.1 Introduction

When the Solar System formed 4.6 billion years ago, the planets formed their cores from solid material in the pre-Solar nebula. In the outer, colder regions of this nebula volatile molecules such as H_2O, CO_2 and CO were frozen out as ices on the surfaces of grains, and later larger bodies. Some of these bodies merged to form the planetary cores, and eventually the Jovian planets, but some of this solid material remained unused by planets, and is still present in our Solar System today as comets.

Comets are made up of partly refractory dust and partly volatile ices. These ices reside deep inside the comets, and they are thought to be pristine samples of the material that was present in the pre-Solar nebula (see review by Mumma & Charnley 2011). Comets are thus interesting because of what they can tell us about the chemical composition in the icy outer pre-Solar nebula 4.6 billion years ago, but also because comets are known to have impacted on the Earth, after having been dynamically scattered towards the Sun from the outer Solar System. The material (volatile and organic) they carry on them has thus added to the chemical make-up of the Earth, and understanding the origin of water and life on the Earth may have traces back to comets.

Comets have been observed from the ground and from space for decades, in various wavelength regimes. Several efforts have gone into detecting molecular species in the comae of comets, and using these to classify them (A'Hearn et al. 1995; Fink 2009; Mumma & Charnley 2011; Cochran et al. 2012; Le Roy et al. 2015). At least two classification groups have been proposed for cometary compositions: "Typical" and "Depleted", where "Depleted" refers to a depletion in organic carbon-chain molecules, compared with the "Typical" compositions (see e.g. Cochran et al. 2012). Hundreds of comets have been analysed for composition. The majority of these (75-91%) fall under the "Typical" category, as found by Cochran et al. (2012). They also find good agreement with the other studies (e.g. A'Hearn et al. 1995; Fink 2009) as to which comets are depleted, and which are not.

However, relating observed cometary species to the actual cometary compositions remains a challenge. This is because some parent species (e.g. NH_3 and HCN) sublimating from the comet get dissociated into chemical daughter species, such as radicals (e.g. NH_2 and CN for parent species NH_3 and HCN, respectively), when moving from the surface to the coma of the comet. Tracing which daughter species originate from which parent species, and how the daughter species abundance in the coma translates to parent species' abundances near the surface is tricky, as pointed out by e.g. Le Roy et al. (2015).

Recently, ESA's *Rosetta* mission visited comet 67P, and orbited the comet for two years with an armada of instruments, providing unprecedented details about the comet. The ROSINA instrument has been particularly powerful for determing chemical composition. The comet showed very different amounts of produced species from the summer to the winter hemispheres (Le Roy et al. 2015), and hence it is difficult to say which amounts of which species are representative of the bulk composition, since temperature plays a role. It is in turn difficult to classify

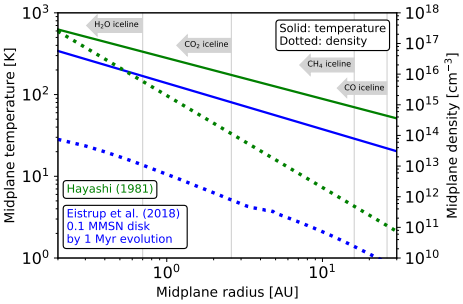

Figure 5.1: Physical structures of the disk midplanes for the pre-Solar nebula from Hayashi (1981) (in green), and for the 0.1 MMSN disk by 1 Myr evolution from Eistrup et al. (2018) (in blue). Solid profiles are for temperature. Dotted profiles are for number density. The vertical grey lines indicate the positions of the icelines of H_2O, CO_2, CH_4 and CO by 1 Myr evolution for the 0.1 MMSN disk in Eistrup et al. (2018). The grey arrows on each of the vertical lines indicate which species each line is associated with, and how the iceline moves over time (all inwards).

this comet's composition according to the "Typical"-and-"Depleted"-scheme.

In this work, a quantitative comparison between the observed cometary abundances and the protoplanetary disk midplane chemical evolution models from Eistrup et al. (2018) will be made. Molecular abundances, observed mainly from remote sensing with infrared (IR) and mm telescopes, for each of the 15 comets presented in Le Roy et al. (2015) will be compared statistically in time and space with volatile abundances from the models. The aim is to test if there is a statistical connection between current cometary abundances, and where and when such abundances were found in the pre-Solar nebula, thereby possibly tracing the formation histories of the comets. Based on this test, a possible "chemical evolution"-taxonomy of comets may be established if multiple comets match the same formation histories.

5.2 Methods

5.2.1 Model description

The modelled volatile ice abundances are taken from Eistrup et al. (2018). A physical disk model evolving in time was used featuring decreasing temperature and density structures from 0 to 30 AU, with the CO iceline residing inside 30 AU. Icelines (or snowlines) mark the radius in the disk midplane beyond which species exist solely in ice form and are thus depleted from the gas. This occurs at the radius where the accretion rate onto grain surfaces (or freezeout) exceeds the desorption rate from grain surfaces due to the negative temperature gradient in the midplane. The position of the midplane iceline for a particular species will depend on its volatility (i.e., its binding energy).

The disk structure used is not the pre-Solar nebula structure proposed by Hayashi (1981), and parameterised in Aikawa et al. (1997). However, the utilised

disk structure here is evolving in time, and chemical evolution model results are readily available from Eistrup et al. (2018). Besides, the locations in the disk important to comet formation are the volatile icelines, which are closer to the star for a colder disk, and further away from it for a warmer disk. Tracking comet formation based on iceline positions therefore means that the exact choice of physical disk structure is less important, and in addition, the 30 AU range of this disk covers all important icelines (including the CO iceline which starts just inside 30 AU).

Figure 5.1 shows a comparison of the midplane temperature and density structures from Hayashi (1981), and from Eistrup et al. (2018) (for the 0.1 MMSN disk by 1 Myr evolution), extending to 30 AU. The structures are different, in that the structure from Hayashi (1981) is warmer (roughly twice as high temperature at any radius) and more massive (more than ten times higher mass) compared to the disk from Eistrup et al. (2018) (hence the "0.1 Minimum Mass Solar Nebula"-designation for this disk). It is noted that the disk from Eistrup et al. (2018) has already lost mass by 1 Myr evolution, so in Fig. 5.1 the density difference between the disks is more than ten times. The disk mass of 0.1 MMSN from Eistrup et al. (2018) is the starting mass of the disk, not the mass by 1 Myr (as plotted in Fig. 5.1).

Results for the high ionisation rate are taken, which includes contributions from galactic cosmic rays, as well as decay products of short-lived radionuclei in the disk midplane (see e.g. Cleeves et al. 2013a; Padovani et al. 2018). A timescale up to 8 Myr is assumed for a long-lived gaseous protoplanetary disk. The high ionisation rate of typically $10^{-17}\mathrm{s}^{-1}$ means that chemical changes occur after a few 10^5 yrs. The disk structure cooling in time means that the volatile icelines move inwards in time.

Two different sets of initial abundances are assumed: inheritance and reset. Inheritance assumes all ices to have survived the trip from the parent molecular cloud to the disk midplane, thereby starting the chemical modelling with neutral molecules that are abundant in interstellar ices. The reset scenario assumes an energetic event to have dissociated all molecules into atoms (chemical reset) upon arrival in the midplane, thereby starting the chemical modelling with highly reactive atoms. This effect was proposed to happen in the hotter regions close to the protostar by e.g. Visser et al. (2009). The inner Solar System is assumed to have undergone some amount of chemical reset (with evidence from studies of chondrules and CAIs, see e.g. Trinquier et al. 2009), followed by a condensation sequence, depending on location in the disk. Comets, on the other hand, are often thought to be pristine, possibly because they formed, and mainly reside in the outer Solar System.

Colour maps of evolving abundances for different volatile ice species with respect to H_2O ice for both reset and inheritance scenarios are shown to the left in Figs. 5.6-5.10 in the Appendix. These plots allow an overview of when and where the different ice species are abundant. It can be seen that there are regions in the radius-time parameter space at which the modeled ice ratios well reproduce the observed ratios for most species. Based on these plots, the ice species considered in the statistical analysis are CO_2, CO, O_2, CH_4, C_2H_6, H_2S, OCS, SO_2, H_2CO and

CH_3OH. It is noted in each panel which molecule is considered, and whether the inheritance or the reset scenario has been assumed. To the right of the colour maps are shown the observed abundances of the given ice species in different comets. The ice species NH_3, HCN, HNCO, CH_3CN and C_2H_2 have all been detected and modelled, but they are excluded from the analysis. This exclusion is based on nitrogen ice chemistry in protoplanetary disks remaining poorly understood (see e.g. Schwarz & Bergin 2014; Walsh et al. 2015). Lastly, C_2H_2 is most likely to be a daughter species, and thus also not constraining the bulk cometary composition.

Daughter species in general have been excluded because the parent species are expected to be dominant in cometary ices, even if the daughter species are abundant in the comae. Since the daughter species in the coma originate from dissociated parent species in the gas after sublimation, the exclusion of daughter species means that the detected abundances of parent species in the coma are likely lower than the actual abundance on the cometary surface.

The detected abundances of each molecule in each comet are taken from Tables, 2, 3, 4 and 5 in Le Roy et al. (2015). If multiple values are given for the abundance of an ices species, then the median is used, and the difference between this median and the lowest given value is taken as the error. If only one abundance value was available, then a conservative error estimate of 50% of the observed value is assumed. This estimate is reasonable when compared with observed errors (see figures A1 to A5).

5.2.2 Statistical comparison between observations and models

With observed abundances of several molecules available for all comets, along with the evolving spatial midplane abundances of those molecules, it can now be quantified how likely it is for a comet to have formed at a given time and place, assuming that the comets acquired all their ices at one time and place, and that the ices remained unaltered thereafter.

For each comet, a log-space χ^2-surface in time t and radius r is computed. We do the analysis in log-space because of the large dynamical range (orders of magnitude) in the modelled abundances; hence, we consider a good agreement to lie within an order of magnitude of the observed ratio. For each set of radius r and time t, the χ^2 value for a given comet is given by

$$\chi^2(r,t) = \sum_{i=1}^{n} \frac{\left(\log(n_{i,\mathrm{obs}}(r,t)) - \log(n_{i,\mathrm{mod}}(r,t))\right)^2}{\sigma'_{i,\mathrm{obs}}(r,t)^2}, \tag{5.1}$$

where $n_{i,\mathrm{obs}}(r,t)$ and $n_{i,\mathrm{mod}}(r,t)$ are the observed and modelled abundance of species i with respect to H_2O ice at (r,t). $\sigma'_{i,\mathrm{obs}}(r,t)$ is defined as

$$\begin{aligned}\sigma'_{i,\mathrm{obs}}(r,t) = \max(&|\log(n_{i,\mathrm{obs}}(r,t) + \sigma_{i,\mathrm{obs}}(r,t)) - \log(n_{i,\mathrm{obs}}(r,t))|,\\ &|\log(n_{i,\mathrm{obs}}(r,t) - \sigma_{i,\mathrm{obs}}(r,t)) - \log(n_{i,\mathrm{obs}}(r,t))|)\end{aligned} \tag{5.2}$$

where $\sigma_{i,\mathrm{obs}}(r,t)$ is the observed or estimated error on the abundance. We use this prescription as it is a more conservative estimate for the error when propagated using a log function. For the case where $\sigma_{i,\mathrm{obs}}(r,t) \ll n_{i,\mathrm{obs}}(r,t)$, one can estimate $\sigma'_{i,\mathrm{obs}}(r,t) \sim \sigma_{i,\mathrm{obs}}(r,t)/n_{i,\mathrm{obs}}(r,t)$; however, here, the errors are of the same order of magnitude as the measurement.

The χ^2-surface for each comet is then transformed into a maximum likelihood function $P(r,t)$ using

$$P(r,t) \propto e^{-\chi^2(r,t)/2} \tag{5.3}$$

and subsequently all sets of $P(r,t)$ for each comet are normalised by the maximum P-value for that comet. The resulting surfaces of maximum likelihood show contours of different colours in different regions of parameter space, with colours depending on how close a region is to the maximum likelihood value for the comet. Regions of parameter space close to the maximum likelihood value for a comet are in turn the regions showing best agreement between the chemical models and the observed cometary abundances.

These maximum likelihood (P-value) surfaces are shown for all comets in Fig. 5.2 which compares observations with models of the reset scenario, and in Fig. 5.3 for models of the inheritance scenario. The x-axes in each panel in each figure are radial distance from the star in AU, and the y-axes are chemical evolution time in Myr. For each contour level the value of the contour indicates where the fraction of the local P-value to the maximum P-value is above a certain level, for each comet. Regions of yellow contour indicate good agreement between models and observations, whereas darker colours indicate poorer agreements.

The comet names, and dynamical types from Cochran et al. (2012), are listed in all panels. In each panel is also given the number of molecular detections for each comet (from Le Roy et al. 2015), with the panels from left to right, and top to bottom featuring decreasing numbers of molecular detections per comet. This way, the first panel with ten molecular detections (Comet 67P-S) can be distinguished from the last panel with only two molecular detections (Comet 21P), in that more molecular detections in a comet should make the comparison between the models and the observations more robust.

5.3 Results

5.3.1 Full sample of species

5.3.1.1 Reset scenario

Fig. 5.2 features the maximum likelihood surfaces for the reset scenario with the full sample of species. For all comets, there are regions of the parameter space that show good agreement between models and observations. All comets are in good agreement with formation between 12-15 AU by $\sim$ 8 Myr evolution, and most comets, excluding comets 67P-W, LINEAR and 17P, also show good agreement with formation between 27-30 AU by $\sim$0.5-1 Myr evolution. For comets Lemmon,

103P, 9P, 6P, 2P, and 21P, the two aforementioned regions of parameter space are connected with the contours at the chosen levels (down to 10^{-4} relative to the maximum likelihood value for each comet). For comets 103P and 2P there is a high degree of degeneracy in radius and time, as the maximum contours for these comets follow a trail spanning from the aforementioned 30 AU by $\sim$ by 1 Myr inwards to $\sim$ 12 AU by 8 Myr evolution. This trail is marked by the red shaded region overplotted for comet 2P, and this trail overlaps with the regions of highest likelihood for all comets, except for comet 17P.

The trail, in turn, roughly traces the CO iceline (at $T \sim 20$ K), as is seen in the left panel of fig. 4 in Eistrup et al. (2018). This figure, amongst others, shows the changing location of the CO iceline in the physically evolving disk midplane utilised in that work. This is interesting, because it points to all the comets here, except comet 17P, agreeing well with formation in the vicinity the CO iceline in the pre-Solar nebula.

Comet 17P, as an outlier, is seen to have several regions of parameter space in which it shows good agreement with formation. These regions are: 2-3 AU by 8 Myr, 5 AU by 0.5 Myr, 11 AU by both <0.5 Myr and by 8 Myr, and a large region at large radii at late evolutionary times. From this point of view, comet 17P is somewhat less constrained with respect to its formation time and location, than the other comets. Although comet 17P does show agreement over the regions of parameter space described above, it appears that this comet does not agree with formation along the CO iceline.

Additionally, all comets, except comets 73P, 6P and 2P, show high likelihood of formation at 5-10 AU by 7-8 Myr, which is roughly at the CH_4 iceline (see again fig. 4, left panel, in Eistrup et al. 2018).

5.3.1.2 Inheritance scenario

Turning to the inheritance scenario the maximum likelihood surfaces for all comets are presented in Fig. 5.3. All comets in this scenario share good agreement with formation at $\sim$ 12 AU by 8 Myr, similar to the case for the reset scenario in Fig. 5.2. All comets also show agreement with late formation (7-8 Myr) from small radii out to 10 AU, and some (103P, 6P, Lovejoy and 21P) also agree well with having formed inside 5 AU at various times during the evolution. The trail along the CO iceline that was seen for the reset scenario is not reproduced for all comets in the inheritance scenario. However, Hale-Bopp, LINEAR, Lemmon, 103P, 9P, 6P and 21P do somewhat agree with parts of the trail (103P and 6P are both in good agreement with the trail).

Most of the comets for the inheritance scenario also agree with formation at 25-30 AU by <1 Myr evolution. However, the best agreements between models and observations are for late evolutionary times. Comet 17P, as was the case for the reset scenario, does not showcase the same trends as the rest of the comets. Overall, the contours for 17P indicate that this comet is largely unconstrained in time and location.

Lastly, addressing both the reset scenario in Fig. 5.2 and the inheritance scenario in Fig. 5.3 it is generally seen that the more species that are observed in

a comet (the top panels of each figure), the smaller the regions in parameter space over which the models well reproduce the observed ratios, thus better constraining the potential formation location.

5.3.2 Correlation for C- and O-carrying species only

Given the interlinked chemical nature of carbon and oxygen, and the fact that the modelled nitrogen and sulphur chemistry is less well understood, it is interesting to have a look at maximum likelihood surfaces for the comets excluding sulphur species, and considering only ice species with carbon and oxygen. In the sample of molecules from Le Roy et al. (2015) these species are: C_2H_6, CO_2, CO, H_2CO, CH_3OH, CH_4 and O_2, thus seven in total.

For these seven ice species maximum likelihood surfaces are shown in Fig. 5.4 for the reset scenario and in Fig. 5.5 for the inheritance scenario. Since sulphur species have only been observed for comets 1P, Hale-Bopp, Hyakutake, LINEAR, 73P, 9P and 67P (both seasons), only these comets are relevant to analyse for differences compared to the analysis with the full sample of species.

Comparing these maximum likelihood surfaces to their counterparts in Fig. 5.2 for the reset scenario and Fig. 5.3 for the inheritance scenario reveals that excluding sulphur species does not significantly change the behaviour in the results. The only apparent difference is found comet Hale-Bopp, which in the reset scenario in Fig. 5.4 without sulphur agrees more broadly with formation at various evolutionary times and locations (though still along the CO iceline) than it did when including sulphur. However, this makes sense because excluding species from the analysis should cause less constraints on the most likely time and location of formation.

5.4 Discussion

Studies of comets and cometary compositions so far have been grouping them by either dynamical characteristics (length of orbit or inclination), or by their molecular contents (see Cochran et al. 2012). A'Hearn et al. (1995) and Cochran et al. (2012) defined standards for molecular abundances ("Typical"), such that cometary measurements could then indicate either enhanced or depleted abundances for a given molecule. While this approach does provide a grouping for comets that fit with the standard, it fails to include the possible chemical evolution of the comet-forming material in setting that standard.

This work attempts to trace the formation histories of 15 comets, by comparing cometary abundances with evolving ice abundances in a protoplanetary disk midplane through statistical tests. This way, rather than simply comparing similarities in the cometary contents, the potential formation times of the comets can also be addressed, since the chemical composition of the comet-forming disk midplane evolves over time. Four different comparison setups were investigated, with two different sets of observed abundances (either including or excluding sulphur-bearing species), and two different models for evolving abundances for the midplane (the

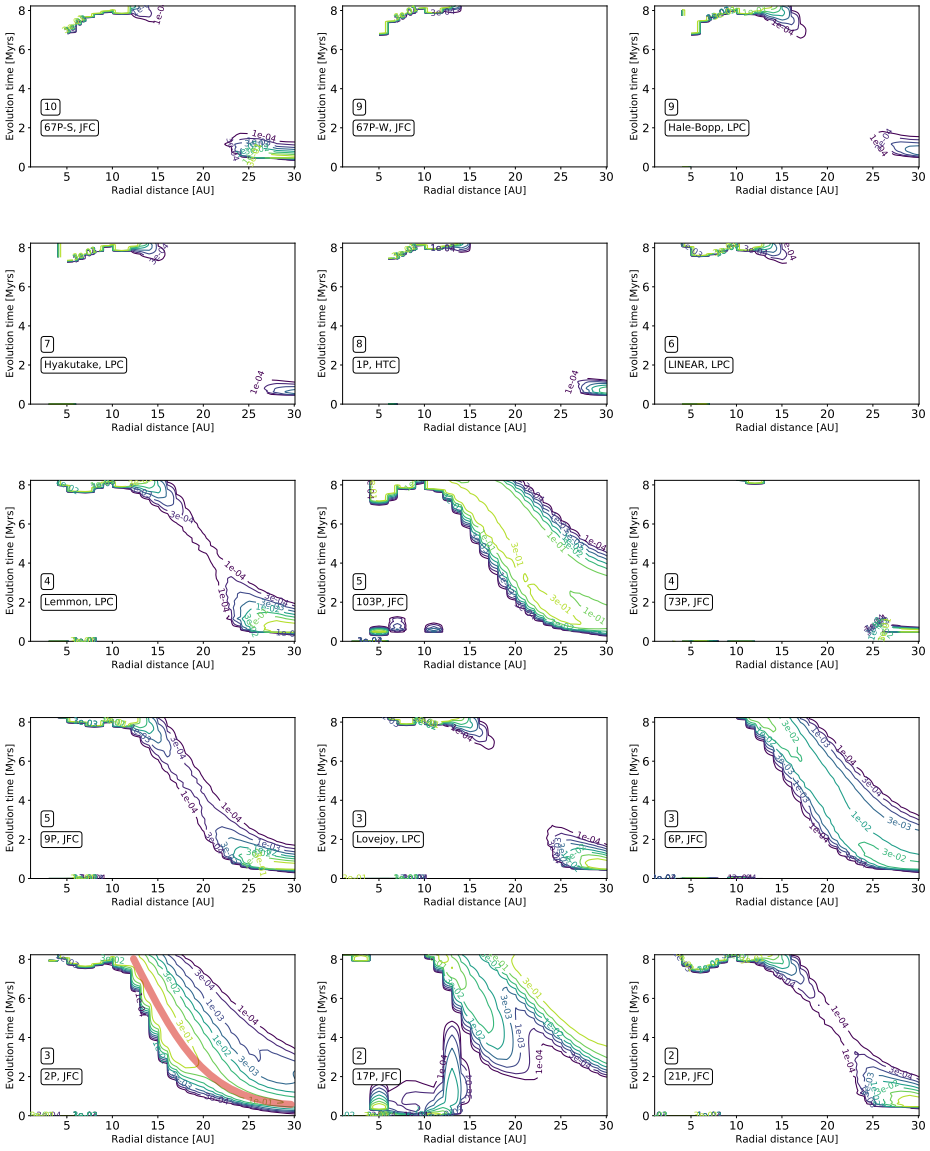

Figure 5.2: Maximum likelihood surfaces for the reset scenario, for the full sample of molecular species. Radius in AU in the physically evolving protoplanetary disk midplane is on the x-axis, and evolution time in Myrs is on the y-axis. The red shaded region for comet 2P indicates the trail through parameter space (largely tracing the vicinity of the CO iceline) on which most of the comets show good agreement with formation.

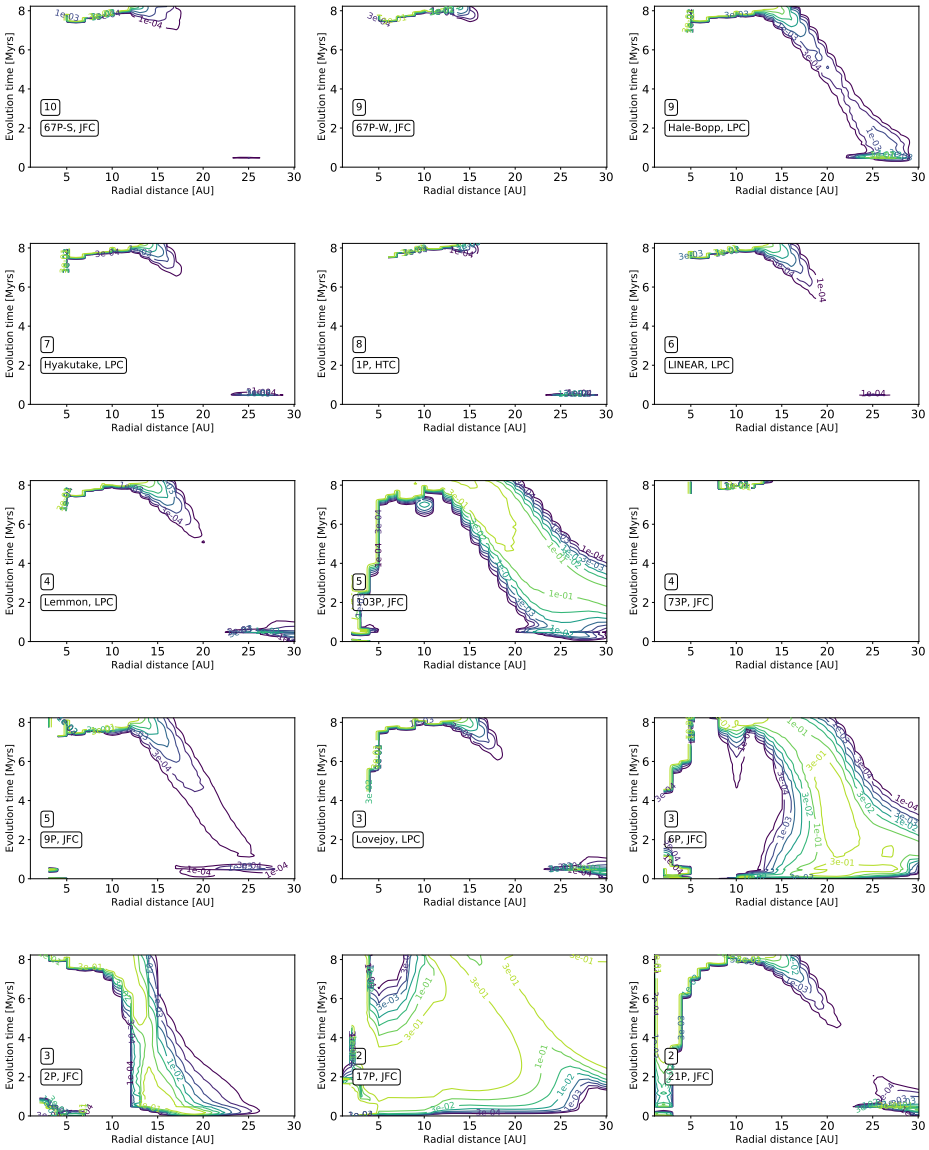

Figure 5.3: Maximum likelihood surfaces for the inheritance scenario, for the full sample of molecular species. Radius in AU in the physically evolving protoplanetary disk midplane is on the x-axis, and evolution time in Myrs is on the y-axis.

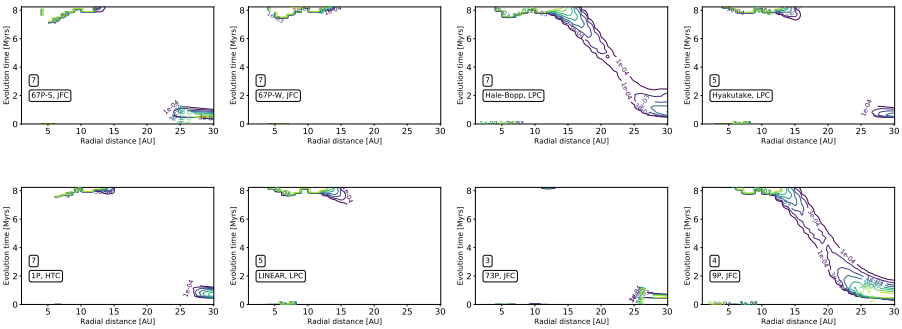

Figure 5.4: Maximum likelihood surfaces for the reset scenario, considering C and O bearing species only. Radius in AU in the physically evolving protoplanetary disk midplane is on the x-axis, and evolution time in Myrs is on the y-axis.

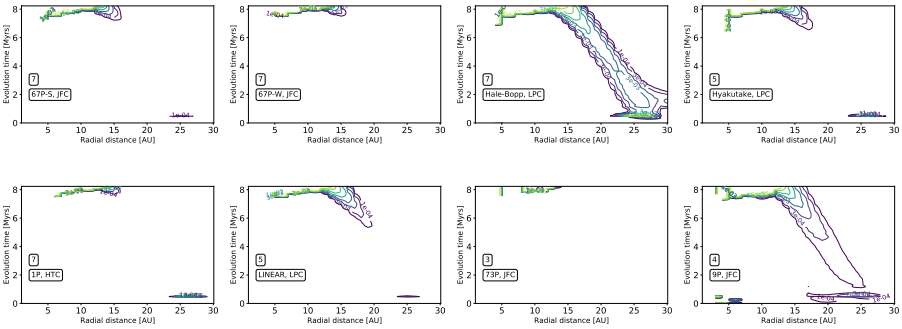

Figure 5.5: Maximum likelihood surfaces for the inheritance scenario, considering C and O bearing species only. Radius in AU in the physically evolving protoplanetary disk midplane is on the x-axis, and evolution time in Myrs is on the y-axis.

inheritance or the reset scenario).

For the reset scenario, good agreement is seen for formation along the CO iceline for 14 out of 15 comets. Comet 17P/Holmes remains largely unconstrained. Note that this comet underwent a so-called extraordinary outburst event (Santana 2007) prior to the observations compiled in Le Roy et al. (2015) (from Dello Russo et al. 2008). Dello Russo et al. (2008) found enhancements in HCN, C_2H_6 and C_2H_2 (by a factor of two to three) relative to other cometary observations; however, it is clear that cometary activity will have a great impact on the bulk composition derived from coma observations (see discussion later regarding comet 67P). The cause of the outburst event for comet 17P remains unknown.

The comets with more species observed in them are constrained to either formation at 27-30 AU by $\sim$ 1 Myr evolution, or to formation at $\sim$ 12 AU by 8 Myr evolution. Comets with fewer observed species agree well with formation along the CO iceline, as indicated by the red shaded region overplotted on the panel for comet 2P in Fig. 5.2. From the left panel in fig. 4 from Eistrup et al. (2018), 30 AU is by 0.5 Myr just outside the CO iceline (at 27 AU), which moves to 15 AU by 8 Myr. The CH_4 iceline is found at 10 AU by 8 Myr. For these 14 out of 15 comets this suggests that cometary formation can be constrained to lie roughly between the icelines of CH_4 and CO, with some degeneracy remaining in the formation time.

For the inheritance scenario, both with and without sulphur-bearing species, the results do not point as strongly to formation along the CO iceline, as is the case for the reset scenario. There is a similarity between the reset and inheritance scenario with good agreement for formation at 10-15 AU by 8 Myr, but this should be seen in the light of the results from Eistrup et al. (2018). It is shown there that the ice abundances for both scenarios tend towards icy disk midplane steady state at late evolutionary times (>5 Myr). That means that the ice abundances after 5 Myr evolution are largely similar across the two scenarios, resulting in similar maximum likelihood surfaces for both (see also the abundance evolution surfaces in Figs 5.6 -5.10).

Generally, the inheritance scenario does not point to a single formation history for all comets, but rather good agreement is seen for multiple formation regions in parameter space, and overall this scenario seems less constraining. This may indicate that our starting molecular abundances for the inheritance scenario do not resemble well those for the particular molecular cloud from which the Sun formed. Although this set of abundances are motivated by observations of ices in protostellar (or interstellar) environments (see Eistrup et al. 2016), it is possible that the Sun formed in a different (warmer) environment to that for nearby well-studied protostellar sources (see e.g. Adams 2010). It would be worth to explore the impact of a warmer interstellar environment on the initial inherited molecular abundances for a comet-forming disk.

Using the analysis here as a test of which chemical starting conditions and evolution best agree with the observations, the reset scenario is seen to generally agree best with the cometary observation. This scenario constrains all but one comet to most likely having formed in the vicinity of the CO iceline. As this iceline resides at a temperature at which grain-surface (ice) chemistry is particularly active, large

changes in the relative abundances of the volatile ice species are seen over time (see Eistrup et al. 2018). This active chemistry could in turn explain the diversity of observed cometary abundances.

That the reset scenario provides better constraints on location and time for comet formation, points to the comet-forming region in the pre-Solar nebula having been seeded with chemically processed material. This chemical processing can have several origins including an accretion shock *en route* into the forming disk, turbulent mixing within the disk once formed, or an accretion outburst caused by material in-falling from the disk onto the star. If any (all) of these processes have occurred, then this supports an early formation of comets (<1 Myr). However, if the pre-Solar nebula formed and evolved in a quiescent manner, a late formation of comets ($\sim$ 8 Myr) is also supported. In this latter case, it cannot be distinguished whether or not the cometary material has an interstellar origin.

Comparing the grouping of 14 comets here with the previous cometary classifications from Cochran et al. (2012) as "Typical", "Depleted" or "Mixed classification" (as of Table 2 in Le Roy et al. 2015) they fall under all these three classes. These 14 comets have thus never been grouped chemically together before. With these 14 comets now grouped together based on likely formation in the vicinity of the CO iceline, it is also possible to propose a formation sequence for this group, based on the peak of the maximum likelihood functions in Fig. 5.4.

Based on this, the following formation time classes from early to late for the 14 comets can be proposed: 67P-S, 73P, 21P, 9P, Lemmon and Lovejoy (all comets feature maximum likelihood peaks from 0.4-0.64 Myr at 28-30 AU), 2P and 103P (by 4.3-7.5 Myr at 14-16 AU), and Hyakutake, LINEAR, 67P-W, 6P, Hale-Bopp and 1P (by 8.23 Myr at 12-13 AU). It is noted that some of these comets have their maximum likelihood peaks located outside of the formation region around the CO iceline. For the sake of focusing on the possible formation time classification around this iceline, only likelihood peaks happening between 0.4 and 8.23 Myr were used for the analysis, thereby ignoring peaks outside of the CO iceline region of the parameter space. This formation time classification creates one group of six comets that possibly formed early, between 0.4-0.64 Myr, one that formed possibly at an intermediate time by 4.3-7.5 Myr, and another group of seven comets that possibly formed later after 7.5 Myr. This hints that comet formation may occur in tandem with disk evolution over $\sim$ 8 Myr timescales.

This formation classes should be considered in light of which comets have more detections. As is evident in Fig. 5.4, the maximum likelihood peaks are very localised (either $\sim$ 14 AU by 8 Myr or at $\sim$ 30 AU by 1 Myr) for the comets that have more detections. The comets with fewer detections are less constrained and thus have larger regions of parameter space with good agreement with the models. The comets with more detections are thus constrained to having formation times similar to each other.

An interesting additional consideration regards which specific species have been detected in which comets, and how that may relate to which regions of parameter space the comets are in best agreement with, and how that may relate to the regions of best agreement in parameter space. Comets 73P, 2P, 9P, 6P and 17P have no CO detections in them, yet in the analysis here these are all constrained to

have formed in the vicinity of the CO iceline. Detection of CO in a comet is thus not a pre-requisite for constraining the comet formation (roughly) to this region. Note that a comet that has formed inside of the CO ice line will naturally be CO poor.

Lastly, it is seen from all plots of comet 67P-S and 67P-W that the summer and winter sides of the comet feature different compositions. Which side, or which relative proportions of the sides are representative of the bulk composition of the comet is still unclear, as was noted in Le Roy et al. (2015). Given that the two seasons of comet 67P fall into different formation classifications (67P-S agrees with early formation, whereas 67P-W agrees with late formation), classifying the formation time of the comet as a whole should be done with caution, although the summer side observations of the comet are likely more comparable to the observations of the other comets. One reason for the differences between the two seasons around 67P, could be that the temperature on its winter side is too low for H_2O ice to sublimate. This, in turn, can lead to increased abundances of the rest of the molecular species, because the all have a lower sublimation temperature than H_2O ice. This is important evidence that cometary activity is an crucial factor to take into consideration when extrapolating abundances measured in the coma to the bulk composition. In future work, it would be worth to explore how the ice ratios vary relative to a different species that is less susceptible to summer and winter effects.

5.5 Conclusion

In this work a statistical χ^2 method has been used to perform a quantitative comparison between observed cometary abundances and modelled chemical evolution in a protoplanetary disk midplane, by computing maximum likelihood surfaces, as a function of disk midplace location (radius) and time. The best agreements between observed and modelled abundances were found when considering the chemical evolution models to be chemically reset at the start, thus assuming that the volatile content of the pre-Solar nebula was (perhaps partially) atomised before dust grains starting building larger bodies. This is consistent with the traditional idea about the chemical start of the inner pre-Solar nebula (Grossman 1972).

Out of 15 comets, 14 were found to have high likelihoods of formation along a trail in time and radial parameter space consistent with the position of the CO iceline. Since CO is the molecule (next to N_2 and H_2) with the lowest binding energy (E_b=855 K) this means that most molecules are in the ice at the point where the comets are most likely to have formed. We do not consider here formation radii outside of the CO iceline, as the abundances in this region are found to be very different from those around the iceline (see Eistrup et al. 2018). There, it is found that the grain-surface chemistry is mainly driven by hydrogenation reactions leading to high abundances of e.g., H_2O, CH_4, C_2H_6, and CH_3OH ices.

Based on the maxima of the likelihood functions for each comet along the CO iceline, it was then determined when during chemical evolution each comet was most likely to have formed. Thereby a formation time classification for 14 comets

was proposed, with some degeneracy remaining between the early (<1 Myr) and late (>7.5 Myr) formation. With more samples of comets with sufficient molecular detections in the future, it will be possible to further test this chemical evolution classification scheme for formation histories of comets. It will be interesting to see if other comets support the idea of a chemical reset start, and if they too show best agreement with formation in the vicinity of the CO iceline.

Acknowledgements: Astrochemistry in Leiden is supported by the European Union A-ERC grant 291141 CHEMPLAN and the Netherlands Research School for Astronomy (NOVA). CW also acknowledges the University of Leeds for financial support.

5.A Evolving modelled abundances and cometary abundances

This appendix features abundance ratio maps (Figs. 5.6-5.10) in radius and time for the molecular species considered in this work, as well as HCN, NH_3, HNCO, CH_3CN and C_2H_2. These abundances are taken from Eistrup et al. (2018). Each row is for one molecular ice species. The left columns of the figures are evolving abundances for the reset scenario ("Atomic"), and the middle columns for inheritance scenario ("Molecular") from the 0.1 MMSN evolving disk from Eistrup et al. (2018). The right column features the observed abundances (with given errors, or, if no error was given, assuming a conservative 50% error relative to the observed species abundance with respect to H_2O ice) of a given ice species, in those of the 15 comets, where the molecule has been observed.

The colourbar next to the right column indicates that high abundance with respect to H_2O ice gives a light colour, and low abundance gives a darker colour. The cometary abundances can also be read off vertically on the y-axis. The colour abundances of the comets are intended to enable easy visual comparison between the modelled (left and middle columns) and observed (right column) abundances.

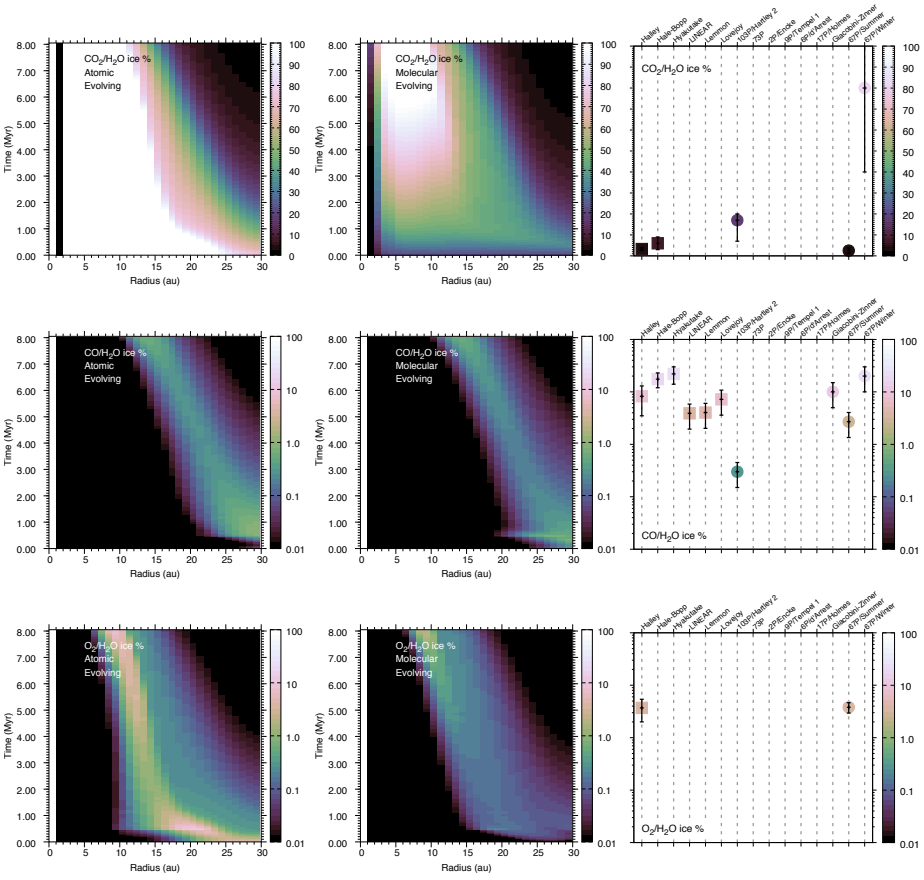

Figure 5.6: Abundance of CO_2, CO, and O_2 ice relative to water ice as a function of radius and time for the protoplanetary disk model with evolving physical conditions and using fully atomic initial abundances (left) and fully molecular initial abundances (middle). Note that the data for CO_2 are shown on a linear scale as opposed to logarithmic because of the low dynamic range in the chemical model results. The right-hand column shows the corresponding values measured for each species in cometary comae. The vertical dashed lines are included solely to guide the eye. Oort cloud comets and Jupiter family comets are represented by the squares and circles, respectively. For comets without a stated observed error (or range), we have assumed a conservative error of 50% of the observed ratio with respect to H_2O ice.

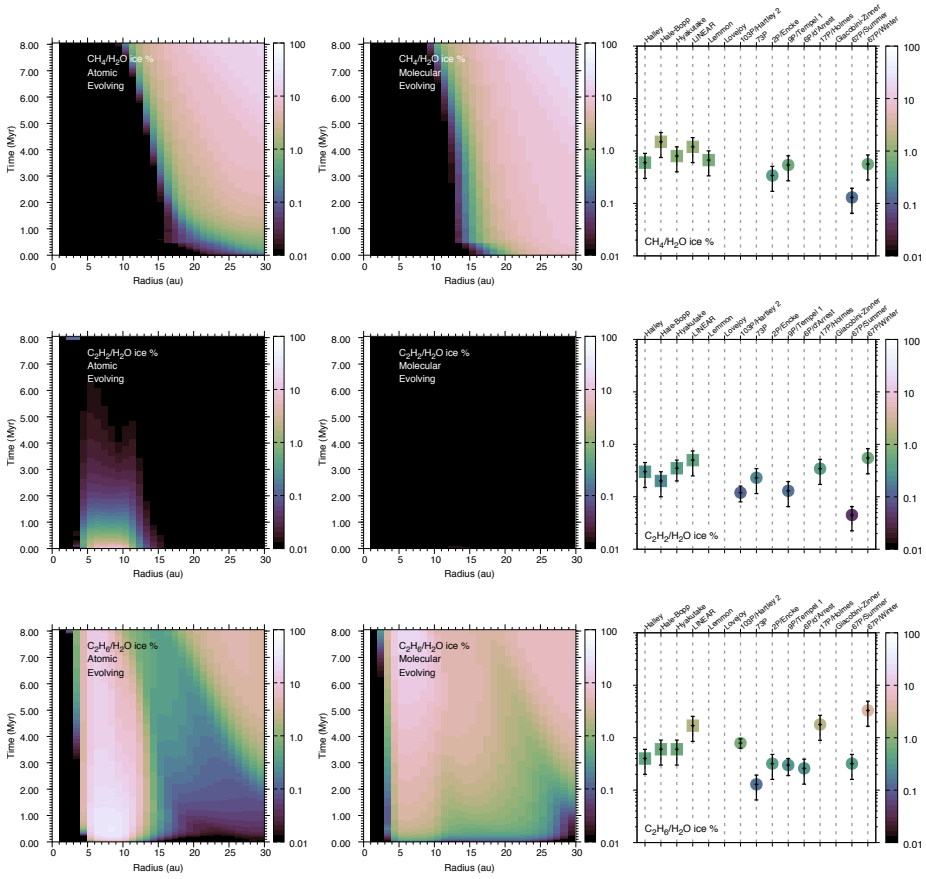

Figure 5.7: Same as Figure 5.6 for CH_4, C_2H_2, and C_2H_6 ice.

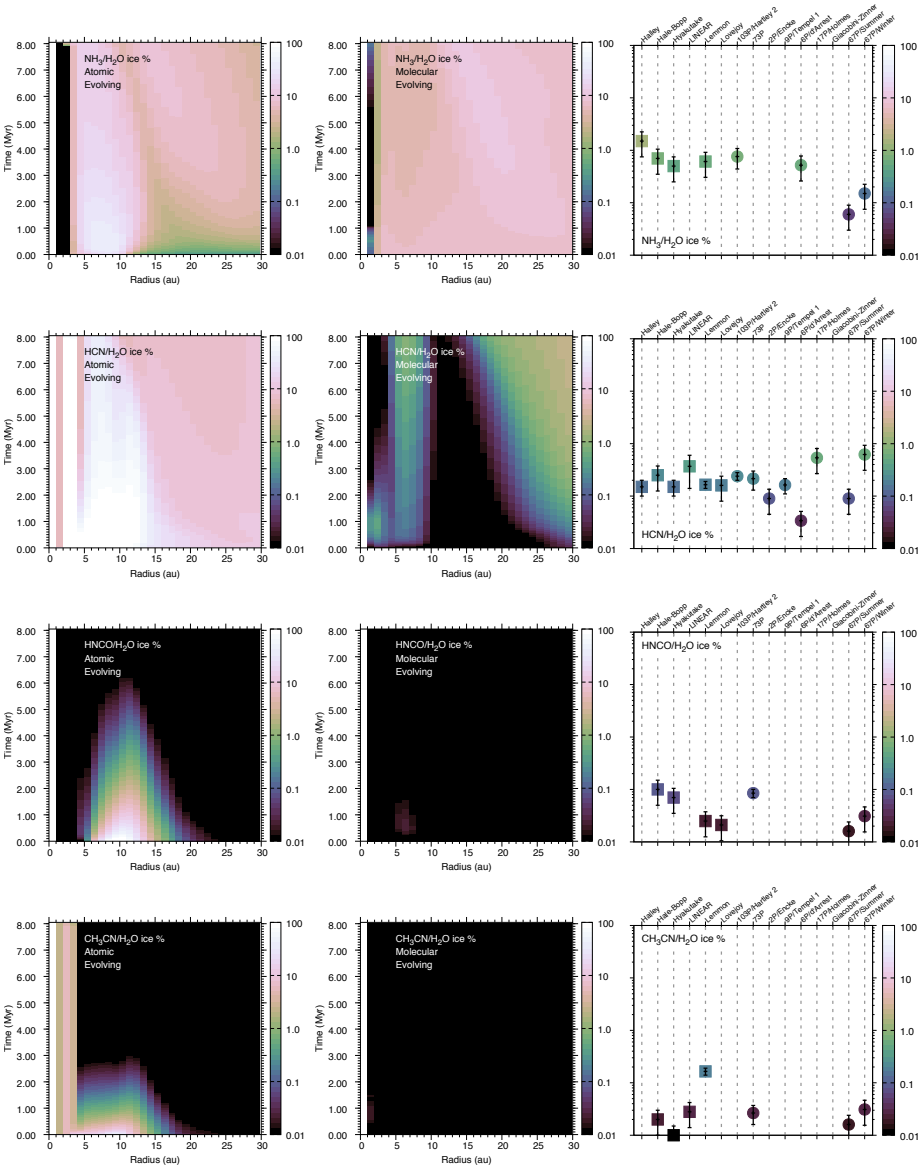

Figure 5.8: Same as Figure 5.6 for NH_3, HCN, HNCO and CH_3CN ice.

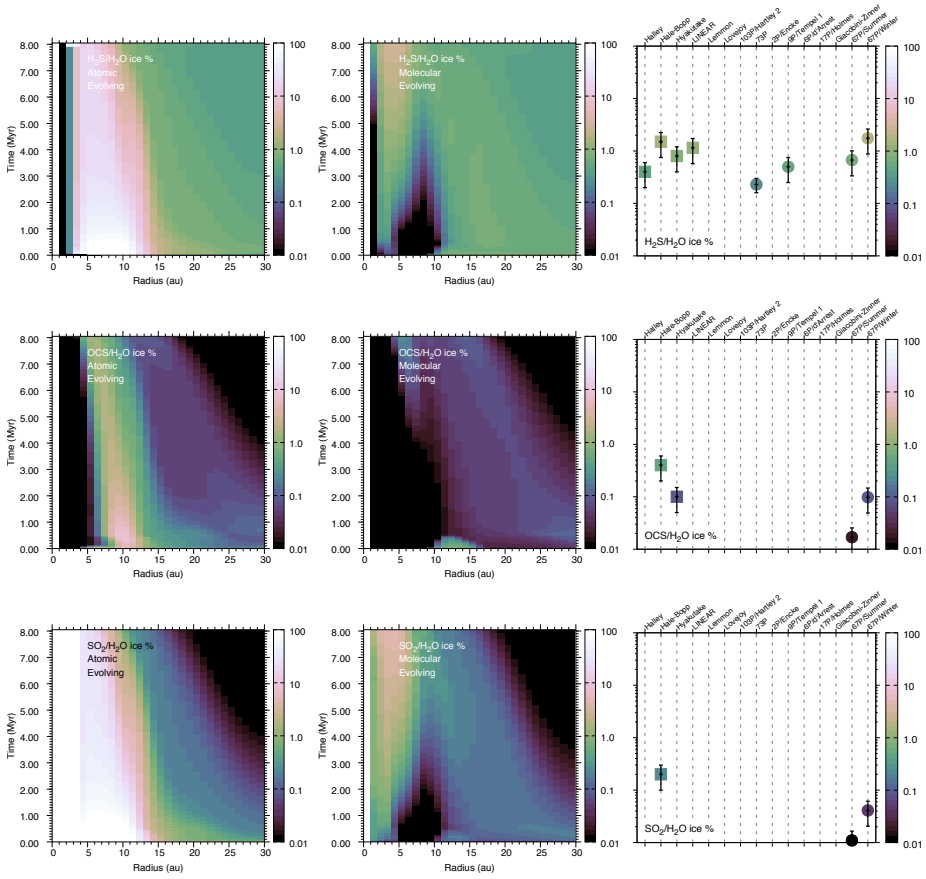

Figure 5.9: Same as Figure 5.6 for H_2S, OCS, and SO_2 ice.

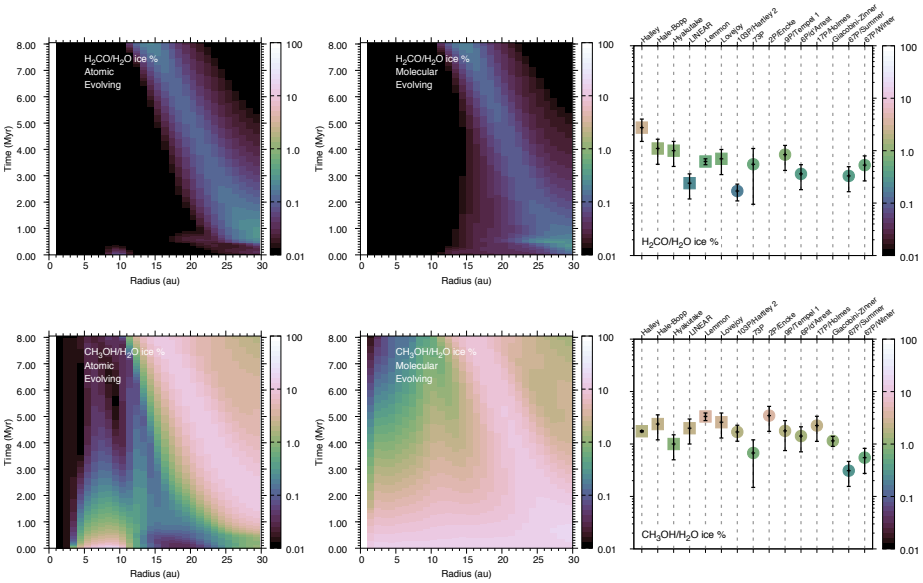

Figure 5.10: Same as Figure 5.6 for H_2CO and CH_3OH ice.

Bibliography

Adams, F. C. 2010, ARA&A, 48, 47
A'Hearn, M. F. 2011, Annual Review of Astronomy and Astrophysics, 49, 281
A'Hearn, M. F., Millis, R. C., Schleicher, D. O., Osip, D. J., & Birch, P. V. 1995, Icarus, 118, 223
Aikawa, Y. & Herbst, E. 1999, A&A, 351, 233
Aikawa, Y., Miyama, S. M., Nakano, T., & Umebayashi, T. 1996, ApJ, 467, 684
Aikawa, Y., Umebayashi, T., Nakano, T., & Miyama, S. M. 1997, ApJL, 486, L51
Aikawa, Y., Umebayashi, T., Nakano, T., & Miyama, S. M. 1999, ApJ, 519, 705
Ali-Dib, M. 2017, MNRAS, 467, 2845
Ali-Dib, M., Mousis, O., Petit, J.-M., & Lunine, J. I. 2014, ApJ, 785, 125
Alibert, Y., Carron, F., Fortier, A., et al. 2013, A&A, 558, A109
ALMA Partnership, Brogan, C. L., Pérez, L. M., et al. 2015, ApJL, 808, L3
Andrews, S. M., Wilner, D. J., Hughes, A. M., Qi, C., & Dullemond, C. P. 2010, ApJ, 723, 1241
Andrews, S. M., Wilner, D. J., Zhu, Z., et al. 2016, ApJL, 820, L40
Armitage, P. J. 2011, ARA&A, 49, 195
Barclay, T., Rowe, J. F., Lissauer, J. J., et al. 2013, Nature, 494, 452
Barman, T. S., Konopacky, Q. M., Macintosh, B., & Marois, C. 2015, ApJ, 804, 61
Batalha, N. M., Rowe, J. F., Bryson, S. T., et al. 2013, ApJS, 204, 24
Benz, W., Ida, S., Alibert, Y., Lin, D., & Mordasini, C. 2014, in Protostars and Planets VI, ed. H. Beuther, R. F. Klessen, C. P. Dullemond, & T. Henning (The University of Arizona Press), 691–713
Bergin, E. A., Aikawa, Y., Blake, G. A., & van Dishoeck, E. F. 2007, in Protostars and Planets V, ed. B. Reipurth, D. Jewitt, & K. Keil (The University of Arizona Press), 751–766
Bieler, A., Altwegg, K., Balsiger, H., et al. 2015, Nature, 526, 678
Birkby, J. L., de Kok, R. J., Brogi, M., et al. 2013, MNRAS, 436, L35
Birnstiel, T., Fang, M., & Johansen, A. 2016, Space Sci. Rev., 205, 41
Bitsch, B. & Johansen, A. 2016, A&A, 590, A101
Bitsch, B., Lambrechts, M., & Johansen, A. 2015, A&A, 582, A112
Blum, J. & Wurm, G. 2008, ARA&A, 46, 21
Boogert, A. C. A., Gerakines, P. A., & Whittet, D. C. B. 2015, ARA&A, 53, 541
Borucki, W. J., Koch, D. G., Basri, G., et al. 2011, ApJ, 736, 19

Brown, W. A. & Bolina, A. S. 2007, MNRAS, 374, 1006
Bruderer, S. 2013, A&A, 559, A46
Bruderer, S., van der Marel, N., van Dishoeck, E. F., & van Kempen, T. A. 2014, A&A, 562, A26
Bruderer, S., van Dishoeck, E. F., Doty, S. D., & Herczeg, G. J. 2012, A&A, 541, A91
Cassan, A., Kubas, D., Beaulieu, J.-P., et al. 2012, Nature, 481, 167
Cazaux, S. & Tielens, A. G. G. M. 2002, ApJL, 575, L29
Cazzoletti, P., van Dishoeck, E. F., Visser, R., Facchini, S., & Bruderer, S. 2018, A&A, 609, A93
Ceccarelli, C., Caselli, P., Bockelée-Morvan, D., et al. 2014, Protostars and Planets VI, 859
Cleeves, L. I., Adams, F. C., & Bergin, E. A. 2013a, ApJ, 772, 5
Cleeves, L. I., Adams, F. C., Bergin, E. A., & Visser, R. 2013b, ApJ, 777, 28
Cleeves, L. I., Bergin, E. A., & Adams, F. C. 2014a, ApJ, 794, 123
Cleeves, L. I., Bergin, E. A., & Adams, F. C. 2014b, ApJ, 794, 123
Cleeves, L. I., Bergin, E. A., Alexander, C. M. O. ., et al. 2014c, Science, 345, 1590
Cleeves, L. I., Bergin, E. A., Alexander, C. M. O., et al. 2014d, Science, 345, 1590
Cochran, A. L., Barker, E. S., & Gray, C. L. 2012, Icarus, 218, 144
Cridland, A. J., Pudritz, R. E., & Alessi, M. 2016, MNRAS, 461, 3274
Cridland, A. J., Pudritz, R. E., Birnstiel, T., Cleeves, L. I., & Bergin, E. A. 2017, MNRAS, 469, 3910
Crossfield, I. J. M. 2015, PASP, 127, 941
Cuppen, H. M., Ioppolo, S., Romanzin, C., & Linnartz, H. 2010, Physical Chemistry Chemical Physics (Incorporating Faraday Transactions), 12, 12077
Cuppen, H. M., Walsh, C., Lamberts, T., et al. 2017, Space Science Reviews, 212, 1
Cuppen, H. M., Walsh, C., Lamberts, T., et al. 2017, Space Sci. Rev., 212, 1
Dalgarno, A. 2006, Proceedings of the National Academy of Science, 103, 12269
Davis, S. S. 2005, ApJ, 620, 994
Dello Russo, N., R. J. Vervack, J., Weaver, H. A., et al. 2008, The Astrophysical Journal, 680, 793
Dong, R., Zhu, Z., Rafikov, R. R., & Stone, J. M. 2015, ApJL, 809, L5
Dressing, C. D. & Charbonneau, D. 2013, ApJ, 767, 95
Drozdovskaya, M. N., Walsh, C., van Dishoeck, E. F., et al. 2016, MNRAS, 462, 977
Du, F., Bergin, E. A., Hogerheijde, M., et al. 2017, ApJ, 842, 98
Du, F., Bergin, E. A., & Hogerheijde, M. R. 2015, ApJL, 807, L32
Dulieu, F., Minissale, M., & Bockelée-Morvan, D. 2017, A&A, 597, A56
Dullemond, C. P. & Dominik, C. 2004, A&A, 421, 1075
Dullemond, C. P. & Dominik, C. 2005, A&A, 434, 971
Dullemond, C. P., Hollenbach, D., Kamp, I., & D'Alessio, P. 2007, in Protostars and Planets V, ed. B. Reipurth, D. Jewitt, & K. Keil (The University of Arizona

Press), 555–572
Eberhardt, P. 1999, Space Sci. Rev., 90, 45
Eistrup, C., Walsh, C., & van Dishoeck, E. F. 2016, A&A, 595, A83
Eistrup, C., Walsh, C., & van Dishoeck, E. F. 2018, A&A, 613, A14
Ennis, C. P., Bennett, C. J., & Kaiser, R. I. 2011, Physical Chemistry Chemical Physics (Incorporating Faraday Transactions), 13, 9469
Facchini, S., Birnstiel, T., Bruderer, S., & van Dishoeck, E. F. 2017, A&A, 605, A16
Favre, C., Cleeves, L. I., Bergin, E. A., Qi, C., & Blake, G. A. 2013, ApJL, 776, L38
Fedele, D., Pascucci, I., Brittain, S., et al. 2011, ApJ, 732, 106
Fedele, D., van den Ancker, M. E., Henning, T., Jayawardhana, R., & Oliveira, J. M. 2010, A&A, 510, A72
Fink, U. 2009, Icarus, 201, 311
Fischer, D. A., Howard, A. W., Laughlin, G. P., et al. 2014, in Protostars and Planets VI, ed. H. Beuther, R. F. Klessen, C. P. Dullemond, & T. Henning (The University of Arizona Press), 715–737
Fraine, J., Deming, D., Benneke, B., et al. 2014, Nature, 513, 526
Furuya, K. & Aikawa, Y. 2014, ApJ, 790, 97
Furuya, K., Drozdovskaya, M. N., & Visser, R. 2016, A&A, in press
Garrod, R. T. & Herbst, E. 2006, A&A, 457, 927
Garrod, R. T., Widicus Weaver, S. L., & Herbst, E. 2008, ApJ, 682, 283
Gibb, E. L., Whittet, D. C. B., Boogert, A. C. A., & Tielens, A. G. G. M. 2004, ApJS, 151, 35
Gillon, M., Triaud, A. H. M. J., Demory, B.-O., et al. 2017, Nature, 542, 456
Grossman, L. 1972, Geochimica et Cosmochimica Acta, 36, 597
Hall, C., Rice, K., Dipierro, G., et al. 2018, MNRAS, 477, 1004
Harsono, D., Bruderer, S., & van Dishoeck, E. F. 2015, A&A, 582, A41
Hasegawa, T. I. & Herbst, E. 1993, MNRAS, 261, 83
Hayashi, C. 1981, Progress of Theoretical Physics Supplement, 70, 35
He, J., Shi, J., Hopkins, T., Vidali, G., & Kaufman, M. J. 2015, ApJ, 801, 120
Helling, C., Woitke, P., Rimmer, P. B., et al. 2014, Life, 4 [[arXiv]1403.4420]
Henning, T. & Semenov, D. 2013, Chemical Reviews, 113, 9016
Hogerheijde, M. R., Bergin, E. A., Brinch, C., et al. 2011, Science, 334, 338
Hollenbach, D., Kaufman, M. J., Bergin, E. A., & Melnick, G. J. 2009, ApJ, 690, 1497
Ida, S. & Lin, D. N. C. 2004, ApJ, 604, 388
Ida, S. & Lin, D. N. C. 2008, ApJ, 673, 487
Indriolo, N., Neufeld, D. A., Gerin, M., et al. 2015, ApJ, 800, 40
Ioppolo, S., Cuppen, H. M., Romanzin, C., van Dishoeck, E. F., & Linnartz, H. 2008, ApJ, 686, 1474
Ioppolo, S., Cuppen, H. M., Romanzin, C., van Dishoeck, E. F., & Linnartz, H. 2010, Physical Chemistry Chemical Physics (Incorporating Faraday Transac-

tions), 12, 12065
Johansen, A., Blum, J., Tanaka, H., et al. 2014a, Protostars and Planets VI, 547
Johansen, A., Blum, J., Tanaka, H., et al. 2014b, in Protostars and Planets VI, ed. H. Beuther, R. F. Klessen, C. P. Dullemond, & T. Henning (The University of Arizona Press), 547–570
Johnson, T. V., Mousis, O., Lunine, J. I., & Madhusudhan, N. 2012, ApJ, 757, 192
Jones, B. M., Kaiser, R. I., & Strazzulla, G. 2014, ApJ, 781, 85
Kama, M., Bruderer, S., Carney, M., et al. 2016a, A&A, 588, A108
Kama, M., Bruderer, S., van Dishoeck, E. F., et al. 2016b, ArXiv e-prints [[arXiv]1605.05093]
Kama, M., Bruderer, S., van Dishoeck, E. F., et al. 2016c, A&A, 592, A83
Kamp, I., Thi, W.-F., Meeus, G., et al. 2013, A&A, 559, A24
Kataoka, A., Okuzumi, S., Tanaka, H., & Nomura, H. 2014, A&A, 568, A42
Keppler, M., Benisty, M., Müller, A., et al. 2018, ArXiv e-prints [[arXiv]1806.11568]
Kreidberg, L., Bean, J. L., Désert, J.-M., et al. 2014, ApJL, 793, L27
Lamberts, T., Cuppen, H. M., Ioppolo, S., & Linnartz, H. 2013, Physical Chemistry Chemical Physics (Incorporating Faraday Transactions), 15, 8287
Lambrechts, M. & Johansen, A. 2012, A&A, 544, A32
Le Roy, L., Altwegg, K., Balsiger, H., et al. 2015, A&A, 583, A1
Li, Z.-Y., Banerjee, R., Pudritz, R. E., et al. 2014, Protostars and Planets VI, 173
Linnartz, H., Ioppolo, S., & Fedoseev, G. 2015, International Reviews in Physical Chemistry, 34, 205
Loomis, R. A., Cleeves, L. I., Öberg, K. I., Guzman, V. V., & Andrews, S. M. 2015, ApJL, 809, L25
Madhusudhan, N., Amin, M. A., & Kennedy, G. M. 2014, ApJL, 794, L12
Marboeuf, U., Thiabaud, A., Alibert, Y., Cabral, N., & Benz, W. 2014, A&A, 570, A35
Marois, C., Zuckerman, B., Konopacky, Q. M., Macintosh, B., & Barman, T. 2010, Nature, 468, 1080
Martín-Doménech, R., Manzano-Santamaría, J., Muñoz Caro, G. M., et al. 2015, A&A, 584, A14
Matrà, L., Dent, W. R. F., Wyatt, M. C., et al. 2017a, MNRAS, 464, 1415
Matrà, L., MacGregor, M. A., Kalas, P., et al. 2017b, ApJ, 842, 9
Mayor, M. & Queloz, D. 1995, Nature, 378, 355
McElroy, D., Walsh, C., Markwick, A. J., et al. 2013, A&A, 550, A36
Min, M., Dullemond, C. P., Kama, M., & Dominik, C. 2011, Icarus, 212, 416
Minissale, M., Congiu, E., & Dulieu, F. 2014, The Journal of Chemical Physics, 140, 074705
Miotello, A., van Dishoeck, E. F., Williams, J. P., et al. 2017, A&A, 599, A113
Mollière, P., van Boekel, R., Dullemond, C., Henning, T., & Mordasini, C. 2015, ApJ, 813, 47

Mordasini, C., van Boekel, R., Mollière, P., Henning, T., & Benneke, B. 2016, ApJ, 832, 41
Moses, J. I., Madhusudhan, N., Visscher, C., & Freedman, R. S. 2013, ApJ, 763, 25
Mousis, O., Lunine, J. I., Picaud, S., & Cordier, D. 2010, Faraday Discussions, 147, 509
Mousis, O., Marboeuf, U., Lunine, J. I., et al. 2009, ApJ, 696, 1348
Mousis, O., Ronnet, T., Brugger, B., et al. 2016, ApJL, 823, L41
Mousis, O., Ronnet, T., Lunine, J. I., et al. 2018, ArXiv e-prints [[arXiv]1804.03478]
Mumma, M. J. & Charnley, S. B. 2011, ARA&A, 49, 471
Musiolik, G., Teiser, J., Jankowski, T., & Wurm, G. 2016, ApJ, 818, 16
Noble, J. A., Theule, P., Borget, F., et al. 2013, MNRAS, 428, 3262
Nomura, H. & Millar, T. J. 2005, A&A, 438, 923
Nomura, H., Tsukagoshi, T., Kawabe, R., et al. 2016, ApJL, 819, L7
Öberg, K. I. & Bergin, E. A. 2016, ApJL, 831, L19
Öberg, K. I., Boogert, A. C. A., Pontoppidan, K. M., et al. 2011a, ApJ, 740, 109
Öberg, K. I., Furuya, K., Loomis, R., et al. 2015, ApJ, 810, 112
Öberg, K. I., Murray-Clay, R., & Bergin, E. A. 2011b, ApJL, 743, L16
Okuzumi, S., Tanaka, H., Kobayashi, H., & Wada, K. 2012, ApJ, 752, 106
Padovani, M., Ivlev, A. V., Galli, D., & Caselli, P. 2018, ArXiv e-prints [[arXiv]1803.09348]
Pérez, L. M., Carpenter, J. M., Andrews, S. M., et al. 2016, Science, 353, 1519
Pinilla, P., Birnstiel, T., Ricci, L., et al. 2012, A&A, 538, A114
Pinte, C., Price, D. J., Ménard, F., et al. 2018, ApJL, 860, L13
Piso, A.-M. A., Öberg, K. I., Birnstiel, T., & Murray-Clay, R. A. 2015, ApJ, 815, 109
Piso, A.-M. A., Pegues, J., & Öberg, K. I. 2016, ApJ, 833, 203
Pollack, J. B., Hubickyj, O., Bodenheimer, P., et al. 1996, Icarus, 124, 62
Pontoppidan, K. M., Salyk, C., Bergin, E. A., et al. 2014, in Protostars and Planets VI, ed. H. Beuther, R. F. Klessen, C. P. Dullemond, & T. Henning (The University of Arizona Press), 363–385
Prasad, S. S. & Tarafdar, S. P. 1983, ApJ, 267, 603
Qi, C., Öberg, K. I., Wilner, D. J., et al. 2013, Science, 341, 630
Reboussin, L., Wakelam, V., Guilloteau, S., Hersant, F., & Dutrey, A. 2015, A&A, 579, A82
Rubin, M., Altwegg, K., van Dishoeck, E. F., & Schwehm, G. 2015, ApJL, 815, L11
Ruffle, D. P. & Herbst, E. 2000, MNRAS, 319, 837
Salinas, V. N., Hogerheijde, M. R., Bergin, E. A., et al. 2016, A&A, 591, A122
Santana, J. A. H. 2007, IAU Circ. 8886
Schwarz, K. R. & Bergin, E. A. 2014, ApJ, 797, 113
Schwarz, K. R., Bergin, E. A., Cleeves, L. I., et al. 2016, ApJ, 823, 91

Seager, S. & Deming, D. 2010, ARA&A, 48, 631
Semenov, D., Wiebe, D., & Henning, T. 2004, A&A, 417, 93
Sing, D. K., Fortney, J. J., Nikolov, N., et al. 2016, Nature, 529, 59
Snellen, I. A. G., de Kok, R. J., de Mooij, E. J. W., & Albrecht, S. 2010, Nature, 465, 1049
Swain, M. R., Vasisht, G., & Tinetti, G. 2008, Nature, 452, 329
Takahashi, S. Z. & Inutsuka, S.-i. 2014, ApJ, 794, 55
Taquet, V., Furuya, K., Walsh, C., & van Dishoeck, E. F. 2016, MNRAS, 462, S99
Teague, R., Bae, J., Bergin, E. A., Birnstiel, T., & Foreman-Mackey, D. 2018, ApJL, 860, L12
Teolis, B. D., Plainaki, C., Cassidy, T. A., & Raut, U. 2017, Journal of Geophysical Research (Planets), 122, 1996
Thiabaud, A., Marboeuf, U., Alibert, Y., Leya, I., & Mezger, K. 2015a, A&A, 580, A30
Thiabaud, A., Marboeuf, U., Alibert, Y., Leya, I., & Mezger, K. 2015b, A&A, 574, A138
Tielens, A. G. G. M. & Allamandola, L. J. 1987, in Astrophysics and Space Science Library, Vol. 134, Interstellar Processes, ed. D. J. Hollenbach & H. A. Thronson, Jr., 397–469
Tielens, A. G. G. M. & Hagen, W. 1982, A&A, 114, 245
Trinquier, A., Elliott, T., Ulfbeck, D., et al. 2009, Science, 324, 374
Udry, S. & Santos, N. C. 2007, ARA&A, 45, 397
Umebayashi, T. & Nakano, T. 2009, ApJ, 690, 69
van der Marel, N., van Dishoeck, E. F., Bruderer, S., et al. 2016, A&A, 585, A58
van der Marel, N., van Dishoeck, E. F., Bruderer, S., et al. 2013, Science, 340, 1199
van Dishoeck, E. F. & Black, J. H. 1986, in Interstellar Processes: Abstracts of Contributed Papers, ed. D. J. Hollenbach & H. A. Thronson, Jr.
van 't Hoff, M. L. R., Walsh, C., Kama, M., Facchini, S., & van Dishoeck, E. F. 2017, A&A, 599, A101
Vasyunin, A. I., Semenov, D., Henning, T., et al. 2008, ApJ, 672, 629
Visser, R., Bergin, E. A., & Jørgensen, J. K. 2015, A&A, 577, A102
Visser, R., van Dishoeck, E. F., Doty, S. D., & Dullemond, C. P. 2009, A&A, 495, 881
Walsh, C., Loomis, R. A., Öberg, K. I., et al. 2016, ApJL, 823, L10
Walsh, C., Millar, T. J., & Nomura, H. 2010, ApJ, 722, 1607
Walsh, C., Millar, T. J., Nomura, H., et al. 2014, A&A, 563, A33
Walsh, C., Nomura, H., Millar, T. J., & Aikawa, Y. 2012, ApJ, 747, 114
Walsh, C., Nomura, H., & van Dishoeck, E. 2015, A&A, 582, A88
Weidenschilling, S. J. 1977, Ap&SS, 51, 153
Willacy, K. 2007, ApJ, 660, 441
Willacy, K., Klahr, H. H., Millar, T. J., & Henning, T. 1998, A&A, 338, 995
Williams, J. P. & Cieza, L. A. 2011, ARA&A, 49, 67

Wirström, E. S., Lerner, M. S., Källström, P., et al. 2016, A&A, submitted
Woitke, P., Kamp, I., & Thi, W.-F. 2009, A&A, 501, 383
Youdin, A. N. & Goodman, J. 2005, ApJ, 620, 459
Yu, M., Evans, II, N. J., Dodson-Robinson, S. E., Willacy, K., & Turner, N. J. 2017, ApJ, 841, 39
Yu, M., Willacy, K., Dodson-Robinson, S. E., Turner, N. J., & Evans, II, N. J. 2016, ApJ, 822, 53
Zhang, K., Bergin, E. A., Blake, G. A., Cleeves, L. I., & Schwarz, K. R. 2017, Nature Astronomy, 1, 0130
Zhang, K., Blake, G. A., & Bergin, E. A. 2015, ApJL, 806, L7

English Summary

Planets and the search for life in space. Humankind has always wondered about its origin. Where do we come from, and are we alone? The latter question concerns life, and how it can erupt. The only life we know of is life here on our own planet, the Earth. The search for life elsewhere in space is thus a search for planets and exoplanets that have environments that are similar to the life-supporting environment we have on the Earth.

The origin of life on our planet may trace as far back in time as the formation of the Earth itself (there is evidence to suggest that there was life of the Earth already 3.6 billion years ago, with the Earth itself being 4.6 billion years old). Life's ingredients originate from the same material that formed the planet, and hence understanding planet formation and which material forms planets is key to understanding, not only the evolution of the Earth, but also of the life on it.

Planet formation. Planets form around stars, which in turn start forming when large regions of space filled with gas and dust collapse due to the pull of gravity from all the material (see "Prestellar Core" in image 5.11, where gravity pulls all the material in the grey cloud inwards, in the directions of the arrows). The formation of planets is an active field of research in astronomy. It attempts to describe, how the process of forming a star from the gas and dust collapsing under gravity can lead to planets forming out of some of this material around the star (illustrated by all six evolution stages in image 5.11). Understanding the size, movements and composition of the resulting planets requires knowledge of both the physical and chemical processes taking place during the formation process.

These processes are studied in several different ways in astronomical research: through theoretically understanding of the processes and predicting what they will lead to, through astronomical observations of space, and through laboratory experiments on the Earth. In the case of planet formation, theoretically understanding of the physical processes taking place has greatly advanced in recent years. Computer simulations have provided predictions about which types of planets form where. Observations of planets, exoplanets and planet-forming regions, in turn, have constrained these predictions. Laboratory experiments have contributed to understanding the molecules that exist in space, how to detect them, and which chemical reactions can happen between them. This all helps to understand the composition of the material that goes into forming planets.

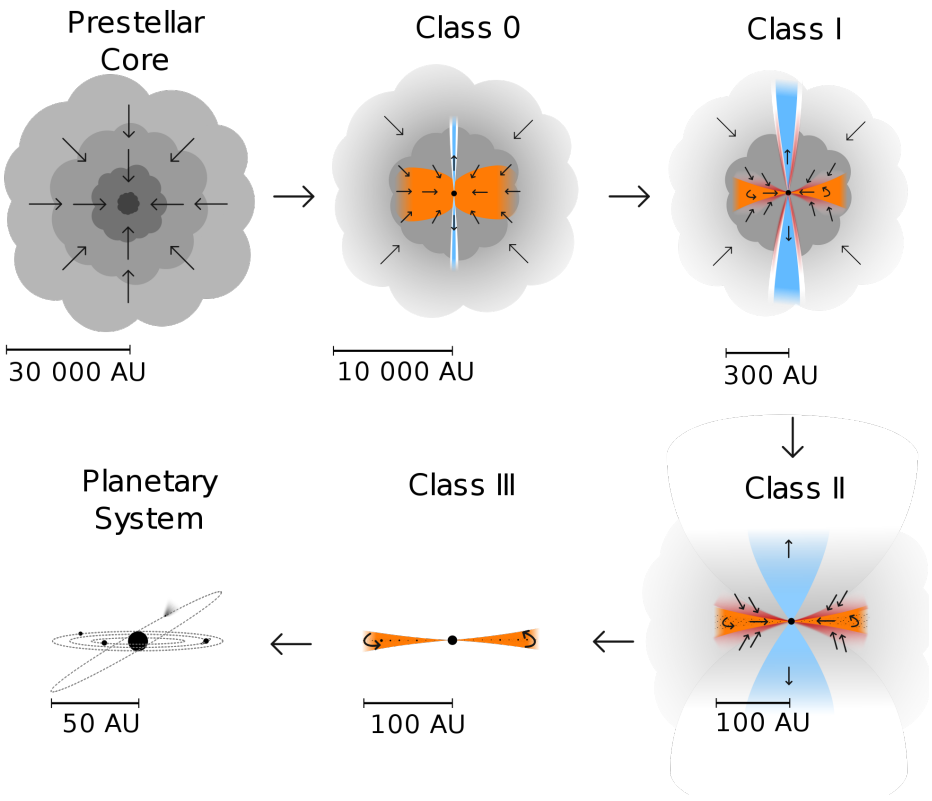

Figure 5.11: Different stages of star and planet formation. The chemical simulations in this thesis focus mostly on classes 2 and 3, but links are made to both the prestellar core, and to the end-product, namely the planetary system. Image credit: "Current view of protostellar evolution" by Dr. Magnus Vilhelm Persson.

Physical and chemical effects during planet formation. The understanding of the physics of planet formation has come far. Alongside that, observations of planet-forming regions, especially with the Atacama Large Millimeter/submillimeter Array-observatory (ALMA) in Chile, have provided a wealth of information on the structure and molecular composition of such regions. ALMA consists of 66 of radio antennas situated at 5000 meters altitude in the driest desert on the Earth. In this environment, ALMA is the best observatory in the world for observing electromagnetic radiation at wavelenghts around 1 millimeter. This makes ALMA optimal for many observations, including observing regions of star and planet formation, and also for detecting signatures of specific molecules in these regions. Amongst other, several so-called icelines have been detected using ALMA. An iceline is the radius in a planet-forming region inside of which it is close enough to the star to be warm enough for a molecule (e.g. carbon monoxide) to be in the gas-phase, but outside of which it is so cold that the molecule exists as ice on the surfaces of dust grains. However, the theoretical understanding of the chemical processes taking place during planet formation, especially in the planet-forming regions before planets start forming, are less well-understood. Chemical reactions between molecules are likely to happen, both in the gas, and when the molecules are in the ice-phase on the surfaces of small grains of dust.

This thesis attempts to understand how chemical reactions in the material that forms planets changes this material over time. How the amounts of different common molecules change over time, and how much material, in particular how much carbon and oxygen, is in the gas and ice-phases, respectively, when planets start forming. Since planet formation models thus far have considered only unchanging chemical compositions of this material, or somewhat simplified chemistry, the goal of this thesis is to explore the trends in which chemical changes occur in planet-forming material before planets start forming. The results could potentially be useful, both for research in planet formation, but also for understanding the presence of certain molecules in the atmospheres of planets and exoplanets, and on comets. These molecules all tell stories about formation and evolution of these planets and comets, and the results here could be used to connect the planets and comets that are observed today to where and how they were formed.

Chapter 2 makes use of a computer code (the BADASS code) that can simulate chemical reactions in space. The code is given information about the physical environment found in planet-forming regions, such as temperature, density, and the level of ionisation (the amount of new ions created from neutral atoms or molecules reacting with energetic cosmic ray particles per second). The code is set to either only simulate chemical reactions in the gas-phase, or to also account for reactions taking place between molecules in the ice-phase on the surfaces of grains of dust. The code simulates an astronomical timescale of 1 million years. The timescale from the beginning of star formation and until the star and surrounding planets are all formed is estimated to be around 10 million years. The question is: will chemical reactions change the composition of the material over time?

It is found there are no significant chemical changes seen to the material only, when the ionisation level is low, and the simulations start off with neutral molecules. Significant changes are seen for all other setups of the simulation,

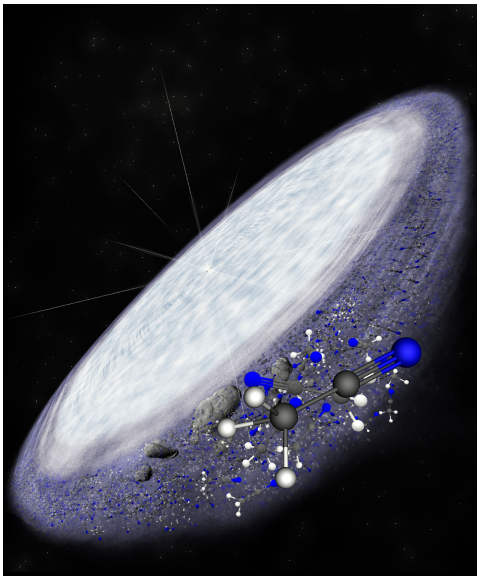

Figure 5.12: A star forming in the middle of a disk of molecules and dust grains (the latter may may appear as rocks). The molecules can react with each other, both in the gas-phase, and when frozen out as ices on the surfaces of the dust grains. Image credit: B. Saxton (NRAO/AUI/NSF).

and both chemical reactions on the surfaces of the dust grains, and the level of ionisation show important effects.

Chapter 3 is an expansion of the simulation setup in Chapter 2. A longer astronomical timescale is assumed (7 millions years), and the physical conditions, such as the temperature, are assumed to evolve (it gets colder) during the 7 million years, whereas in Chapter 2 they were kept static. Taking a changing physical environment into account does complicate the calculations, but this is a more realistic scenario, as not just the chemistry, but also the physical environment in the planet-forming region changes over time.

It is found that chemical evolution changes the chemical composition of the planet-forming material continuously up until at least 7 million year. The evolving physical conditions do not cause much different effects from the static conditions from Chapter 2, except that when the temperature decreases with time, then more molecules will become ices on dust grain. Only close to the star, where it is warm enough, will most molecules be in the gas-phase. It also turns out that the chemical composition of the material by 7 million years of evolution has evolved towards a steady state in which the composition is independent of what chemical composition (purely atoms or purely stable molecules) the simulation starts out with. This steady state chemical composition, in turn, is found to be very different than the typical compositions assumed in traditional planet formation models with a more simple treatment of chemistry.

The idea for **Chapter 4** is triggered by the detection of large amounts of molecular O_2 ice in comets 1P and 67P in the Solar System, and the fact that the

simulations in Chapter 2 (for certain model setups) shows that O_2 ice is produced in similar amounts as those detected in the comets. In this chapter it is investigated how and under which conditions O_2 ice can be produced on the surfaces of dust grains in the region where comets formed at the time, when our Solar System was still under construction. Several chemical parameters for how reactions between ice molecules take place were explored, and O_3 ice is included into the chemical code, which is not included in Chapter 2.

The results show that after including O_3 ice into the code, O_3 ice, and not O_2 ice is produced in large amounts, which does not match with the detected amounts of those molecules in the two comets. It turns out that the results from the code only agree with the comet detections for a very specific simulation setup, and it is therefore more likely that the O_2 ice was already there in the comet-forming region around the Sun, before chemical reactions took place there, instead of being produced by these reactions. However, chemical reactions on the surfaces of dust grains are less well-understood than reactions in the gas-phase, and the chemical interactions between O_2 ice, O_3 ice and some other chemically related atoms and molecules may need to be understood better before ruling out that that the O_2 ice could have been produced via chemical reaction on the surfaces of the grains, leading to the detected amounts in the comets.

Chapter 5 continues in the cometary track. Chapter 3 provides simulated amounts of many different icy molecules both as a function of astronomical evolution time, and as a function of distance (radius) from the star. The idea is to statistically match these relative amounts of each icy molecule to the amounts of each molecule detected in different comets. Such data on the amounts of each molecule in different comets are available in the scientific literature. A χ^2-method is used for this statistical comparison. The goal is to check if this investigation, using the molecular amounts of several different icy molecules, both detected and simulated, would will result in pointing out where in the planet -and comet-forming region around the Sun the comets were most likely to have formed.

Using a set of 15 different comets with detected amounts of various icy molecules, this statistical analysis points to 14 of the comets to likely have formed in the vicinity of the iceline of carbon monoxide (CO), although probably at different times during the evolution of the Solar System. This method showcases a possible new way of categorising comets: instead of categorising them directly based on the amounts of each molecule that are detected in them, this new method takes into account the chemical changes that can happen to the material during the evolution of the Solar System, and the new method shows that 14 out of 15 comets may have formed around the same iceline, although at different times.

Main conclusions drawn from this thesis:

- Chemical evolution in planet -and comet-forming regions can change the chemical composition of its material significantly over time. Ionisation of this material, as well as chemical reactions between molecules in the ice-phase, are both important factors contributing to the chemical evoution. The evolution may influence the chemical compositions of the planet, exo-

planets and comets, that form. Models that simulate planet formation and composition would therefore benefit from incorporating better treatments of chemical reactions in planet-forming material.

- The amount of O_2 ice detected in comets 1P and 67P remains best explained by the O_2 ice having formed before the chemical simulations were run. That is to say, the O_2 ice was most likely already present, before the Solar System started forming.
- Chemical evolution models can be used to speak about the formation histories of, not only planet, but also comets. With a statistical comparison between detected molecules in comets in the Solar System, and simulated amounts of molecules in a comet-forming region, almost all the investigated comets show likely formation around the CO iceline.
- Chemical reactions between icy molecules on the surfaces of dust grains play an important role in changing the chemical composition of material in regions of planet formation. However, these reactions are less well-understood than reactions in the gas-phase. Future laboratory experiments on the Earth will help to better understand these reactions, and this improved understanding will be valuable in codes simulating chemical evolution in space.

Nederlandse Samenvatting

Planeten en de zoektocht naar leven in het heelal. Waar komen we vandaan en zijn we alleen? Dit zijn vragen waar de mensheid zich altijd al mee bezig heeft gehouden. De laatste vraag betreft het leven en hoe het kan ontstaan. Het enige leven dat we kennen is het leven hier op onze eigen planeet, de aarde. De zoektocht naar leven elders in het heelal is dus vaak een zoektocht naar planeten en exoplaneten die op de aarde lijken.

Het leven op onze planeet zou bijna net zou oud kunnen zijn als de aarde zelf. Ter vergelijking: het eerste leven begon waarschijnlijk 3,6 miljard jaar geleden en de aarde is 4,6 miljard jaar oud. De ingrediënten van het leven zijn gebaseerd op hetzelfde materiaal dat onze planeet heeft gevormd, en daarom is het begrijpen van planeetvorming en van welk materiaal planeten worden gevormd, de sleutel tot het begrijpen van zowel de evolutie van de aarde, als het leven daarop.

Planeetvorming. Planeten vormen rondom sterren, die op hun beurt vormen wanneer grote wolken van gas en stof instorten onder invloed van de zwaartekracht van al het materiaal dat zich daarin bevindt (zie "Prestellaire Kern" in figuur 5.13, waar de zwaartekracht al het materiaal van de grijze wolk naar binnen trekt, in de richting van de pijlen). De vorming van planeten is een actief onderzoeksgebied in de astronomie. Het probeert te beschrijven hoe het proces van stervorming kan leiden tot planeetvorming uit het materiaal rondom de ster (geïllustreerd door alle zes evolutiestappen in figuur 5.13). Het begrijpen van de grootte, de bewegingen en de samenstelling van de resulterende planeten vereist kennis van zowel de fysische als chemische processen die plaatsvinden tijdens het vormingsproces.

Deze processen worden op verschillende manieren bestudeerd in astronomisch onderzoek: door theoretisch inzicht in de processen en het voorspellen waartoe ze zullen leiden, door astronomische waarnemingen van het heelal en door laboratoriumexperimenten op de aarde. In het geval van planeetvorming is het theoretisch inzicht in de fysische processen die zich voordoen recentelijk enorm verbeterd. Computersimulaties hebben voorspellingen gedaan over welke soorten planeten zich op welke plek vormen. Waarnemingen van planeten, exoplaneten en planeetvormende gebieden hebben op hun beurt deze voorspellingen bevestigd of ontkracht. Laboratoriumexperimenten hebben bijgedragen aan het begrip van de moleculen die in het heelal bestaan, hoe we ze kunnen detecteren en welke chemische reacties er tussen hen kunnen plaatsvinden. Dit alles helpt om de samenstelling van het materiaal waaruit planeten vormen te begrijpen.

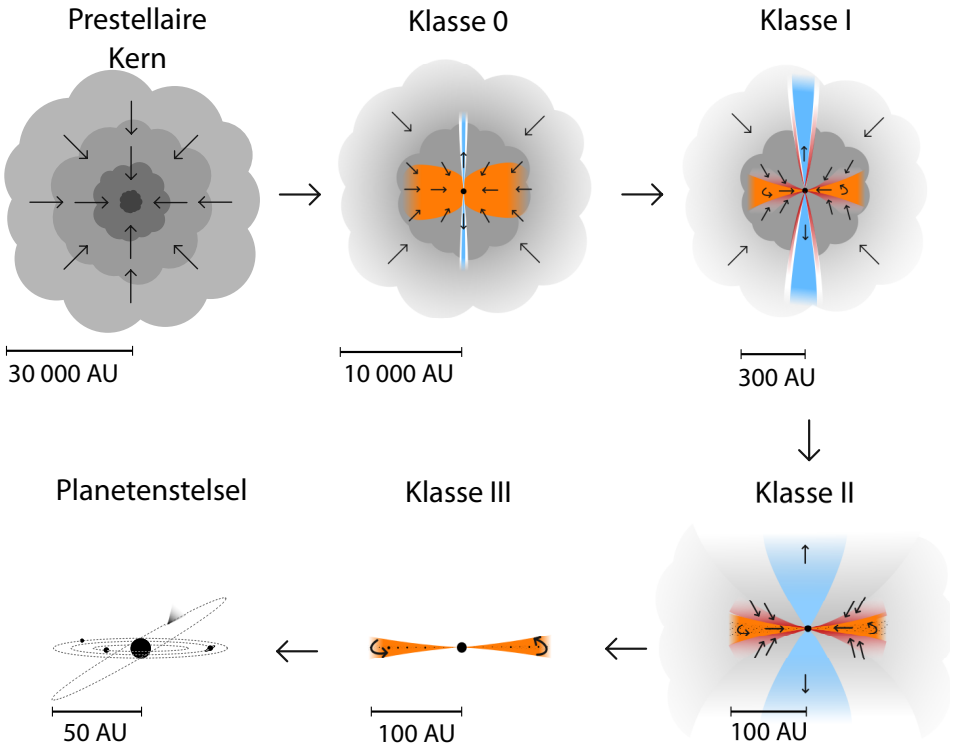

Figuur 5.13: Verschillende stadia van ster- en planeetvorming. De chemische simulaties in dit proefschrift concentreren zich voornamelijk op klassen 2 en 3, maar er worden koppelingen gemaakt met zowel de prestellaire kern als het eindproduct, namelijk het planetenstelsel. Afbeelding: "Current view of protostellar evolution" door Magnus Vilhelm Persson.

Fysische en chemische effecten tijdens planeetvorming. Het begrip van de fysica van planeetvorming is ver gekomen. Daarnaast hebben waarnemingen van planeetvormende gebieden, vooral met de Atacama Large Millimeter / submillimeter Array (ALMA) in Chili, een schat aan informatie opgeleverd over de structuur en moleculaire samenstelling van dergelijke gebieden. ALMA is een telescoop die bestaat uit 66 radioantennes gelegen op 5000 meter hoogte in de droogste woestijn op aarde. In deze omgeving is ALMA het beste observatorium ter wereld voor het waarnemen van elektromagnetische straling op golflengten van ongeveer 1 millimeter. Dit maakt ALMA optimaal voor vele waarnemingen, inclusief die van ster- en planeetvormingsgebieden, en ook voor het detecteren van specifieke moleculen in deze gebieden. Onder andere zijn zogenaamde ijslijnen van verschillende moleculen gedetecteerd met behulp van ALMA. Een ijslijn markeert het gebied in de schijf dichtbij de ster waar het warm genoeg is voor een molecuul (bv. koolmonoxide) om zich in de gasfase te bevinden. Buiten de ijslijn is het zo koud dat het molecuul alleen als ijs op het oppervlak van een stofkorrel bestaat. Het theoretisch inzicht in de chemische processen die plaatsvinden tijdens de planeetvorming, vooral voordat de planeten zich beginnen te vormen, is echter minder goed begrepen. Chemische reacties tussen moleculen zullen waarschijnlijk, zowel in het gas- als in de ijsfase op het oppervlak van kleine stofkorrels plaatsvinden.

Dit proefschrift probeert te begrijpen hoe planeetvormend materiaal in de loop van de tijd wordt veranderd door deze chemische reacties. Ook onderzoekt het hoe de hoeveelheden van verschillende gangbare moleculen veranderen in de loop van de tijd en hoeveel materiaal, met name hoeveel koolstof en zuurstof, respectievelijk in de gas- en ijsfase aanwezig is wanneer planeten zich beginnen te vormen. Omdat planeetvormingsmodellen tot nu toe alleen onveranderde chemische samenstellingen van dit materiaal, of enigszins vereenvoudigde chemie, hebben overwogen, is het doel van dit proefschrift om de trends te verkennen waarin chemische veranderingen plaatsvinden in planeetvormend materiaal voordat planeten beginnen te vormen. De resultaten kunnen mogelijk nuttig zijn, zowel voor onderzoek naar planeetvorming, als voor het begrijpen van de aanwezigheid van bepaalde moleculen in de atmosferen van planeten, exoplaneten en kometen. Deze moleculen vertellen verhalen over de vorming en evolutie van deze planeten en kometen, en de resultaten van dit proefschrift zouden kunnen worden gebruikt om de planeten en kometen die vandaag worden waargenomen te verbinden met waar en hoe ze werden gevormd.

Hoofdstuk 2 maakt gebruik van een computercode (de BADASS-code) die chemische reacties in het heelal kan simuleren. Deze code bevat informatie over de fysische toestanden van planeetvormende gebieden, zoals temperatuur, dichtheid en het niveau van ionisatie (de hoeveelheid nieuwe ionen die per seconde gemaakt worden door interacties van energetische kosmische deeltjes met neutrale atomen of moleculen). De code is ingesteld om alleen chemische reacties in de gasfase te simuleren, of om ook rekening te houden met reacties die plaatsvinden tussen moleculen in de ijsfase op de oppervlakken van stofkorrels. De code simuleert een astronomisch interval van 1 miljoen jaar. De tijdschaal vanaf het begin van de stervorming tot aan de tijd dat de ster en de omliggende planeten allemaal zijn gevormd, wordt geschat op ongeveer 10 miljoen jaar. De vraag is: zouden

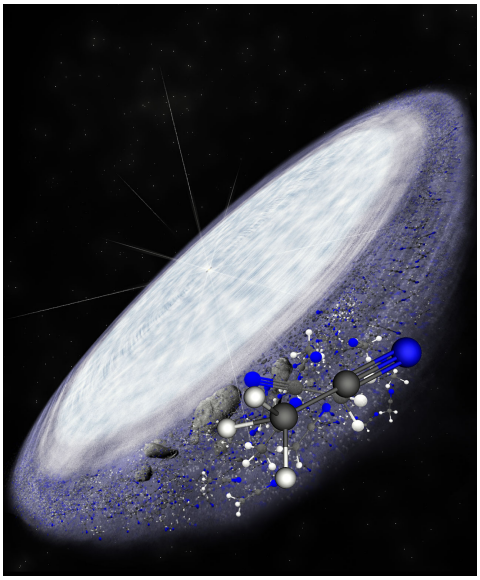

Figuur 5.14: In het midden van een schijf van moleculen en stofkorrels (die eruit kunnen zien als rotsen) vormt zich een ster. De moleculen in de schijf kunnen met elkaar in contact komen, zowel in de gasfase, als bevroren als ijs op de oppervlakken van de stofkorrels. Credit: B. Saxton (NRAO/AUI/NSF)

chemische reacties de samenstelling van het materiaal in de loop van de tijd kunnen veranderen.

Het blijkt dat alleen wanneer het ionisatieniveau laag is, en de simulatie begint met neutrale moleculen, er geen significante chemische veranderingen in het materiaal worden waargenomen. Significante veranderingen worden gezien voor alle andere versies van de simulatie, en zowel chemische reacties op de oppervlakken van de stofkorrels als het niveau van ionisatie veroorzaken belangrijke effecten.

Hoofdstuk 3 is een uitbreiding van de simulatie-opzet in hoofdstuk 2. Er wordt uitgegaan van een langere astronomische tijdschaal (7 miljoen jaar) en de fysische omstandigheden, zoals de temperatuur, worden verondersteld te evolueren (af te koelen) gedurende de 7 miljoen jaar. Dit in tegenstelling tot in hoofdstuk 2, waarin ze constant worden gehouden. Het rekening houden met veranderende fysische omstandigheden bemoeilijkt de berekeningen, maar dit is een meer realistisch scenario, omdat niet alleen de chemie, maar ook de fysische omgeving in het planeetvormende gebied in de loop van de tijd verandert.

Er is vastgesteld dat chemische evolutie de chemische samenstelling van het planeetvormende materiaal continu verandert tot ten minste 7 miljoen jaar. De zich veranderende fysische omstandigheden veroorzaken geen sterk verschillend effect in vergelijking met de onveranderlijke omstandigheden uit hoofdstuk 2, behalve dat wanneer de temperatuur met de tijd afneemt, er meer moleculen zich in ijs op de stofkorrels bevinden. Alleen dicht bij de ster, waar het warm genoeg is, zullen de meeste moleculen zich in de gasfase bevinden. Het blijkt ook dat de chemische

samenstelling van het materiaal na 7 miljoen jaar geëvolueerd is tot een stabiele toestand, waarbij de samenstelling onafhankelijk is van de chemische samenstelling (enkel atomen of zuiver stabiele moleculen) waarmee de simulatie was begonnen. Deze steady-state chemische samenstelling blijkt op haar beurt weer heel anders te zijn dan de typische samenstellingen die in traditionele planeetvormingsmodellen worden verondersteld met een eenvoudigere behandeling van de chemie.

Het idee voor **Hoofdstuk 4** is geïnspireerd door de detectie van grote hoeveelheden moleculair zuurstofijs (O_2-ijs) in kometen 1P en 67P in ons zonnestelsel en het feit dat de simulaties in hoofdstuk 2 (voor bepaalde modelopstellingen) aantonen dat O_2-ijs in vergelijkbare hoeveelheden wordt geproduceerd als die werden gedetecteerd in de kometen. In dit hoofdstuk is onderzocht hoe en onder welke voorwaarden O_2-ijs kan worden geproduceerd op de oppervlakken van stofkorrels in het gebied waar kometen werden gevormd in de periode waarin ons zonnestelsel nog in aanbouw was. Verschillende chemische parameters voor de manier waarop reacties tussen ijsmoleculen plaatsvinden, worden onderzocht en O_3-ijs wordt opgenomen in de chemische code in tegenstelling tot in hoofdstuk 2.

De resultaten tonen aan dat na het opnemen van O_3-ijs in de code, O_3-ijs in plaats van O_2-ijs in grote hoeveelheden wordt geproduceerd, wat niet overeenkomt met de waarnemingen van die moleculen in de twee kometen. Het blijkt dat de resultaten van de code alleen overeenkomen met de waarnemingen van de kometen voor een zeer specifieke simulatie-opzet, en het is daarom waarschijnlijker dat het O_2-ijs zich al in de komeetvormende regio rondom de zon bevond voordat daar chemische reacties plaatsvonden, in plaats van te worden geproduceerd door deze reacties. Chemische reacties op de oppervlakken van stofkorrels zijn echter minder goed begrepen dan reacties in de gasfase. De chemische interacties tussen O_2-ijs, O_3-ijs en enkele andere chemisch gerelateerde atomen en moleculen moeten misschien eerst beter onderzocht worden voordat we kunnen uitsluiten dat het O_2-ijs geproduceerd kan zijn via chemische reacties op de oppervlakken van de stofkorrels, leidend tot de gedetecteerde hoeveelheden in de kometen.

Hoofdstuk 5 gaat verder in op de kometen. Hoofdstuk 3 biedt gesimuleerde hoeveelheden van vele verschillende bevroren moleculen als een functie van astronomische tijd en als een functie van afstand (straal) van de ster. Het idee was om deze relatieve hoeveelheden van elk bevroren molecuul statistisch te matchen met de hoeveelheden van elk molecuul die in verschillende kometen zijn gedetecteerd. Dergelijke gegevens over de hoeveelheden van elk molecuul in verschillende kometen zijn beschikbaar in de wetenschappelijke literatuur. Een χ^2-methode wordt gebruikt voor deze statistische vergelijking. Het doel van dit onderzoek is om door het vergelijken van hoeveelheden van moleculen in simulaties en in waargenomen kometen de meest waarschijnlijke locaties van de komeet- en planeetvormende gebieden rondom de jonge zon te bepalen.

Met behulp van een set van 15 verschillende kometen met gedetecteerde hoeveelheden van verschillende bevroren moleculen, suggereert deze statistische analyse dat 14 van de kometen waarschijnlijk in de buurt van de ijslijn van koolmonoxide (CO) zijn gevormd, hoewel op verschillende tijdstippen tijdens de evolutie van het zonnestelsel. Deze methode toont een mogelijke nieuwe manier aan om kometen te categoriseren: in plaats van ze rechtstreeks te categoriseren op basis

van de hoeveelheden van elk molecuul die in hen werden gedetecteerd, houdt deze nieuwe methode rekening met de chemische veranderingen van het materiaal tijdens de evolutie van het zonnestelsel. De nieuwe methode toont aan dat 14 van de 15 kometen zich rond dezelfde ijslijn hadden gevormd, hoewel op verschillende tijdstippen.

De belangrijkste conclusies van dit proefschrift zijn:

- Chemische evolutie in planeet- en komeetvormende gebieden kan de chemische samenstelling van het materiaal in de loop van de tijd aanzienlijk veranderen. Dit kan van invloed zijn op de chemische samenstelling van de planeten, exoplaneten en kometen die zich vormen. Modellen die planeetvorming en -samenstelling simuleren, zouden er goed aan doen om hier rekening mee te houden.

- De hoeveelheid O_2-ijs gedetecteerd in kometen 1P en 67P blijft het best te verklaren met O_2-ijs dat is gevormd voor de periode waardoor de chemie werd gesimuleerd. Dat wil zeggen dat het O_2-ijs waarschijnlijk al aanwezig was voordat het zonnestelsel begon te vormen.

- Chemische evolutiemodellen kunnen worden gebruikt om te spreken over de geschiedenis van de vorming van niet alleen planeten maar ook kometen. Uit een statistische vergelijking tussen gedetecteerde moleculen in kometen in het zonnestelsel en gesimuleerde hoeveelheden moleculen in een komeetvormingsgebied, blijkt dat bijna alle onderzochte kometen waarschijnlijk rond de CO-ijslijn zijn gevormd.

- Chemische reacties tussen bevroren moleculen op de oppervlakken van stofkorrels spelen een belangrijke rol bij het veranderen van de chemische samenstelling van het materiaal in gebieden waarin planeten vormen. Deze reacties zijn echter minder goed begrepen dan reacties in de gasfase. Toekomstige laboratoriumexperimenten op aarde zullen helpen om deze reacties beter te begrijpen, en dit verbeterde begrip zal waardevol zijn in codes die de chemische evolutie in het heelal simuleren.

Dansk Resumé

Planeter, og jagten på liv i rummet. Siden tidernes morgen har vi mennesker spekuleret over vores oprindelse. Hvor kommer vi fra, og er vi alene? Det sidste af disse spørgsmål relaterer sig til liv, og hvordan det kan opstå. Det eneste liv, vi kender og ved noget om, er livet her på vores egen planet: Jorden. Jagten på liv i det ydre rum er derfor ofte en søgen efter omgivelser og betingelser i verdensrummet, der minder om de livsunderstøttende omgivelser, vi har her på Jorden.

Livets oprindelse på vores planet går formentlig helt tilbage til planetens dannelse (der er fundet tegn på, at der allerede var liv på Jorden for ca. 3,6 millarder år siden, hvorimod Jorden selv er 4,6 milliarder år gammel). De ingredienser, der er nødvendige for at liv kan opstå, er kommet hertil sammen med det materiale, som i sin tid dannede Jorden. For at forstå planetens udvikling, og hvordan liv er opstået, er det derfor vigtigt, både at forstå hvordan planeten blev dannet, men også hvilket materiale, den blev lavet af.

Planetdannelse. Planeter dannes rundt om stjerner, og stjerner dannes når store områder i rummet fyldt med gas og stjernestøv kollapser på grund af tyngdekraften (se "Prestellar Core" i figur 5.15, hvor tyngdekraften trækker alt materialet ind mod midten af den grå sky, i pilenes retninger). Planetdannelse er et aktivt forskningsfelt indenfor astronomi. Feltet forsøger at beskrive, hvordan stjernedannelsesprocessen kan føre til at dele af materialet ender med at lave planeter, der kredser rundt om stjernen (illustreret ved de seks udviklingsstadier in figur 5.15). For at forstå diversiteten af de dannede planeter, for eksempel deres størrelser, sammensætninger, og deres baner rundt om deres stjerner, kræves der både viden om de fysiske og de kemiske processer, der finder sted under dannelsesprocessen.

Disse processer studeres på flere forskellige måder indenfor astronomisk forskning. Det sker gennem teoretisk forståelse af processerne, og derigennnem forudsigelser af, hvad de vil føre til. Derudover sker det igennem astronomiske observationer af rummet, og det sker gennem laboratorieforsøg på jorden. I tilfældet med planetdannelse er den teoretiske forståelse af de fysiske processer skredet betydeligt frem i de seneste par år. Computersimuleringer har leveret forudsigelser om hvilke typer planeter, der bliver dannet, og hvor. Observationer af planeter, exoplaneter og planetdannende områder har afgrænset hvilke forudsigelser der stemmer overens med observationer, og laboratorieforsøg har bidraget til at forstå de molekyler, der eksisterer i rummet, hvordan man opdager dem og hvilke kemiske reaktioner, der ske imellem dem. Alt dette hjælper med til at forstå sammensætningen af det materiale, som planeterne bliver dannet af.

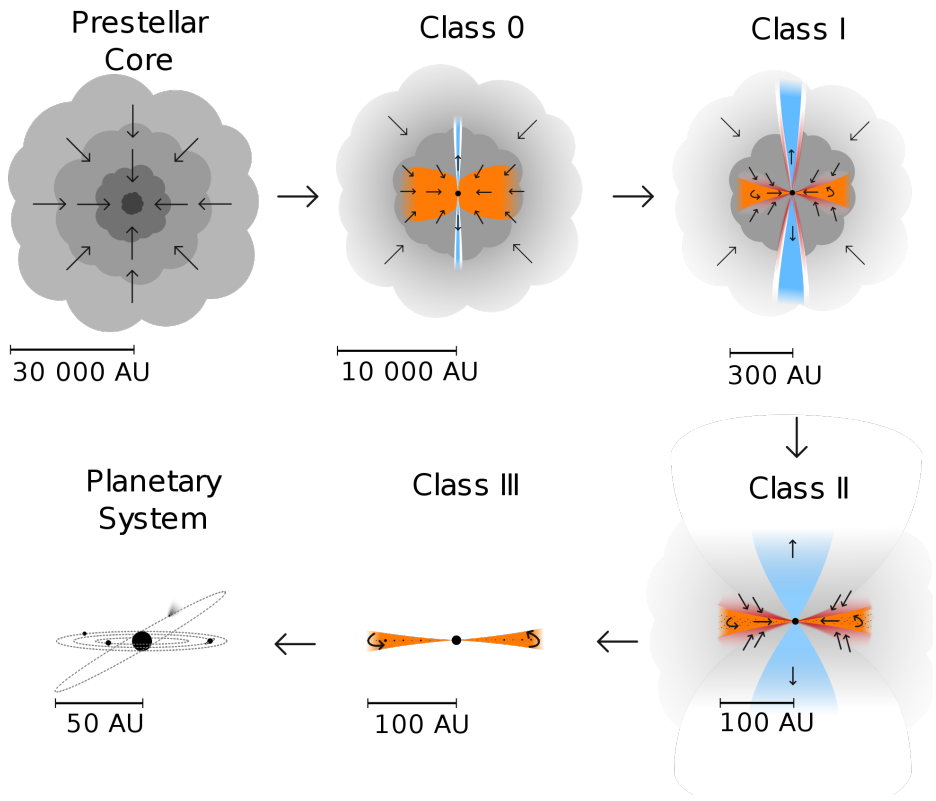

Figur 5.15: Forskellige stadier af stjerne -og planetdannelsesprocessen. De kemiske simuleringer i denne afhandling fokuserer hovedsageligt på klasse 2 og 3, men der trækkes tråde til både den præstellare kerne, og til slutproduktet, nemlig planetsystemet. Billedkilde: "Current view of protostellar evolution" af Magnus Vilhelm Persson.

Fysiske og kemiske processer under planetdannelsen. Udover den fremskredne forståelse af fysikken bag planetdannelse, har observationer af planetdannende områder i rummet (især med Atacama Large Millimeter / submillimeter Array Observatory (ALMA) i Atacamaørkenen i Chile), givet et væld af nye informationer om, og ny indsigt i, strukturen og de molekylære sammensætninger af sådanne områder. ALMA består af 66 radioantenner, der er placeret i 5000 meters højde i den tørreste ørken på Jorden. På grund af disse omgivelser er ALMA det bedste observatorium i verden til observationer af elektromagnetisk stråling med bølgelængder på omkring 1 millimeter. Det gør ALMA optimal til mange anvendelser, heriblandt til observationer af områder hvor stjerne- og planetdannelse finder sted, og til detektion af specifikke molekyler i områderne. Blandt andet er der blevet påvist flere såkaldte islinjer ved anvendelse af ALMA. En islinje er radiusen fra den centrale stjerne i et planetdannende område, der afgrænser tilstandsformen for et givent molekyle. Inden for islinjen er stjernen tæt nok på til at et molekyle (for eksempel kulilte) eksisterer på gasform, men udenfor islinjen er det så koldt, at molekylet kun kan eksistere som is på overfladen af støvkorn. De kemiske processer, der foregår under planetdannelsen, især i de planetdannende områder inden planeterne bliver dannet, er imidlertid ikke nær så velforståede. Kemiske reaktioner mellem molekyler i disse områder vil sandsynligvis finde sted både i gasfasen og når molekylerne er frosne på overfladen af små støvkorn.

Planetdannelsesmodeller har hidtil enten kun anvendt forenklede kemiske modeller til at tage højde for kemiske reaktioner i planetdannende materiale, eller antaget, at der ikke sker nogle kemiske reaktioner, så materialets sammensætning ikke ændres over tid. I den forbindelse forsøger denne afhandling at forbedre forståelsen af, hvordan netop kemiske reaktioner i materialet, ændrer materialets sammensætning over tid. Det drejer sig især om, hvordan mængderne af forskellige molekyler ændrer sig over tid, og hvor meget af dette materiale, især hvor meget kulstof og ilt, der er i henholdsvis gas- og isfasen, når planeterne begynder at dannes. Det sker, ved at anvende en specialiseret computermodel der kan simulere en bred vifte af forskellige kemiske reaktioner, og ved at bruge modellen til at undersøge, hvilke tendenser i de kemiske forandringer af materialet der forekommer, i det planetdannende materiale, før planeterne bliver dannet. Resultaterne er til gavn for forskning i planetdannelse, men også i forhold til at forstå forekomsten af bestemte molekyler i planeters og i exoplaneters atmosfærer, og forekomsten af molekyler på kometer. Molekyler fortæller nemlig historier om dannelsen og udviklingen af disse planeter og kometer, og resultaterne her kan potentielt bruges til at forbinde planeter og kometer til hvor og hvordan, de blev dannet.

Kapitel 2 gør brug af et computerprogram (BADASS-koden), der kan simulere kemiske reaktioner i rummet. Kapitlet undersøger, om kemiske reaktioner i det planetdannende materiale ændrer materialets sammensætning over tid. BADASS-koden gives oplysninger om det fysiske miljø, der findes i planetdannende områder, såsom temperatur, densitet og ioniseringsniveauet (hvor mange nye ioner per sekund, som bliver dannet af reaktioner mellem neutrale atomer eller molekyler og energisk kosmisk stråling). Programmet indstilles til, enten kun at simulere kemiske reaktioner i gasfasen, eller til også at tage højde for reaktioner, der finder sted mellem molekyler i isfasen på overfladen af støvkorn. Koden simulerer på

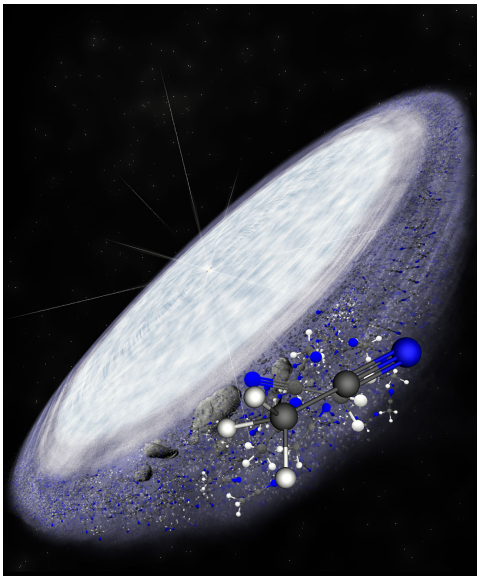

Figur 5.16: En stjerne bliver dannet i midten af en skive af molekyler og støvkorn (sidstnævnte kan ligne stykker af sten). Molekylerne kan reagere med hinanden, både i gasfasen, men også når de ligger som is på overfladerne af støvkornene. Billedkilde: B. Saxton (NRAO/AUI/NSF).

den baggrund en astronomisk tidsskala på 1 million år. Tiden, fra begyndelsen af stjernedannelsen, og indtil stjernen og de omkringliggende planeter alle er dannet anslås til at være omkring 10 millioner år.

Resultaterne af projektet viser, at kun i tilfælde hvor ioniseringsniveauet er lavt, og simuleringen starter med neutrale molekyler, er der ingen betydelige ændringer i den kemiske sammensætning af materialet. Der ses betydelige ændringer for alle andre begyndelsesbetingelser, og både kemiske reaktioner på støvkornenes overflader og ioniseringsniveauet viser sig at have stor indflydelse på, hvordan den kemiske sammensætning ændres.

Kapitel 3 er en udbygning af simuleringsopsætningen fra Kapitel 2, igen med fokus på planetdannende områder i rummet. Der antages en længere astronomisk tidsskala (7 millioner år), og det antages at de fysiske forhold, såsom temperaturen i området, udvikler sig i løbet af de 7 millioner år (det bliver koldere med tiden), hvorimod de fysiske forhold i den anvendte model i Kapitel 2 ikke udvikler sig over tid. Hensyntagen til et ændret fysisk miljø komplicerer beregningerne, men det er mere realistisk, da ikke kun kemien, men også det fysiske miljø i det planetdannende område, rent faktisk forandrer sig over tid.

Vi finder frem til, at kemisk udvikling forårsager kontinuerte ændringer af den kemiske sammensætning af det planetdannende materiale indtil mindst 7 millioner år. Derimod gør udviklingen af de fysiske forhold ikke den store forskel for den kemiske sammensætning set i forhold til de statiske forhold fra Kapitel 2. Dog ser vi, at når temperaturen falder med tiden, så går flere molekyler fra at være i gas-fasen til at være is på overfladen af støvkorn. Kun tæt på stjernen, hvor

det forbliver varmt nok, vil de fleste molekyler stadig være i gasfasen. Det viser sig også, at den kemiske sammensætning af det planetdannende materiale efter 7 millioner års udvikling har udviklet sig hen imod en stabil tilstand, hvor sammensætningen er uafhængig af hvilken kemisk sammensætning (kun atomer eller kun stabile molekyler) simuleringen begynder med. Ovenikøbet er den stabile kemiske sammensætning ved simuleringens afslutning meget forskellig fra de kemiske sammensætninger der typisk bliver antaget i traditionelle planetdannelsesmodeller, som behandler de kemiske reaktioner i materialet mere simpelt.

Ideen til **Kapitel 4** udspringer af fundet af de store mængder af molekylær O_2 is i kometerne 1P og 67P i Solsystemet, og det faktum at simuleringerne (for visse modelopsætninger) tilbage i Kapitel 2 viser, at O_2 is bliver produceret i kemiske reaktioner i mængder svarende til dem, der findes i de to kometer. I Kapitel 4 bliver det undersøgt, hvordan, og under hvilke betingelser, O_2 is kan produceres gennem kemiske reaktioner i isen på overfladerne af støvkorn i det område, hvor kometer blev dannet, tilbage dengang, da vores Solsystem stadig var under dannelse. Flere kemiske parametre for, hvordan reaktioner mellem ismolekyler finder sted, bliver undersøgt, og O_3 is (som ikke er inkluderet i Kapitel 2) er som noget nyt inkluderet i programkoden, der bruges til simulationerne.

Resultaterne viser, at O_3 is inkluderes in simulationerne, så er det O_3 is, og ikke O_2 is, der bliver produceret i store mængder. Det resultat stemmer ikke overens med mængderne af disse molekyler i de to kometer. De kemiske simuleringer kan kun reproducere de fundne mængder i kometerne, når simulationerne kører under nogle meget specifikke betingelser. Derfor er det mere sandsynligt, at O_2 isen fundet på kometerne allerede befandt sig i det stjerne -og planetdannende område som dannede Solsystemet (Prestellar Core-stadiet i figur 5.15), før Solen blev dannet, i stedet for at været blevet dannet af kemiske reaktioner, efterfølgende. Imidlertid er kemiske reaktioner på overfladen af støvkorn ikke så velforståede som kemiske reaktioner i gasfasen. Derfor er de kemiske vekselvirkninger mellem O_2 is, O_3 is og andre, kemisk beslægtede atomer og molekyler, muligvis nødt til at blive undersøgt og studeret bedre, før det kan udelukkes, at O_2 isen fundet i kometerne kunne være blevet produceret gennem kemiske reaktioner på de isbelagte støvkorns overflader, undervejs under dannelsen af Solsystemet.

Kapitel 5 fortsætter på sporet af kometer. Kapitel 3 leverer simulerede mængder af mange forskellige ismolekyler, både som funktion af den astronomiske tidsudvikling, og som funktion af afstanden (radius) fra stjernen. Tanken er, at der kan laves et statistisk match mellem de simulerede mængder af ismolekyler, og mængderne af hvert molekyle detekteret i forskellige kometer. Målinger af mængderne af bestemte molekyler i forskellige kometer er tilgængelige i den videnskabelige litteratur. En χ^2 - metode anvendes til den statistiske sammenligning. Målet er at undersøge, om der kan drages statistiske konklusioner om, hvor det er mest sandsynligt, at kometerne oprindeligt blev dannet på baggrund af sammenligningen.

Ved hjælp af data fra 15 forskellige kometer med detekterede mængder af forskellige ismolekyler, peger vores statistiske analyse på, at 14 af kometerne sandsynligvis blev dannet i nærheden af islinjen for kulilte (CO). Dog er kometerne sandsynligvis blevet dannet på forskellige tidspunkter undervejs i dannelsen af Solsystemet. Metoden præsenterer derfor en mulig ny måde at kategorisere kome-

ter på: i stedet for at kategorisere dem direkte ud fra mængderne af hvert molekyle, der er detekteret i dem, så tager denne nye metode hensyn til de kemiske forandringer, der kan finde sted i materialet under udviklingen af Solsystemet, og den nye metode viser altså, at 14 ud af 15 kometer kan have dannet sig omkring den samme islinje, dog blot på forskellige tidspunkter.

Hovedkonklusionerne fra denne Ph.D.-afhandling er som følger:

- Kemisk udvikling i planet -og kometdannende materiale, kan ændre materialets kemiske sammensætning betydeligt over tid. Dette kan påvirke de kemiske sammensætninger af både planeter, exoplaneter og kometer, som alle bliver dannet ud af materialet. Modeller, som simulerer planeters dannelse og sammensætning, ville drage fordel af at tage de kemiske forandringer af det planetdannende materiales sammensætning i betragtning.

- Den bedste forklaring på mængden af O_2 is som er detekteret i kometerne 1P og 67P er fortsat, at O_2 isen er blevet dannet, før de kemiske forandringer præsenteret her i afhandling fandt sted. Det vil sige, at O_2 isen sandsynligvis allerede var tilstede, før Solsystemet blev dannet.

- Modeller, som simulerer kemisk udvikling i det ydre rum, kan bruges til at adressere, hvordan både planeter og kometer er blevet dannet. En statistisk sammenligning mellem detekterede molekyler i kometer i Solsystemet, og simulerede mængder af molekyler i et kometdannende område peger på, at næsten alle undersøgte kometer sandsynligvis blev dannet i nærheden af CO-islinjen.

- Kemiske reaktioner mellem iskolde molekyler på overfladerne af støvkorn spiller en vigtig rolle i forhold til at ændre den kemiske sammensætning af materialet i områder, hvor planeter bliver dannet. Disse reaktioner er imidlertid ikke ligeså velforståede som reaktioner mellem molekyler i gasfasen. Fremtidige laboratorieeksperimenter på Jorden vil være vigtige for fortsat at opnå en bedre forståelse af disse overfladereaktioner, og denne forbedrede forståelse vil være værdifuld i programkoder, som simulerer kemiske reaktioner i det ydre rum.

Publications

Refereed Publications

Setting the volatile composition of (exo)planet-building material. Does chemical evolution in disk midplanes matter?
C. Eistrup, C. Walsh, E. F. van Dishoeck, 2016, A&A , 595, 83.

Molecular abundances and C/O ratios in chemically evolving planet-forming disk midplanes
C. Eistrup, C. Walsh, E. F. van Dishoeck, 2018, A&A , 613, 14.

Formation of cometary O_2 ice and related ice species on grain surfaces in the midplane of the pre-Solar nebula
C. Eistrup, C. Walsh, 2018, A&A , *in press*

Publications in preparation

Matching protoplanetary disk midplane chemical evolution to cometary compositions
C. Eistrup, C. Walsh, D. Carr, M. Drozdovskaya, E. F. van Dishoeck, A&A *In prep*

Refractory carbon depletion leading to super-stellar C/O in planetary atmospheres
A. J. Cridland, **C. Eistrup**, E. F. van Dishoeck, MNRAS *In prep*

Hot-Jupiter atmospheric compositions formed from a chemically evolved disk midplane
S. Notsu, **C. Eistrup**, H. Nomura, C. Walsh, A&A *In prep*

Curriculum Vitae

I was born on 4 July 1988 in Hørsholm, Denmark to Kirsten and Carl Eistrup. I grew up with my little sister, Astrid, and dogs in the house. My childhood and teenage years were filled with weekly activities, as I was boy scouting, sailing, rowing, playing basketball, dancing and playing the contrabass. I was not particularly talented in any of the disciplines, but I gave them all my full commitment. I came to like sports and physical exercise, I learned perseverance, and especially rowing built my physical stamina. I also grew accustomed to spending much time away from home and meeting new people constantly.

My primary school physics teacher at Hørsholm Skole, Jens Terkelsen, inspired me much and got me enrolled in a LEGO robotics competition, and with that I learned my first basic programming. I continued on a scientific path in high school at Birkerød Gymnasium, where Niels Erik Wegge and Hanne Gjerløff opened up a world of physics and astronomy to me, and taught me to solve physics and astronomy textbook problems. I vividly remember how Niels Erik caught the attention and interest of the entire classroom during his lessons, how the Big Bang, CERN physics and Einstein's relativity permeated our curriculum, and how he kept us up-to-date on the frontiers of science. As a final project, Niels Erik provided me with exoplanet radial velocity data for me to analyse, and with that exoplanetary science and an eargerness to search for life in space became clear interests for me to further persue.

I enrolled as a physics undergraduate student at the Niels Bohr Institute at the University of Copenhagen, and I was inspired by both CERN physics and exoplanets. For my undergraduate final project I was supervised by Dr. Uffe Graae Jørgensen on a project about transiting exoplanets. As the loud and talkative person that I am, and with a growing fascination with and understanding of science, I caught on to the idea of teaching physics, during my undergraduate studies. Thus, upon earning my degree at age 21, I went into teaching physics and astronomy at my old high shool for a year. And what an experience! Seeing the fascination in my students' eyes when I went through the newest scientific results, their puzzled faces when faced with something seemingly inexplicable, and their excitement when they finally understood it, or suddenly succeeded in deducing or calculating the correct results themselves, sparked an incredible eagerness in me to continue to teach, pass on excitement and inspire people around me and everywhere, with science.

With my mind set to return to teaching at a later point, I continued my studies as a Master's student in physics and astronomy at the Niels Bohr Institute. As a

part of it, I went to Hawai'i, USA for a semester to study astronomy as an exchange student at the University of Hawai'i at Manōa. Here, I took part in the activities at the NASA Astrobiology Institute, along with, among others, Dr. Karen Meech and Dr. Bo Reipurth, and I had my first experience with theoretical astrochemistry in a course taught by Prof.dr. Ralf Kaiser. Back in Copenhangen, I decided to explore yet another exoplanetary detection method as my Master's degree final project, and did this project on gravitational microlensing, again supervised by Dr. Uffe Graae Jørgensen.

Nearing the end of my Master's, Dr. Jes Kristian Jørgensen at the University of Copenhagen suggested I applied to enter the PhD program at Leiden Observatory. My interests at that time were still very much on the detection of exoplanets, and the search for biosignatures. Thus, I applied for two exoplanetary PhD projects in Leiden, as well as a somewhat more peripheral project on the chemistry of planet formation with Prof.dr. Ewine van Dishoeck and Dr. Catherine Walsh. I thought it would be interesting to explore the astrochemistry I learned in Hawai'i further, and I was fortunate enough to be offered the astrochemistry position.

My PhD started with me emerging into an entire new field: star formation, planet formation and protoplanetary disks. A world of disk -and astrochemical models, and ALMA data and results being discussed over coffee and lunch. Like many beginnings, this was not an easy one. But my PhD project evolved in interesting ways. I went from exploring some of the astrochemistry that takes place before planets start forming, to making connections to what is detected in exoplanet atmospheres, and in comets nowadays. Importantly, I realised that as a theoretical astrochemist working with disks and planet formation chemistry, and with a strong interest in and intention to couple this to planets, I was somewhat floating in-between more traditional scientific communities, focusing on different fields of science (from star formation to disks to planet formation and to exoplanets) using different means and observing in different wavelengths. This has led to many interesting discussions, new ideas and a platform from which I feel that I can contribute to multiple scientific fields at the same time. In that context, I have been privileged to meet many brilliant and talented scientists, amongst others Kamber, Tim, Jenny, Ryan, Thomas, Dr. Steffen Kjær Jacobsen, Dr. Richard Teague, Dr. Sebastiaan Krijt, Dr. Myriam Telus, Dr. Bertram Bitsch, Dr. Ágnes Kóspál, Prof.dr. Fred Ciesla, Prof.dr. Christoph Mordasini, Prof.dr. Hubert Klahr and Prof.dr. Anders Johansen, and to travel to many interesting meetings in many places around the world to present my work.

I am now so lucky that I can pursue some of my research ideas, as an Origins Postdoctoral Fellow, first for two years at University of Virginia in Charlottesville, US, working with among other Dr. Rob Garrod and Prof.dr. Eric Herbst, and subsequently for two years at Chalmers University of Technology in Gothenburg, Sweden, with Prof.dr. Jonathan Tan. I hope that I will be able to make an impact to advance the scientific fields of planet formation, planets and exoplanets.

With my heart still beating loudly to share the world of, and fascination with science with people everywhere, I have been fortunate enough to be introduced to Universe Awareness at Leiden Observatory during my PhD. UNAWE has helped me become a better communicator, story-teller, and, through that, also a better

scientist. With skills learned from working with UNAWE, I took up the challenge of condensing my research interests down to a three-minute pitch, and with that I won the Leiden heat of the FameLab 2017 science communication competition, and was subsequently invited to talk about my research at NEMO Science Center for the Museum Night in Amsterdam 2017.

I will continue to communicate and inspire people with astronomy, everywhere I go. Becoming a scientist, doing research and being in touch with the frontiers of astronomy have made me a better communicator. Communicating my research, and why science is exciting and important, in turn, has made me a better scientist. For me, research and communication go hand-in-hand, and are both very important parts of my job, and my identity, as a scientist.

Acknowledgements

I may be the author of this PhD thesis, but it is the product of countless interactions and discussions with, suggestions from, support by, and answers to questions by many, many people. Each and everyone whom I have encountered on my way from arriving at Leiden Observatory, and until printing my thesis have affected me, and hence my thesis, in one way or another.

Catherine and Ewine. I deeply appreciate that you have stood by my side throughout these four years. I have found my research difficult, and becoming an expert in astrochemical modelling has been extremely challenging and hard work for me. You have taught me astrochemistry from scratch and till where I am now, even though I assume that I was not always an easy PhD student to advise and guide. Yet, you gave me space, but also both encouraged and pushed me at critical times so I could accomplish and be proud of this thesis, and you allowed me, not only to engage with all the different scientific communities relevant to my research interests, but also to devote precious time and energy to my outreach. Thank you for making me the scientist I am today!

My research group in Leiden (and Garching) has counted so many people over four years. Thanks to Magnus, Mihkel, Joe, John, Maria, Irene, Xioahu, Kenji, Niels, Ko-Ju, Vianney, Daniel, Anna, Paolo, Stefano, Alvaro, Andreas and Sierk for countless coffees, L-G telekon discussions, and for making the corridor such a relaxed, yet lively place place to work. Special shout-outs to Arthur, Alan and Daniel for your programming help and advise when I was new to Python and much else down that alley. Merel, I have enjoyed our discussions in the office, and when trying to decipher scripture. Nadia, you are ever positive and patient, also when faced with me getting started with an ALMA proposal. Nadia, Paola and Nienke, I have appreciated your understanding, empathy and warm hugs when times were tough. And Łukasz: a small step for a barista has been a giant LEAP(S) for coffee at Leiden Observatory. Thanks for being appropriately snobbish about coffee, and for coffee crawls during which significant parts of this thesis were written. Lastly, Alex, it was good to get even more spirit of planets and planet formation into the group. My corridor was also shared with people from the laboratory. Jeroen, Danna and Pablo it has been much fun to know actual lab people. Vincent, see you in D.C.! Michał, another person with passions in both astronomy and CrossFit, keep going as you are. And Kirstin, the original hipster at Leiden Observatory, and fellow dog-lover. You're a weird and amazing person, I look forward to running into you again at the other side of the pond!

Andrew, Mike, Chris, Eva, Aayush and Mieke, we shared a crazy and fun first-

year experience, and we have had many great moments since then. Aayush, Mieke, Ann-Sofie, Allison and Ricardo H., those many strolls outside brought the needed energy back on so many afternoons. Thank you to Marcelo and Liz for a delicious drink of Delirium Tremens that lead to the pink elephant on my conference posters. It has become an important part of my presentations at meetings. I also had the pleasure of spending a year of my time in Leiden sharing roofs with Nico and Ann-Sofie. Nico, you and Wijnand have been ever laughing, ever loving, ever direct, and ever comforting towards me back then. I wish you happy lives together! Ann-Sofie, tak! Tak for at vi kunne skælde ud og brokke os til hinanden på dansk, over forskningen og livet. Tak for alle gåturene, al kaffen og øllene. Tak for alt lindy hopperiet. Tak for alt det sjove, det irriterende, alle de gode grin, og fordi du gad lytte og give mig svar, hårdt for usødet. Tak også til Eva, Chris og Henriette, det har været en god og sjov tid med stor dansk tilstedeværelse i Leiden. Henry, tak for korrekturlæsningen og |RUM|-tiden. Luke and Valeriya, the Haguesperts. You two are amazing! Luke, your "English" is completely incomprehensible, but I appreciate that you came to Val's rescue on the dance floor, when my attention was elsewhere.

Being a PhD student in Leiden gives you a country-wide network of colleagues. Claudia, Edgar, Veronica, Kaustubh, Lukas, Kataryna and many others, you all made the PEPSci meetings exciting and fruitful, yet there was a casual and friendly atmosphere surrounding the meetings that made me look especially forward to them all. During my visits to the University of Leeds I have come to know the astronomy graduate students there. Alice, Abi, James and the rest of you, I have felt so welcome in Leeds because of you, and I enjoyed all the discussions! Shota-san and Hideko-san, it has been a pleasure and very interesting collaborating with you both! I also had the honor of serving as Assistant Coordinator of the NOVA Network 2. Carsten Dominik, Rik van Lieshout, Ignas Snellen and Eleanor Spring, it has been a pleasure to co-organise the meetings with you, and thanks to the entire network for your engagement during the meetings.

It was not clear to me throughout my PhD that I would continue in academia afterwards, as other career ideas also caught my interest. However, the professional career advice from Prof.dr. Edwin Bergin, Prof.dr. Karin Öberg, Dr. Nikku Madhusudhan, Dr. Jes Jørgensen and Dr. Ilsedore Cleeves helped me decide to continue in academia, and also helped me shape and sharpen my research ideas and plans. Special thanks to Madhu for always being patient, for having time, and for always looking on the bright side of life with a smile and a laugh. You suggested I do outreach next to being a scientist, rather than vice versa, and I am now confidently following that advice. Lastly, Ted! Thank you for believing in me and my research proposal, and for your tireless reference letter writing.

My PhD was made more exciting because I could mix it with astronomy outreach, which was made possible through Universe Awareness. Thank you to Pedro, Tibisay, Jorge, Michael, Kyra, Rafa, Bruno (and Fatima), Audrey (and Maciej), Wouter, Erik (and Martha), Thilinah and George for introducing me to the world of UNAWE. Sarah, Edward, Sævar, Mathieu and Oana, you also inspired me with new outreach ideas. All of you helped me understand what good astronomy outreach is, and how it can be done. You were a large part of the reason for my success

in the FameLab science communication competition in 2017! Kyra and Rafa, you guys have meant so much to me, the trips to Spain have been fantastic, and every time I see you is a new adventure - Rafa, a f***ing hot dance! Ricardo G.: your introduction to podcasts helped me to make a good one for astronomy outreach. Your enthusiasm is contagious! Singapore Science Center, and UNAWE Singapore Coordinator Gerardyn, I appreciate you having me twice to give exoplanet talks to the interested children. It was much fun, exciting and inspiring to be there, and I hope to come back!

My time in Leiden would not had been the same without CrossFit 071. Peter-Jan and Rob, I appreciate you welcoming me to the box, and trusting me to become a trainer, so I could give classes and share my CrossFit passion with all the great members of the box. To the team of trainers, to Mirte, Eline, Francette, Alex, Michał and all the other members of the box, it has always been putting a smile on my face, and butterflies in my stomach, to enter the box, and to conquer a WOD with y'all! Learning Dutch was a priority for me when I came to Leiden. I wanted to talk the local language with the Dutch and get in touch with the culture. But that is not easy, since the Dutch are now the best in the world (after the Danes) at English as second language, meaning everything is just much easier to do in English. One of the first people to bother speaking slow Dutch, so I could follow, was Kasper S.. Mannetje, you have been so patient with me and my funny Dutch, and you have given me so much. We have shared CrossFit og hiking, I gave astronomy lessons in Dutch to your students. We have had good coffees. You, and Pyne, have made me feel at home in Leiden, and I wish you two happy lives together. Other people to practice my Dutch on have been Simon, Cora, Desiree, Maks, Reinier, Martijn, Siroon, Thom, Elzemieke and Aart. I feel privileged to have gotten to know you all, I have enjoyed it so much. Leiden is not the first city to catch the newest trends. But Lindy Hop did arrive here during my time, thanks to Ron and Lotte, and learning swing-dancing has been much fun. Also, a few decent coffee places have opened in Leiden while I have been here, and I hope they will stay, because they are needed. Van Der Leur, and barista Anna, I have written so many pages of my thesis at your table, whilst sipping your delicious flat whites.

Leaving Denmark for a job in the Netherlands was both exciting and a scary. I was excited about moving abroad, but I also worried that I would lose contact with my friends in Denmark. Emil, tak for pool, for indsatsen med vores astro-podcast, og alt andet. Ubeskrivelige tider, BS! Ana, du er bare dejlige dig og du har altid været der, som dig. Du er som en ekstra søster for mig. Malte, du er sådan en fantastisk ven, du har været en enorm støtte gennem tiden, og vi har haft så mange fantastisk sjove og dejlige stunder sammen i så mange år nu. (Michael) Küffi, du og Schnathorst har en ganske særlig plads i mit hjerte, og du gør vores fælles astronomi rigere. Henrik and Sara, I gjorde mig til FCB fan, og I er fantastiske! Kasper M., du er skør og dejlig, om vi så har været i Leiden eller i Rotten. Og til alle jeres dejlige partnere, Cíntía, Nanna, Lisbeth, Giulia og Birgitte, og lille Aja og Alexander: jeg har været så glad for alle de gode tider, og glad for at lære jer at kende! Thank you all for visiting me, and for seeing me when I am in Denmark. For the calls and the texts. It has warmed my heart. I feel our friendships have

maybe even grown stronger, and I am now not afraid of losing contact with you, even though I am not returning to DK anytime soon.

Ook bedankt aan mijn Nederlandse familie, Lies, Ewout, Eric en Charissa. Jullie betekenen allemaal heel veel voor mij. Ik voel me bij jullie zo thuis. Ook met jullie hulp spreek ik nu beter Nederlands, bedankt voor jullie geduld. Ik zie er zo naar uit om met jullie de toekomst te ervaren.

Mor, far og Astrid. Jeg elsker jer alle tre! You have supported me to pursue science since I was young. You supported me in moving abroad, first to Hawai'i and then to Leiden. You encouraged me to take som big steps, to challenge myself. I miss you every day, but even being across the globe from each other doesn't mean I don't feel we are a small and loving family. Aarhus, Tisvilde and Singapore are all like homes to me, with all the lovely people around those places as well. In particular, Akhil you have made Singapore feel even more like home, likewise have the dear people at the Danish Seamen's Church. And really nice to also have you around now, Lars!

My personal life has changed dramatically since I arrived in Leiden. And that is in a large part because of one person: Iris. You have done so much for me. You have supported and helped me with translations and much more so I could write this thesis, and become better at outreach along the way. You have taught me Dutch. I love you, and I can't wait to explore the World with you during our lives together. And I also like our cats.